**Modelling Sensory Innervation of Cancer
using Organ-on-Chip Technology**

Dissertation

zur Erlangung des Grades eines
Doktors der Naturwissenschaften
der Mathematisch-Naturwissenschaftlichen Fakultät
und
der Medizinischen Fakultät
der Eberhard-Karls-Universität Tübingen

vorgelegt von

Matthijs L. van der Moolen

aus Zaanstad, Niederlande

2024

Tag der mündlichen Prüfung: 19. Juli 2024.

Dekan der Math.-Nat. Fakultät: Prof. Dr. Thilo Stehle
Dekan der Medizinischen Fakultät: Prof. Dr. Bernd Pichler

1. Berichterstatter: Prof. Dr. Peter Loskill

2. Berichterstatter: Prof. Dr. Stefan Liebau

Prüfungskommission: Prof. Dr. Monilola Olayioye

                             Prof. Dr. Peter Loskill

                             Prof. Dr. Stefan Liebau

                             Prof. Dr. Philipp Kahle

Wisdom is doubt

Summary

Research contained in this thesis focuses on the advancement of organ-on-chip technology for the exploration of peripheral sensory innervation in cancer. Simultaneously, it describes an extensive attempt at creating a practical platform that can be leveraged to uncover novel approaches in combating cancer-induced pain and gain insight into the intricate relationship between diseased tissues and pain development at a cellular level. Development of this platform is also expected to produce a versatile system capable of addressing the often-neglected importance of peripheral innervation of various kinds in various organs and tissues. Peripheral nerves are essential in modulating tissue responses to environmental changes and maintaining tissue homeostasis, consequently, when innervation maladapts in conditions such as cancer, it has been associated with the development of pain states and tissue dysfunction. Having a technology that can accurately replicate these processes could prove valuable in facilitating the development of therapeutics aimed at alleviating pain and restoring tissue integrity.

Concurrently, I believe organ-on-chip or microphysiological system approaches modelling innervation couple greater control over neuron-cell interactions with sensitive and multivariate readout compared to e.g., *in vivo* animal research, while also addressing ethical concerns associated with animal studies on pain. Utilizing a modality-agnostic approach, these technologies can develop into platforms that could replicate biological innervation interactions in various organs and tissues, surpassing the limitations of simplistic neuronal outgrowth models lacking relevant electrophysiological readouts and considering automation-friendly design parameters. The innovative microphysiological innervation system or INV-MPS, represents a significant advancement over current *in vitro* models, allowing for the coculturing of peripheral neurons alongside three-dimensional (cancer-)tissues embedded in hydrogels within a glass microfluidic assembly. Additionally, incorporation of a substrate-integrated microelectrode array enables real-time monitoring of nerve activity on top of high-resolution imaging of nerve-tissue interactions. This combination provides a comprehensive approach for studying the dynamic interactions between nerves and tissues in a controlled and physiologically relevant setting.

Before seeding cancer spheroids and primary dorsal root ganglion neurons together inside the INV-MPS, I successfully showcased sensory fiber chemoattraction through the exogenous application of nerve growth factor, mimicking a nerve guidance process that closely resembles *in vivo* conditions. Then, omitting nerve growth factor supplementation, cancer spheroids were also capable of driving nerve guidance of excitable nociceptors that remained functional while innervating target tissues. These dual aspects together underline the platform's potential for monitoring excitability and outgrowth in neurotrophin-induced settings with high neurite densities, but also in tracking more discrete cancer-induced axonal growth and disease-induced changes in neuronal electrophysiology.

Aside from its demonstrated versatility in current setup, the INV-MPS should be able to serve researchers in exploring various applications beyond cancer-induced pain and cancer, faithfully reproducing three-dimensional peripheral innervation in various tissues. Its purposeful design enables the modelling of complex *in vitro* biology, offering great potential for those in the microphysiological systems field and beyond, studying interactions between the peripheral nervous system and innervated tissues. However, within this thesis, the development of a microelectrode array integrated microphysiological system for the study of peripheral neurons is highlighted to aid primarily the discovery and screening of new therapeutics for cancer-related pain. Point is, understanding obtained on how to effectively incorporate recordable innervation within a microphysiological system could then be utilized to also advance modeling (sensory) innervation of many types of tissues *in vitro*.

Zusammenfassung

Die in dieser Arbeit enthaltenen Forschungsarbeiten konzentrieren sich auf die Weiterentwicklung der Organ-on-Chip-Technologie zur Erforschung der peripheren sensorischen Innervation bei Krebs. Gleichzeitig wird ein umfassender Versuch beschrieben, eine praktische Plattform zu schaffen, die zur Aufdeckung neuer Ansätze bei der Bekämpfung krebsbedingter Schmerzen und zur Gewinnung von Erkenntnissen über die komplizierte Beziehung zwischen erkranktem Gewebe und der Schmerzentwicklung auf zellulärer Ebene genutzt werden kann. Die Die Entwicklung dieser Plattform soll auch ein vielseitiges System hervorbringen, das in der Lage ist, die oft vernachlässigte Bedeutung der peripheren Innervation verschiedener Arten in verschiedenen Organen und Geweben zu untersuchen. Periphere Nerven sind für die Modulation von Gewebereaktionen auf Umweltveränderungen und die Aufrechterhaltung der Gewebehomöostase von entscheidender Bedeutung. Wenn die Innervation bei Krankheiten wie Krebs gestört ist, wird dies mit der Entwicklung von Schmerzzuständen und Gewebedysfunktionen in Verbindung gebracht. Eine Technologie, die diese Prozesse genau nachbilden kann, könnte sich als wertvoll für die Entwicklung von Therapeutika erweisen, die auf die Linderung von Schmerzen und die Wiederherstellung der Gewebeintegrität abzielen.

Gleichzeitig glaube ich, dass Organ-on-Chip- oder mikrophysiologische Systemansätze, die die Innervation modellieren, eine bessere Kontrolle über die Interaktionen zwischen Neuronen und Zellen mit sensiblen und multivariaten Messwerten ermöglichen als z. B. In-vivo-Tierversuche und gleichzeitig die ethischen Bedenken ausräumen, die mit Tierversuchen zu Schmerzen verbunden sind. Unter Verwendung eines modalitätsagnostischen Ansatzes können sich diese Technologien zu Plattformen entwickeln, die biologische Innervationsinteraktionen in verschiedenen Organen und Geweben nachbilden und die Grenzen einfacher neuronaler Wachstumsmodelle ohne relevante elektrophysiologische Messwerte und unter Berücksichtigung automatisierungsfreundlicher Designparameter überwinden. Das innovative mikrophysiologische Innervierungssystem, INV-MPS, stellt einen bedeutenden Fortschritt gegenüber den derzeitigen In-vitro-Modellen dar und ermöglicht die Kokultur von peripheren Neuronen neben dreidimensionalen (Krebs-)Geweben, die in Hydrogelen eingebettet sind, in einer mikrofluidischen Glasanordnung. Darüber hinaus ermöglicht die Integration eines substratintegrierten Mikroelektroden-Arrays die Echtzeit-Überwachung der Nervenaktivität zusätzlich zur hochauflösenden Bildgebung von Nerven-Gewebe-Interaktionen. Diese Kombination bietet einen umfassenden Ansatz zur Untersuchung der dynamischen Interaktionen zwischen Nerven und Gewebe in einer kontrollierten und physiologisch relevanten Umgebung.

Vor der gemeinsamen Aussaat von Krebs-Sphäroiden und primären Spinalganglien-Neuronen im INV-MPS habe ich erfolgreich die Chemoattraktion sensorischer Fasern durch die exogene Anwendung von Nervenwachstumsfaktor vorgeführt und damit einen Nervenleitprozess nachgeahmt, der den Bedingungen in vivo sehr ähnlich ist. Ohne Zugabe des Nervenwachstumsfaktors waren die Krebs-Sphäroide auch in der Lage, die Nervenführung erregbarer Nozizeptoren zu steuern, die funktionsfähig blieben und das Zielgewebe innervierten. Diese beiden Aspekte zusammen unterstreichen das Potenzial der Plattform für die Überwachung der Erregbarkeit und des Wachstums in Neurotrophin-induzierten Umgebungen mit hoher Neuritendichte, aber auch für die Verfolgung von diskreterem krebsinduziertem axonalem Wachstum und krankheitsbedingten Veränderungen der neuronalen Elektrophysiologie.

Abgesehen von seiner nachgewiesenen Vielseitigkeit im derzeitigen Aufbau sollte das INV-MPS Forschern bei der Erforschung verschiedener Anwendungen jenseits von krebsbedingte Schmerzen und Krebs helfen können, indem es die dreidimensionale periphere Innervation in verschiedenen Geweben originalgetreu nachbildet. Sein zweckmäßiges Design ermöglicht die Modellierung komplexer In-vitro-Biologie und bietet ein großes Potenzial für diejenigen, die im Bereich der mikrophysiologischen Systeme und darüber hinaus die Interaktionen zwischen dem peripheren Nervensystem und innervierten Geweben untersuchen. In dieser Arbeit wird jedoch die Entwicklung eines integrierten mikrophysiologischen Systems mit Mikroelektroden-Array für die Untersuchung peripherer Neuronen hervorgehoben, das in erster Linie der Entdeckung und dem Screening neuer Therapeutika für krebsbedingte Schmerzen dienen soll. Die Erkenntnisse darüber, wie man die aufzeichenbare Innervation effektiv in ein mikrophysiologisches System integrieren kann, könnten dann auch dazu genutzt werden, die Modellierung der (sensorischen) Innervation vieler Gewebetypen in vitro voranzutreiben.

Acknowledgements

Declaration of Contributions to the Dissertation

The dissertation work was carried out at the Natural and Medical Sciences Institute in Reutlingen under the supervision of Dr. Paolo Cesare and Prof. Dr. Peter Loskill.

The INV-MPS (Microphysiological System for Innervation) research titled "**Cancer-mediated Axonal Guidance of Sensory Neurons in a MEA-based Innervation MPS**", illustrated in **Chapter. 7**, was designed in collaboration with Dr. Paolo Cesare.

Outlined in the *Author Contributions'* section of the published article in **Biofabrication Iopscience.iop.org** (doi: 10.1088/1758-5090/ad218a) and in the pre-print available on **Biorxv.org** (doi: 10.1101/2023.10.18.562227)

> *"Matthijs van der Moolen and Dr. Paolo Cesare designed research; Matthijs van der Moolen and Dr. Paolo Cesare performed biological and microfabrication research; Fulya Ersoy aided microfabrication; Dr. Andrea Lovera and Sacha Mommo created glass devices; Matthijs van der Moolen and Paolo Cesare analyzed data; Matthijs van der Moolen, Prof. Dr. Peter Loskill and Dr. Paolo Cesare wrote the paper."*

I performed the majority of biological and microfabrication research and together with Dr. Paolo Cesare performed associated imaging and electrophysiological readout. I received ample assistance from Dr. Paolo Cesare with regards to data analysis, and statistical analysis was, additionally, carried out under his supervision.

I confirm that the written text in this thesis, pertaining to the INV-MPS work was written by myself, with input/correction from Dr. Paolo Cesare and Prof. Dr. Peter Loskill.

Signed by: **Matthijs L. van der Moolen**   Date: **16-03-2024**

Abbreviations

OOC	Organ-on-Chip
MPS	Microphysiological system
INV-MPS	Microphysiological innervation system
SLE-MPS	Selectively laser-etched microphysiological innervation system
MEA	Microelectrode Array
MF	Microfluidic
PNS	Peripheral nervous system
CNS	Central nervous system
DRG	Dorsal root ganglion
DH	Dorsal horn
CIP	Cancer-induced pain
NGF	Nerve growth factor
TrkA	Tropomyosin receptor kinase A
RTK	Receptor tyrosine kinase family
HT-29	Human colorectal adenocarcinoma cell line
PANC-1	Human pancreatic cancer cell line
3D	Three-dimensional
2D	Two-dimensional
TRPV1	Transient receptor potential vanilloid 1
TRPA1	Transient receptor potential ankyrin 1
TRPM8	Transient receptor potential melastatin 8
CGRP	Calcitonin-gene related peptide
SP	Substance P
Ach	Acetylcholine
NMDA	N-methyl-D-aspartate
ASIC	Acid-sensing cation channels
Nav	Voltage-gated sodium channels
Cav	Voltage-gated calcium channels
Kav	Voltage-gated potassium channels
VGIC	Voltage-gated ion channels
LGIC	Ligand-gated ion channels
GPCR	G-protein coupled receptors

BBB	Blood-brain-barrier
PDMS	Polydimethylsiloxane
TME	Tumour microenvironment
PNI	Perineural invasion
PGE_2	Prostaglandins
ATP	Adenosine triphosphate
ROS	Reactive oxygen species
NO	Nitric oxide
IL-8	Interleukin - 8
TNF-α	Tumour necrosis factor α
GDNF	Glial cell-derived neurotrophic factor
BDNF	Brain-derived neurotrophic factor
GPCR	G-protein-coupled receptors
NSAIDs	Nonsteroidal anti-inflammatory
RPOA	Rapid onset osteoarthritis
qPCR	Quantitative polymerase chain reaction
ELISA	Enzyme-linked immunosorbent assay
GECI	Genetically encoded calcium indicators
PTX	Picrotoxin
GABA	Gamma-aminobutyric acid
GFP	Green fluorescent protein
GcaMP6f	Ca^{2+}-sensitive GFP
CME	Covered microelectrode
OME	Open microelectrode
ML	Media layer
GL	Gel layer
MFR	Mean firing rate
IPSC	Induced pluripotent stem cells
DMEM	Dulbecco's modified eagle medium
AAV	Adeno-associated virus
SYN1	Synapsin I
DIV	Days *in vitro*
MEMS	Microelectromechanical systems

PFOTS	Perfluorooctyltrichlorosilane
SiNx	Silicon nitride
PECVD	Plasma enhanced vapor deposition
PEB	Post-exposure bake
SB	Soft-bake
HB	Hard-bake
SU-8	EPON SU-8 photoresist resin
Ordyl SY300	Dry film negative photoresist
ADEX	Dry film negative photoresist
FRP	Free radical photo-polymerization
PAG	Photoacid generator
TDFS	Thin dry film sheet
SNR	Signal-to-noise ratio
TiN	Titanium nitride
CMH	C-fiber mechano-heat-sensitive
AMH	A-fiber mechano-heat-sensitive
MSA	Mechanically sensitive afferents
MIA	Mechanically insensitive afferents
AP	Action potential
ACC/PCC	Anterior and posterior cingulate cortex
PAG	Periaqueductal gray
SEM	Standard error of the mean
p75NTR	P75 neurotrophin receptor
CRC	Colorectal cancer
PDAC	Pancreatic ductal adenocarcinoma
GI-tract	Gastrointestinal tract
ENS	Enteric nervous system
FCS	Fetal calf serum
RPOA	Rapid onset osteoarthritis
VEGF	Vascular endothelial growth factor
IL-1β	Interleukin - 1β
IL-6	Interleukin – 6
WHO	World Health Organization

Table of Contents

Chapter 1: General Introduction

1.1 Introduction

Organ-on-chips (OoCs) and the broader field of microphysiological systems (MPSs) have emerged as innovative technologies that provide a platform for investigating complex biological interactions in a controlled environment. These systems generally contain engineered or natural miniature tissues grown inside microfluidic chips, which enable the precise tuning of cell microenvironments and recapitulation of tissue-specific functions. Consequently, the field of *in vitro* scientific development has allowed researchers to mimic human physiology more accurately. However, despite the significant strides made in recapitulating organs and tissues, OoC/MPS-scientists often overlook the essential role of peripheral innervation (nerve ingrowth) in proper tissue function [1, 2]. The peripheral nervous system (PNS) is a network of nerve fibers that extend throughout the body and connects to all types of tissues. The peripheral innervation of skin, bone and visceral organs plays a crucial role in mediating responses to changes in the environment and aiding in safeguarding tissue homeostasis. Additionally, the PNS is responsible for relaying information from purely sensory organs, such as the eyes, to the brain and for transmitting signals from the brain to the limbs for coordinated movement (motor). Nerve bundles also assist in arranging vascular networks by aligning blood vessels. Effectively mediating vessel contraction and relaxation which controls blood pressure and ensures proper circulation throughout the body (Table. 1).

Type	General function	Notable finding	Refs
SKIN (SENSORY & SYMPATHETIC)	C and Aδ fibers expressing specific receptors responding to various environmental stimuli (cold, mechanical and polymodal) and autonomic fibers regulate gland function	Disruption of nerve ending pruning by keratinocytes leads to pathological itch	**Takahashi, S. [3]** **Laverdet, B. [4]**
SKELETAL MUSCLE (MOTOR & SENSORY)	Development of the neuromuscular junction (NMJ - synapse connecting neurons and myofibers) is key for improving muscle function and muscle growth	Acetylcholine (ACh) released by motorneurons can prevent atrophy (denervation induces weakness conversely)	**Lepore, E. [5]** **Cisterna, B. A. [6]** **Guo, X. [7]**
SMOOTH MUSCLE (SENSORY, SYMPATHETIC & PARASYMPATHETIC)	Convey high-threshold sensations like e.g., discomfort, distension and urgency and facilitate gastrointestinal motility	Sodium channels (NaV) are involved in colonic visceral hypersensitivity and react to inflammatory mediators	**Erickson, A. [8]** **Brierley, S. M. [9]**

BONE (SENSORY & SYMPATHETIC)	Neural regulation of blood flow, protective pain and whole-body homeostasis	Large percentage of sensory nerve fibers innervating bone express tropomyosin receptor kinase A (TrkA)	**Brazill, J. M. [10]** **Castañeda-Corral, G. [11]**
LIVER (SYMPATHETIC & PARASYMPATHETIC)	Transmitting information about osmolality, glucose and lipid concentrations, while receiving signals regarding blood flow, bile secretion and metabolism	Hepatic inflammation and fibrosis can decrease hepatic nerve innervation affecting control	**Nam, S. W. [12]** **Mizuno, K. [13]**
HEART (SYMPATHETIC & PARASYMPATHETIC, SENSORY)	Autonomic nervous system controls heart rate, blood pressure and all associated cardiac function	Activation of vagal afferents causes a profound bradycardia (lowering of heart rate)	**Rajendran, P. S. [14]** **Kapa, S. [15]**
CORNEA (SENSORY)	C and Aδ fibers expressing specific receptors responding to various environmental stimuli (cold, mechanical and polymodal)	High density sensory nerve innervation triggers avoidance responses to potential eye damage	**Guerrero-Moreno, A. [16]** **Paunicka, K. J. [17]**
FAT (SENSORY & SYMPATHETIC)	Paracrine factors like e.g., leptin enable adipocyte-neuron communication for glucose homeostasis	Sensory nerve ablation in adipose tissue increases fat storage and heat production	**Wang, Y. [18]** **Guilherme, A. [19]**

Table. 1: Differential innervation of bodily tissues and organs.

From the table above, it is clear that the degree of innervation an organ receives can even serve as a metric for determining whether a tissue has been damaged or not (denervation occurs in some damaged tissues). Worth mentioning separately also is the integral peripheral nerve involvement in maintaining a stable heart rhythm, among other vital bodily functions. Hence, OoC/MPS-scientists need to carefully consider and even prioritize the incorporation of nerves into their complex three-dimensional (3D) constructs, when trying to model organs. Because effective integration could then lead to the development of more accurate and complete 3D tissue models that significantly improve the translational value of this branch of *in vitro* approaches. The table also suggests that the involvement of sensory nerve fibers is especially widespread. Vast literature available on the somatosensory system mostly involves nociceptive fibers (pain sensing) and comes from *in vivo* research, currently deemed the gold-standard for assessing e.g., tissue-damage related pain [20]. As a result, additional ethical concerns associated with *in vivo* pain research in addition to general pro-*in vitro* considerations (more control, higher throughput etc.)

should drive the OoC-field and MPS-field to incorporate particularly sensory innervation in their models. But before describing the development of new *in vitro* technologies for studying e.g., nerve-tissue interplay in pain, it is important to have a basic understanding of the pain field and its players.

1.2 Relevance for Pain Research and Sensory Innervation

(Sensory neurons, Nociception, Pain mediators, Ion channels and Schwann cells)

The somatosensory system is responsible for providing us with information about the external environment, and includes; touch (mechanoception), proprioception (sense location/movement), temperature (thermoception), pain (nociception) and itchy/tickly stimuli. For humans, pain often prompts taking further protective actions, thus, playing a major role in ensuring our survival in a potentially harmful environment [20, 21]. However, pain can outlive its evolutionary usefulness as an acute warning system and instead become debilitating and chronic (sciatica, cancer pain, arthritis etc.).

Nociception specifically refers to the neural encoding of harmful noxious stimuli (can be measured in terms of objective parameters), while pain is the unpleasant sensory and emotional experience associated with actual or potential tissue damage [22]. Peripheral sensory neurons called nociceptors - unmyelinated C-fibers and myelinated Aδ-fibers - carry receptors that can be activated by various forms of noxious stimuli such as intense heat (threshold >43-50°C), cold, mechanical pressure and certain exogenous and endogenous chemicals like capsaicin (present in cayenne pepper) [23-25]. Upon activation, sensory input will propagate from the periphery to the central nervous system (CNS) after generation of an action potential following stimuli-induced depolarization at the nerve terminal of these nociceptors.

Acute pain, which typically lasts from a few minutes up to 1-3 months and often results from an injury, can be classified as nociceptive pain. Generally caused by ongoing noxious input from tissue damage and distinctly different from neuropathic (chronic) pain [20, 26]. Neuropathic pain arises from an injury or illness directly affecting either the PNS (primary afferent nociceptive fibers) or the CNS, altering pain processing. Certain chronic pain disorders have well-defined phenotypes and are believed to originate from both nociceptive and neuropathic involvement. There also exists a third classification of pain which comprises conditions lacking clear evidence of either nociceptive or neuropathic components. In 2016, nociplastic pain, was introduced to mechanistically describe pain states that exhibit altered nociceptive function but no obvious activation of nociceptors or neuropathy, "but in whom clinical and psychophysical findings suggest altered nociceptive function" [27]. This type of pain is difficult to characterize and arises from

modified pain-related sensory pathways particularly in the CNS, resulting in heightened sensitivity (Figure. 1). However, before the term nociplastic pain was coined, central sensitization (alterations to centrally regulated pain sensitivity) was considered part of neuropathic pain and remains acknowledged as a component of both.

Nociceptive Pain	Neuropathic Pain	Nociplastic Pain
Due to activation of nociceptors by damaging stimuli	Due to lesion or disease of the somatosensory system	Due to disturbance in pain processing
• Inflammation • Mechanical irritant • Injury	• Peripheral neuropathy	• Central sensitization
Examples	Examples	*"Hypersensitivity after a traumatic noxious stimulus in the periphery could be mediated by both peripheral and CNS changes"*
• Osteoarthritis and rheumatoid arthritis • Cuts/Burns/ Bruises • Cancer	• Phantom limb • Diabetic neuropathy • Carpal tunnel syndrome • Complex regional pain syndrome	Examples • Fibromyalgia • Tension-type headache • Low back pain

Figure. 1: Classification of different types of pain. Produced with input from [20, 27]. ---- Reproduced from [28] with permission ©Oxford University Press (license num. 5721920974905) & Dr. Kathleen Sluka.

When discussing afferent (sending information *to*, the brain) nociceptive fibers – one generally separates first-order (primary) afferent fibers and second-order (secondary) afferent fibers. First-order nociceptive fibers have their cell bodies located in the dorsal root ganglia (DRG) for the body and in the trigeminal ganglia for the face. DRG soma are enveloped by immunomodulatory satellite glia cells (SGCs) and are effectively insulated from external stimuli as they reside within the bony boundaries of the intervertebral foramen and are largely protected by the blood-brain-barrier (BBB) [29, 30]. In order to send pain signals to the CNS, nociceptors have a peripheral branch that combines with the ventral root (contains motor neurons) to form a spinal nerve (e.g., sciatic) ultimately innervating the target organ and a central axonal branch that terminates in the spinal cord - synapsing onto second-order fibers with soma in the dorsal horn (DH) that relay to the brain. Aδ and C fibers are considered the two main kinds of nociceptors (primary afferents), as Aβ fibers only respond to innocuous mechanical stimulation like e.g., light touch [20, 24].

The acute, well-localized "first" or "fast" pain, which is characterized by a strong, distinct sensation that is quickly localized to a particular area of the body, is mediated by small diameter myelinated-Aδ fibers. Myelination status indicates whether or not the peripheral fibers are insulated by Schwann cells (Oligodendrocytes in the CNS) for rapid electrical impulse transmission [31]. Unmyelinated-C fibers, on the other hand, transmit poorly localized, dull, or "second" pain. High-threshold mechanical nociceptors, sometimes referred to as Aδ type I fibers, are capable of responding to both chemical and mechanical stimuli with high heat threshold (>50°C). Contrarily, type II fibers have a high mechanical threshold but a significantly lower heat threshold. C fibers are also generally mechanically and thermally sensitive [20]. Both Aδ and C fibers can become 'sensitized' at their nerve endings as a result of damage, causing exaggerated pain sensation at lower noxious thresholds [24]. In Chapter 5: Pain Electrophysiology & Cancer-Neuron coculture, we delve deeper into how pain scientists distinguish different nerve fibers and elaborate on the processing of pain electrophysiology data, but an introductory summary is given here.
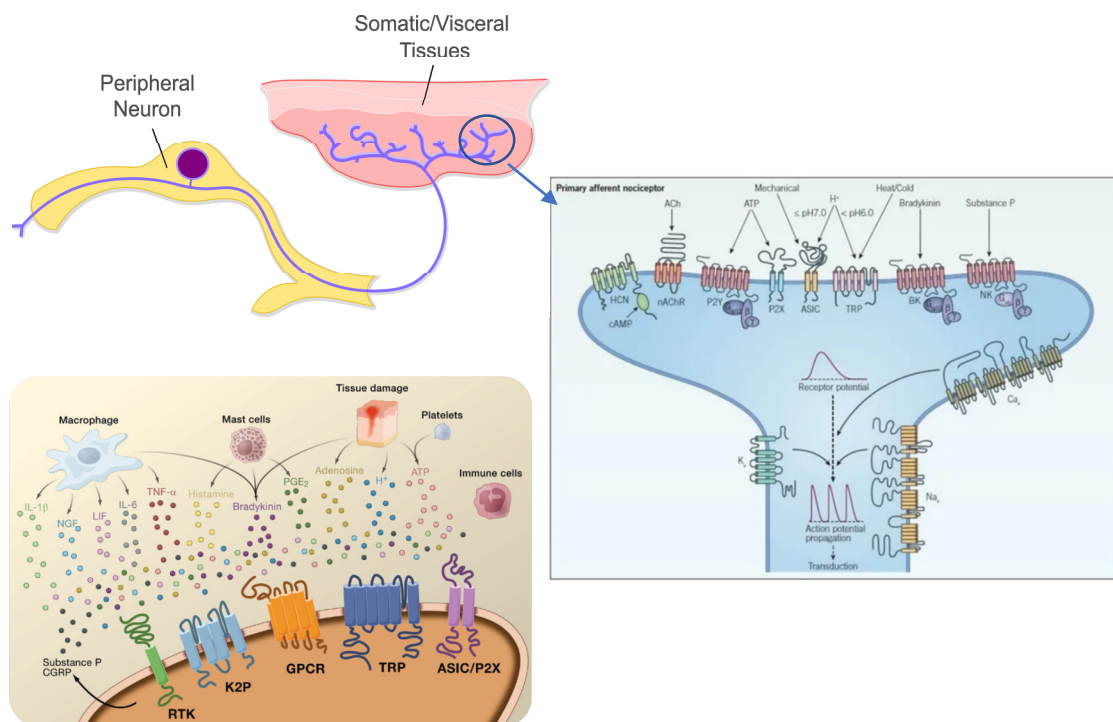
Figure. 2: DRG physiology with characteristic receptors and ligand/voltage-gated ion channels (VGICs/LGICs). Free nerve endings are covered with ligand-gated and voltage-gated receptors/channels that can be activated by compounds released during inflammation that ultimately drive pain states. Reproduced from reference [32] (CC BY 4.0) ©IOP Publishing. All rights reserved. Reproduced from [24] with permission ©Elsevier (license num. 5721940230082). Reproduced from reference [33].

DRG neurons have a unique structure called pseudo-unipolar, where both central and peripheral terminals bifurcate from a common axonal stalk, unlike prototypical neurons with dendrites and axons (Figure. 2). Both terminals can be activated by endogenous moieties (chemical agonists, neurotransmitters and changes in pH), however, peripheral terminals are the only one to respond to environmental stimuli. As mentioned, these stimuli ultimately induce a membrane depolarization that leads to sensory input propagation from the periphery up the spinal cord. In injury, nociceptors release excitatory neurotransmitter glutamate onto DH neurons which opens postsynaptic ion channels gated by N-methyl-D-aspartate (NMDA)-type glutamate receptors to propagate the signal (persistent release can drive DH hypersensitivity – central sensitization) [21].

Characteristic cellular markers and simultaneous actors in depolarization of (peptidergic) nociceptors are the tropomyosin kinase A receptor for nerve growth factor (NGF – neural development and survival), the transient receptor potential vanilloid type 1 (TRPV1 – general sensor of noxious heat) channel, TRPM8 (cold) and TRPA1 for chemical irritants [34]. Pioneering work by Prof. David Julius (UC San Francisco, USA) indicates LGIC TRPV1 rearranges its structure upon capsaicin binding or activation by noxious heat, allowing influx of ions such as Na^+ and Ca^{2+} leading to generation of an action potential [35]. Nociceptors also express, among other things, voltage-gated sodium (Na_v) and calcium (Ca_v) channels, a variety of potassium (K_1) channels and acid-sensing cation channels (ASIC) – which increase their gating response (opening) upon voltage-sensing. Important to note is that VGICs like Na_vs primarily contribute to action potential generation after depolarization by facilitating inward current during the rising phase and are located just beyond the neuron's input region or 'trigger zone' (Figure. 2 on the right) [21, 36, 37]. At the input region, specific disturbance of charge separation at the membrane (in- outflow of cations or anions) induce depolarization after breaching the activation threshold (membrane potential rises from -75 mV to -55 mV).

Peptidergic means peripheral terminals release neuropeptides when activated by painful stimuli (e.g., TRPV1), namely calcitonin-gene related peptide (CGRP) and substance P, which can also contribute to vasodilation and plasma protein extravasation in neurogenic inflammation [38]. These neuropeptides undergo vesicular transport to the nerve endings and are subsequently released through fusion with the membrane. In Figure. 2 on the left, it is additionally portrayed that activity of nociceptors is regulated by products of inflammation acting on G-protein coupled receptors (GPCRs), including prostaglandins (PGE_2), adenosine triphosphate (ATP), histamine, bradykinin and protons (H^+).

Depicted release of specific cytokines, NGF, reactive oxygen species (ROS), nitric oxide (NO) by e.g., immune cells or tissue damage can lower noxious thresholds of sensory fibers and also directly sensitize TRPV1 channels (enhancing TRPV1-evoked responses). TRPV1 sensitization is a protein specific intracellular mechanism that facilitates its gating and strengthens the currents that are triggered when it is activated [38]. Additionally, intracellular vesicles also transport membrane proteins from their sites of synthesis to insertion at functionally appropriate targets (damaged tissue innervating terminals) to increase regional receptor/channel density [20, 21]. Emerging evidence suggests that within the field of oncology, crosstalk between cancer and nerves might involve such upregulation of surface receptors and could even lead to malformations and hypersensitivity of sensory nerve fibers innervating the inflammatory tumour milieu.

1.3 Sensory Nerve Fibers and the Tumour Microenvironment

40%-70% of cancer patients experience moderate to severe pain, particularly those with advanced cancer [39]. This pain significantly impairs their quality of life, affecting essential activities like eating, sleeping and working, ultimately exerting a heavy emotional toll. Profound impact underscores the urgent need for discovery of new effective cancer-pain management strategies. Interaction between sensory fibers innervating certain tissues subject to cancer cell growth has become a highly relevant area of research for understanding the development of cancer-induced pain (CIP) and also cancer dissemination. Researchers even suggest that neuro-oncological interplay can be deemed a new hallmark of cancer [40]. Several reviews have covered the topic of cancer innervation and few published articles have already identified mechanisms of action that potentially mediate the interaction. General consensus is that factors released into the tumour microenvironment (TME) play a role in influencing nerve outgrowth and morphology (sprouting) based on observations of cancer-induced erratic innervating fiber behaviour and guidance of nerves to the TME through tumour-mediated chemoattraction [41-45]. Release of cytokines, exosome-packaged molecules and neurogenic factors like e.g., IL-8, TNF-α, Artemin, NGF, EphrinB1, glial cell-derived neurotrophic factor (GDNF) and brain-derived neurotrophic factor (BDNF) have already been implicated as potential drivers of associated axonogenesis (nerve outgrowth) / hyperinnervation / neurogenesis (nerve generation) / reprogramming (gene regulation affecting phenotype) (Figure. 3). Important to note is that the process by which cancer cells receive tumourigenic input from nerves and spread along peripheral nerves, called perineural invasion (PNI), is a lot more advanced than describing nerve-cancer associated pain (when sensory afferents are involved) (Figure. 3D). NGF signaling specifically has been shown to facilitate migration of pancreatic cancer cells and by blocking this signaling pathway (via KO or

neutralizing antibodies), perineural invasion could be prevented to limit spread [46]. Which, when taken together, make the field of nerve-cancer crosstalk even more intriguing.
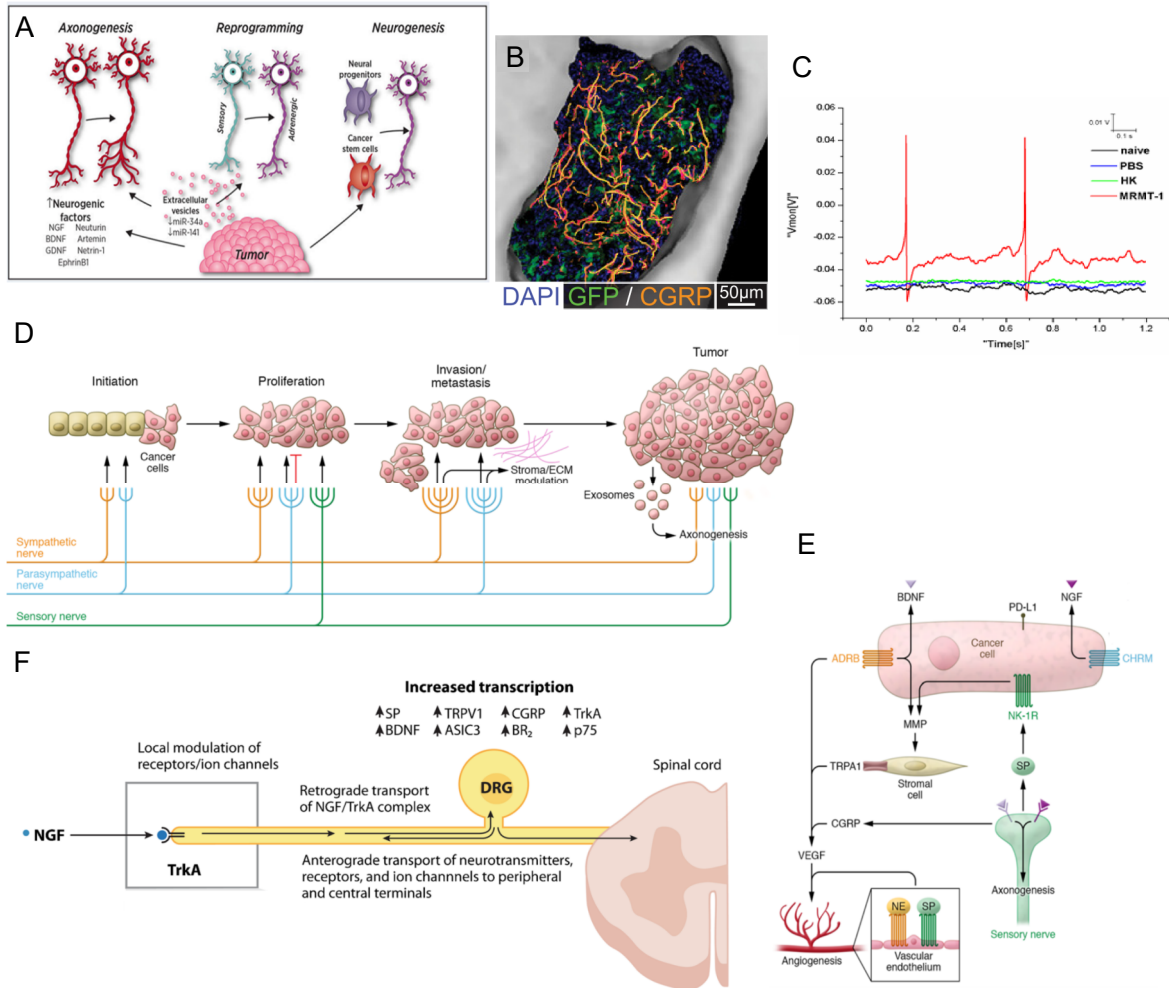
Figure. 3: Cancer-peripheral nerve interactions. (A) (B) Tumour-derived neurogenic factors (potentially transported as exosomal cargo) can drive alterations in morphology (axonogenesis - ectopic sprouting and arborization) and (C) induce spontaneous firing and/or changes in sensitivity towards depolarizing stimuli in nociceptors. (D) (E) Vice versa, various types of peripheral nerves have been implicated in facilitating tumour growth and e.g., angiogenesis by neuropeptide release. (F) TME generated NGF binds terminal TrkA and modulates nociceptor function. ---- Reproduced from [44] with permission ©The American Association for Cancer Research (license num. 5722021005343). Reproduced from reference [47] (CC BY 4.0) ©Society for Neuroscience and [48] (CC BY 4.0) ©SAGE Publications Inc. Reproduced from [41] with permission ©The American Society for Clinical Investigation (license num. 1446693-1/1446694-1). Reproduced from [49] with permission ©Springer Nature (license num. 5726650312581)

Highly relevant, with regards to cancer pain, is research done by Prof. Patrick W. Mantyh (University of Arizona, USA) and his associates into the consequences of cancer metastasis on the sensory nerves innervating bone by demonstrating pathological reconfiguration of sensory nerve fibers in murine tumour-bearing tissue (Figure. 3B).

They found that the majority of sprouting sensory nerve fibers express the TrkA gene (part of the receptor tyrosine kinase family - RTK), pointing towards the NGF/TrkA mechanism driving this maladaptation. NGF-TrkA, in this context, is internalized and transported to the soma in the DRG and influences gene expression that regulates neurotransmitter, receptor and ion channel cycling, which consequently drives pain states [50] (Figure. 3F). Anti-NGF antibody administration (binding NGF) ameliorated sprouting and pain, however, cancer cells did not always show upregulated expression/release of NGF (MDA-MB-231-BO human breast cancer did, ACE-1 canine prostate did not). This indicates cancer cells but also tumour-associated stromal cells in the TME were able to drive pathological remodeling of surrounding TrkA+ sensory nerve fibers via the release of NGF [47, 51].

Non-behavioural study of cancer-induced alterations in electrogenic properties and excitability of DRG neurons was performed using whole-cell patch-clamp recordings a few years later [48] (Figure. 3C) (cancer pain is already known to induce mechanical and thermal hyperalgesia *in vivo* [52]). Neurons became more excitable after injection of MRMT-1 rat breast carcinoma cells in the rat tibial canal, evidenced by spontaneous and tonic (ongoing) excitatory discharges. Seemingly self-explanatory is then linking TME-induced nerve alterations (sprouting) and pain profiles, however, establishing a clear causal relationship between morphology and functionality is not trivial. What is known is that NGF might be the key player that could provide this link. Outside the context of cancer, anti-NGF therapy targeting affected innervating fibers has already effectively reduced osteoarthritis pain in patients [53]. Intravenously admitted NGF monoclonal antibody Tanezumab, is being studied as a potential treatment for osteoarthritis pain in people who do not respond to or are unable to take NSAIDs (nonsteroidal anti-inflammatory drugs). Tanezumab was more effective than NSAIDs and opioid analgesics in treating OA pain, but risk of reporting peripheral sensation abnormalities and joint issues (RPOA – rapid onset osteoarthritis) outweigh the benefits currently. [54]. It is, therefore, important to continue exploring alternative methods for mitigating pain in osteoarthritis and cancer patients by studying inhibition of relevant receptor-ligand interactions like e.g., NGF-TrkA or blocking of downstream effectors. Identifying peripherally acting candidates could ultimately reduce the necessity for administering opioids to patients, while still effectively managing pain.

1.4 State-of-the-Art *in vitro* Approaches Modelling Peripheral Nerve Injury

As described above, available literature on CIP is limited to tumours of particular origin (namely breast and prostate cancer metastasis to bone) and research is generally performed *in vivo*. Furthermore, it makes sense to explore alternative avenues for studying morphology and neuronal excitability in this context. 3D MPSs provide a controllable yet physiologically relevant *in vitro* platform to develop interventive therapies inhibiting specific cancer-induced axonal growth / nerve sprouting and associated changes in neuronal electrophysiology. Arguably, compatible neuronal systems have been developed previously. These generally implement micropatterned structures separating soma from terminals for the manipulation of solely axons by e.g., mechanical injury and/or growth factor cocktails (Table. 2). This feature also enables high resolution characterization of protein complex trafficking in axons and largely eliminates the interference from supportive cells such as fibroblasts and Schwann cells on terminals. It also facilitates the study of peripheral hyperexcitability in DRG axons and how it affects the expression of nerve ending ion channels and receptors. Focusing on models that incorporate the equivalent of peripheral sensory afferent fibers, some key insights looking at the *in vitro* approaches modelling peripheral nerves and their interactions with tissue(-derived molecules) are summarized.

Model (2D/3D)	*in vitro* device/technology	Readout(s)	Notable finding	Refs
2D DISSOCIATED EMBRYONIC RAT DRG CULTURE	2 chamber XonaChips® (Xona Microfluidics™) - Compartmentalized PDMS-based system with microtunnels (extra ref: Park, J. W. [55])	Neurite outgrowth, Calcium imaging, Immunocytochemistry	Observable contrast in proton sensitivity between peripheral neurites and cell soma	**Clark, A. J. [56]**
2D DISSOCIATED EMBRYONIC RAT DRG AND DH COCULTURE	3 chamber XonaChips® (Xona Microfluidics™) - Compartmentalized PDMS-based system with microtunnels	Calcium imaging, Extracellular patch clamp, Immunocytochemistry, qPCR	Decrease in the involvement of NaV1.8 and NaV1.7 channels in synaptic transmission following axotomy	**Vysokov, N. [57]**
2D DISSOCIATED POST-NATAL PORCINE DRG CULTURE	3 chamber Campenot device (extra ref: Campenot, R.B. [58]) – Teflon divider structure attached on silicon grease with microtunnels	Neurite outgrowth, ELISA	GDNF-cultured soma extend laterally without added growth factors, unlike those cultured in NGF	**Klusch, A. [59]**
3D HUMAN SENSORY NEURON AND INTERNEURON PROGENITOR ORGANOIDS IN MATRIGEL®	Stereolithographic printing of polycarbonate devices and membranes, placed inside a 24-well Cytoview MEA plate (Axion Biosystems™)	MEA-based recordings, Immunocyto-chemistry, with cryosections, qPCR	THC and capsaicin cotreatment eliminated the increase in MFR caused by capsaicin	**Ao, Z. [60]**

2D DISSOCIATED POST-NATAL RAT DRG AND PANCREATIC/BREAST/ PROSTATE CANCER COCULTURE	2 chamber - Compartmentalized PDMS-based system with microtunnels	Cancer migration, Immunofluorescence, ELISA	Prostate and pancreatic cancer cells migrated more than breast cancer cells	**Lei, Y. [61]**
2D POST-NATAL MURINE DRG EXPLANTS CULTURE EXPOSED TO OSTEOCLAST SECRETOME	2 chamber XonaChips® (Xona Microfluidics™) and similar microElectrode–microfluidic (µEF) on MEA	MEA-based recordings, qRT-PCR, Neurite outgrowth	Osteoclasts' secretome triggers sensory neurons, implicating nerve sensitization by bone	**Neto, E. [62]**
3D HUMAN IPSC-DERIVED PERIPHERAL NEURON AND SCHWANN CELL SPHEROIDS IN MATRIGEL®	Single keyhole chamber PEGDMA/LAP stereolithography combined with Transwell® (Corning™) inserts	Immunocyto-chemistry, Extracellular patch clamp, Transmission electron microscopy (TEM), Histology	Mini-nerve portion of the coculture system comprises densely underlined myelinated, thinly myelinated and unmyelinated axons	**Sharma, A. D. [63]** (Axosim™)
2D(-3D) HUMAN IPSC-DERIVED SENSORY NEURONS AND HUMAN PRIMARY KERATINOCYTES	2-3 chamber NeoBento MEA Pro (Netri™ with Axion Biosystems™) - Compartmentalized PDMS-based high-throughput system with microtunnels	Neurite outgrowth, MEA-based recordings, Calcium imaging, Immunocyto-chemistry, qPCR/ELISA	Optimal growth achieved by cultivating cells with their respective culture medium.	**Guichard, A. [64]** Unpublished (Netri™)

Table. 2: *In vitro* **models replicating sensory nerve physiology and tissue innervation**

Polydimethylsiloxane (PDMS)-based models are widely adopted and recognized for their affordability, ease of patterning, translucency and gas permeability. Relevant participants in this field include Xona Microfluidics™ and Netri™, who provide researchers with standardized chambered devices, particularly those with limited access to microfabrication tools at their institutions. With these kinds of chips, brightfield imaging and/or immunocytochemistry can be used to precisely measure neurite outgrowth. Moreover, the conditioned medium can be collected and examined for the presence of specific regulating proteins. What stands out is that the majority of available models are limited to two-dimensional (2D) space – which makes them inappropriate for innervation of intricate structures, such as (cancer) organoids and spheroids. Additionally, systems are inherently low-throughput (not scalable for drug discovery) and often do not harbor electrophysiological readouts for monitoring activity of 3D tissue' innervating fibers.

Because, although Ca^{2+} imaging can provide a measure of nerve terminal activation, monitoring responses in a multiplexed 3D setting remains technically challenging and time-consuming (same goes for patch-clamp recordings). Notably, the collaboration between Netri™ and Axion Biosystems™ stands out for its potential to enhance the throughput of electrophysiological screening performed in PDMS-based innervation systems. The companies have appropriately adopted integration with standard wells plate formats (Society for Biomolecular Sciences - ANSI-Standards), commonly used in large assay infrastructure and incorporated a robust electrophysiological readout via substrate-embedded microelectrode arrays.

1.5 Electrophysiological Recordings in Pain Neuroscience & Microelectrode Arrays

Sensory neurons convert physical stimuli into electrical activity. Stimuli generate graded/summed potentials (duration and amplitude) and are compared to the spike threshold in the axon hillock (bifurcation near the soma). If the threshold is exceeded, an action potential is generated. As the amplitude of the input signal increases, the frequency of the generated action potentials also increases. Meanwhile, the absolute number of action potentials is determined by the duration of the input signal. This information is then transmitted to the synaptic terminal in the DH, where it triggers the release of neurotransmitters, serving as output signal [20, 21]. When establishing a model for studying pain, it is essential that you integrate an electrophysiological readout that can generate this action potential fingerprint. Because a neuron's electrophysiology is the most reliable indicator of its current state and it is the only functional parameter that can produce observable changes within the range of milliseconds. When developiong a high complex *in vitro* strategy for pain-related neuroscience, one must prioritize the inclusion of this readout over all other considerations.

Patch-clamp electrophysiological recording is considered the gold standard for high-resolution *in vitro* electrophysiological readout (Figure. 4A). This technique involves bringing a glass pipette, filled with a physiological saline solution, to a cell's surface and creating a seal between the cell membrane and the pipette. By connecting an amplifier (through wires) to the glass pipette isolating this "patch" and to a pipette inside the culture bath, it is possible to record the activity of individual ion channels (generally displayed on an oscilloscope) [65]. The patch-clamp technique enables direct observation of the microstates of single ion channel proteins. However, characterizing isolated single cells (no complex networks) one at a time, requires highly trained personnel and is time-consuming. Making it difficult to effectively scale for complex drug discovery efforts. Researchers have attempted to use the patch-clamp method for monitoring the activity of intricate networks. One approach involves the development of patch-clamp array chips, which utilize

planarized patch-clamp technology with multiple substrate-embedded apertures. The bottom bath is divided into microfluidic channels, with each channel dedicated to a single aperture. However, there are not many of these models available and they still require cells to sit flat on a 2D surface (Figure. 4B) (described in [66] and [67]). Dr. Ramin Raouf was slightly more successful at integrating patch-clamp electrophysiological readouts into higher complexity cultures of DRG neurons. He used the Xona Microfluidics™ 3-chamber platform and modified it to grant access to a glass micropipette to assay conduction of evoked action potentials in naïve, damaged or sensitized DRG axons for detailed electrophysiological characterization (also in [57]) (Figure. 4C) [68].
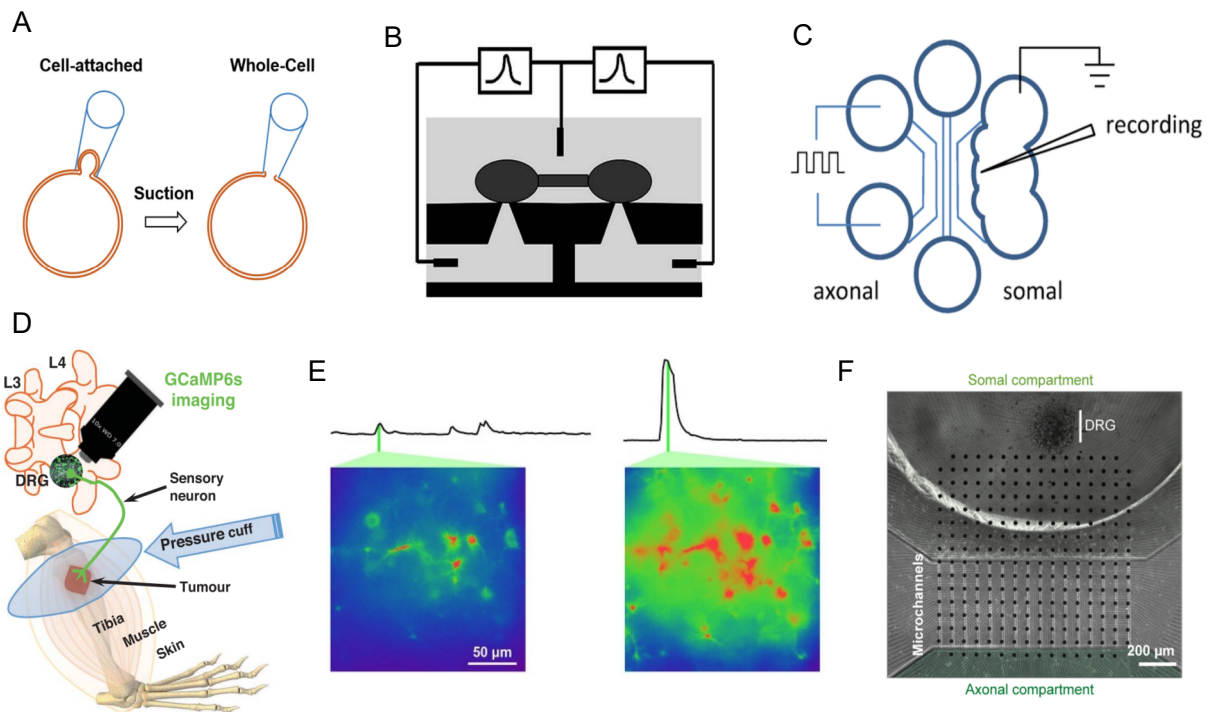
Figure. 4: Patch-clamp, calcium imaging and MEA for complex *in vivo* and complex *in vitro* cultures. (A) Patch clamp technique: cell-attached, whole-cell. Membrane rupture grants access to the cell's intracellular space, allowing electrical access to ion channels across the entire cell membrane. (B) (C) Patch-clamp array chips and modified Xona Microfluidics™ for pain research. (D) (E) *In vivo* and *in vitro* confocal imaging GCaMP6f (using adenoviral transduction) in DRG sensory neurons and hippocampal cells. (F) MEAs are generally combined with patterned culture chips to position electrodes conform microfluidics. --- Reproduced from reference [69] (CC BY 4.0) ©Frontiers Media, reference [66] (CC BY 4.0) ©Frontiers Media S.A., reference [68] (CC BY 4.0) ©Public Library of Science, reference [70] (CC BY 4.0) ©Wolters Kluwer Health, reference [71] (CC BY 4.0) ©IOP Publishing and reference [62] (CC BY 4.0) ©Springer Nature.

Calcium Imaging is another commonly implemented electrophysiological readout which uses genetically coded calcium indicators (GECI) like e.g., GcaMP6f (Ca^{2+}-sensitive GFP), in conjunction with fluorometric microscopy to identify variations in Ca^{2+} levels in the cell cytoplasm. As calcium flow (through voltage-gated calcium channels) is largely mediated by action potentials. Monitoring the spatiotemporal patterns of intracellular Ca^{2+} dynamics has been used to examine disease states in animal models (bone cancer in anaesthetized rats [70]) and *in vitro* study of brain slice preparations/cell cultures [72]. Previous work from the nMPS-lab also includes the stimulation of a 3D culture of primary hippocampal neurons transduced with pAAV.Syn.GCaMP6f (Figure. 4E) [71]. Administration of picrotoxin (PTX - GABA blocker) evoked seizure-like behaviour visible as Ca^{2+} transients across the entire network. GABA (gamma-aminobutyric acid) is the principal inhibitory neurotransmitter in the cerebral cortex and maintains the inhibitory tone that counterbalances neuronal excitation [73]. There are, however, several downsides to using calcium imaging. Firstly, when monitoring the calcium dynamics of a complex 3D *in vitro* culture, you are limited by the field of view and Z-plane in which you operate. This means that when measuring the action potentials you evoke, you can generally only observe a tiny fraction of your culture which makes it difficult to scale for drug discovery assays. Secondly, Ca^{2+} signals do not possess the temporal resolution required for accurately resolving key neuronal activity characteristics like e.g., duration, number and frequency from rapidly firing neurons. And thirdly, Ca^{2+} transients are a surrogate marker for spiking activity, which means spontaneous transients can occur without actual action potentials having been generated.

Substrate-integrated microelectrode arrays (MEAs) provide a third, and highly efficient method for recording electrophysiological activity. Using microfabrication technology, hundreds of electrodes (transduce ionic current to electronic current) are precisely integrated into a biocompatible surface allowing for the recording of both passive and stimulated electrophysiology from cells cultured on top. MEAs were partially developed in response to the difficulties associated with electrical activity data collection from a sufficient number of similar neurons for statistical analysis [74]. Intracellular electrophysiological information, furthermore, provides valuable insights into the activity of ion channels and synapses of individual cells, but it also requires invasive membrane manipulation. Spatially resolved extracellular signals (obtained by MEA recordings) can prove just as valuable by having the ability to look at larger populations and sort their action potentials to still accurately analyze individual cells. Some initiatives have employed small MEAs (5 μm diameter) decorated with 3D plasmonic nanoelectrodes shaped like nanopillars to, nevertheless, record intracellular electrophysiology [75]. These nanoelectrodes penetrate the cell after optoporation (cell membrane rupture by pulse administration) and establish an interface to record intracellular action

potentials, while the planar electrode underneath simultaneously records the extracellular activity. However, researchers in the advanced *in vitro* sensory model field commonly use commercially available planar substrate-embedded MEAs, such as AlphaMED2™, Axion-Biosystems™, Ayanda™ and Multi-Channel-Systems™, as mentioned in Table. 2. These MEA providers offer electrode arrangements that can be tailored to suit culture requirements. Alternatively, standard MEA templates can be purchased and culture designs can be customized accordingly. Good example of such application with relevance for *in vitro* investigation of sensory innervation can be seen in recent research by Dr. Neto et al. (2022) [62]. They demonstrated the outgrowth of sensory neurons could be induced by soluble factor release from bone-resorbing cells, namely osteoclasts. They then transferred the culture to a standard MEA-integrated glass substrate coupled with PDMS microfluidics (see Table. 2 and Figure. 4F). This allowed them to expose only the nerve terminals to stimuli while recording the electrical propagation through the neuronal extensions towards the cell soma, finding that increases in mean firing rate (MFR) were related to the secretome from mature osteoclasts sensitizing the nerve endings.

1.6 Current Research: Aims, Method(s) and Approach

Having summarized the current state-of-the-art in the field of OoC and MPS research, with respect to the incorporation of (sensory) innervation in complex *in vitro* models and nerve-cancer interplay in pain, a novel MPS innervation technology is proposed. The approach considers the various pitfalls and strengths of alternative approaches described in the literature and aims to omit these or draw valuable insights from them. Current research sets out to develop a Microphysiological Innervation System (INV-MPS) (Figure. 5) and directly apply it to the investigation of sensory innervation of cancer spheroids to understand cancer-induced axonal growth, nerve sprouting and associated changes in neuronal electrophysiology. This focus is motivated by the significance of CIP and the ethical concerns surrounding *in vivo* animal research in this field.

The INV-MPS is a technological approach that builds upon previous research conducted at NMI. This includes culturing of murine primary neuronal cells in fused silica-based microfluidic devices with integrated MEA and a standardized protocol for arranging neurons in 3D neuronal networks using biomimetic hydrogels as extracellular scaffolds. Aim is to effectively utilize available knowledge/infrastructure and create a similarly multimodal platform (as previously described [71]) by developing a novel microfluidics-based bioreactor (the INV-MPS), which will combine sensory neurons embedded in Matrigel® scaffolds with the formation of 3D tumour structures to monitor their innervation by recordable sensory nerve terminals (Figure. 5).
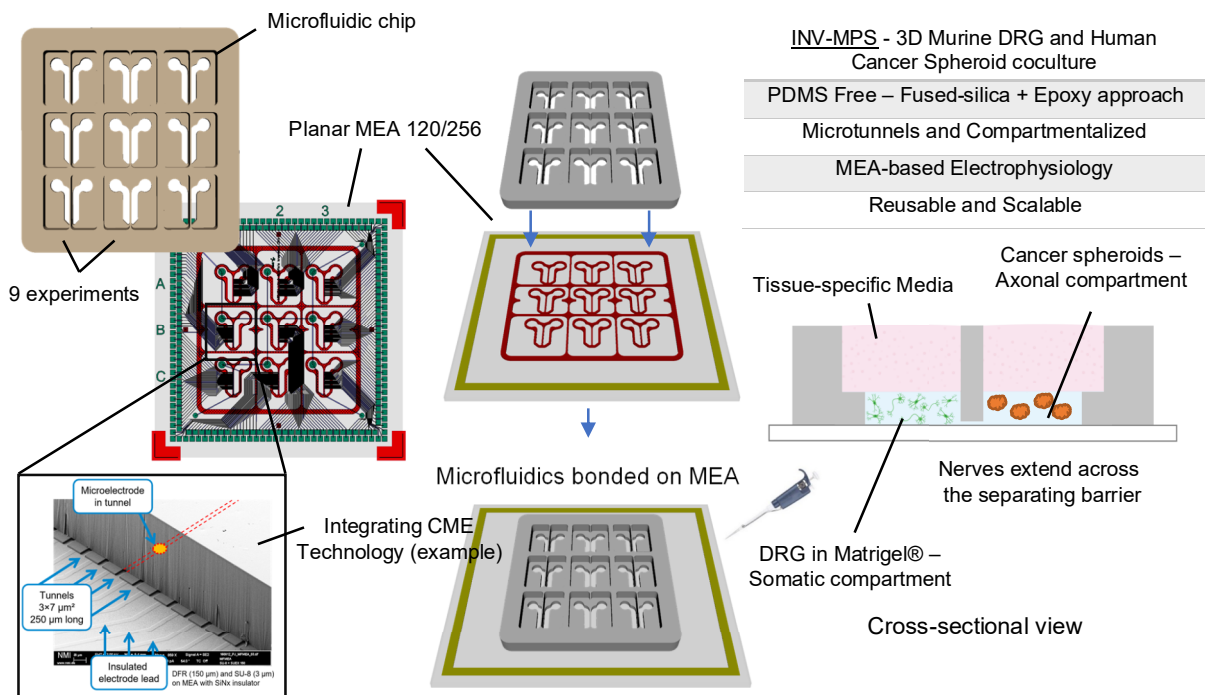
Figure. 5: Methodology includes design of a fused-silica microfluidic (MF) chip (FEMTOprint SA, Zwitserland) **which matches the MEA** (NMI TT, Reutlingen)**.** MF chip is mounted on the MEA with the incorporation of photoresist patterning conform patented Covered Microelectrode (CME) technology which enables recording from 3D tissues [71]. In the cross-section on the right one sees how the coculture will arrange itself with the help of glass-embedded microtunnels and dedicated cell seeding channels.

A compartmentalized system, connected via microtunnels, enables the manipulation and analysis of solely axons innervating and interacting with tumour-like tissue. This arrangement can also eventually provide a reliable measure of the engagement of receptors and ion channels localized at distinct locations (terminal vs. somatic), effectively influencing pain states [57]. In addition, it is postulated that the microtunnel-integrated platform combined with a 3D hydrogel component, creates a system that more accurately mimics *in vivo*-like innervation physiology. While this added complexity makes the system more challenging to develop, it is necessary to create a useful tool for researchers in the OOC and MPS field who are interested in exploring the value of more complex yet functional *in vitro* models. Moreover, traditional 2D systems can flatten and disrupt the natural physiology of organoids and spheroids, making them less suitable for this type of research. Current model also avoids using PDMS and perfusion as integrating these components in a scalable manner is challenging. Associated perfusion methods typically require specialized equipment and PDMS-based devices are susceptible to small molecule absorption, involve laborious moulding processes and are generally not ideal for 3D cultures because they lack an open top, which can make it difficult to apply compounds.

FEMTOprint SA (Zwitserland) is a collaborator that specializes in producing fused-silica microfluidic chips using a subtractive, direct-write microfabrication process. They utilize a femtosecond laser and etching technique to create glass 3D microsystems with micrometer precision [76]. Utilizing this high resolution made it possible to accurately define hydrogel parameters by creating fine glass edges for containment and the use of glass also enabled highly reproducible assembly and strong bonding of the two-component model (MF chip - MEA). As electrophysiological readout, high-density MEA (and Ca^{2+} imaging) was employed to continuously measure excitability along nerve fibers non-invasively under a range of physiological and pathological conditions to study CIP. Furthermore, the device is designed to be optically transparent and open-top (promotes essential air-liquid gas exchange), which allows for high-resolution imaging of controlled coculture conditions. The transparency of the device enables the coupling of visible alterations in neuron morphology (confocal fluorescence) to changes in excitability. Finally, compatibility with automated imaging and pipetting systems was ensured to smoothen the path to adoption of the INV-MPS for drug discovery endeavours.

In Table. 3 the applied techniques and key research developments are outlined that ultimately led to publishing the work surrounding the INV-MPS technology [32]. The INV-MPS technology will be highlighted in the second to last chapter of this thesis in edited form. Briefly summarizing events - introductory research included getting accustomed to 3D culture of DRG neurons using PDMS (Chapter. 2). This included primary DRG isolation through a murine dissection protocol and live confocal fluorescence microscopy, serving as essential techniques and readouts in this project. Hereafter, a bonding strategy was developed using a patternable photoresist (Ordyl SY300) to bond MEA and MF chip, aiming to avoid issues caused by standard epoxy glue bonding and introducing the concept of barrier-integrated microtunnels, highlighted in Chapter 3: Microfabrication Part 1. Ordyl SY300-based Glue-free Bonding Strategy. After improving the understanding of microfabrication parameters and specific needs i.e. incorporating CME technology in the microtunnels embedded in the separating barrier, Chapter. 4. is introduced, where photoresist layering expertise is exploited to potentially satisfy compartmentalization / microtunnel / bonding requirements. Concurrently, the feasibility of a single-channel coculture was assessed and this is described in Chapter 5: Pain Electrophysiology & Cancer-Neuron coculture. Reliant on available existing technology at the nMPS lab, this approach generated a number of biological insights that were used to further develop the model. From these insights, a monolithic imaging chip (no electrodes) was produced and its use for demostrating neurite outgrowth and fluidic separation is illustrated in Chapter 6: Monolithic Imaging Chip (IMGchip / SLE INV-MPS).

The thesis concludes with an original draft of the INV-MPS technology research paper that has since then been edited extensively for publication. Chapter. 7 should be treated as the result of effectively applying the knowledge gathered from the different experimental successes and failures of the preceding methodologies. In Chapter. 8 Concluding Insights, the thesis contents are summarized and connected to generate a suitable outlook for this field of research.

CHAPTER	Contents	Methods/Readouts
2. STANDARD PROCEDURE & 3D DORSAL ROOT GANGLION NEURONS IN PDMS	Detailing of a widely used PDMS-based microfluidic chip production (introduction to microfabrication and mask/chip design) and seeding of primary DRG neurons inside using Matrigel®	Stereolithograpy, Clewin5.4 photomask design, PDMS casting, mice dissection and DRG isolation. Fluorescence microscopy and analysis of previously generated Rheology data.
3. MICROFABRICATION PART 1. ORDYL SY300-BASED GLUE-FREE BONDING STRATEGY	Ordyl SY 300 is a permanent dry film photoresist that can be used for sealing applications. Here, an attempt is made to utilize it for both microtunneling and channel sealing.	Stereolithography, Bonding, Clewin5.4 photomask design, Autodesk MF chip design, Fluorescence imaging
4. MICROFABRICATION PART 2. SU8 ADEX BARRIER STACKING	SU8 and ADEX are essential for CME technology and can be leveraged for high-resolution microtunnel production.	Stereolithography, Bonding, Clewin5.4 photomask design, Autodesk MF chip design, Fluorescence imaging, stylus profilometry Dektak
5. PAIN ELECTROPHYSIOLOGY & CANCER-NEURON COCULTURE	Exploring the interaction of DRG neurons and various cancer cells lines. With the available nMPS-technology I assess whether CME works well for 3D cultures of sensory neurons.	Cancer cell culture, DRG-Cancer co-culture, Autodesk MF chip design and MEA-based electrophysiology, Fluorescence imaging
6. MONOLITHIC IMAGING CHIP (SLE INV-MPS)	Expanding on the promising DRG-cancer interaction I see, I incorporate microtunnels and emulate the final system. Eventually proves highly relevant for the published work.	Cancer cell culture, DRG-Cancer co-culture, Autodesk MF chip design, Fluorescence imaging, Neurite outgrowth assay (NGF), Dextran diffusion
7. CANCER-MEDIATED AXONAL GUIDANCE OF SENSORY NEURONS IN A MEA-BASED INNERVATION MPS	First draft of the published work that details the emergence of electrode-integrated INV-MPS technology .	Cancer cell culture, DRG-Cancer co-culture, Autodesk MF chip design, Fluorescence imaging, Neurite outgrowth assay (NGF), Dextran diffusion, MEA-based electrophysiology, Calcium Imaging
8. CONCLUDING INSIGHTS	Illustrating how the INV-MPS research was able to deliver on the aims of the thesis and exploring interventive therapies in CIP	

Table. 3: Approaches and methodology that led to the production of the INV-MPS. Important to note is that development and improvement of methodology is equal in relevance to readout.

Chapter 2: Standard Procedure & Three-dimensional Dorsal Root Ganglion Neurons in Polydimethylsiloxane

2.1 Introduction

In order to effectively exploit the potential of the MEA-integrated INV-MPS platform introduced in the general introduction, initial approach prioritized understanding and consistently generating viable 3D cultures of DRG neurons. Achieving this involved adopting a well-established and widely used protocol for producing microfluidic chips based on PDMS [77]. Plating in PDMS resulted in obtaining fast proficiency in the murine dissection protocol and DRG isolation, as well as the appropriate processing techniques required for enzymatic digestion and seeding of neurons inside these chips using Matrigel®. As previously stated, the fundament of MF chip-based biological experiments with neurons involves this process of dissection, isolation, digestion, and seeding. In subsequent chapters, this protocol will be referenced for the sake of simplicity, while highlighting adaptations for the different designs. Notable distinction in current approach is that researchers generally plate neurons in 2D (not 3D) when using standard PDMS templates – as templates are often not open top, which makes it difficult to homogenously apply compounds to PDMS-embedded 3D constructs rendering the setup impractical for further research. However, PDMS-based microfluidics are highly cost-effective and the abundance of available master templates will provide ample opportunity for hands-on experimentation to familiarize with various technologies in real-time. Producing prototypes with MEA and glass MF chips for familiarizing and improving standard protocol is not cost-effective in the early stages of the project.

Optimizing the DRG enzymatic dissection protocol is critical for the progression of the project and this requires consistent (bi-) weekly practice [78]. DRG (sensory) neurons originate from a subset of neural crest cells during embryogenesis and migrate downward to form cell accumulations in sac-like spinal ganglia [79]. Achieving a consistent yield of viable sensory neurons from these ganglia (DRGs) with the dissection protocol enables accurate evaluation of microfluidic culture chip parameters. Isolating DRG neurons from adult mice is relatively easy because they are significantly larger in size than those from post-natal mice. However, as the mouse develops from an embryo to a fetus and then into an adult, there is a decrease in the potential for neurite outgrowth [80]. In short, researchers found that growth onset, initial growth rate and pattern of changes in growth rate over time *in vitro* exhibit age-dependent variations. It was observed that neurites from perinatal (immediately before and after birth) ganglionic explants emerge the earliest, typically within 5-13 hours and have the fastest initial rate of growth, ranging from 370-

660 µm/day. In contrast, the initial growth rates are lower when increasing post-natal age (beyond P16). These initial growth rates range from 70-176 µm/day, followed by a subsequent rise to an intermediate rate of 200-250 µm/day (up to P30). Therefore, it is important to establish a specific window for DRG isolation, as this will affect the time it takes for neurite outgrowth to reach the adjacent axonal compartment (see Chapter. 1 - Figure. 5). Interesting to note also, is that postnatally, DRGs contain mostly maturing neurons and little neural progenitors still actively undergoing differentiation, as neurogenesis primarily occurs around E9 to E13 during embryonic development [79]. Primary neurons are used as a robust and easily accessible cell source to improve current model as much as possible. While induced pluripotent stem cell (IPSC)-derived sensory neurons are available [63], they are expensive and not as well-established as primary DRG neurons. Therefore, when satisfied with the *in vitro* innervation model, seeding with e.g., IPSC-derived sensory neurons can be explored to assess whether similar levels of innervation can be achieved. Furthermore, embedding sensory neurons in an appropriately stiff 3D Matrigel® scaffold has its advantages and disadvantages. The primary reason for doing so is to achieve a high level of biomimicry in the *in vitro* model, considering that cell-cell interactions occur in 3D space inside the human body and should be replicated in the model accordingly. However, the actual relevance of this approach is the subject of debate [81]. Regarding DRG neurons specifically, there has been some research conducted on comparing the morphology of 2D and 3D sensory neurons. Sensory neurons grown in 3D collagen gels obtained a more complex neurite structure, which is reminiscent of *in vivo* axons, with a higher degree of branching for receiving information from multiple regions. More than 65% of the neurons cultured in 3D had two or more branching points, whereas fewer than 35% of the neurons cultured on collagen-coated coverslips demonstrated this branching pattern [82]. Disadvantage is obviously that it is more challenging from a technical and biological standpoint to generate a 3D *in vitro* model for assessing axonal outgrowth and electrophysiology than for a 2D model. Thus, utilization of 3D Matrigel® scaffolds for embedding DRG neurons has the potential to enhance the biomimetic nature of *in vitro* models and can recapitulate neural behaviour effectively but complexity should be managed. Additionally, there exists a general trend towards creating more complex organoid and spheroid technologies in the MPS and OoC-field, all of which grow in 3D space. Therefore, it is not logical to reduce these constructs to 2D space merely to be compatible with current platform. Researchers may not be willing to place their constructs inside the INV-MPS to receive innervation if they simultaneously lose a significant portion of their 3D morphology. The INV-MPS ultimately aims to recognize the progression of the MPS/OoC-field towards creating *in vivo*-like tissue models and simultaneously integrate a non-invasive electrophysiological readout.

2.2 Materials & Methods

PDMS device preparation

As described in pioneering work from the group of George M. Whitesides at the Dep. of Chemistry and Chem. Biology, (Harvard University, USA) the production of a PDMS-based microfluidic chip involves the design of a master which is generally created by contact photolithography. The master is a thin film (photoresist) deposited on a silicon wafer substrate which is exposed to UV light through a patterned mask to polymerize specific regions and subsequently remove others. Dedicated photomasks were designed using CleWin5.4 CAD software (WieWeb software, Netherlands) and ordered from Delta Mask B.V. (Enschede, the Netherlands). In this work, the resist(s) is (are) generally the photo-curable epoxy, SU-8 (MicroChem, USA) (spin coated to ≈ 5 µm) and a second layer of 100 µm thick ADEX/SUEX resist (MicroChem, USA) (laminated).
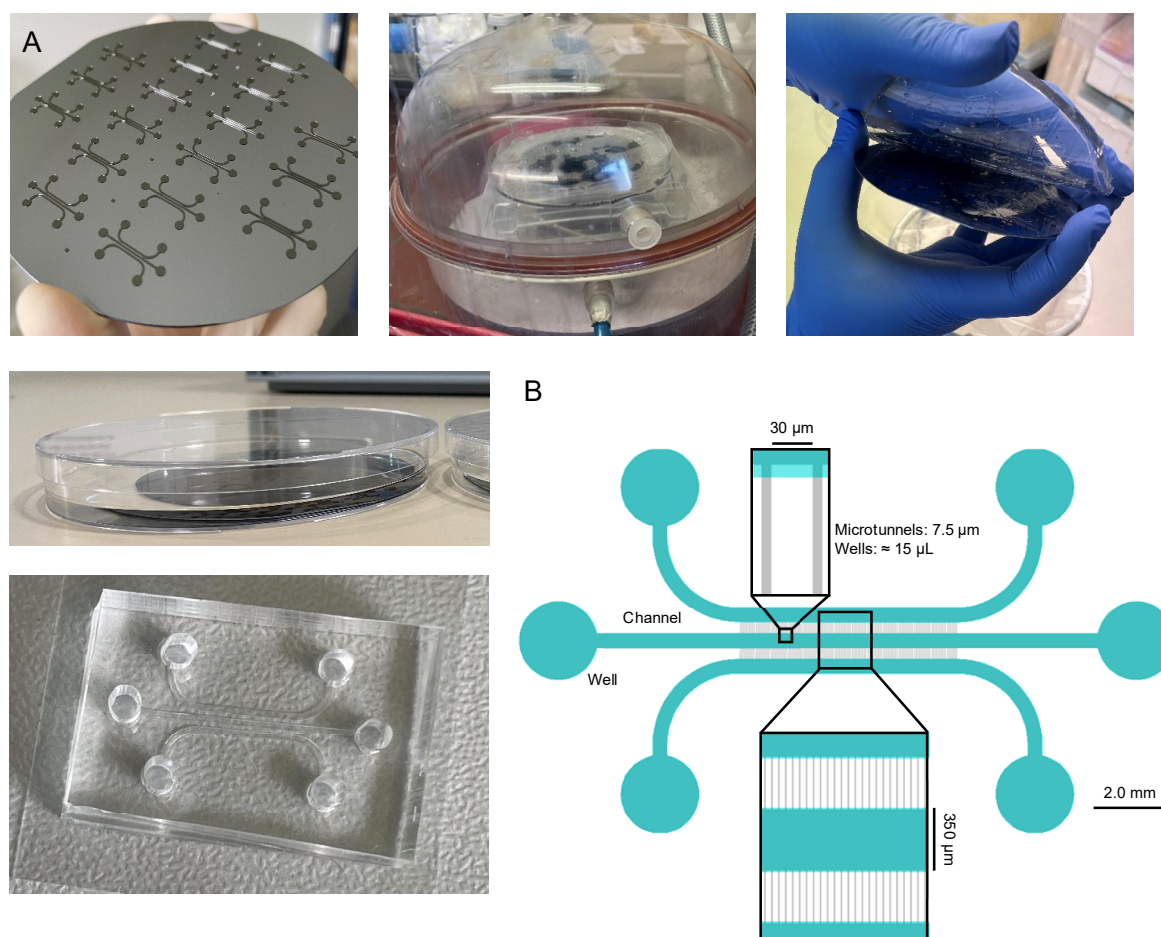

Figure. 6: Fabrication of PDMS-based microfluidic systems using replica molding. (A) Workflow producing a PDMS/Glass microfluidic chip from a SU8/SUEX Master. (B) 3-channel unit overview.

The master is the positive relief of what is produced in PDMS (negative relief) by replica molding after the unpolymerized photoresist is dissolved in a mildly alkaline solution (Figure. 6A). Where the unexposed portion of the photoresist is neutralized and made soluble [83]. Replica molding involves pouring the PDMS prepolymer over the master, degassing, curing the polymer in an oven at low temp. and then extracting it from the master before hard-baking. Before pouring the PDMS prepolymer, the master is treated with a silane solution containing fluorinated functional groups, such as perfluorooctyl trichlorosilane (PFOTS). This creates a monolayer that prevents the silicon and PDMS from bonding irreversibly. Once masters have been correctly created – PDMS chips can be produced as follows: PDMS (Sylgard® 184 Silicone Elastomer Kit) comes as a kit with two parts; curing (crosslinking) agent and monomer base mix. These are combined in a 1 : 10 mix ratio, then poured in a plastic cup and mixed at 2000 rpm for 2 min in a Speed MixerTM (DAC 150.1 FVZ-K, Hauschild & Co. KG, Hamm). Then a master (contains 18 positive reliefs per mold) is placed inside a 145 mm Petri dish (639102, Greiner Bio One International GmbH) and ≈ 59.0 grams of PDMS-mix is poured on top (this eventually equates to a 4.0 mm thick gel). Petridish is then transferred to a desiccator for degassing as bubbles are created during mixing (Nalgene, Paul Merienfeld GmbH & Co. KG, Germany). PDMS is then left to cure over night at RT on a flat top table – before transfer to a heating oven to be baked at 40 ºC for 12 hrs.

Using a blade and isopropanol – PDMS is then extracted from the petridish whilst leaving the master completely intact to be reused – and then baked again at 100 ºC for 12 hours to complete polymerization. Now 18 individual chips are diced using a blade and 6 holes are punched with a biopsy punch (Harris Uni-Core 2.0, Sigma-Aldrich Chemie GmbH, Munich) as designated by master imprint. Important to note – the depth of the imprint is determined by the thickness of the photoresist present on the master – in this case, that is roughly 105 µm as a single SU-8 2002 base with a SUEX K100 secondary layer was layered (details of photolithograpy are illustrated in the next chapters) (Figure. 6B). PDMS chips and thin glass substrates are rinsed with bidistilled water and sonicated in isopropanol (VWR® Ultrasonic Cleaner, VWR International, LLC) before air plasma treatment (Plasma cleaner/sterilizer PDC-32G, Harrick Plasma, Ithaca, US) for 2 min at high RF (18 W) (Figure. 7). PDMS chips bonded on the glass substrates by collecting them with tweezers and placing on top under a microscope (Figure. 6A).

DRG dissection and dissociation

DRG neurons were extracted from spinal ganglia at all levels by modification of a previously published protocol [78]. Postnatal Swiss mice (Janvier Labs, France) (P5-P9) were sacrificed, in accordance with the European Union (EU) legislation by CO_2 inhalation before disinfection with 70% ethanol. For P9 DRG, narrow incision through the skin and muscle is made, starting from the tail, from which 2 cuts are made along the spine to separate the vertebral column. Column is separated from the head and place in a petridish with Hanks' Balanced Salt Solution (HBSS without Ca^{2+} and Mg^{2+}). Here, the column is cleaned with a scalpel and then cut longitudinally along the spine to expose the spinal ganglia (up to 40 individual DRGs). For P2-P5 ganglia, it is not necessary to excise the entire spinal column as there is not a lot of fat and connective tissue you need to remove before being able to access the spine. One can simply cut straight through the skin of the back and directly cut open the column. Ganglia can then be collected and cleaned with forceps and incubated in Dulbecco's Modified Eagle Medium (DMEM) with GlutaMAX™ (Thermo Fisher, #31966021) containing 1.5 mg/mL collagenase (IV) (Worthington, #LS004186) and dispase 3 mg/mL (Worthington, #LS02109) for 40 minutes, followed by manual dissociation in DNAse solution (Worthington, #LS002139), straining through a 70 µm filter (MACS® Smart Strainers, Miltenyi Biotec, Germany) and centrifugation. Then a gradient centrifugation is performed to remove dead cells and debris from the pellet. For this, 4 solutions of DMEM / OptiPrep™ (Iodixanol) (Stemcell, #07820) are layered into a 15 ml falcon tube according to Table. 4. Working Solution is a master mix of DMEM / OptiPrep™ at ratio 1 : 2 and cell pellet is resuspended in 28% solution. 1.0 mL DMEM is placed at the bottom of the falcon, followed by 8% solution and 15% solution. 28% solution with suspended cells is placed at the bottom of the falcon using a spinal needle and the falcon is centrifuged at 800 g for 22 minutes.

	Working Solution (ml)	DMEM medium (ml)
28% solution	2.8	1.2
15% solution	1.5	2.5
8% solution	0.8	3.2

Table. 4: Gradient centrifugation DRG neurons

Live cells are collected from the interface between the 8% and 15% solution before mixing with Neurobasal-A (Thermo Fisher, #10888-022) and centrifugation. Cell pellet is then resuspended in Neurobasal-A (culture media) with GlutaMAX (Thermo Fisher, #35050-038), SM1 (Stemcell, #5711), N2 Supplement-A (Stemcell, #7152), 0,5% Penicillin-Streptomycin (Sigma, #P4333) and 100 ng/ml Nerve Growth Factor 2,5S (Promega, #G5141) at the desired concentration after careful removal of the supernatant. Cell suspension is then counted using a NucleoCounter NC-200 (ChemoMetec A/S, Denmark) and mixed with Matrigel® Growth Factor Reduced (1 : 4 ratio or 75%) (Corning, #356230) inside an Eppendorf to stand. conc. of 500 cells/µL (2000 cells/µL before mixing). This is kept in a cold rack to prevent Matrigel® polymerization during plating.

DRG neuron plating

To ensure efficient filling of microtunnels and channels with hydrogel when extruding ≈ 10.0 µL DRG-mix with the tip (Purple low retention tips, Integra) placed inside the peripheral wells, the assembled glass-PDMS chip must be treated with air plasma again. O_2 (or air) plasma treatment enhances the hydrophilicity of the surface by eliminating organic material and introduces -OH groups through a chemical reaction with extremely reactive oxygen radicals. The result is the presence of silanol (Si-OH) groups on the surface, which improves surface wettability (Figure. 7). Up to 6 PDMS devices can be simultaneously sterilized/hydrophilized by air plasma treatment. Depending on the goal of the experiment – cells are seeded in selected channels and bare 75% Matrigel® is placed inside the remaining channels – to monitor outgrowth into these channels. All peripheral wells are then topped off with another ≈ 10.0 µL of culture media which is refreshed every other day (also see Figure. 8). Part of previous work published in Molina-Martínez et al. (2022) [71] – included rheological measurement of the 75% Matrigel® for 3D cultivation of neurons (Rheometer Gemini 150, Cellendes) and obtained data is more elaborately illustrated here.
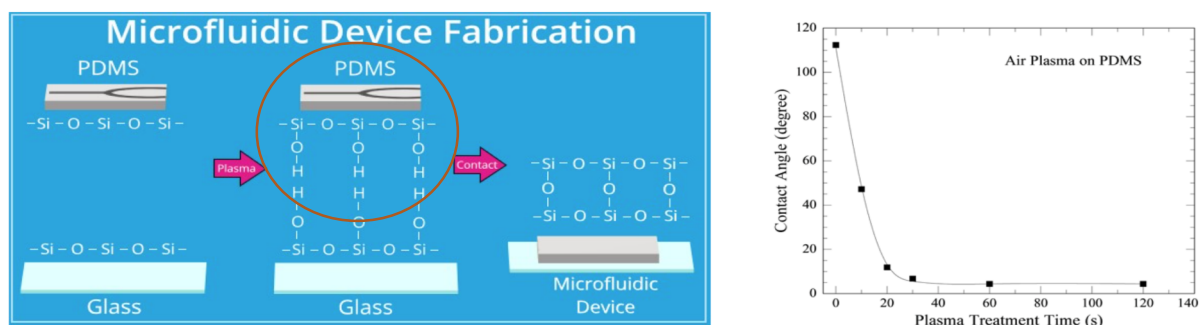
Figure. 7: PDMS activation using plasma cleaner. PDMS and glass are both oxidized before attachment which creates a strong covalent siloxane (Si-O-Si) bond. Reproduced from [84] ©harrickplasma.com. Reproduced from [85] with permission ©American Chemical Society.

AAV1-eGFP transduction

Live fluorescence imaging of green fluorescent protein (GFP) (virally delivered) is used to accurately monitor neurite outgrowth. This approach enabled conducting bi-weekly cultures instead of waiting for lengthy incubation steps required by immunocytochemistry protocols developed for 3D cultures. Murine DRG neurons were transduced with AAV1.Syn.eGFP, which is an adeno-associated virus (AAV)-based viral vector containing a promotor and reporter. AAV vectors are commonly used for viral vector-mediated transgenesis (foreign gene insertion for transcription – AAVs do no integrate into host genome) in both animal models, to study physiological and pathological states, and gene therapy approaches in humans. Additionally, AAV vectors are compatible with Biosafety Level 1 (BSL1) and can be used in mixed-use laboratory spaces [86]. Nonetheless, work with enveloped and non-enveloped viruses was only commenced with thorough pre-disinfection of surfaces using Dismozon® plus (Paul Hartmann AG, Germany) as prescribed by the RKI (Federal Ministry of Health, Germany). Promoter of the human Synapsin 1 (SYN1)-gene (involved in synaptic vesicle regulation) was particularly effective in current experiments, as it allowed discerning sensory neurons from non-neuronal cells by restricting the long-term expression of the eGFP reporter gene to solely neurons [87]. Only drawback is that it takes up to 4 days before neurons start to express the inserted gene.

Imaging

3D neurite outgrowth is monitored daily using a standard table top EVOS™ M5000 Imaging System (Invitrogen, #AMF5000). At 4-5 days in vitro (DIV) imaging was performed using confocal fluorescence microscopy with a spinning disk head Zeiss Cell Observer® System (20x/10x objective) equipped with ZEN software (blue edition, ZEISS) followed by image-processing with open-source image processing software, FIJI (ImageJ, http://imagej.nih.gov/ij/). To excite the AAV1-eGFP, an Alexa Fluor 488 laser was used and Z-stacks were generated of single tiles or e.g., 3x3 tile scans with the EC Plan-Neofluor 10x/0.30 and the Plan-Apochromat 20x/0.8 M27.

3.3 Results & Discussion

As previously stated, at the early stage it was sensible to gain experience with the necessary techniques and readout methods by employing a simpler PDMS-based standardized approach. Concordantly, the PDMS-based microfluidic system was utilized to get accustomed to the dissection protocol and at the same time obtain initial insights into the most suitable age of rodent for current application, the optimal seeding density for outgrowth and the plating of a hydrogel inside a closed PDMS-based system. In this context, a closed system (not open top) refers to a microfluidic platform where the hydrogel channel portions cannot be directly supported by a media layer to which compounds can be applied for drug screening. Instead, this layer only sits on top of the hydrogel present in the six individual wells located at the end of the channels (Figure. 8A). As Matrigel® is a three-dimensional network of polymer chains with the capability to absorb and retain substantial amounts of water, some may argue that compounds would nevertheless diffuse through the gel and reach the target cell population inside these channels. However, in this configuration, such diffusion would not uniformly activate or sensitize the cell population (applying noxious chemical stimuli), leading to a potentially skewed readout. In Chapter.1 - Figure. 4C, Dr. Raouf and colleagues perforated the peripheral/axonal channel (contains no soma) with a biopsy punch to create a large connected open top space, which could potentially be a way to mitigate this issue but has not been tested in a 3D setting [68]. Figure. 8B illustrates the choice of filling the middle channel with DRG neurons and monitoring the culture for up to 6 days as the neurites located the microtunnels (300 µm x 7.5 µm x 5 µm) present at the glass-interface on either side of the channel (4.0 mm x 300 µm x 105 µm). Particular age range was identified, approximately P4-6, where there was a pronounced natural drive for neurite outgrowth, yet the size/maturity of the animal did not hinder the effective collection of ganglia. This age range could be considered ideal for these purposes and is in agreeance with axon regeneration (PNS) literature [80].

Similar to previous literature, established dissociation protocol involves the axotomy or severing of nerve fibers emanating from the murine DRGs and after dissociation into single cells (also includes non-neuronal such as Schwann cells) their neurites regrow in culture. Additionally, in this case, they become randomly trapped inside nearby microtunnels to enable accurate study of their growth behaviour.

It is additionally important to consider the seeding density, as higher densities can lead to more neurite outgrowth both in absolute and relative terms, since DRG neurons tend to support each other when they are in close vicinity and receive ample trophic support from non-neuronal cells present [88]. However, there is an upper limit to density, as a culture that is too densely packed can lead to cells competing for nutrients and space within the 3D hydrogel. In Figure. 8C, nerve endings extend and arborize extensively in 3D space ([82]) after exiting the microtunnels that connect the somatic and axonal channels. Not particularly trivial is that nerves that grow attached to a substrate tend to remain attached and not release. In the current set up, the nerves therefore either release from the substrate or never attach to it.

This provides an excellent opportunity for innervating 3D tissues in the axonal compartments of developed microfluidic platforms as neurites will be able to enter into the 3D space these added constructs inhabit for interaction.
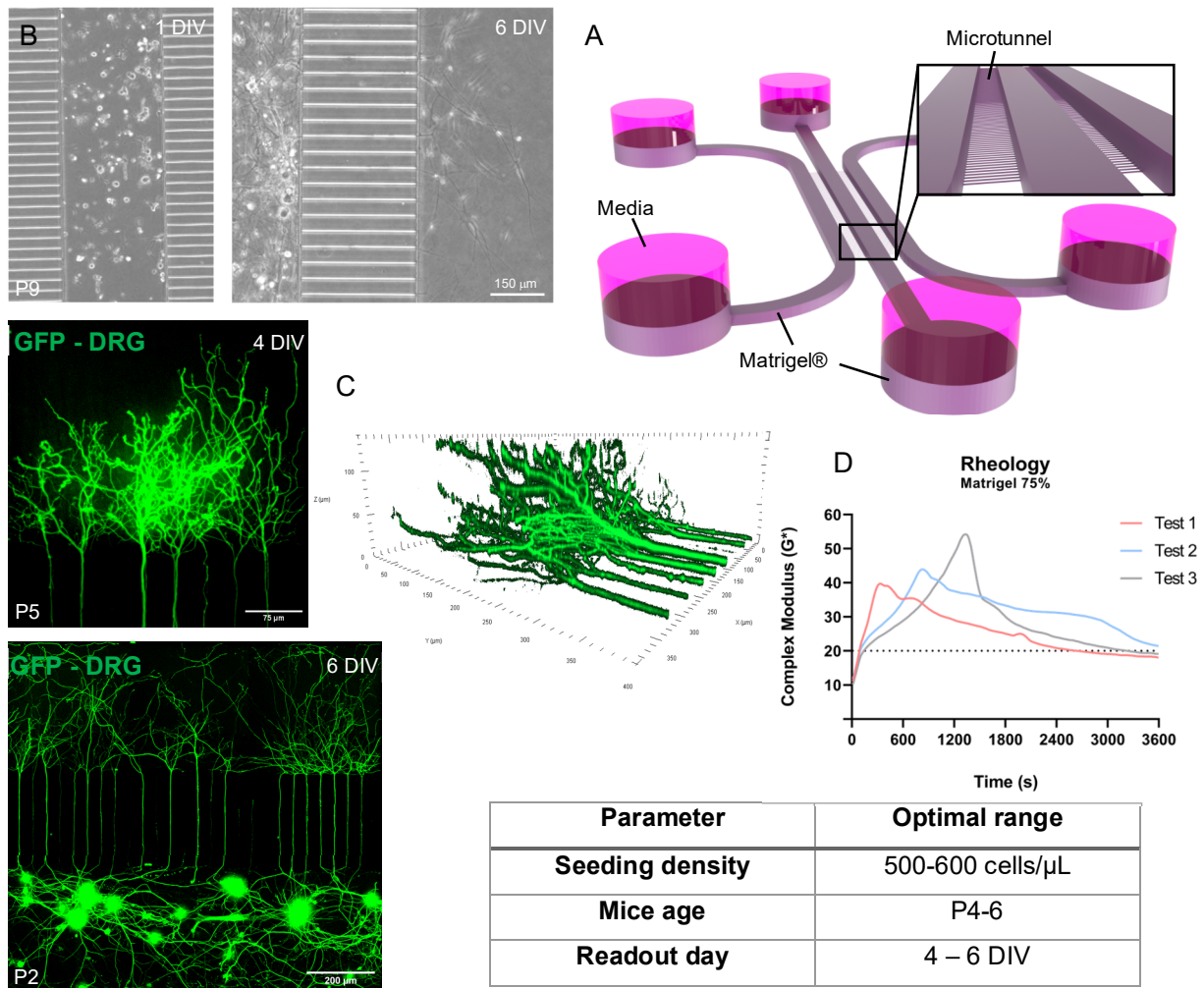
Figure. 8: Culturing DRG neurons in a compartmentalized Glass-PDMS microfluidic system provides an important foundation for *in vitro* 3D innervation. (A) Overview of the gel and media loaded microfluidic setup. (B) Dissociated cells are obtained from P9, P5 and P2 and are seeded in the center channel for monitoring (up to 6 DIV). With strong GFP-expression in sensory neurons after 4 DIV and further optimization of parameters. (C) Neurites grow in 3D space as they emerge from the microtunnels. (D) Rheological measurement of 3 hydrogel samples.

Additionally, the rheological measurement of the 75% Matrigel® used for 3D cultivation of neurons, provided a valuable insight into the mechanical properties of *in vitro* culture constructs (Figure. 8D). Matrigel® is a murine basement membrane (BM) extract composed of a complex mixture of proteins, including type IV collagen (30%), laminin (60%) and entactin (8%) as major components. At 75% dilution, this equates to a laminin and collagen IV concentration of ≈ 4.1 mg/mL and ≈ 2.0 mg/mL respectively (Certificate of Analysis [89]).

Hydrogels were spun for 5 minutes at 1 Hz (full rotation per second) while raising the temperature to 37 °C and stabilizing there. From this I obtain an estimation of the various moduli that can be used to describe the mechanical properties of a material under deformation like e.g., substrate stiffness. Particularly the complex modulus (G* in Pascal or Newton/m^2) is the most comprehensive measure of a material's mechanical behaviour, as it takes into account both the elastic (stretching without breaking or permanently deforming) and viscous (resisting flow) components of a material's resistance to deformation under an applied force. Where G' is storage/elastic modulus and G'' is loss/viscous modulus [90]

$$G^* = \sqrt{(G'^2 + G''^2)} \qquad (1)$$

Elastic modulus (or Young's modulus = stress/strain) represents the energy stored in a material during deformation, while the loss modulus represents the energy lost as heat during deformation. In the case of hydrogels, which are viscoelastic materials, the loss of energy described by the loss modulus, can be relatively low compared to the elastic modulus (>99% of G*). As I am interested in the long-term mechanical behaviour of the hydrogel culture, the stabilizing of all three measurements around a complex modulus of 20 Pa is the most relevant for this application [91]. This is described as providing insight into the behavior of the hydrogel after an approximation of real use. Furthermore, 20 Pa is relatively soft, but optimal for neurite outgrowth and in line with previous literature looking at dissociated sensory neurons in 3D cultures [92].

Fine-tuning dissociation and culture parameters, and making first contact with nerve outgrowth in microfluidic systems were important first steps in the project. Focus now shifts away from PDMS and moves towards developing methods of production for the Glass-MEA based system (see Chapter. 1 - Figure. 5). Considerable challenge here is assembling the MEA and microfluidic chip in an effective manner, preferably without manual application of epoxy adhesive.

Initial attempts at bonding the microfluidic chip to glass have involved the use of Ordyl SY 300, a permanent dry film photoresist suitable for sealing applications. Following chapter will illustrate how its potential for microtunneling and channel sealing purposes was explored in a glass microfluidic prototype.

Chapter 3: Microfabrication Part 1. Ordyl SY300-based glue-free Bonding Strategy

3.1 Introduction

Before delving into the process of bonding glass microfluidics to microelectrode arrays using photoresist-based adhesives, it is essential to first discuss the initial conceptualization of the 3D INV-MPS system. A platform was envisioned that incorporates a separating barrier that would perform three functions: mediate fluidic containment and separation to minimize diffusion between compartments, physically separate nerve terminals and cell soma, and integrate carefully positioned microelectrodes. Microelectrodes would record from only those fibers that traverse the barrier into the axonal compartment and ultimately innervate targets (Figure. 9A). Postulating that this would be the most effective way to capture and translate the effects of nerve-tissue interaction to recordable electrical activity. This is also the approach that others have elected for MEA-recording from 2D neurite outgrowth in microfluidic chips [62, 64]. Placement of microelectrodes elsewhere in the system either means that; the population of nerves that are recordable now includes also those that do not extend into the axonal compartment and/or probability of recording meaningful activity is affected. Understanding of the relationship between the INV-MPS platform and DRG cultures developed over time, and it was later discovered that there are viable alternative options available for the placement of microelectrodes within the system. Despite this, the bonding techniques investigated here focus on embedding the recording electrodes inside (below) the separating barrier.

Simultaneously, it will become clear that incorporating microelectrodes into a 3D culture system for neural recordings requires modification of individual electrodes of the MEA-substrate. Recording from neurons that are suspended in 3D space and not situated directly on top of an electrode means it is necessary to record from their axonal projections. In order to accomplish this, it is essential to restrict dissipation of extracellular ionic currents around these projections when action potentials are generated. This follows from what has been previously demonstrated for MEA-recordings from 3D cultures of hippocampal neural networks [71]. Failure to do so will result in ions diffusing rapidly into the 3D space, making it impossible to differentiate an actual spike from background noise. This concept will be further examined in subsequent chapters.

INV-MPS approach

During (ideal) assembly, the MF chip (9-well INV-MPS details in Chapter. 4) is placed on top of the MEA and centered, allowing the separating barrier to align with the substrate-embedded microelectrodes (Figure. 9B). This assembly process involves the use of a Fineplacer® lambda (Finetech GmbH, Germany) to also guarantee a fine seal between microfabricated photoresist structures and the flat bottom glass chip. However, approaches that elect to etch microtunnels in the glass barrier bottom and seal them upon assembly are not appropriate. It is therefore crucial that a UV-patternable photoresist adhesive is incorporated that can establish microtunneling, bonding, standardization and scalability of this process. Simultaneously, this could then eliminate the need for manual dispensing of epoxy for bonding.
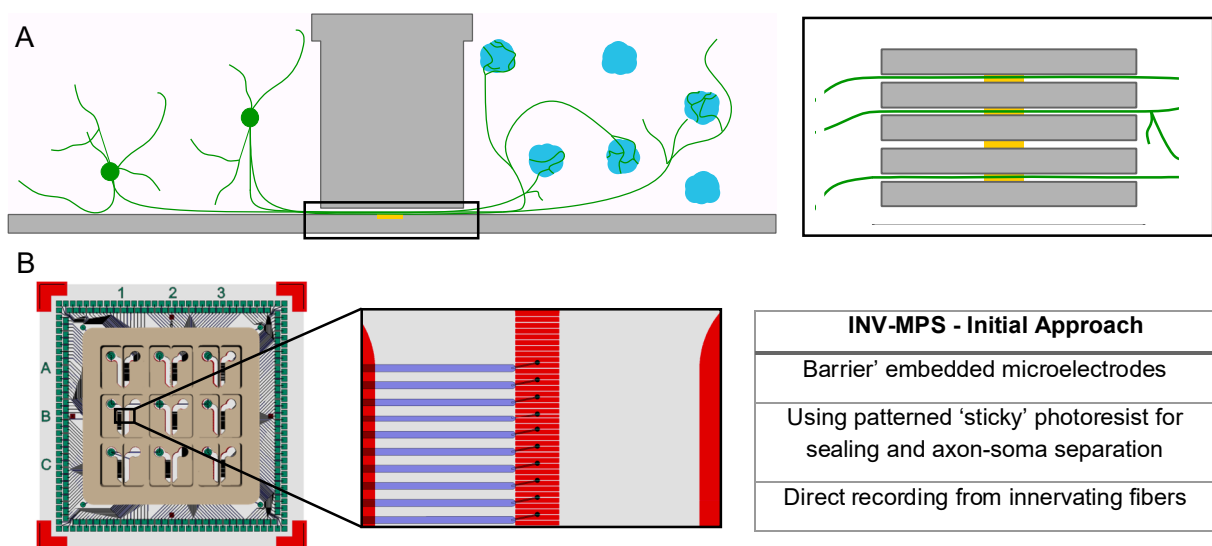
Figure. 9: Overview of barrier' embedded microelectrode INV-MPS approach. (A) Sensory fibers emanating from 3D neurons traverse the fluidic barrier and innervate 3D targets peripherally while electrodes record their activity. (B) Patterning photoresist spaced along the separating barrier should enclose axonal and somatic channels leaving room for traversing neurites.

Ordyl SY300 is a type of permanent dry film negative photoresist developed by Elga Europe Srl. (Milan, Italy) and distributed within Germany by Microchemical GmbH (Ulm, Germany). The term "permanent" indicates that this dry film cannot be removed once it has been applied and cured like e.g., SU-8 and ADEX/SUEX. This grants the opportunity to selectively remove (weaker) patterned resist and reuse MEAs for reassembly with a new MF chip, if needed. Ordyl's reported use in specialized microelectromechanical systems (MEMS) applications generally commend its usefulness for sealing of designated structures. Dr. Paul Vulto (CEO and co-Founder of Mimetas)

and his colleagues have previously expressed a preference for using Ordyl-based bonding over SU8-based bonding [93]. Based on the notion that Ordyl processing does not require both substrates to be patterned in order for successful bonding to occur, also not possible in current situation. Dr. Vulto defines Ordyl SY300 as an acrylic resist with epoxy groups, which would classify it as a multifunctional epoxy acrylate resin. Acrylic resins are more thermoplastic (can consistently deform after heat application) than solely epoxy-based resins, such as SU-8. It could therefore be speculated that it has the mechanical and chemical stability of an epoxy resin (typically more thermosetting) while also softening effectively to adhere glass or silicon [94, 95]. Before extensively exploring the application specific matter, it makes sense to first provide some comprehensive explanation of the distinct categories of chemistry that are relevant here. However, since the exact formulation of Ordyl SY300 is not publicly known and it is not as widely recognized as SU-8, it is more practical to explain implicated polymerization chemistry using SU-8 as a reference while highlighting the similarities with Ordyl SY300.

Photopolymerization theory

(UV-)Photopolymerization is a process by which a polymer is formed from a monomer using light as a catalyst [96]. The most common form of photopolymerization is free radical photo-polymerization (FRP) (generally used for acrylic resins) [97]. In this process, the absorption of light by a so-called photoinitiator induces a set of complex reactions that generates the release of free radicals (highly reactive molecular fragments = unpaired electrons). These fragments interact with the present monomer molecules (potentially methyl-methacrylate-epoxy for Ordyl SY300) (Figure. 10A) which initiates a chain reaction that propagates through the exposed resist. FRP breaks down into; initiation, propagation and termination [97] [98].

Photoinitiator + hv (photon of UV light) → Photoinitiator* (I*) (excited state)

Photoinitiator* (highly sensitive to cleavage) → • I* + • R' (other radical)

• I* + Monomer (attacked by radical) → I* - Monomer • (initiation)

Monomer + I* - Monomer • → Polymer • (propagation)

Polymer • + Polymer • → Polymer (termination)
(combination of radicals)
or
Polymer • + Polymer • → Polymer + • R'
(disproportionation – radical transferred elsewhere)
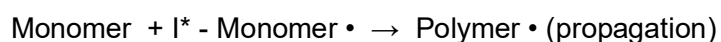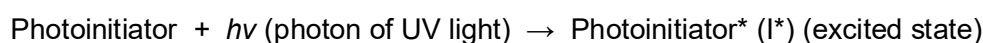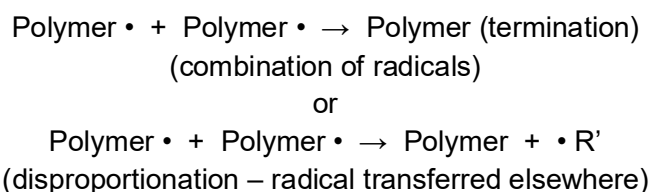
Free radical photopolymerization is widely used in the manufacturing of polymers for various applications, including coatings, adhesives and electronics. Interestingly, in the case of Ordyl SY300 you are potentially dealing with both free radical- and cationic photopolymerization, as epoxy groups generally polymerize following the generation of H^+ ions by exciting a photoacid generator (PAG). H^+ ions cleave the epoxy rings present on the monomers, which can then cross react to form covalent bonds and produce a 3D polymer network. For SU-8 (also cationically polymerizes and widely used) this looks like this [99, 100];

Photoacid generator (PAG) + hv → PAG^* (excited state)

PAG^* (salt decomposition to ions) → H^+ + R^-

H^+ + BADGE (SU-8 epoxy monomer) → 'SU8'$^{+}$-OH (epoxy ring cleaved) + H_2O

'SU8'$^{+}$-OH (also attacks epoxy rings) + BADGE → SU8-O-SU8 (polymer extended)
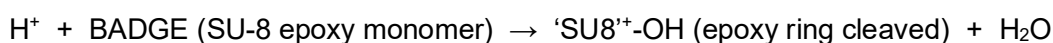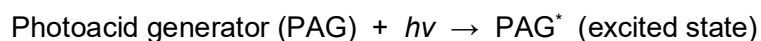
EPON® SU-8 negative resist has been originally developed and patented by IBM (NY, USA) and is currently sold by Kayaku Advanced Materials (MA, USA) under a license-agreement [101] [102]. SU-8 resin is mixed with a solvent like e.g., GBL or PGMEA, controlling its viscosity, as SU-8 is a wet resist that is generally spin-coated rather than laminated. Throughout the reaction mechanism, the excited PAG continues to generate H+ ions that protonate undisturbed epoxy rings on BADGE SU-8 monomers (Figure. 10B). Which generates reactive hydroxyl (-OH) groups that act on other monomers, extending the polymer.

A

Methyl
Methacrylate

Alkoxysilane

Bisphenol A
Novolac epoxy
(BADGE)

B
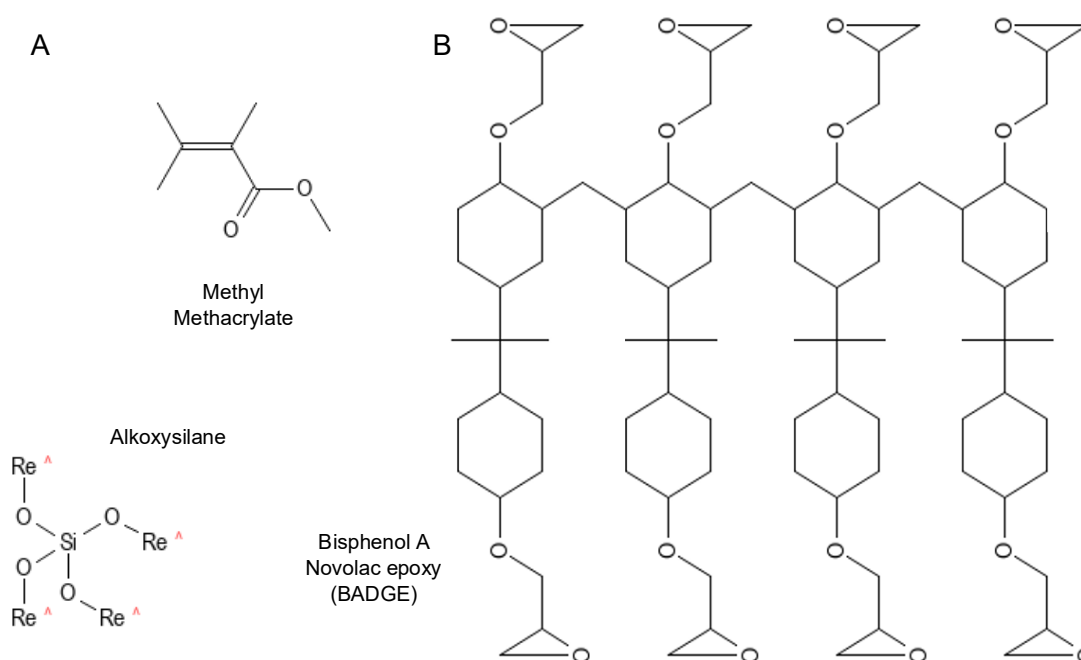
Figure. 10: Acrylic and epoxy monomers present in photoresists. (A) Methyl methacrylate is the most common acrylic monomer and polymerizes via addition to the C=C of the vinyl group (CH_2=CH-). Ordyl SY300 also contains an alkoxysilane group which can engage in the formation of (Si-O-Si) bonds that improve crosslinking and adhesion. (B) SU-8 derives its name from the eight epoxy groups present on the four connected symmetrical BADGE monomers. Adapted from [103] and [102]. Reproduced from reference [104] (CC BY 4.0) ©Springer Nature.

Reiterating that with regards to the exact formulation of Ordyl SY300 we are relatively in the dark relative to SU-8, therefore the chemistry illustrated here is an example of what cationic polymerization of its epoxy groups could look like. Ordyl SY300 incorporation will now be examined on its ability to enhance the standardization and scalability of glass microfluidic - MEA bonding under the parameters sketched in Figure. 9.

3.2 Materials & Methods

Repurposed glass MF and photomask design

Bonding capabilities of Ordyl SY300 were evaluated through repurposing stored glass MF technology. A 3-channel chip that closely resembles the PDMS device discussed in the previous chapter was utilized and this particular glass device was previously used for 2D culture of sensory neurons (Figure. 11).
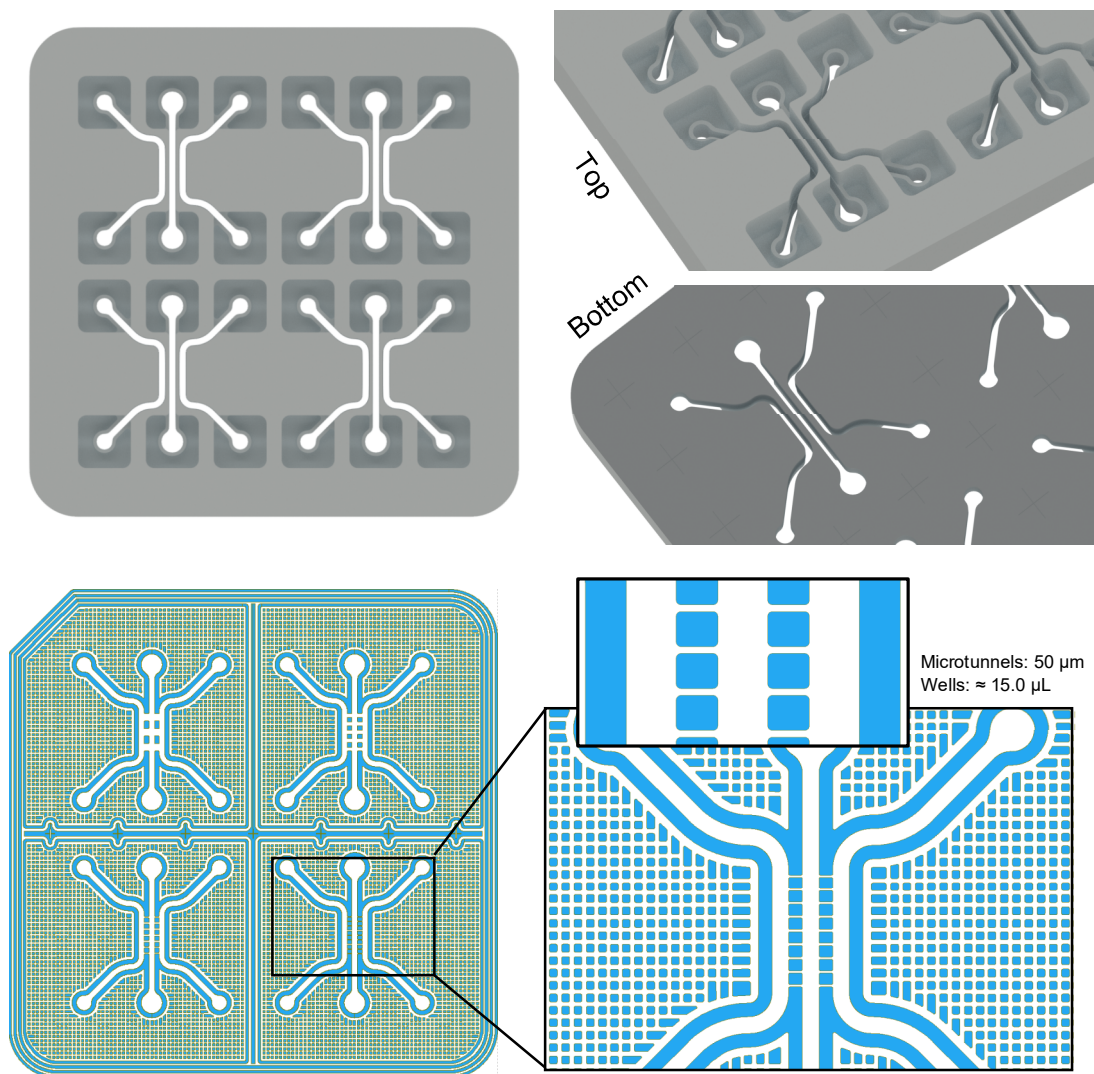
Figure. 11: Triple-channel glass MF chip and complementary photomask. Selectively laser-etched (SLE) MF chip (3.00 mm thick) produced by FEMTOprint SA (Switzerland) featuring 4 individual experiments. Photomask design features carefully crafted pillars spanning the MF surface and a 350 – 400 µm channel rim.

In this section, this device was utilized to attempt consolidating an effective bonding protocol using Ordyl SY300 for the culture of recordable 3D sensory neurons. Objective was to seal the individual compartments while allowing the neurites to pass through the patterned microtunnels within the photoresist-glass barrier. This means that in this particular approach the glass MF chip does not contain any embedded microtunnels (etched into the glass) - but confined spaces for neurite extension are created by sealing the MF chip to a substrate (MEA or 49.0 x 49.0 mm float glass) (see Figure. 9). Subsequently, the feasibility of etching microtunnels directly within the glass barrier itself also became apparent. Dr. Andrea Lovera (collaborator, FEMTOprint SA) indicates that their fabrication method for glass MF chips is a subtractive, direct-write microfabrication process. They integrate 3D microsystems with high precision using a femtosecond laser and etching [76] (Figure. 12). During the laser exposure step, it is possible to generate highly localized material changes and depending on the laser focusing optics, these adjustments typically range from 10 to 100 µm in the Z-axis and 2 µm in the XY-axis.

Figure. 12: High-resolution MF defines liquid-gel interface and Ordyl SY300 separates axons and soma. (A) Single experiment with a 1.0 mm high repurposed 'Gel Layer' (GL) and a covering 3.0 mm high 'Media Layer' (ML). (B) Precisely spaced photoresist ensures neurons remain in the center channel upon plating and extend axons to the peripheral channels.

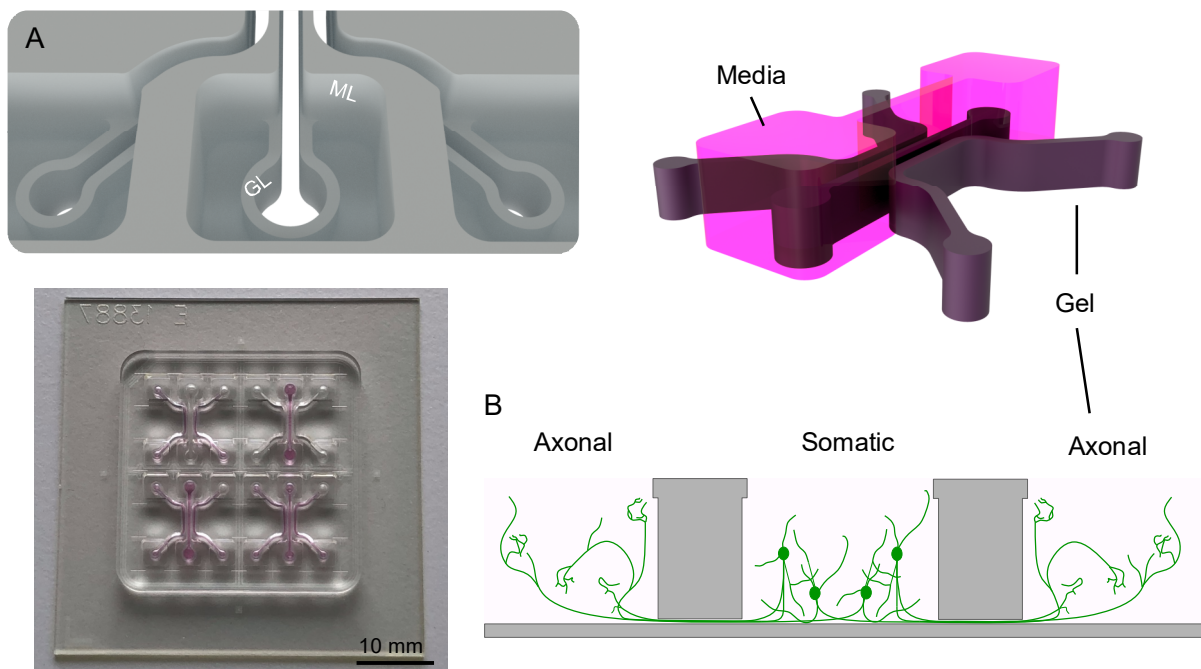The etching rate within the exposed material increases locally in the changed regions (focal spot or voxel) and enables creation of e.g., buried structures (microtunnels). The exposed material is later etched in potassium hydroxide (KOH) based solution to create 3D devices. In the upcoming chapters, I will exploit this potential to my advantage.

Ordyl development and bonding

Float glass substrates diced to 49.0 x 49.0 x 1.0 mm, are obtained from NMI TT (Reutlingen). These substrates are coated with a silicon nitride (SiNx) layer applied via plasma enhanced vapor deposition (PECVD). A SiNx layer serves as a passivation layer, providing an electrical insulation that prevents the transfer of electrical charges across different layers, thereby protecting underlying electronics [105]. When improving bonding parameters much of what will be relevant for actual processing/bonding of MEAs is incorporated, thus also the use of this insulating SiNx layer for passivation of the embedded circuits. SiNx surfaces can be treated further to enhance their hydrophilicity. This is done through either an oxygen plasma or a UV/Ozone treatment, resulting in the creation of a silanol (Si-OH) layer on the surface. This silanol layer can form covalent siloxane bonds with the photoresist following dehydration reactions, as detailed in the previous chapter. Before the lamination process using Ordyl SY300 (55 μm thick), the glass substrates are vigorously cleaned to eliminate any potential adhesion-inhibiting contaminants. These contaminants could be small dust particulates settling from the surrounding environment, residual organic matter from prior processing or chemical residues, including remnants of etching or cleaning steps. The thorough cleaning regimen for the glass substrates includes sonication in boiling water, acetone and isopropanol, 10 minutes each. After these cleaning steps, substrates are dried in an oven set at 120°C for 20 minutes after which they are stored until use.

On the day of lamination (Figure. 13), substrates first undergo an oxygen plasma treatment at 300 V (related to power applied to generate plasma) and 1800 mPa pressure (Piccolo, Plasma Electronic GmbH, Germany). Plasma can be created by applying a magnetic field to a bundle of gas molecules – creating reactive free radicals and ions. Oxygen plasma (O• radicals), is more potent than air plasma (which consists of 78% Nitrogen and 21% Oxygen) and induces more prominent surface modification. Modification involves raising surface energy which increases the reactivity with materials brought into contact and improves wettability [106]. Plasma also cleans off hydrocarbon contaminants and turns them into carbon dioxide and water, which is pumped out of the chamber [107]. If deemed necessary, the substrates can undergo a baking process post-plasma treatment.

This step assists in stabilizing the modifications induced on the substrate surface by the plasma and also aids in eliminating any residual moisture from the surface before proceeding with the lamination process. A basic pouch laminator, the GMP Photonex@325 (model EF02015), is used for the lamination of Ordyl SY355 and other dry resists. Here set to a temperature of 100°C, validated using a thermocouple. Ordyl SY300 product sheet recommends - a lamination temperature of 105 – 125°C, roll pressure of 2.5 – 3.5 bar, and a speed of 1 – 3 m/min, but the lack of precise measurements for pressure and speed in my setup and the fact that values derive from SiO_2 wafer processing, means that these parameters must be adjusted and fine-tuned according to my specific requirements [95]. Ordyl SY355 is ordered from Micro Resist Technology GmbH (Germany) and comes as a roll - the resist is protected by two polymer sheets that are removed right before lamination and right before exposure. After laminating - substrates are rested 5-10 minutes before transferring them to the SÜSS MA6 mask aligner (Süss Microtec SE, Germany).
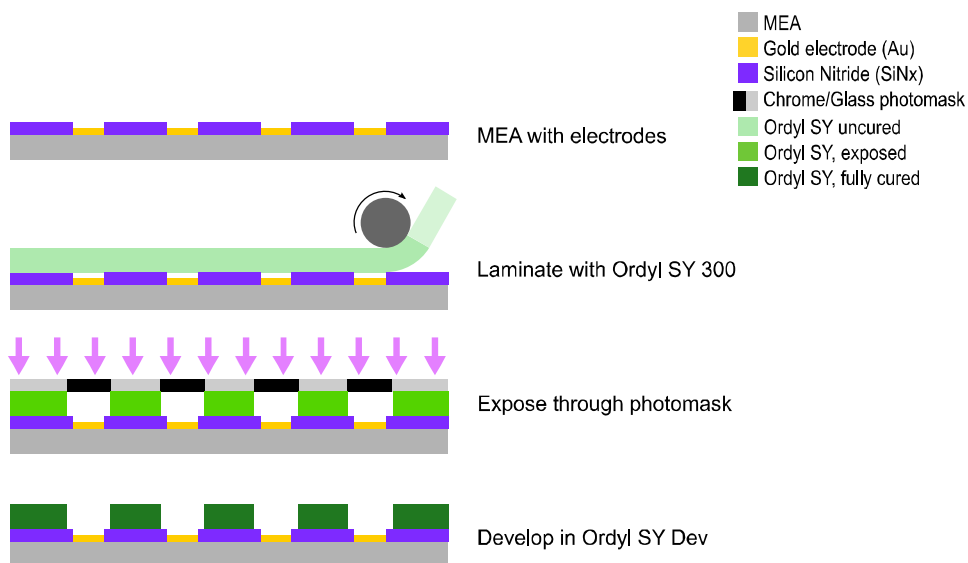
Figure. 13: Ordyl SY300 photoresist development.

Substrates coated with resist are exposed through the glass-chromium photomask I position inside the MA6, utilizing an I-line filter and soft contact, at an approximate dose of 300 mJ/cm^{-2}. Upcoming chapter will provide a more detailed description of these parameters and their impact on the resultant structures. It is worth mentioning at this stage that I maintain a relatively low exposure dose to ensure the resist remains adhesive post-development.

High exposure dosages (and extended high temperature bakes) can lead to a significant amount of resist crosslinking, which consequently reduces the resist's ability to adhere post-development [94]. After exposure, substrates are subjected to a post-exposure bake (PEB) on a hotplate. This bake is essential for cross-linking resists, particularly negative resists like SU8, ADEX and Ordyl SY300. It facilitates, among other things, the dehydration reactions needed for polymerization, which is initiated during exposure. As a result of this cross-linking process, the exposed structures become insoluble in the developer [108]. Substrates are submerged in Ordyl SY 300 Developer XFB, which is a dedicated solution that dissolves unexposed resist leaving behind the patterned structures.
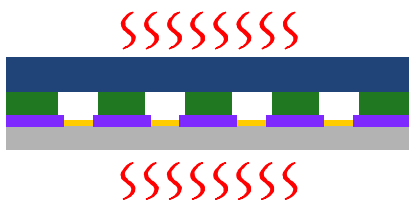
■ Glass MF chip

Bond MF piece on top and Bake
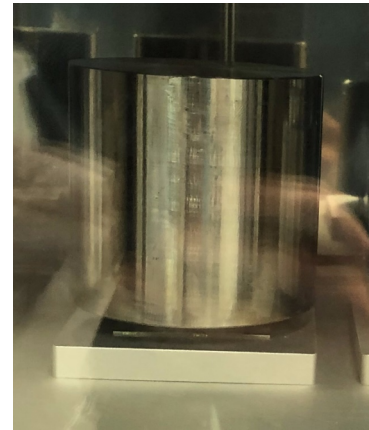
Figure. 14: Ordyl SY300 bonding.

As mentioned, I utilize a Fineplacer® to ensure precise placement of the microfluidic piece (similarly cleaned and oxygen plasma treated) onto the substrates coated with patterned Ordyl SY355. Subsequently, a 2 kg weight is applied, resulting in a force of ~20 N. It follows from the formula

$$F = M * A \tag{2}$$

, where A represents acceleration/gravity (9.81 m/s²) and M is mass (2 kg). Moreover, this force can be converted into a pressure using the formula

$$P = F / A \tag{3}$$

The area (A) is determined by the surface of the MF chip, which is approx. 32.5 mm * 32.5 mm = 1056.25 mm² = 1056.25 * 10^{-6} m², the resulting pressure is approx. 20.000 Pa (20 kPa) (Figure. 14). It is worth noting that this pressure is significantly lower (approximately 30 times less) compared to the pressure applied in the work of Dr. Vulto, who utilizes a dedicated wafer bonder with temperature control [109].

DRG isolation and plating

DRG neurons were extracted from spinal ganglia as previously outlined (see Chapter. 2 Materials & Methods). After resuspending cells collected from centrifugation in Neurobasal-A with GlutaMAX, SM1, N2 Supplement, 0.5% Penicillin-Streptomycin and 100 ng/ml Nerve Growth Factor 2,5S (Promega, #G5141) at the desired concentration, they are mixed with Matrigel® (1 : 4 ratio or 75%) to stand. conc. of 500 cells/µL (2000 cells/µL before mixing). Channels and microtunnels of devices are, again, filled with hydrogel by extruding ≈ 10.0 µL DRG-mix with the pipet tip placed inside the peripheral wells (Figure. 12A) after air plasma treatment. Cells are seeded in the center channel and bare 75% Matrigel® is placed inside the adjacent channels – to monitor outgrowth. In contract to the PDMS-based device, supporting media can now be placed on top of the complete hydrogel to support the cultured neurons.

AAV1-eGFP transduction & imaging

3D neurite outgrowth is monitored daily using a standard table top EVOS™ M5000 Imaging System and at 5-6 DIV I perform confocal fluorescence microscopy on DRG neurons transduced with AAV1.Syn.eGFP using the Zeiss Cell Observer® System (20x objective) followed by image-processing with FIJI. To excite the AAV1-eGFP, I use an Alexa Fluor 488 laser and generate Z-stacks of single tiles or e.g., 4x4 tilescans with the Plan-Apochromat 20x/0.8 M27.

3.3 Results & Discussion

Efforts were focused on facing the challenges associated with manual dispensing of adhesive, a complex and error-prone step that often required a significant time investment. Concurrently, I aimed to enhance the uniformity and scalability of MF-MEA bonding by integrating a UV-patternable photoresist, Ordyl SY300.
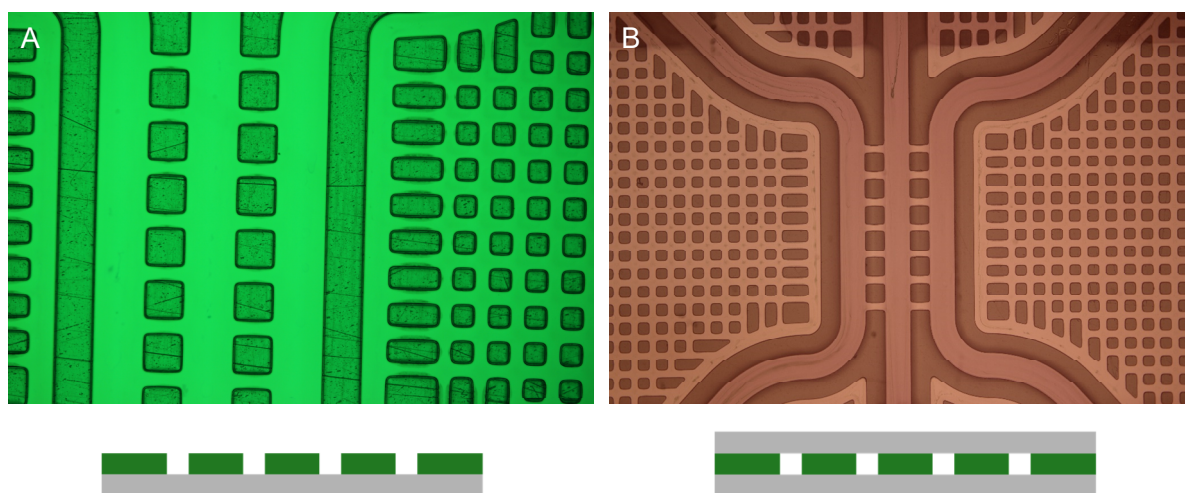
Figure. 15: Ordyl SY355 effectively seals microfluidic compartments. (A) After development. (B) After bonding.

As stated – Figure. 9 describes the objective: to create a glue-free system, in which processed electrodes are integrated into the separating barrier, but results obtained here did not align perfectly with this vision. However, the process of fabricating these Ordyl SY300-based devices provided important insights. Insights which aided in adjusting strategy effectively as working with Ordyl SY300 presented substantial challenges in application.

Initially a different thickness was utilized before transitioning to the 55 µm thick Ordyl SY300. Using a resist of this thickness for fluidic separation is not practical, as it would create an excessively large space for neurite growth, thereby negatively affecting the recording of extracellular currents (cannot be appropriately constricted). Instead, trials commenced with a 20 µm thick Ordyl SY300. However, it was quickly realized that this particular batch of Ordyl SY300 was extremely difficult to rid of unexposed resist during the development phase of the fabrication process. It was elected to persist with the thicker Ordyl SY300, aware that it might pose recording difficulties in the future. Mitigating strategies were already considered to counter these potential issues, elaborated on in the upcoming chapter.

In brief, my proposed solution involved employing the high-resolution photoresist SU-8, to create confined spaces for neurite growth over the barrier-embedded microelectrodes. These SU-8 islets (similar to the Ordyl islets in Figure. 15 and Figure. 16A) would then be covered or 'tented' with a secondary layer of resist, potentially Ordyl SY355 or another suitable resist. This layer would facilitate bonding with the MF chip placed on top.

Figure. 15 demonstrates that effective bonding of the entire surface could be achieved, provided the surface area of Ordyl SY300 pillars and rim structures were kept around 300 x 300 µm. This is because larger areas with minor imperfections could lead to complete delamination or detachment after repeated use. Interestingly, the developed Ordyl SY300 rim, which seals the fluidic channels, appears to be highly suitable for lining compartments. This approach will make a reappearance in a slightly modified but related manner in the next chapters.

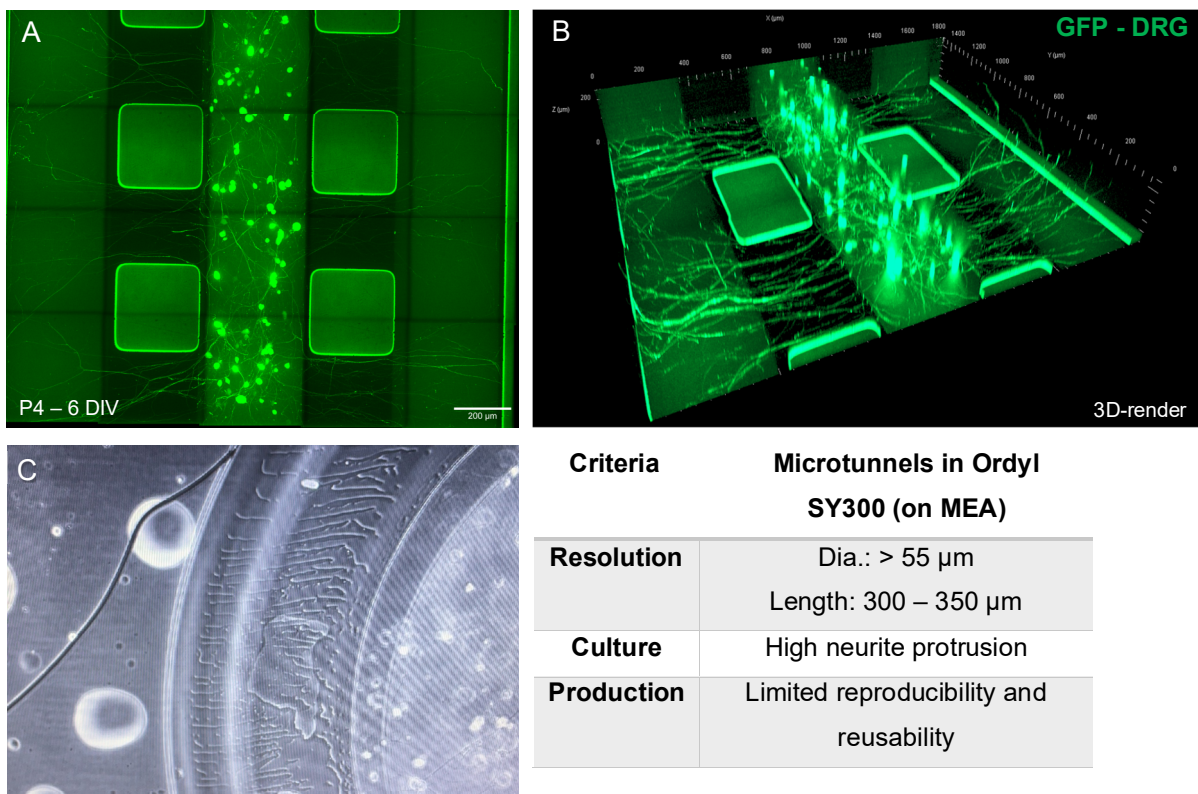| Criteria	Microtunnels in Ordyl SY300 (on MEA)
Resolution	Dia.: > 55 µm Length: 300 – 350 µm
Culture	High neurite protrusion
Production	Limited reproducibility and reusability

Figure. 16: Neurite outgrowth inside the Ordyl SY300 bonded 3-channel chip. (A) (B) Live-cell confocal images of GFP-transduced DRG neurons protruding into adjacent channels in 3D after 6 days in culture. (C) Channel rim suffering moisture eroding adhesion.

Here represented is the first official instance where hydrogel-embedded DRG neurons were cultured within the open top two-component (MF piece and substrate) model, as similarly detailed in Molina-Martinez et al. (2022) (Figure. 16) [71]. However, as a 3-channel model does not hold particular biological relevance (a 2-channel model is more suitable), I will not delve deeper into the culture parameters here. Nevertheless, critical observations from the nerve outgrowth experiments within the Ordyl SY300 bonded chip include that, when the plating protocol is followed accurately – i.e., bare Matrigel® is plated first in the axonal channels, followed by the DRG neurons in Matrigel in the central channel – the cells stay focused in the center upon seeding and do not cross over, despite the fairly large exits from the center channel. This offers a good perspective for approaches involving tunnels with larger openings. Still, as noted earlier, the recording capabilities are compromised when the tunnel size is increased excessively.

Furthermore, bonding the two-component system with Ordyl SY300 is feasible, but mere bonding is insufficient. It must be robust and long-lasting. Given the substantial cost of the platform, which is currently not suitable for single use, it is essential that it is reusable at least ten times to reduce the cost per experiment. MEAs ordered from NMI TT are roughly priced at €275,- , while etched glass MF chips currently cost between €750,- and €1000,- each. Figure. 16C illustrates how Ordyl SY300 started showing visible signs of wear after only a few uses, which is not acceptable for current requirements. This realization prompted a shift towards a method previously hinted at: integrating the high(er)-resolution resist SU-8 to ensure the quality of electrophysiological recordings while guaranteeing a more robust and durable bonding by coupling with a tenting polymer and the manual application of adhesive but in a modified setting. I integrate a distribution guide for glue application, thus enhancing workflow and standardization. Details on this are presented in the following chapter.

Chapter 4: Microfabrication Part 2. SU8 ADEX Barrier Stacking

4.1 Introduction

CME technology

In previous work we outlined the development of a system with potential utility for investigating brain disorders, such as Alzheimer's and Parkinson's disease [71]. The study aimed to address the absence of reliable *in vitro* models that are capable of assessing both structure and electrophysiology of brain tissues by creating a platform that merges real-time monitoring of electrical activity and morphology of neural networks in 3D.
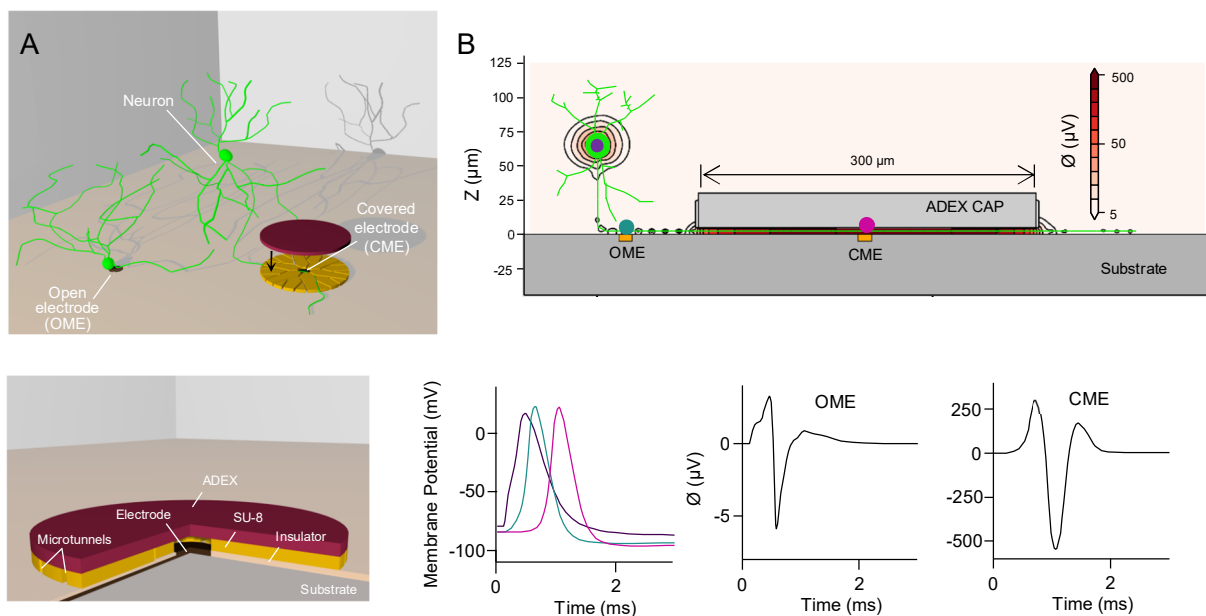
Figure. 17: Published method for capturing electrical activity from 3D neuronal networks. (A) Neurons can only be recorded if their soma is on an open microelectrode (OME). When neurons are spread throughout a 3D volume, monitoring them becomes challenging. Only way to detect their activity is through their neurites, which extend towards the lower substrate. Process involving photoresist was used to develop covered microelectrodes (CMEs) that enable recording from trapped neurites. (B) Collaborators modelled the electrical kinetics of ionic currents present in the system and found CMEs enhance recordings substantially. Reproduced from reference [71] (CC BY 4.0) ©IOP Publishing.

Conventional methods used for recording from 2D neuronal cultures are inefficient for 3D arrangements and published 3D electrophysiology technologies employ devices not compatible with the throughput and cross-platform integration required for drug discovery.

Reason this is mentioned here is because a distinguishing feature of the previously published system is the innovative approach of processing substrate-integrated microelectrodes, enabling continuous monitoring of activity from the neurites of 3D neural tissues (Figure. 17). Neurites extending in 3D space within designed hydrogel-based structures are captured inside covered microelectrodes (CMEs). CMEs are capable of providing a non-invasive measurement of electrical activity in 3D neuronal circuits with high sensitivity, hold scalable throughput and the usability required for effective preclinical research.

Through the simulations performed by Dr. Torbjørn V Ness, it was confirmed that the rapid dissipation of recordable extracellular ionic currents arising from active neurons is problematic in 3D cultures. In Figure. 17B, it can be seen how the associated voltage of transduced extracellular currents, originating from the firing of membrane potentials at the soma (represented in purple) falls below 10 µV — which is indistinguishable from noise — when moving ~15 µm away. Proximal segment of the axon (depicted in green) over an OME produces similarly undetectable changes in voltage over the electrode surface. Conversely, the distal segment of the axon (illustrated in pink) inside the CME limits the dispersion of extracellular transmembrane currents and generates voltages that reach up to ~250 - 500 µV.

When a neuron fires an action potential, there is a fast change in voltage across the neuron's membrane due to the movement of ions in and out of the cell [21]. Resulting extracellular ionic flux is converted into electronic currents by a nearby electrode, known as transduction. With the help of an amplifier, this current (I) can then be transformed into a change in voltage (V), which is easier to interpret and measure [110]. Electrodes used in MEAs for neural recordings generally have 'moderate to high' impedance (Z) of e.g., ~0,45 MΩ, which is a measure of resistivity towards charges crossing the solution-electrode interface [111, 112]. Rather than using $V = I * R$, known as Ohm's Law here, impedance Z ($V \sim I * Z$) better describes 'resistance' in biological signals like neuronal action potentials, as these are more complex e.g., frequency dependent (relevant range ~1 kHz) [110]. High impedance and a small electrode surface (~30 µm diameter) guarantees sensitivity towards potential changes and allows the resolve of microvolt range signals of single units [113]. However, higher impedance is not always beneficial as raising it exponentially will also increase recording noise intrinsic to the electrode, called thermal noise.

When setting out to amplify an electrical signal, one has to consider the balance between enhancing the desired signal and limiting the amplification of background noise, a relationship commonly referred to as the signal-to-noise ratio (SNR). Modifying certain electrode parameters, such as choosing specific electrode materials like e.g., gold (highly conductive) or titanium nitride (TiN), may improve SNR to some extent [113]. On the other hand, alterations like changing the electrode's size or geometry might not significantly improve the SNR. You might amplify relevant signal but also enhance e.g., biological noise (emanating from distant neurons), which could interfere with accurate electrical readings. Theorizing about the possibility of selectively improving signal while limiting noise resulted in the development of the CME. Acting as an insulator, the CME selectively allows signals from target neurons to reach the electrode, effectively shielding it from other unwanted signals, enhancing the specificity of signal acquisition and improving SNR [71]. Here, the principle of confining transmembrane currents to enhance extracellular potential is similar to the concept of seal resistance in patch-clamp recordings. Where formation of a tight seal between the cell membrane and the recording pipette, minimizes ionic current leakage and allows effective measurement of voltage change [113, 114].

INV-MPS template

Extrapolating this to the 3D coculture of sensory neurons innervating target tissues, it was reasoned that Ordyl SY300 had the potential (aside from bonding) to similarly limit the dispersion of extracellular membrane currents around axons that cross the separating barriers in cocultures. Nevertheless, achieving a tunnel resolution of less than ~20 μm (at least) with Ordyl SY300, a necessary condition for obtaining the level of amplification required for recordings, proved technically unfeasible. As a result, it was concluded that it would be more beneficial to attempt the integration of the standard SU8 - ADEX (dry laminated resist) setup, as represented in Figure. 17. Supported by the fact that with SU-8, it is well-documented that a sub-5 μm microtunnel resolution can be achieved, in both the Z and X,Y axes and record spikes [115]. Ordyl SY300 also does not tent inserted spaces as effectively as ADEX does [94]. However, both SU-8 and ADEX are not suitable for direct bonding, therefore, a method will be devised for combining this SU8 - ADEX structure with standard epoxy adhesive to bond the microfluidic piece and MEA. Important to highlight at this stage is the design of the basic prototype of the 2-channel INV-MPS (microfabrication workhorse), which includes 9 coculture experiments and a separating barrier within each. Device shares similarities with the previously published 18-well chip [71], employing the same partitioning of liquid and gel. This platform has already been briefly mentioned in the general introduction and further details of its overall geometry are indicated in Figure. 18.

'Under' the barrier

9-Well INV-MPS (x2)			
Media Layer (ML) ~ 62.5 µL	**A.**	Height (mm)	2.0
	B.	Width (mm)	3.9
	C.	Length (mm)	8.0
Gel Layer (GL) ~ 8.7 µL	**D.**	Height (mm)	1.0
	E.	Width (mm)	1.0
	F.	Base (mm)	8.7
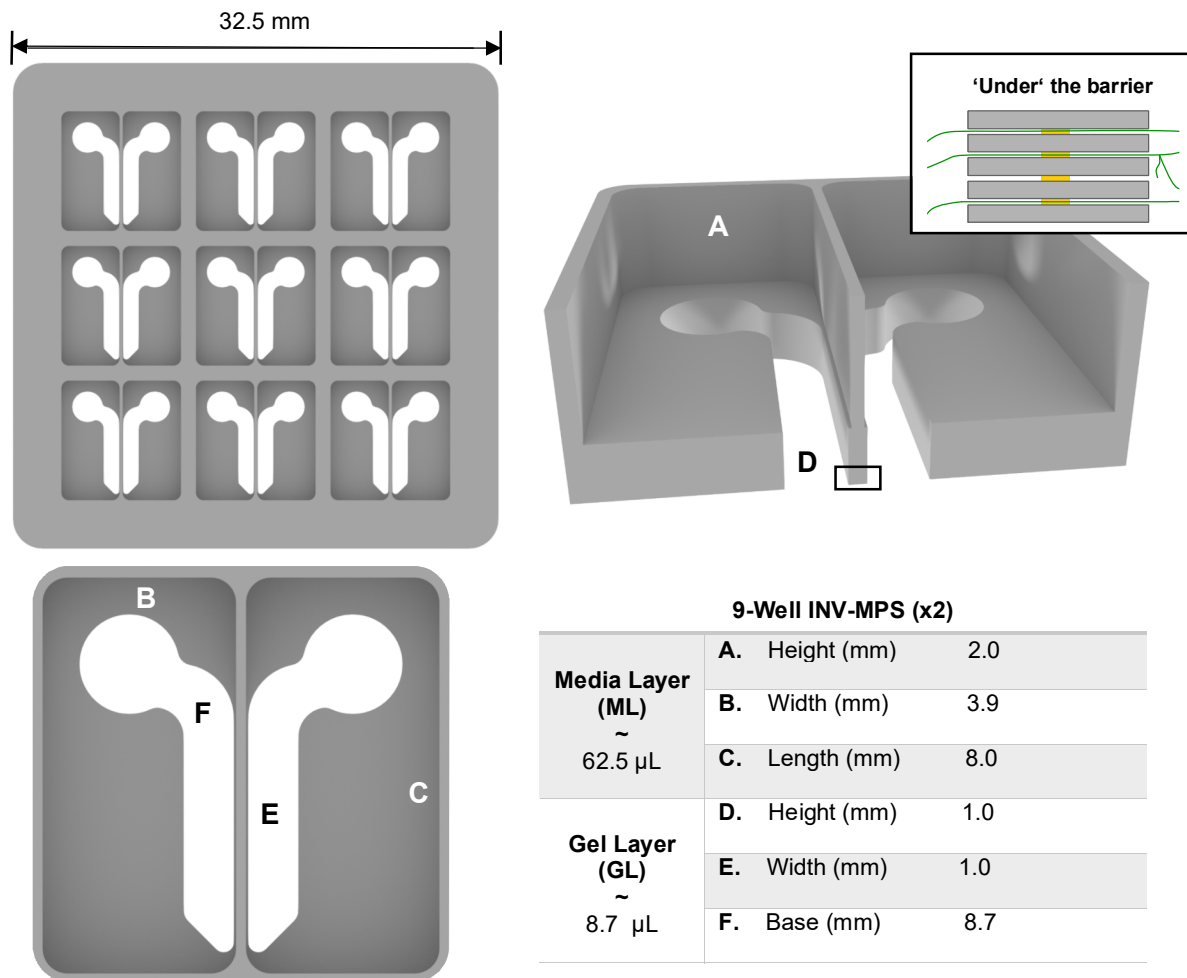
Figure. 18: 9-well INV-MPS prototype. Microfluidic devices were originally diced from a fused-silica sheet of ~ 3.0 mm thickness and selectively laser-etched to create gel layers (GL) and media layers (ML). Designed with Autodesk Inventor Software (Autodesk Inc. CA, USA).

In this chapter, a final attempt is made at employing photoresist to construct a barrier component that not only maintains fluidic separation between compartments, but also permits neurite extension through it. Simultaneously, photoresist structuring should adequately enclose the barrier-centric microelectrodes to ensure recording from neurites that traverse and ultimately innervate the target tissues in the adjacent compartment. SU8 - ADEX processing will be extensively detailed here and subsequent chapters using the same methodology will refer back to the detailed description provided here, although the context and parameters may differ.

4.2 Materials & Methods

Photomask design(s) and glue guide MF

Bonding process is tested glass to glass before proceeding with glass to MEA, as it is not practical to waste MEA during the iterative fine-tuning of the bonding process. Figure. 19 depicts the theoretical outline of the microfluidic piece to be centered on the MEA, aligning the photoresist counterpart of the glue guide rim with guide etched in the MF chip (Figure. 20).
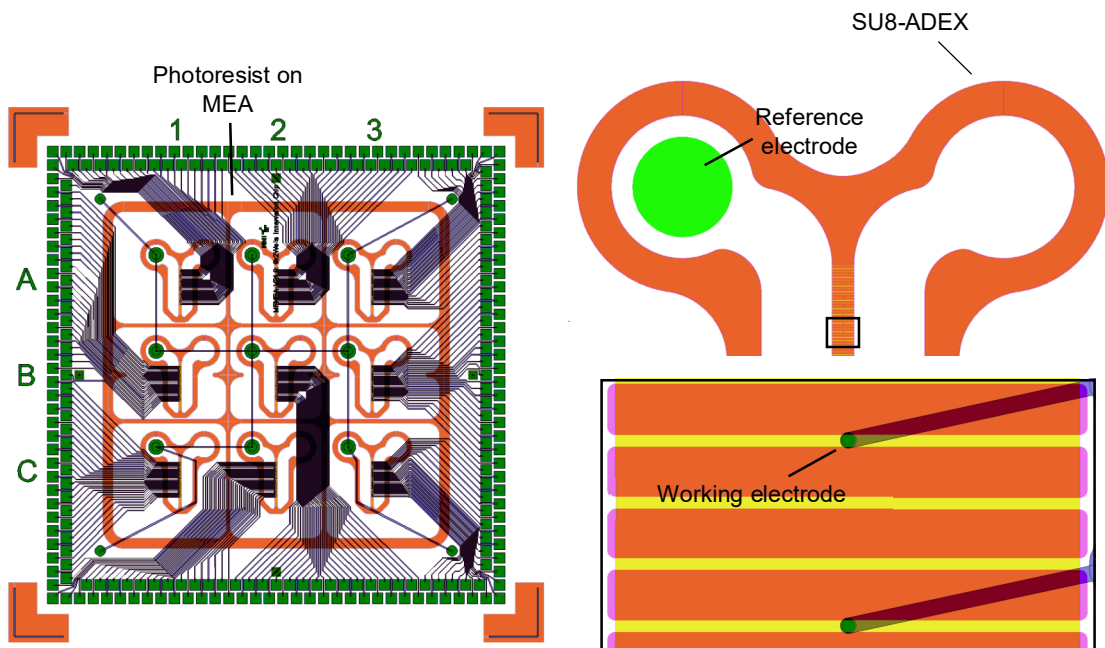
Figure. 19: SU8-ADEX photoresist patterned on MEA (theoretical). Rim segments surround the MF chip perimeter to create a tight seal and individual wells have rims around both channels and connect to the separating barrier. SU-8 (orange) and ADEX (yellow) are layered on top of each other to create a confined space around the recording electrodes (7.5 µm x 300 µm with 32.5 µm spacing). Every well has an interconnected (large) reference that helps reduce electrical noise. Designed with CleWin (WieWeb, the Netherlands).

Together with collaborators at FEMTOprint SA (Switzerland) it was decided to etch out some designation for the epoxy adhesive used to bond the MEA and MF chip to smoothen distribution and standardization. Particularly relevant for this approach as the main difficulty here is fine placing the MF chip on top of the patterned photoresist in a way that does not cause any epoxy adhesive to enter the microtunnels underneath.
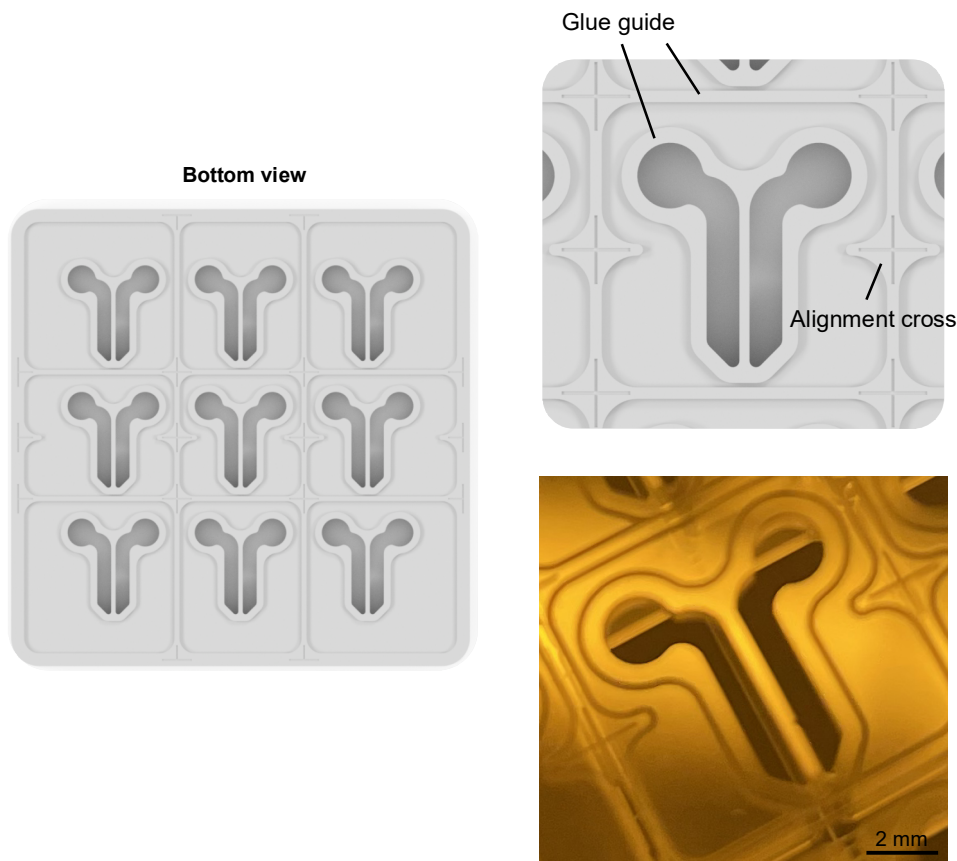
Figure. 20: Profile on MF chip bottom includes glue guide and alignment. Original to the photoresist on MEA - rim segment surrounds both channels and connects to the separating barrier. Non-essential segments can either be completely etched out or confined by a trench.

SU8 - ADEX microfabrication

SU8-ADEX process is included in the 2022 publication [71] and is also an integral part of the INV-MPS outlined in Chapter. 7. Process details will be discussed here in the context of its potential use as a barrier component in the 2-channel INV-MPS. Modulating parameters like e.g., hard baking (affects adhesive properties), is context dependent and therefore varies between CME production and current goal. Key differences will be highlighted accordingly to prevent confusion in later chapters.

As described previously, SiNx coated glass substrates are cleaned extensively the day before use in any of my processes. First step in SU8-ADEX microfabrication (Figure. 21) is spin-coating SU-8 2002 (Kayaku Advanced Materials, USA) to a thickness of approximately 3 μm. Before doing so, substrates are treated with oxygen plasma (Piccolo, Plasma electronic GmbH, Germany). Followed by a bake at 150 °C for 1 hr to eliminate moisture from the surface and stabilize the introduced silanol groups. Noting that, in the previous chapter, I detailed cationic polymerization chemistry and formulation of EPON® SU-8 as a tool to aid in general understanding of UV-photolithography – here, focus is on the exact processing.

Substrates are collected from the oven and left to cool down for ~15 minutes while preparing the Spin Coater 1001 S (CONVAC, GmbH). Here, spincoating involves the covering of activated SiNx surfaces with liquid photocurable SU-8 by applying 1 mL of solution with a pipet. Chuck holding the substrate in place spins at 500 revolution per minute (RPM) for 10 s to remove large excess polymer and then accelerates to 1000 RPM and spins for another 30 s to achieve desired thickness. Parameters are adapted from the product sheet provided by KAM, which includes detailed thickness vs. spin speed indications for various SU-8 resists [116]. Substrates are then transferred to a hotplate where they are baked for 1 min at 95 °C and left to cool down in what is called a softbake (SB). Soft baking evaporates solvent and gives the film some initial density as it stabilizes its adhesion to the substrate. Also, exposure is performed in 'contact mode' which means photomask and substrate are in direct contact and a soft liquid resist will stain the mask.

For SU-8 exposure I use the SÜSS MA6 mask aligner (Süss Microtec SE, Germany) with the integrated I-line filter. The I-line filter allows passage of only 365 nm wavelength light as SU-8 is insensitive above 375 nm and does not crosslink optimally below 350 nm. Substrates are exposed at 150 mJ/cm^2, through photomasks designed in CAD-software CleWin (WieWeb, the Netherlands) and ordered from Deltamask (the Netherlands). Exposure dose in UV-photo-lithography is generally expressed in millijoules per square centimeter (mJ/cm^2) and follows from multiplying the UV lamp (350 W Hg) light intensity (mW/cm^2) by the exposure time (s) [117]

$$Dose = Time * Intensity \qquad (4)$$

To achieve an exposure dose of 150 mJ/cm^2, one first reads off the lamp intensity from the MA6 or uses a radiometer to measure it. With an intensity of ~ 6 mW/cm^2, this means an exposure time of 25 seconds is necessary to obtain required dose.

For clarification, watt (W) is a unit of power and equivalent to one joule (energy) per second, thus, total energy delivered to the substrate is expressed in mJ/cm^2. Furthermore, SU-8 is a negative photoresist which means that UV-light exposed resist will become cross-linked and unexposed resist will be solubilized.

Completion of the cross-linking reaction (initiated by UV photoacid activation) is again done through a PEB. Substrates undergo a PEB of 1 min at 95 °C – where a ramp at 35% of the max ramp (max. ~7.5 °C/min) is instated to provide a gradual heating and reduce thermal stress in the resist. However, one should consider the effect ramping has on the overall baking time and adjust parameters accordingly. Lastly, substrates are developed in mr-Dev 600 (Micro Resist Technology GmbH, Berlin, Germany) for 10-15 s and then rinsed in isopropanol.
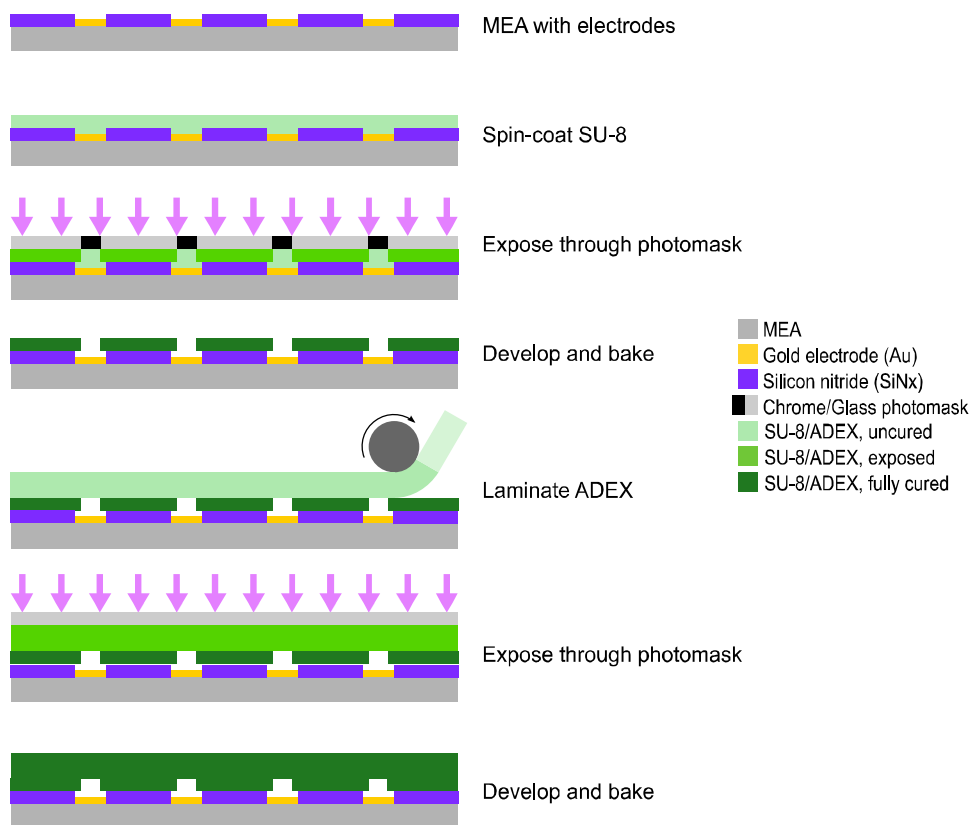

Figure. 21: Production scheme SU8-ADEX

SU8 is then baked in a convection oven at 150 °C for 30 minutes which helps prevent overdevelopment of the resist in subsequent developer steps included in the ADEX process (on day 2). ADEX™ (and SUEX™) is a dry film photoresist created by DJ MicroLaminates Inc. (Boston, USA) and is sold in Germany by Micro Resist Technology GmbH (Germany). ADEX is similarly an epoxy-based resin, but as it comes as a film it has been partially pre-cured, unlike SU-8. Cross-linking occurs via cationic polymerization with the use of a PAG (photoacid generator). Lastly, ADEX comes sandwiched between two protective layers of polyester (PET) (like Ordyl SY300) and is stored at RT while kept away from white light [118]. ADEX TDFS (Thin Dry Film Sheet) A20 (20 µm thickness) is laminated on top of the SU-8 channel rim base – which as you can see in Figure. 19 – is almost identical to the final ADEX structures, except for the spaced SU-8 in the separating barrier. ADEX will tent/overhang these spaces and create microtunnels (Figure. 21). Resist is laminated using a pouch laminator (GMP Photonex@325, EF02015) at 3 mm s^{-1} heated to 75 °C and left to stabilize for 10 – 15 minutes before exposure. ADEX is exposed at 600 mJ/cm^2 under the i-line filter, but not in 'contact mode'. A 10 µm proximity exposure is elected, as with higher exposure dose, one risks fusing hard-to-remove resist to the chromium mask. PEB is 1 hr at 65 °C followed by 1 hr cooldown.

Development is rather strenuos (8+ minutes) as scum (unexposed solubilized resist) tends to collect inside the tight microtunnel spaces and needs to be cleaned out. ADEX is developed in cyclohexanone and rinsed with isopropanol. Stacked SU-8 and ADEX was hard-baked (30 min at 170 °C with a 6 hr ramp) prior to bonding – as it is not the resist that will be bonding directly to the MF chip (unlike with Ordyl SY300). Hard-baking photoresist improves thermal stability, raises stiffness and drives out excess solvent that might still be present [115]. Substrates with structures are then stored until a bonding date is set.

Pre-treatment & Bonding
MF chip is glued to resist structures on the MEA (simple SiNx coated substrate here) with EPO-TEK 301-2FL (Epoxy Technology, Billerica, MA, USA). EPO-TEK 301-2FL is a two-component epoxy resin, that starts cross-linking upon mixing of the curing agent and the base epoxy-solution [119]. Before applying the adhesive along the designated glue guide (Figure. 22), it is made sure that MF chips are bond-ready. Through becoming increasingly experienced with preparing fused silica MF chips for assembly, it was found that a mild cleaning without sonication – but rather – swishing manually in acetone and isopropanol, followed by a 20 minutes drying run at 120 °C – was satisfactory.

Performing this either the day before bonding or the morning of, followed by an air plasma treatment (Plasma cleaner/sterilizer PDC-32G, Harrick Plasma, Ithaca, US) for 2 min at high RF (18 W). This followed from the finding that it did not attack surfaces as aggressively as oxygen plasma treatment, appearing less wettable than the latter, which is desirable for the gluing process.
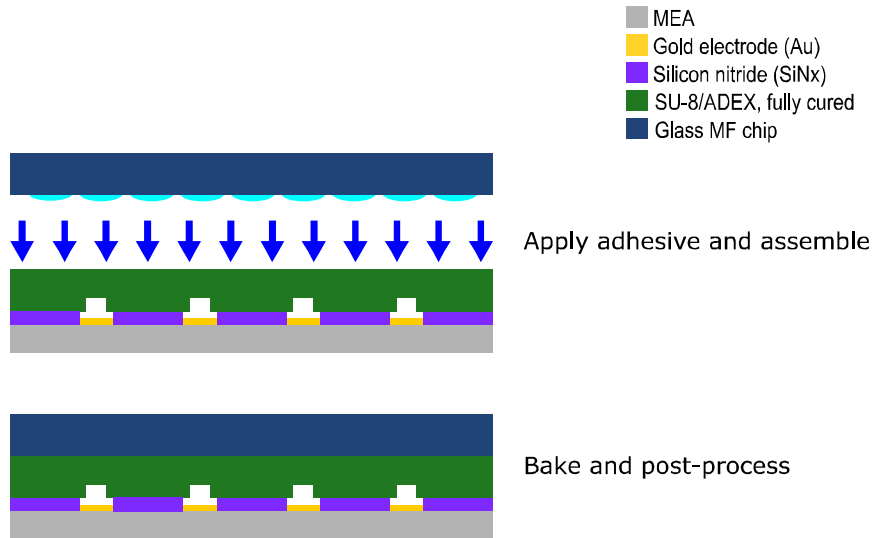
Figure. 22: Bonding scheme SU8-ADEX epoxy adhesive

EPO-TEK 301-2FL is mixed and transported to a setup with; Fineplacer® lambda (Finetech GmbH, Germany), glue dispenser, light microscope and oven. Adhesive is dispensed along the guide on the bottom of the MF chip. Chip is then mounted inside the Fineplacer and placed on top of the structured substrates. Devices are then cured at 80 °C for 3 hrs (with a 6 hr ramp) and stored for later use.

Profilometry

Stylus profilometry (DektakXT, Bruker UK Ltd.) was performed to characterize SU8-ADEX height. Both SU8 (no ADEX cover) and SU8-ADEX (with cover) were measured by using a 2 µm tip. Both sets of measurements were processed and analyzed using dedicated Vision64 software (Bruker UK Ltd.).

DRG isolation and plating

DRG neurons were extracted from spinal ganglia as previously outlined (see; Chapter. 2 Materials & Methods). After resuspending cells collected from centrifugation in Neurobasal-A with GlutaMAX, SM1, N2 Supplement, 0.5% Penicillin-Streptomycin and 100 ng/ml Nerve Growth Factor 2,5S (Promega, #G5141) at the desired concentration, they are mixed with Matrigel® (1 : 4 ratio or 75%) to stand. conc. of 500-750 cells/µL (2000-3000 cells/µL before mixing). To ensure efficient filling of microtunnels and channels with hydrogel when extruding ≈ 8.5 µL DRG-mix with the tip placed inside the keyhole basin, the assembled glass-MF chip is similarly hydrophilized with air plasma. Cells are seeded in the left (somatic) channel and bare 75% Matrigel® is pipetted inside the right (axonal) channel – to monitor outgrowth into these channels.

AAV1-eGFP transduction & imaging

3D neurite outgrowth is monitored daily using a standard table top EVOS™ M5000 Imaging System and at 5-6 DIV I perform confocal fluorescence microscopy on DRG neurons transduced with AAV1.Syn.eGFP using the Zeiss Cell Observer® System (20x objective) followed by image-processing with FIJI. To excite the AAV1-eGFP, I use an Alexa Fluor 488 laser and generate Z-stacks of single tiles or e.g., 2x3 tile scans with the Plan-Apochromat 20x/0.8 M27.

4.3 Results & Discussion

Illustrated in this chapter is the refinement of the separating microelectrode-integrated barrier by incorporating a structured high-resolution photoresist stack (SU8 – ADEX), drawing from acquired knowledge in producing CMEs. Concurrently, the prototype of the automation-friendly 2-channel INV-MPS is detailed, which was designed to integrate seamlessly with the 3D photoresist stack, as depicted in Figure. 23.

Before delving into the microfabrication, it should be noted that microfluidic technology should similarly cater, to some degree, to the demands of pharmaceutical and biotechnological industry, which adhere to specific standards for their cell culture. INV-MPS wells consistently maintain a fixed spacing of 4.5 mm for multi-channel pipettes (standard cone distance) and device fits a 3 x 3 matrix for ample biological replicates [120].
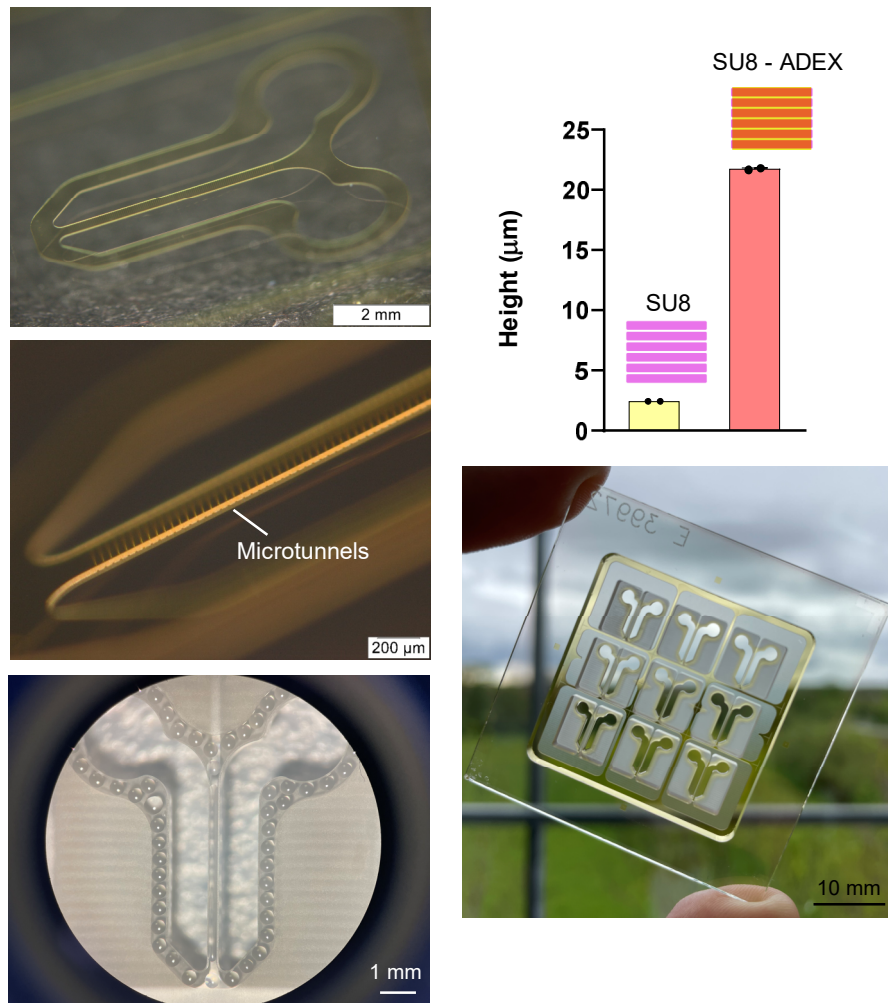
Figure. 23: 2-channel INV-MPS with barrier' integrated photoresist. SU8-ADEX stack structures complement the channel rim etched into the MF chip. Epoxy adhesive easily distributes across the designated glue guide pattern.

While this does limit flexibility to generate certain culture designs, it establishes a streamlined transition towards future pre-clinical adoption. And while the compatibility of this specific platform design with a photoresist-based barrier remains to be evaluated, the development of the INV-MPS glass MF prototype by itself is highly significant for future system iterations. Depicted in Figure. 23. is the production of an INV-MPS with SU8-ADEX microtunnels successfully integrated into larger structures that represent the etched glue guide on the MF chip (Figure. 19 and 20). Total resist stack height ranges from 22.5 to 23 µm, suggesting that the spin-coated SU-8 layer is precisely at the intended 2.5 - 3 µm, considering the ADEX layer used is 20 µm thick.

Additionally, the glue guide functioned as anticipated, and in Figure. 24. it is apparent that by manipulating the barrier thickness - between 100 and 300 µm – it was possible to govern how the glue dispersed across the barrier during bonding. This method effectively preserved the underlying microtunnels, allowing neurons to extend through them undisturbed.
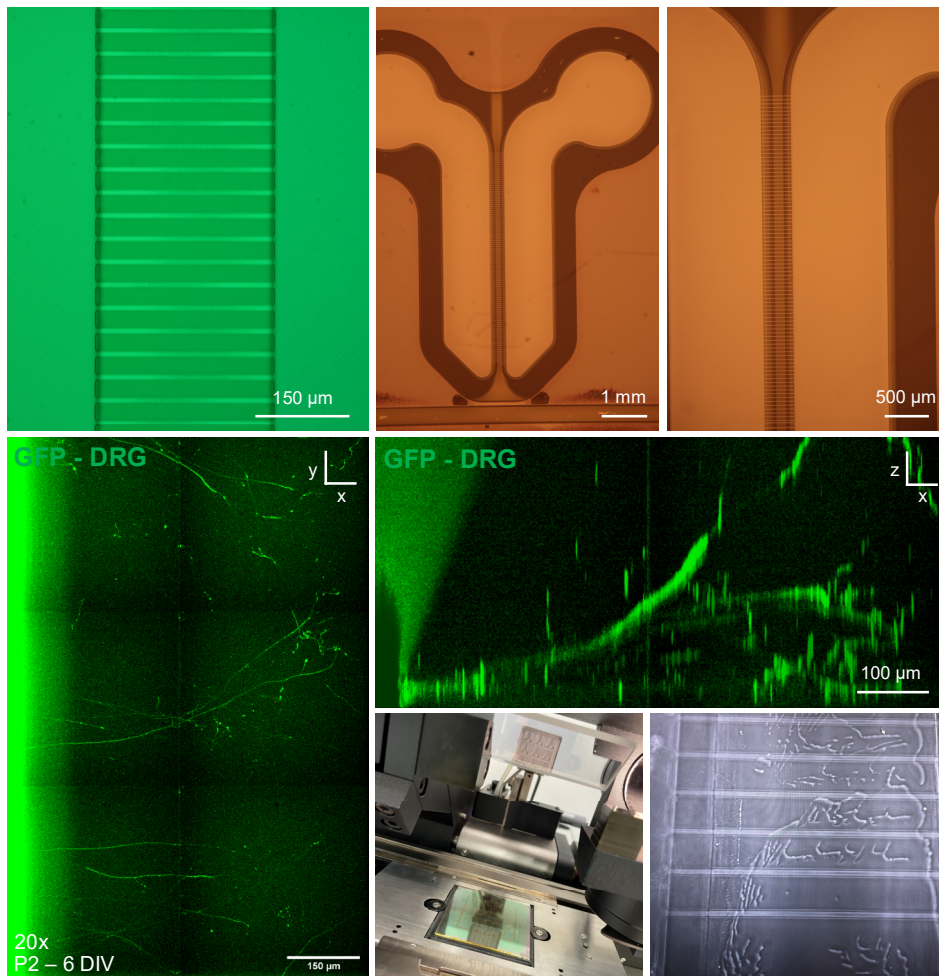
Figure. 24: Neurite outgrowth from SU8-ADEX barrier. Uninterrupted bonding of entire barrier + channel rim. Open microtunnels accommodate neurite growth and extension into 3D space post-exit. Fine placement methodology and wear on the epoxy after 2 cultures.

However, upon objective evaluation of neurite outgrowth, it can be observed that neurites appear to have difficulty identifying the entrances to the microtunnels. This could be attributed to the shifted positioning of these openings relative to the glass barrier (bonding required a tiered structure). As a result, neurites that encounter and grow alongside the barrier are unlikely to find an entrance to a tunnel for extension. Instead, they find a continuous border where the rerouting

required to find an entrance is not a usual projection path. Additionally, the rinse-and-repeat protocol for these devices, as described [71], unfortunately was not compatible with the delicate seal of microfluidic compartments. Epoxy adhesive seems to be negatively impacted by moisture infiltrating the bonding area, which degrades the attachment of the barrier. Therefore, creating a reusable device with which it is possible to significantly cut down the cost per experiment by ensuring multiple successful experimental runs is unfeasible here. Nevertheless, the value of current approach should be recognized as it produced the INV-MPS MF design and associated glue guide, which are both important components for standardization in approaches down the line. Shortcomings of photoresist-based barrier approach steered us away from extensive microfabrication and towards barrier-integrated strategies that utilize a glass barrier with solely an epoxy adhesive. This implies that if the separating barrier requires microtunnels, they would need to be directly etched into the glass, as opposed to being fabricated using a complementary method.

However, before commencing further barrier-integrated strategies, present hurdle prompted a reassessment of overall strategy as replicating sensory innervation of cancers inside these devices started to seem unachievable. It was postulated that, if required, single-well devices from the previous work [71] could be utilized, under the condition that within these devices a method could be found to separate the target tissue and sensory neuron soma at least physically. Meaning no separating barrier integration and consequently an inability to culture the different cell types in their unique media due to the lack of fluidic separation in a single compartment model. However, it was hypothesized that making progress in comprehending both the behaviour of cancer spheroids and the neuron-cancer symbiosis could propel us forward with regards to understanding the relevant biology and how devices should/can be set up. Furthermore, with the 'V19' devices at my disposal, I also possessed a straightforward method that allowed direct examination of the electrophysiology of 3D DRG neurons using CME technology (Figure. 17).

Chapter 5: Pain Electrophysiology & Cancer-Neuron coculture

5.1 Introduction

Progress in devising a robust method for incorporating a CME-inspired separating barrier for the 3D recording from neuron-tissue cocultures came to a standstill after determining the incompatibility of a photoresist-based approach. As mentioned, I previously speculated about the possibility of directly integrating microtunnels into the glass barrier by etching. But this method would eliminate the possibility of incorporating microelectrodes for direct recording from axons that extend through this barrier. Still, throughout the project, I extensively explored the option of having barrier-etched microtunnels, keeping it as a potential alternative once it was established how to combine it with a feasible recording approach. Key developments here will be discussed in the next chapter and it will become clear, from data presented in the following chapter, that barrier-etched microtunnels are a viable approach for designing an INV-MPS. Primary emphasis of this chapter, however, is on advancing the understanding of sensory neuron electrophysiology, but it will also contain illustration of potential characteristics of neuron-cancer crosstalk and describe morphological features observed in cocultures.

Throughout microfabrication efforts, the target tissues, which would eventually be innervated within the axonal compartment, only appeared in hypothetical discussion. Choice was made to go ahead and initiate direct cell-cell contact to find out whether the interaction would provide any meaningful insights. Particularly into whether cell types would repel or attract each other and the associated optimal way of introducing the cells to the system (plating protocol) for the most desirable effect. As outlined in the general introduction, interplay between sensory fibers innervating cancer has emerged as a potentially pivotal factor in cancer spread and the onset of CIP. Preceding CIP, communication between peripheral nerves and cancer has been shown to direct local fibers towards the TME via chemoattraction, facilitated by the tumour-mediated release of cytokines and neurogenic factors (see Chapter. 1 - Figure. 2 and [20] Chapter. 8 Clinical States: Cancer Pain). This interaction can subsequently lead to abnormal axonogenesis and hypersensitivity. Approach proposed in Figure. 25, aimed to bring together sensory neurons and cancer spheroids within the single compartment nMPS technology previously published, with the goal of observing such attraction and axonogenesis/sprouting. Simultaneously, the single compartment chip was used to evaluate how DRG neurons perform in the 3D recording platform and catch a glimpse of what electrophysiological behaviour was to be expected.
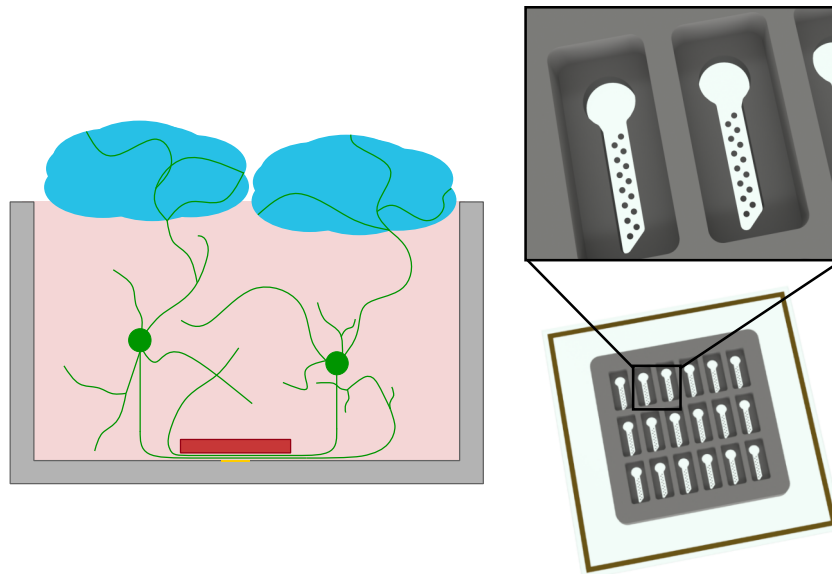
Figure. 25: Single well V19 neuron-cancer coculture design. Hydrogel-embedded DRG neurons will innervate proximal cancer spheroids on top of the gel. Using the 256-MEA 18-well chip with 14 CMEs per experiment.

Nociceptive fibers

As one of the main aims of the current work is to develop an advanced model for the study of cancer pain, it is appropriate to devote some time here to describing current *in vitro* and *in vivo* methods for measuring pain. Not only in the context of cancer but also in general pain electrophysiology, thereby aiding the understanding of basic pain-related concepts in sensory neuron recordings. Hypothesizing that this base knowledge will help comprehension of the potential changes I observe in the electrophysiology of nerves influenced by the cancers introduced to them. In the general introduction, I overviewed sensory fibers in the DRG, namely C-fibers and myelinated Aδ-fibers (Type I and II), with a brief mention of touch-related Aβ fibers. In the table below, neurons are categorized using common pain research terminology, which includes CMH (C-fiber mechano-heat-sensitive >70% [121]) and AMH (A-fiber mechano-heat-sensitive >86% [122]) or polymodal nociceptors ([20] Chapter.1: Neurobiology of Pain). As in most nociceptor studies, receptive fields (tissue areas responding to stimuli, mainly cutaneous) are often activated by both mechanical and heat stimuli – and responding fibers often also react to chemical inputs. Fibers are further divided into MSA (mechanically sensitive afferents) and MIA (mechanically insensitive afferents), where MSAs have a relatively low mechanical threshold, making it easy to define their receptive field and MIAs are slightly more elusive.

MIAs do not show direct response to mechanical stimuli but they develop a response to prolonged mechanical stimulation (tonic stimulus). Portion of MIAs are also termed silent nociceptors, as these have a very high mechanical (or absent) threshold that can be lowered during inflammation, allowing them to start firing in response to near non-noxious mechanical stimuli that previously had no effect [123]. CMHs and AMHs do not undergo a lowering of their mechanical threshold during inflammation but they can show a more intense response to already depolarizing stimuli [124]. Some of these concepts will be discussed in more detail here, as they are relevant for analyzing the effects of cancer on neuronal potential generation.

SENSORY FIBER	GENERAL RESPONSE BEHAVIOUR	ACTION POTENTIAL GENERATION	HEAT THRESHOLD / MECHANICAL THRESHOLD / CAPSAICIN RESPONSE	FUNCTION, CONDUCTION VELOCITY AND SIZE	NOCICEPTIVE POPULATION IN DRG
AΔ TYPE I (AMH) - FREE NERVE ENDINGS - THINLY MYELINATED	High heat threshold – mostly MSA – 'hot spots' for mechanical stimuli	Gradually increasing response to heat with long peak discharge latency – intense throughout the stimulus	High (>50 °C) / Low / Some, but most are insensitive [125]	Mean at 5-25 m/s with Max of 55 m/s (monkey) - pricking, pain during a sustained high-intensity heat stimulus – 1-6 μm	10% of DRG neurons – recognized by NF200, CGRP and TrkA expression [126]
AΔ TYPE II - FREE NERVE ENDINGS - THINLY MYELINATED	Low heat threshold mechanoreceptors – mostly MIA	Early (after stimulus) peak frequency and an adapting response	Low (41 – 49 °C) / High / Yes	15 m/s – sharp, signal first pain sensation from heat – 1-6 μm	10% of DRG neurons – recognized by NF200, CGRP and trkA expression
C (CMH AND C-MIA) - FREE NERVE ENDINGS - UNMYELINATED	Similar to Aδ type II – both MSA and MIA - **Extra:** Low-threshold C-fibre mechanoreceptors mediate pleasant touch	Early peak frequency and an adapting response – brisk at onset - increases with increased stimulus	Low (41 – 49 °C) / Both high and low / CMH no, C-MIA yes [25] with ~ 65-75% expressing TRPV1 [126]	< 2 m/s – burning pain sensation – 0.2-1.5 μm	70% of DRG neurons - 50% are peptidergic and express trkA and CGRP [126]
AB - ENCAPSULATED ENDINGS – THICK MYELINATION	Respond to light touch (Merkel), skin stretch (Ruffini), or vibration (Pacinian)	Do not encode stimulus intensity	NA, Low, don't express TRPV1	> 30-75 m/s – tactile - 6-10 μm	20% of the rapidly conducting Aα/β fibres are nociceptive [122]

Table. 5: Characterization of neuronal contents of dorsal root ganglia (general input from [20, 21, 24, 127]).

Differentiating nociceptive fibers in the DRG generally involves assessing conduction velocities, myelination status/fiber diameters and the various thresholds for response generation (or single-cell transcriptomes [128]). Additionally, studying how Type I and Type II Aδ and C-fibers discharge action potentials upon stimulation can further improve the understanding of individual differences. Generally Aδ-fibers respond with faster and with higher discharge frequencies than C-fibers – causing the information they provide to the central nervous system to be more robust (pricking and sharp vs. burning). In Figure. 26, using the 'teased fiber' technique (isolating nerves *ex vivo*), distinct responses to heat stimuli are observed in Type I and II Aδ nociceptors in monkeys [129]. Key characteristics of neuronal responses, namely onset latency (time to peak from stimulus), peak response (highest Hz) and response duration are analyzed through action potential (AP) frequency histograms. For a 53°C, 30-second stimulus, neurons displaying a longer peak discharge latency are classified as Type I heat responders, while those exhibiting a short latency with a peak discharge near stimulus onset are categorized as Type II. Type II heat responses are predominantly found in the MIA group, while Type I are common in the MSA group (Table. 1).

Nociception analysis & sensitization

Electrophysiological data can be shown in numerous ways. In the example comparing fiber responses, detected action potentials had been segmented into 0.2 second bins and the mean spike frequency (in Hz) was calculated per bin, for 30 seconds post-heat stimulus for the consecutively recorded neurons (Figure. 26B). However, before data can be analyzed, it needs to go through a process that generally begins with a raw continuous signal typically obtained via an electrode. This raw signal is filtered using a bandpass filter to remove signals with frequencies outside the relevant range – relevant is 1 kHz for action potentials (duration of an AP ~ 1-2 ms). Tailored algorithms are then employed to distinguish actual spikes from the background noise, providing the data for frequency (or rate) histograms (Figure. 26A). Worth noting is that the amplitude of a single neuron's action potential does not vary with stimulus strength, when the input threshold is reached the 'all-or-nothing principle' states all APs are equal. It is rather the frequency of action potentials that changes with stimulus intensity; a more intense stimulus generally prompts more frequent neuronal firing [21]. Importantly, nociceptor activity does not always correlate directly with pain perception. Low-level nociceptor discharges, for instance, may not result in pain sensation and this perception is mediated by the central nervous system (in conjunction with the periphery). Neuroimaging has elucidated the brain's perceiving " pain matrix" to include e.g., the thalamus, anterior and posterior cingulate cortex (ACC/PCC), amygdala and the periaqueductal gray (PAG), and this comprises a completely separate field of research [130].

However, highly specialized *in vivo* microneurography (recording activities in peripheral nerves like the median nerve at the wrist in awake humans [131]) and teased fiber techniques in monkeys – has facilitated comparisons of action potential discharge rates in response to nociceptor stimulation to pain ratings, suggesting a strong overlap between nociceptor activity and painfulness (Figure. 26C). Therefore, when solely observing the periphery in e.g., DRG cultures *in vitro*, it is common to consider an action potential as an output that generates pain.
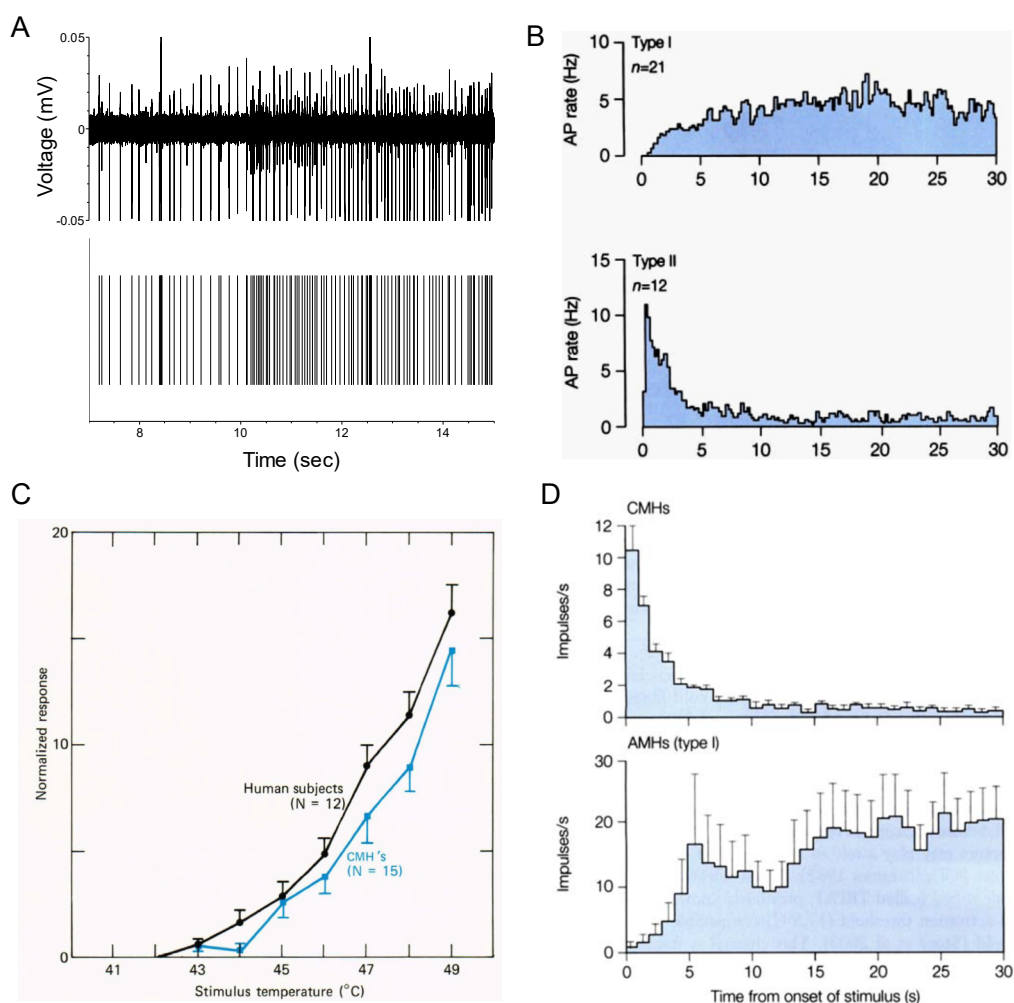
Figure. 26: Collection of key concepts and findings in nociceptor electrophysiology. (A) Filtered continuous signal from a microelectrode with counted spikes in a culture of DRG neurons (own data). (B) Type I and II Aδ nociceptors in monkey discriminating high (slowly adapting) and low (rapidly adapting) heat threshold responses. (C) Correlation between monkey C-fiber nociceptor responses and human heat pain ratings suggests C-fibers' role in sensing heat pain. (D) CMH respond to heat (53°C) similar to Type II Aδ --- Reproduced from [20] ©Elsevier (within STM Guidelines) and from [129, 132, 133] ©The American Physiological Society (license num. 501880804), The Johns Hopkins University Applied Physics Laboratory LLC and with permission from ©The American Association for the Advancement of Science (license num. 5723271330740).

Correlating stimulus input to pain generation is more complex. In the general introduction I briefly touched on a relevant pain concept, namely hyperalgesia, where there is pain sensation that is excessive in comparison to the noxious input stimulus. This follows from what is called 'sensitization', which refers to the heightened responsiveness of nociceptors. Sensitization (fiber response) lowers AP threshold, enhances AP discharge in response to noxious stimuli and can drive continuous spontaneous activity. Sensitization basically shifts the relationship between response and stimulus intensity to the left (less stim. for more response) and makes correlating stimuli strength to pain experience less straightforward. This also holds for normally innocuous stimuli – in allodynia, another form of sensitization, the perception of pain from normally non-painful stimuli (below AP threshold – indicates lowering) is enhanced (Figure. 27) [134].
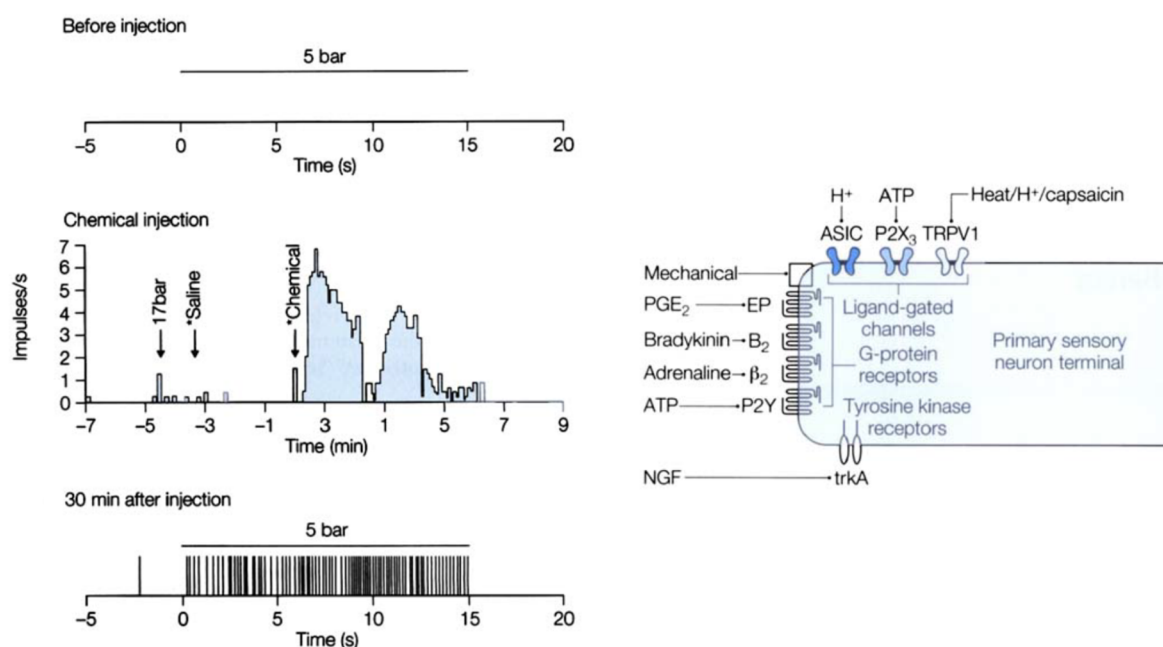
Figure. 27: Allodynia in a MIA Aδ nociceptor by inflammation induced sensitization 10-bar AP threshold fiber initially does not respond to 5-bar von Frey (mechanical stimulus). After exposure to inflammatory soup (bradykinin, prostaglandin, serotonin and histamine) – AP threshold drops to 4-bar and vigorous response is observed. Reproduced from [20] ©Elsevier (within STM Guidelines) and from [134] with permission from ©The American Psychological Society (license num. 501881669).

As depicted in Figure. 27, sensitization may be triggered by free nerve endings found within inflamed tissues, seen in the heightened mechanosensitivity of nerves within arthritic joints. Driven by chemical factors released by damaged tissues and associated inflammatory mediators,

excitability of peripheral terminals is increased via receptor binding and subsequent signaling cascades, leading to upregulated receptor expression [135]. More detailed examination of some of these exact processes will follow, but it is important to distinguish here, that focus is on peripheral sensitization, not central sensitization. Central sensitization refers to a heightened sensitivity of central pain-signaling neurons, specifically the DH neurons that share the 1st synapse with DRG neurons in the spinal cord. Well supported example of how central sensitization can occur is through 'wind-up', a process where persistent or repetitive noxious stimuli (causing excessive glutamate or neuropeptide release into the synapse) progressively amplify the firing rate of certain DH neurons [136]. In this model, primary focus is on potentially recapitulating peripheral sensitization, as I solely consider excitability and morphological alterations of pseudo-unipolar fibers originating from the DRG. Analogous to the affected functioning of free nerve endings in inflamed tissues, I set out to examine alterations in the physiology of nerves innervating cancerous tissues. Specifically, investigating a heightened responsiveness and/or spontaneous activity of these nerves when cocultured with or directly innervating cancer.

Cancer pain

Chronic pain is a prevalent issue among cancer patients and a large majority of patients with advanced disease, ranging from 75% to 90%, face the burden of chronic pain severe enough to require opioid therapy [52]. Additionally, over one-third of patients in remission continue to report pain after treatment, which could point at definitive damage to close-proximity innervation surrounding the tumour site. Currently, majority of studies on CIP have been conducted in animal models. Primarily mouse and rat models offer valuable mechanistic insights, which have proven valuable for the development of potential novel analgesics. In the study of cancer pain, it is common practice to introduce carcinoma cells into the tibia. This approach is preferred due to the ease of studying cancer-related pain in bone, as the injected cancer cells remain localized and the bone exhibits a high density of nociceptor innervation. By conducting behavioural assessments (Figure. 28A), researchers demonstrate significant increase in both mechanical allodynia (heightened sensitivity to non-painful mechanical stimuli) and weight-bearing differences (animals avoid bearing weight on the affected limb) compared to control rats [137]. These behavioural markers are often complemented by detailed electrophysiological measurements obtained through the implantation of a parylene-coated tungsten electrode in the aforementioned dorsal horn, which receives input from afferent C-fibers and A-fibers originating from the cancer-bearing limb (Figure. 28B) [138].

The results clearly indicate that rodents in the cancer condition exhibit higher frequencies of action potential discharges in response to the same type of stimuli. Nevertheless, scientists involved in these studies confirm the primary focus on central sensitization, demonstrating hyperexcitability in DH neurons. In T. K. Kaan et al. (2010) researchers additionally explored the direct interaction between cancer cells and peripheral sensory neurons using a coculture system involving MRMT-1 rat breast carcinoma cells and dissociated primary rat DRG neurons [137]. However, this work is limited to solely investigating the phosphorylation (activation) of key messengers within the peripheral signaling cascade for induction of a sensitive phenotype, not electrophysiology.

Table 1
A comparison of the mean electrical-evoked responses of lamina V dorsal horn neurones in MRMT-1-injected and sham-operated rats

	Sham	MRMT-1
Input	322 ± 40	$433 \pm 35*$
A-β	113 ± 7	116 ± 7
A-δ	89 ± 8	91 ± 8
C-fibre	359 ± 23	$430 \pm 28*$
Post-discharge	191 ± 16	$272 \pm 27*$
Wind-up	295 ± 29	376 ± 57
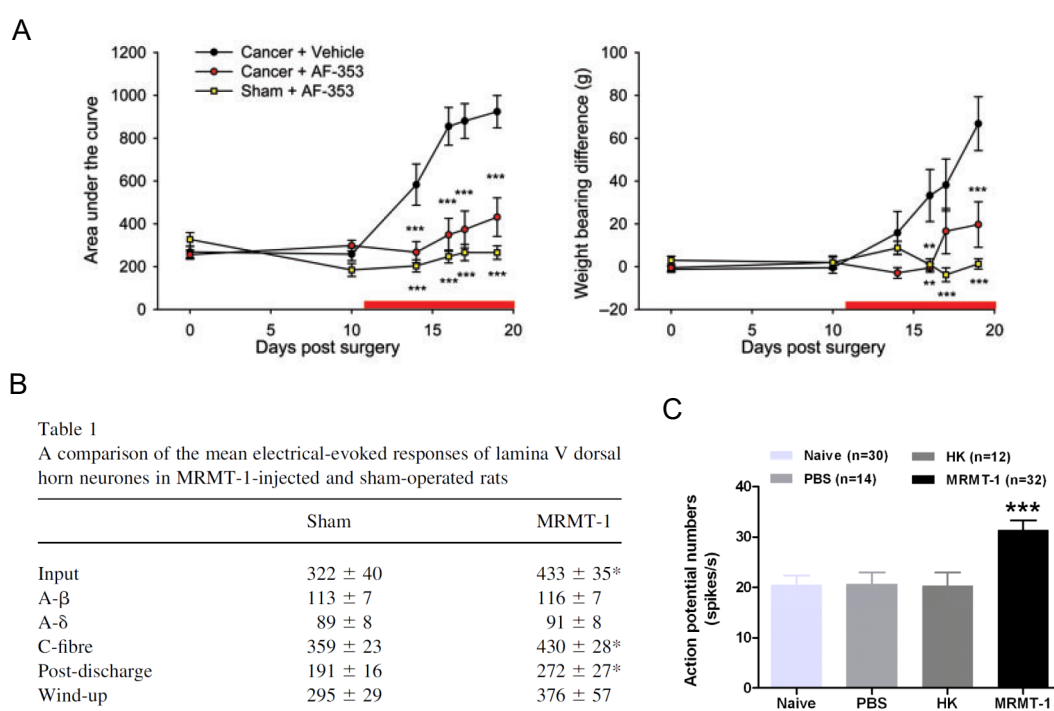
Figure. 28: Assessment of pain sensitivity in cancer through behavioural and electrophysiological methods. (A) Mechanical allodynia represented as AUC of withdrawal responses against Von Frey ([139]) filament force. Weight-bearing difference measured using a force transducer that evaluates downward force applied by each hindlimb, reflecting injury. (B) *In vivo* DH recordings of C-fiber-evoked responses, input (baseline response) and post-discharge (aftereffects of a stimulus) neuronal responses, were significantly higher in rats injected with MRMT-1 cells compared to sham-operated rats. (C) Whole-cell patch clamp recording of small-sized DRG neurons from minced DRGs 28 days post intra-tibial injection of, also, MRMT-1 cells. Reproduced from reference [137] with permission ©Oxford University Press (license num. 5725270294891), reference [138] with permission ©Wolters Kluwer Health, Inc. (license num. 5725261481273) and reference [48] (CC BY 4.0) ©SAGE Publications Inc.

Work by Zheng et al. (2012) is nevertheless highly relevant and also concordantly mentioned in the general introduction. As researcher here performed *in vitro* patch clamp recording techniques on DRG neurons associated with the site of injection of MRMT-1 cells in the rat tibial canal [48]. Zheng's study aligns closely with our own objectives, as they observed cancer-induced alterations in the electrogenic properties and excitability of DRG neurons (Figure. 28C). Alterations included a lowered depolarizing current threshold (current clamp - changes in membrane potential are recorded in response to injected current, such as a 1-second, 300-pA pulse), an increased frequency of evoked action potentials and the occurrence of spontaneous discharges. With this in mind, it should make sense that coculturing these cell types together could induce similar changes.

Furthermore, having gained a comprehensive understanding of pain related electro-physiological concepts, it is possible to anticipate certain changes in neuronal electrophysiology when combining DRG neurons with cancer in electrode-integrated cocultures. Accordingly, potential driving chemical factors released by pathological tissues, inducing excitability of peripheral terminals via receptor binding and subsequent pain signalling cascades (e.g., NGF-TrkA), will be discussed later on as they present themselves. Expected electrophysiological changes should now be noted in addendum to the anticipated changes in neuronal morphology, as mentioned in the general introduction. Reiterating these include; the guidance of fibers (rather than repelling) to the TME through chemoattraction by tumour-mediated release of cytokines/neurogenic factors and visible increases in axonogenesis / sprouting surrounding cancer tissue [47, 51]. With the single well V19 system (Figure. 25) I now attempt to initiate an observable interaction between these two cell types that is reminiscent of what is seen *in vivo*.

5.2 Materials & Methods

General overview

For direct clarification, neurons and cancers in the V19 single well device will not be cocultured with the intent of studying electrophysiology but solely for morphological assessment.
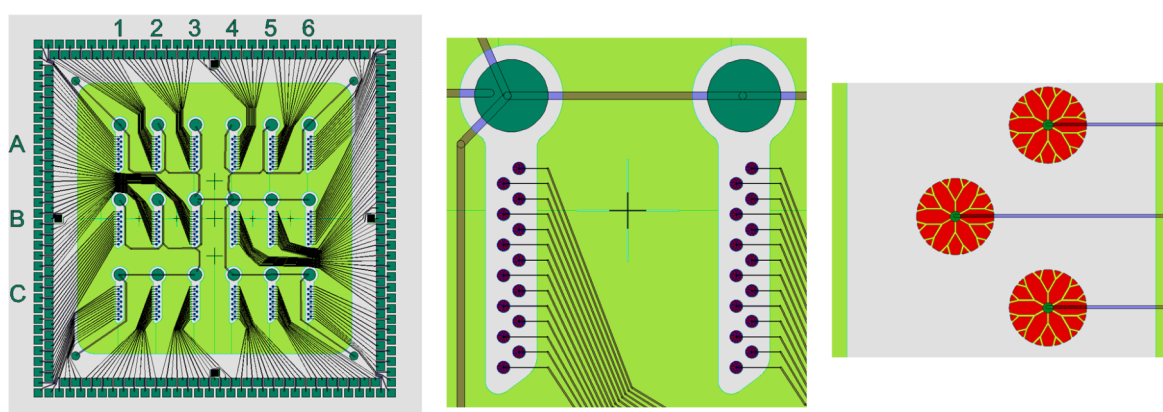

Figure. 29A: nMPS 18-Well V19 Device 256-MEA overview with 14 SU8-ADEX CMEs per well. Produced with Wieweb - Clewin 5.4.
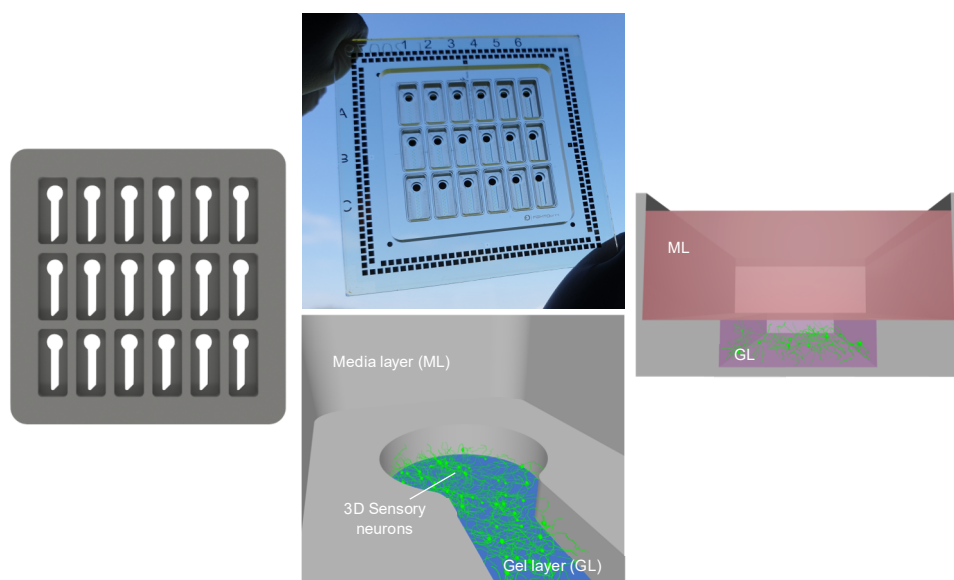
Figure. 29B: Culturing 3D sensory neurons in the nMPS bonded to the MEA substrate. It should be noted that this original setup is the basis from which the innervation approach is an extension. Reproduced from reference [71] (CC BY 4.0) ©IOP Publishing.

Single well arrangement does not provide a viable methodology for obtaining meaningful electrophysiological outputs from this coculture. However, cancer cells and neurons were brought together to investigate their morphological interactions, which provided promising and valuable insights into how to optimize culture conditions. Electrophysiology discussed in this chapter solely involves recordings from a 3D culture of DRG neurons monoculture in the V19 system. These recordings granted an understanding of the formatting and processing of electrophysiological data and how to utilize different agonists, such as capsaicin, to induce action potential generation. Due to the extensive characterization of this device previously [71], I provide a concise recapitulation here without delving into detailed descriptions (Figure. 29).

DRG isolation and plating
DRG neurons were extracted from spinal ganglia as previously outlined (see Chapter. 2 Materials & Methods). After resuspending cells collected from centrifugation in Neurobasal-A with GlutaMAX, SM1, N2 Supplement, 0.5% Penicillin-Streptomycin and 100 ng/ml Nerve Growth Factor 2,5S (Promega, #G5141) at the desired concentration, they are mixed with Matrigel® (1 : 4 ratio or 75%) to stand. conc. of 500-750 cells/µL (2000-3000 cells/µL before mixing). To ensure efficient filling of microtunnels and channels with hydrogel when extruding ≈ 8.5 µL DRG-mix with the tip placed inside the keyhole basin, the assembled glass-MF chip is similarly hydrophilized with air plasma. Cells are seeded in the single channel and monitored for outgrowth.

MEA-based electrophysiological recordings

Electrophysiology of 3D sensory neurons was recorded using a MEA2100-System (Multi Channel Systems MCS GmbH, Germany) with a headstage for 256 electrodes at 5 days in culture. During experiments, a customized MEA incubation chamber (Okolab Srl., Italy) was used to continuously monitor temperature, CO_2 and humidity (Figure. 30). Temperature was set to 36◦C, humidity at 85% and CO_2 at 5%. MEAs were allowed to acclimate inside the MEA chamber before applying agonists and inflammatory mediators to the axonal compartment. Recordings were acquired using MC_Rack v. 4.6.2 (Multichannel Systems MCS GmbH, Germany) and filtered using a fourth-order bandpass filter (60-6000 Hz), before processing with NeuroExplorer (version 5.300) for spike detection and further analysis. Details of electrophysiological data processing will be discussed in association with the results obtained.
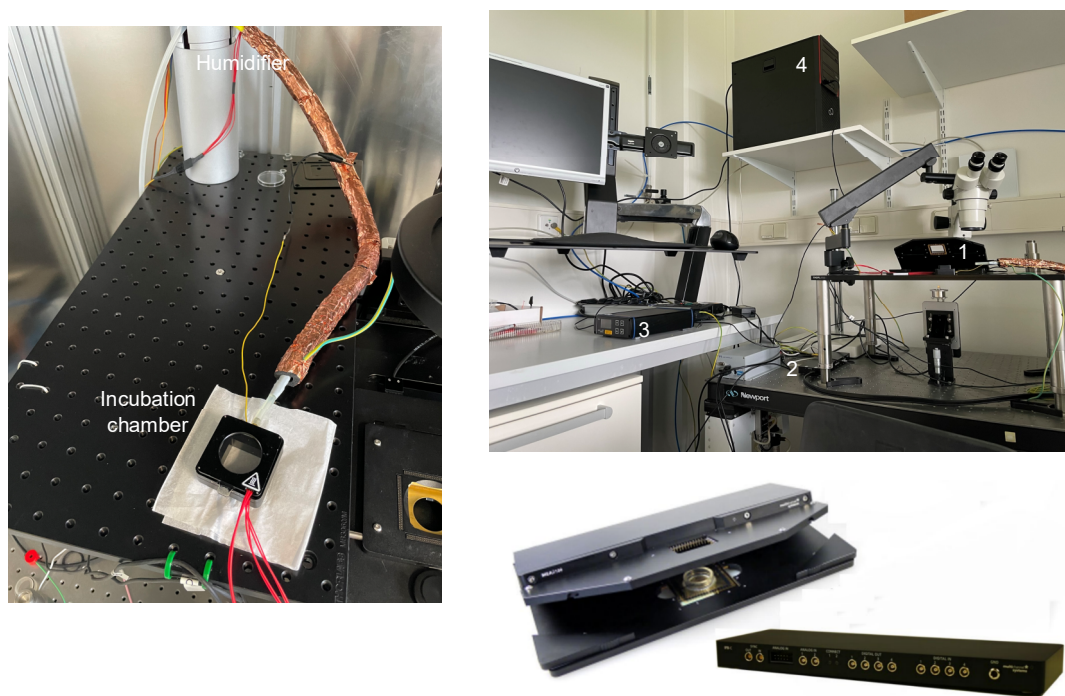
Figure. 30: Electrophysiological recording setup. 1. Headstage equipped with 256 electrodes and amplifier (sampling frequency of 50 kHz per channel – ideal for neural recordings) 2. Interface board with integrated signal processor. 3. Temperature controller TC02 guarantees constant temperature conditions for the biological sample, placed on the MEA. 4. PC with monitor to directly visualize recorded signals. ©Multi Channel Systems MCS GmbH. All rights reserved.

Cancer spheroid culture preparation for coculture

Human colorectal adenocarcinoma (ATCC, #SK809) and human pancreatic carcinoma (ATCC, #CRL1469) cells were grown in McCoy's 5A medium (Gibco, #16600082) and Dulbecco's Modified Eagle's medium (Gibco, #11965092), respectively, both supplemented with 10% Fetal Bovine Serum (Gibco, 10499044) and 1% Penicillin-Streptomycin (Sigma, #P4333). Cells were seeded onto uncoated T75 flasks at a density of $1.0 * 10^6$ cells per flask (Figure. 31). On spheroid formation day, cells were detached with Trypsin-EDTA 0.25% (Sigma, T4049) for 3 min at 37 ∘C, enzymatic digestion was then blocked using DMEM (Gibco, 31966-021) with 10% FBS and cells were spun down before resuspending in complementary cancer media.
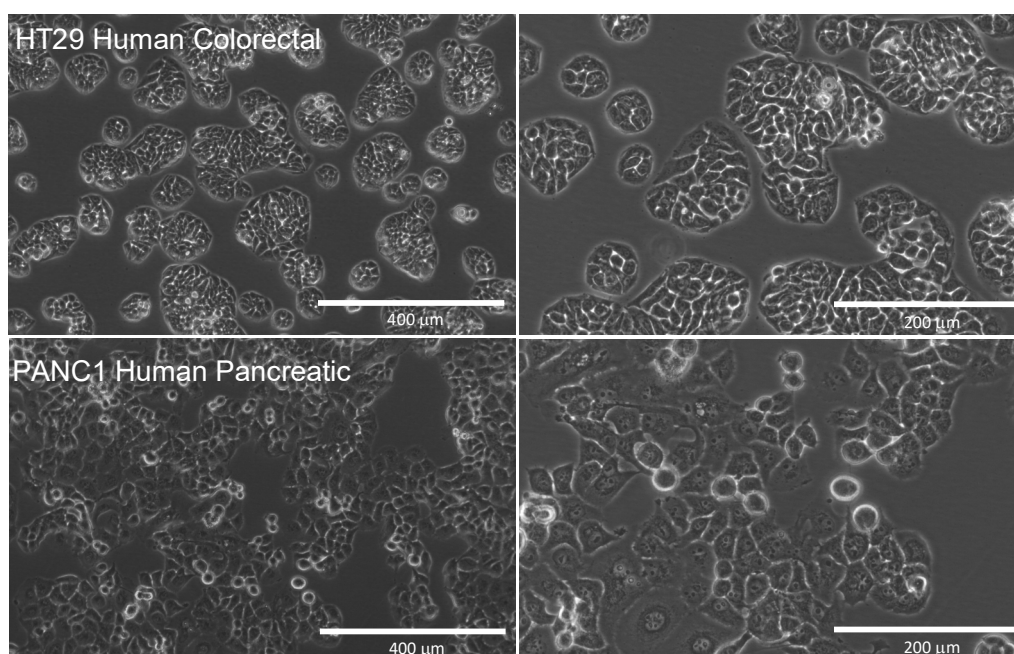
Figure. 31: HT29 Human Colorectal adenocarcinoma and PANC1 Human Pancreatic carcinoma cultured on T75 flasks.

Spheroids are generated in Thermo Scientific™ Nunclon™ Sphera™ low-attachment surface 96 Well Plates (Thermo, # 174927). As an example calculation – I count $1.36 * 10^6$ per mL in 10 mL (75-cm^2 plate or T75 flask of HT-29 colorectal adenocarcinoma cells). Where, per well – consider adding 50 µL solution into each well containing the desired amount of 1000 cells – for a total of ~ 50 wells. 50 wells x 50 µL = 2500 µL needed (calculate 3000 µL) 3000 µL – 44.1 µL → add 2955.9 µL complete media and homogenize. With this master mix I then make serial dilutions to plate appropriate conditions as illustrated in Figure. 32.

µL	Cells
50	1 000 (needed)
1000	20 000
1000	1.36E6 (counted)
14,7	20 000
3000	2.08E6
3 x 14.7 = 44.1 (cell suspension)	60 000 (mix)
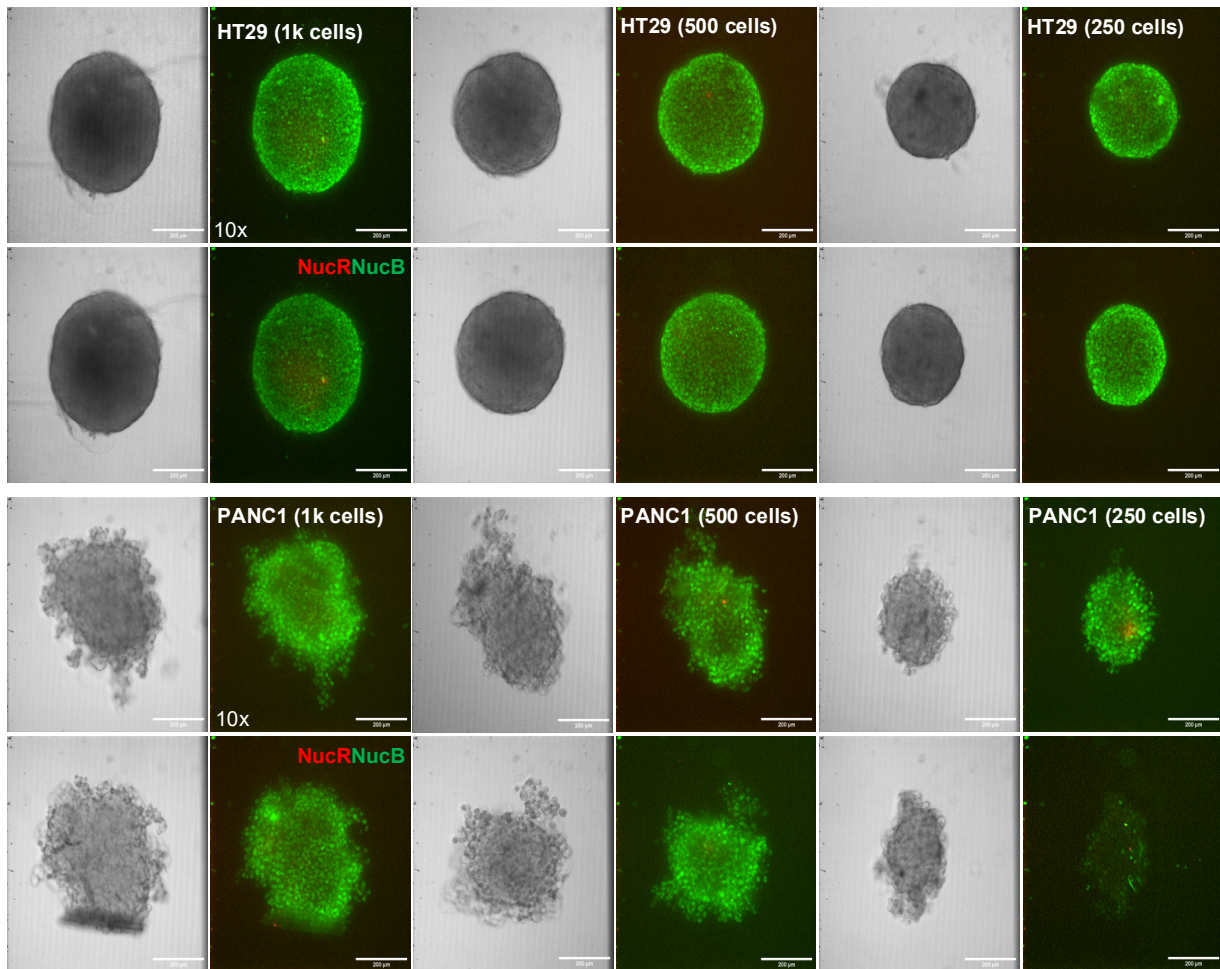
Figure. 32: Spheroid development at 5 DIV (plating on 0 DIV) from cancer spheroids generated with 1000 cells, 500 cells and 250 cells of HT29 and PANC1. Cancer spheroids stained for nuclei (NucBlue - green) and dead cells (NucRed - red).
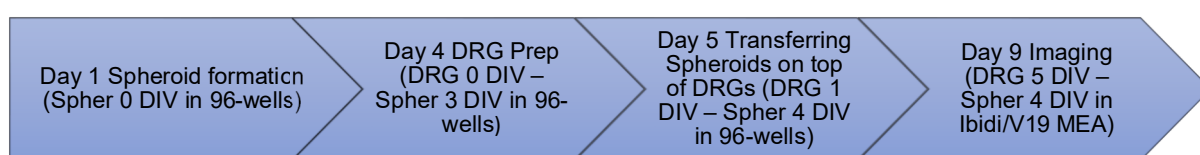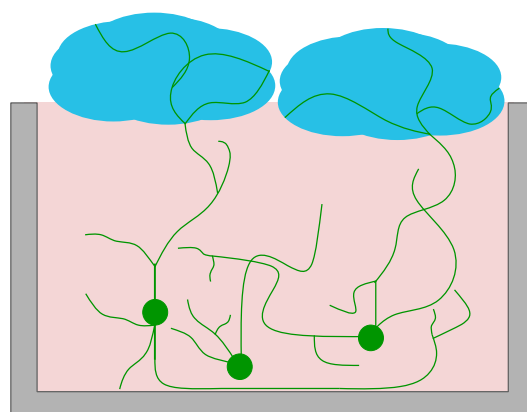
Coculture plating

For imaging and fine-tuning the dissociated DRG neurons & Cancer Spheroid coculture, I generally use μ-Slide 15 Well 3D (formerly μ-Slide Angiogenesis) plates from Ibidi GmbH, Germany. These plates allows me to generate a gel layer / media layer arrangement similar to our INV-MPS. Protocol for aligning cancer spheroid generation with DRG neurite outgrowth is as follows, briefly. On day 1, I form spheroids in low-attachment 96-well plate (Spher 0 DIV). On day 3, I prepare the enzymes and media for the DRG neuron preparation on day 4. On day 4, the spheroids have now grown for 4 days (Spher 3 DIV) and will be transferred on top of the neurites one day after plating (DRG 1 DIV). Similar to the 'DRG neuron monoculture', I prepare my neurons in complete Neurobasal-A (culture media) and mix them with Matrigel® inside an Eppendorf tube at 500-1000 cells/μl (2000-4000 cells/μl before mixing). Ibidi plate holds approximately 10.0 μL of the DRG-mix, which is plated at room temperature with a concentration of 800 cells/μl (3200 cells/μl before mixing) before the addition of 50.0 μl of Neurobasal-A to the media layer. On day 5, I transfer the spheroids on top of the DRG neurons (DRG 1 DIV in Ibidi - Spher 4 DIV in 96-Well plate). At 4-5 DIV in Ibidi, I then perform confocal fluorescence imaging.

Imaging

At 4-5 DIV I perform confocal fluorescence microscopy using a spinning disk head Zeiss Cell Observer® System (20x/10x objective) equipped with ZEN software (blue edition, ZEISS) followed by image-processing with open-source image processing software, FIJI (ImageJ, http://imagej.nih.gov/ij/). To excite the AAV1-eGFP, I used an Alexa Fluor 488 laser and generated Z-stacks of 2x2 tilescans with the Plan-Apochromat 20x/0.8 M27. Spheroids are visualized by pre-incubating the coculture before imaging with (90 min at 37◦C) of NucRed Dead 647 ReadyProbes™ Reagent (TO-PRO-3 iodide) (Invitrogen, #R37113) for dead cells and NucBlue Live ReadyProbes™ Reagent (Hoechst 33342) (Thermo Fisher, #R37605) for all nuclei.

5.3 Results & Discussion

General

As stated in the introduction to this chapter, objective was to enhance understanding of sensory neuron electrophysiology (literature study), monitor the interaction of nerve fibers and cancer tissue, and potentially recapitulate electrophysiological characteristics of neuron-cancer crosstalk described in literature. However, it was quickly discovered that the method of coculturing neurons and cancers in a single well (V19) for the purpose of studying both morphology and electrophysiology was impractical. Concerns will be elucidated in both sections of the results.

Furthermore, with the single well nMPS device available, opportunity was seized to assess the performance of DRG neurons in the 3D recording platform and gather direct insights into the electrophysiological fingerprint of evoked responses. Concise overview of the associated generation and processing of electrophysiological data is provided here, noting that this workflow is similar for later iterations of MEA-integrated sensory neuron cultures. Therefore, detailed description here also serve as in depth background for electrophysiological content included in the INV-MPS chapter.

DRG neuron electrophysiology

Data is captured, analyzed, graphed and reviewed using the Multi Channel Suite (MC_Rack), developed by MCS GmbH. Illustrated below, raw data obtained from the MEA2100 recording system, processed through a high pass filter (100 Hz). Filtered data is then presented, showing signal streams for 14 CMEs within a single well (total of 18 wells).
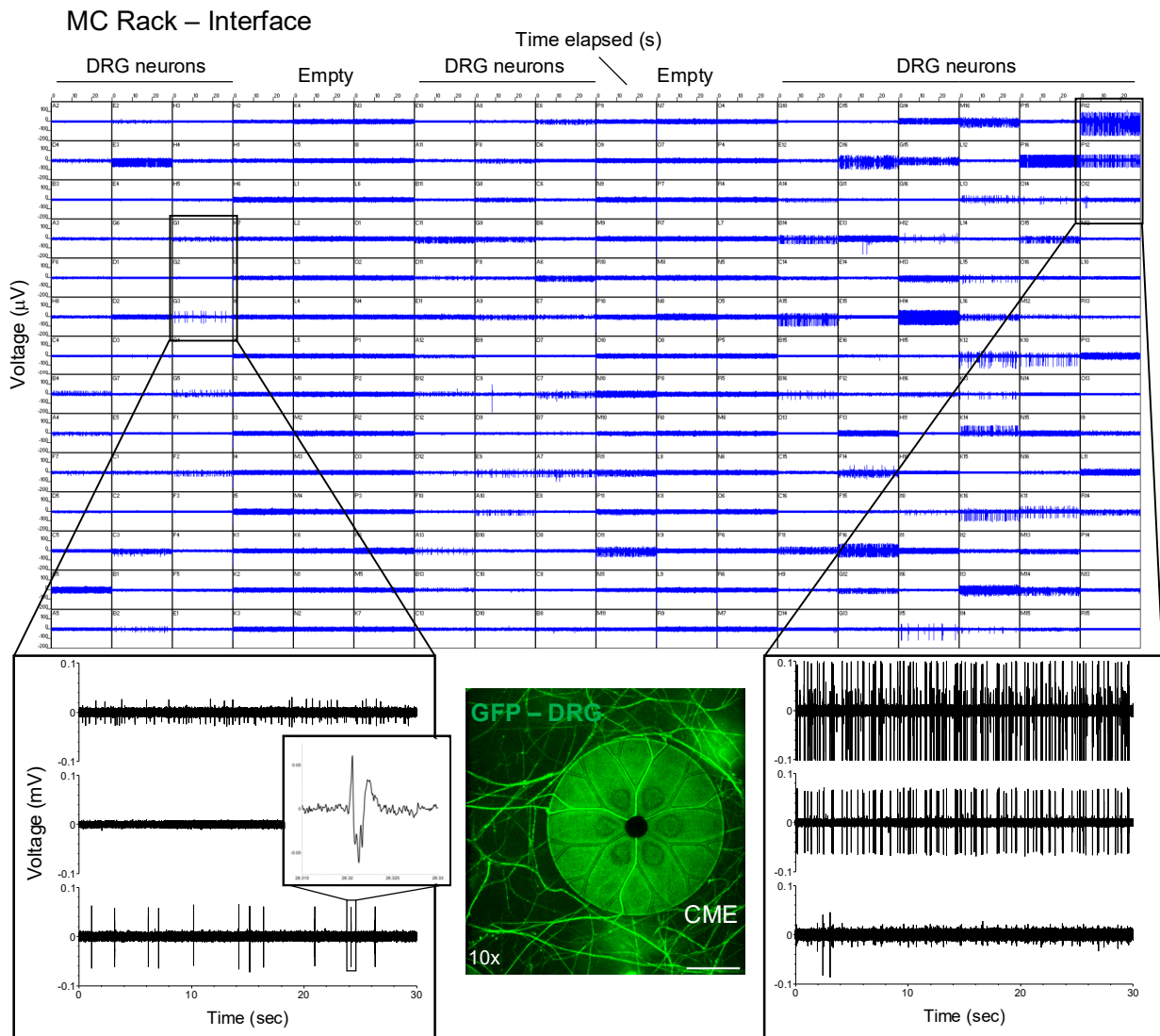
Figure. 33: 18-Well 256-MEA MC Rack user-interface with 14 SU8-ADEX CMEs per well. DRG neurites grow inside CMEs enabling the resolve of spontaneous and evoked action potentials. GFP-transduced DRG entering CMEs (scale bar: 75 µm.)

As discussed in the previous chapter, when evaluating neural recording data, one commonly assesses the SNR. SNR is dimensionless ratio and calculated using the formula [140]

$$SNR = {}_{Variance}Spike \, / \, {}_{Variance}Noise \qquad (5)$$

where,

$$Variance \, (\sigma^2) = \, \Sigma(\pm \, Peak \, amplitude)^2 * 1 \, / \, N \qquad (6)$$

Variance of spikes (σ^2_{spike}) and noise (σ^2_{noise}) is calculated by taking the average of selected squared signal amplitudes. In this case, since I generally observe a spike amplitude between ±50 to ± 100 microvolts (zoom from Figure. 33) and noise amplitude between ±10 to ± 20 microvolts, the variance can be simply computed as follows:

$$\sigma^2_{spike} = [(50^2 + (-50)^2) \, / \, 2] = (2500 + 2500) \, / \, 2 = 5000 \, / \, 2 = 2500 \, \mu V^2 \, (or \, 10000 \, \mu V^2)$$

$$\sigma^2_{noise} = [(10^2 + (-10)^2) \, / \, 2] = (100 + 100) \, / \, 2 = 200 \, / \, 2 = 100 \, \mu V^2 \, (or \, 400 \, \mu V^2)$$

$$SNR = 2500 \, / \, 100 = 25$$

SNR based on a signal amplitude of ±50 microvolts and a noise amplitude of ±10 microvolts equals 25. Obtained SNR is not as high as initially predicted by the electrophysiological model generated by colleagues at the Max Planck Institute. Spatially constricted membrane currents inside CMEs supposedly resulted in spike amplitudes exceeding 250 microvolts for SNR of 62.5 with similar noise levels [71]. However, it is still encouraging to observe that results compare favorably to existing literature on 3D recordings from neuronal cultures using microelectrodes. In a particular study, signal amplitudes ranging from 100 to 400 microvolts and noise levels of 10 to 20 microvolts were reported, but the requirement was for the cell body to be attached to the electrode surface [75]. Therefore, it is remarkable that satisfactory SNR recordings solely from neurites is obtained, without the need for cell soma attachment.

Interestingly, a degree of spontaneous activity in certain wells was observed, with electrodes even capturing action potentials from multiple spontaneously firing sensory neurons (Figure. 33). One might attribute this activity to the presence of 100 ng/mL NGF (promotes survival and aids phenotypic specifications of sensory neurons [20]) in the culture, as chronic NGF treatments have been known to induce hyperexcitability in adult rat DRG neurons *in vitro* [141]. However, in later chapters, minimal to no spontaneous activity with similar levels of NGF present is generally observed. This suggests that in 3D cultures of mouse DRG, induction of sporadic spontaneous activity can be attributed to NGF levels, but pathologically high seeding densities (single compartment) and/or media quality (refresh rate) should also be considered influential. Moreover, in culturing relatively young DRG neurons with NGF, consensus is it that NGF can sensitize the responses of nociceptors to capsaicin or noxious heat during postnatal development. With studies demonstrating that rat DRG neurons acquire sensitivity to the hyperalgesic effects of NGF between postnatal days 4 – 10, but do not generally become hyperactive [142]. Consequently, in order to generate an action potential, neuronal activity commonly still need to be evoked through the application of a noxious stimulus.
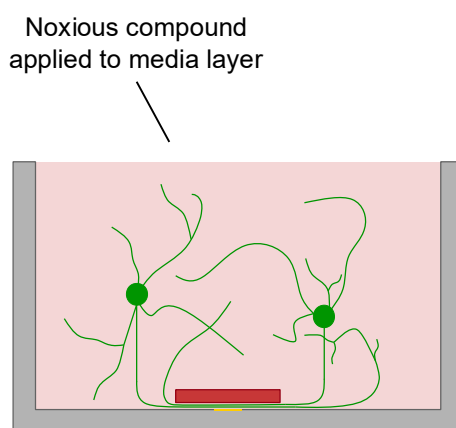
Figure. 34: Excitatory compounds are applied to the media layer atop the 3D nerve terminals, as seen in Figure. 29B
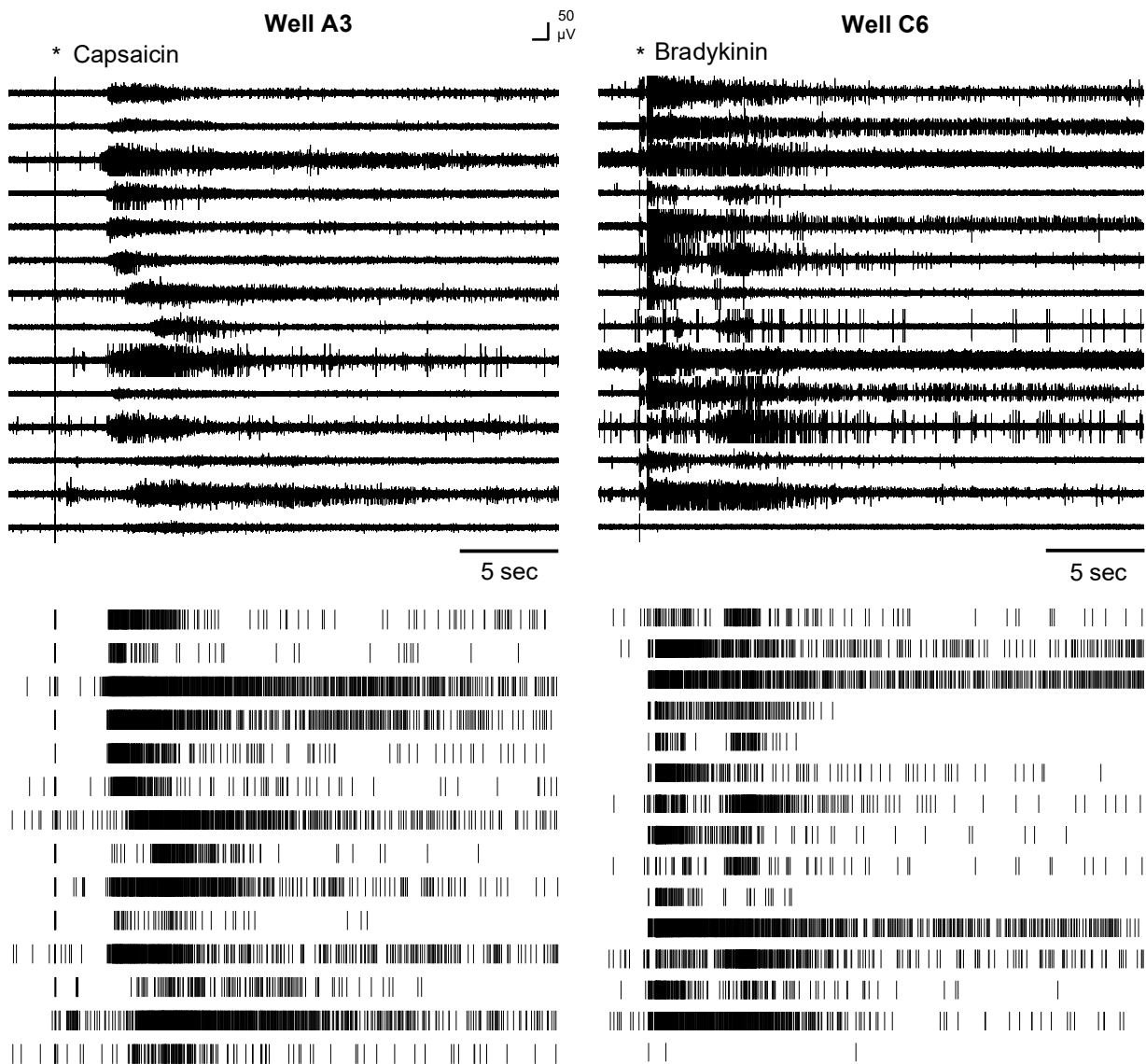
Figure. 35: Trace plots depicting the activity recorded by 14 CMEs after the application of 1.0 µM Capsaicin (indicated by a black asterisk) and 8.0 µM Bradykinin. Raster plots indicate the discerned individual spikes from the filtered signals within the 25 seconds surrounding the application.
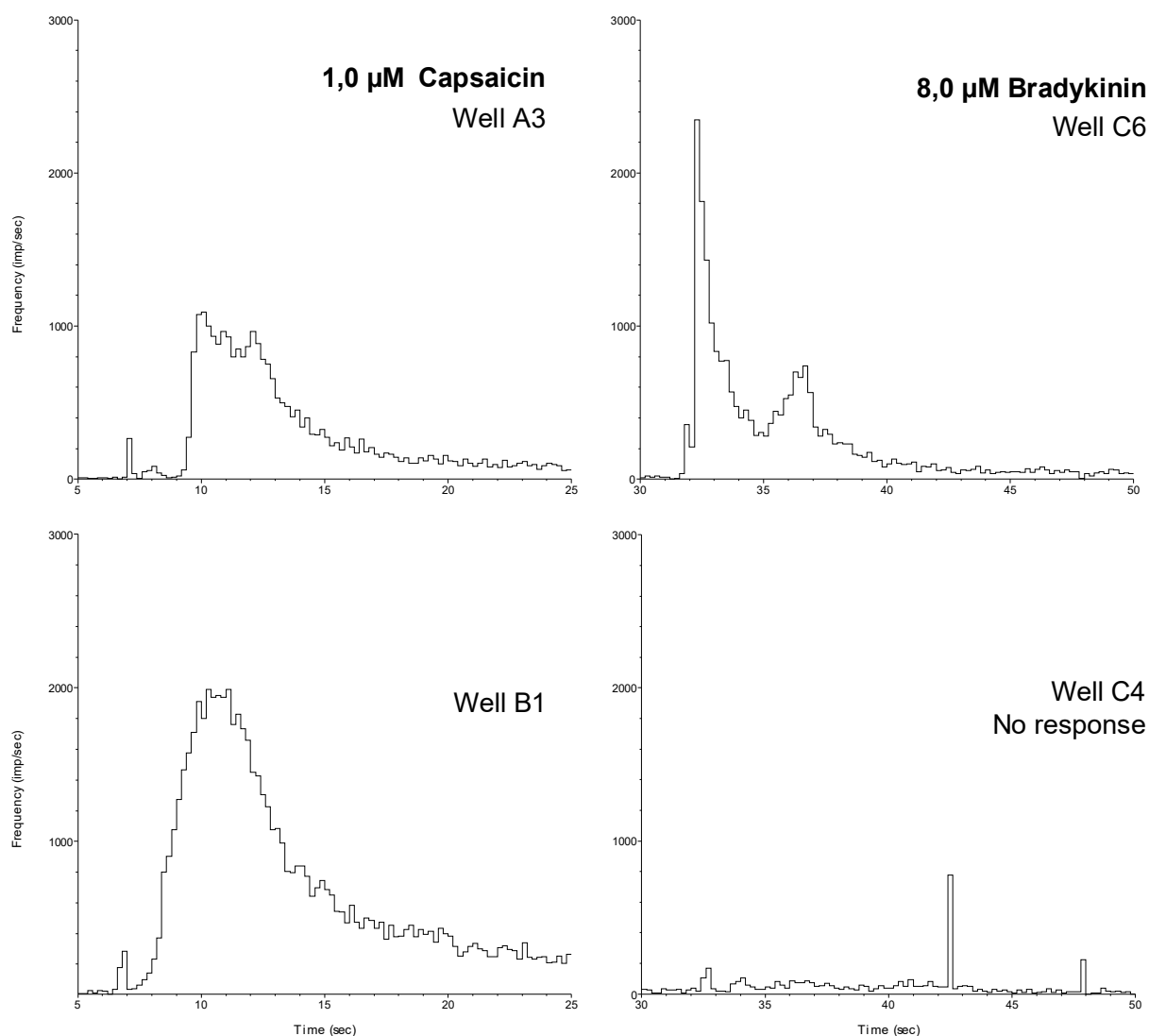
Figure. 36: Rate histograms show temporal dynamics following application with detected action potentials segmented into 0.2 second bins with mean spike frequency (Imp/s or Hz) calculated per bin (similar to Figure. 26).

In the introduction, I mentioned the responsiveness of nociceptors to various chemical stimuli, particularly capsaicin. Capsaicin belongs to the capsaicinoid family and is the active component responsible for the "heat" or tingling sensation experienced when consuming chili peppers. Table. 5 highlights the presence of a capsaicin response in a portion of both unmyelinated C-fibers and Type II myelinated Aδ-fibers, through expression of the capsaicin receptor known as TRPV1. Capsaicin acts as an agonist for the ligand-gated nonselective cation channel TRPV1, binding to

this receptor on the free nerve endings of sensory afferents and triggering a burning sensation. As mentioned in the general introduction, the research conducted by Prof. Julius suggests that TRPV1 undergoes structural rearrangement upon capsaicin binding or activation by noxious heat [35]. Rearrangement then facilitates the influx of ions such as Na^+ and Ca^{2+}, depolarizing the neuron and leading to the generation of an action potential in nociception. Bradykinin is recognized as a powerful endogenous substance responsible for inducing pain and acting as an inflammatory mediator [143]. It is produced at sites of injury or inflammation through the release of proteases from mast cells and basophils. Effects of bradykinin are mediated by specific receptors, namely B_1 and B_2 (as shown in Figure. 27). It has been observed that bradykinin has the ability to elicit acute pain by depolarizing the cell membranes (particularly through increasing membrane permeability to Na^+ ions) and increasing the firing of action potentials [144].

During the assessment of cocultures, three key metrics for evaluation of responses obtained are typically considered. Metrics include the CME-occupancy development, correlated to the percentage of electrodes with DRG neurons responding to stimuli (assessed by presence of a burst – train of >4 spikes longer than 0.02 s), the total number of spikes recorded per electrode within a 60-second timeframe after application, and the overall number of spikes recorded per well (Figure. 35). In addition, by examining the rate histograms (Figure. 36), one can extract information such as peak AP frequencies and temporal dynamics, providing further insights into the neuronal activity patterns. For the capsaicin response 42/42 electrodes responded across the 3 wells tested, giving a 100% response rate with an average of 642 spikes ± 233 (SEM) per electrode for the 60-sec post application. Average spikes recorded per well was 8994 spikes ± 3262 (SEM). In comparison, for the bradykinin response 28/42 electrodes responded across the 3 wells tested, giving a 67% response rate with an average of 273 spikes ± 43 (SEM) per electrode. Average spikes recorded per well was 2622 spikes ± 821 (SEM). Generally signifying a high degree of responsiveness to both compounds which gives us a strong comparative readout for future coculture applications. Frequency histograms of evoked activity show the presence of peak response at approximately 1000-2000 Hz per well (avg. 70-140 Hz per electrode with potentially multiple occupying neurons), directly after the stimulus. From this, it can concluded that average total well responses exhibit a characteristic pattern observed in unmyelinated C-fibers and Type II myelinated Aδ-fibers, as described in the literature (Table. 5). Displaying an initial peak frequency shortly after the stimulus, followed by an adapting response.

However, working with a mixed population and each well holding 14 CMEs means different types of DRG neuron can occupy individual CMEs, which can be closely examined by analysing the differences between individual trace plots (Figure. 35). Furthermore, it is also essential to highlight that when culturing DRG neurons (rather than performing *in vivo* electrophysiological experiments) myelination status of my neuronal population is lost. As a result, it becomes challenging to distinguish between different types of nociceptors based solely on their response profiles, especially concerning e.g., conduction velocity, which is permanently altered for Aδ-fibers without myelination. Key insight gained from this experiment is that the application of noxious compounds can be used to quantify and compare the responses of DRG neurons in cocultures with cancer. Additionally, both compounds act on TRPV1, either directly or through downstream effects on secondary signalling pathways [35, 143]. Therefore, enhanced TRPV1-evoked responses during inflammation and/or influenced by factors released within the TME (such as NGF, prostaglandins and H^+) might be registered [20]. However, there are clear limitations to the single well model with regards to being able to accurately delineate cancer-induced alterations in neuronal electrophysiology. In addition, biomimicry is significantly compromised when both the soma of DRG neurons and their free nerve endings are exposed to cancer, as cancer cells should only directly interact with the nerve terminals. In the next part of this results section, efforts at mitigating this issue by partially separating the cell types are discussed.

Rationale behind separating the soma and nerve endings also includes the spatial variation of specific receptors and ion channels on the neuron's surface [20, 21]. Coculturing both cell types in a single well does not effectively facilitate establishing potential links between observed changes in DRG electrophysiology and the (receptor-ligand binding induced) changes in morphological parameters observed in innervating' nerve terminals. As mentioned, morphological parameters include; increased fiber density surrounding the tumour tissue and the sprouting/arborization of tumour-associated nerve terminals [41-45]. In a single well, it will be challenging to derive conclusions about alterations in fiber arrangement based off obtained morphological data as guidance of fibers is solely in a condensed Z-plane and effective standardization of culture parameters is hampered (spheroid placement matters, 3D DRG distribution matters etc.). Keeping this in mind, promising interaction observed between nerve endings and cancer spheroids in cocultures is demonstrated here. These findings drove us forward with regards to what is possible from a biological standpoint in this setting and shaped the path towards a compartmentalized model that captures the same interaction, in a more electrophysiologically relevant platform.

DRG neuron innervating cancer spheroids

Main focus of the shortcut exploration of cell-cell contact was on understanding whether nerve fibers and cancers would repel or attract each other (and if so, what that would look like) and identifying the optimal method of seeding the cells inside the system What greatly facilitated analysis and fine-tuning of coculture conditions, was utilizing the μ-Slide 15 Well 3D plates from Ibidi GmbH. Plates enabled quick evaluation and refinement of the coculture setup. Through experimentation, technique was devised of "sinking" the DRG neurons to the lower 3rd of the hydrogel matrix in which they are embedded. By adjusting the temperature-dependent crosslinking parameters of Matrigel® during the plating process, it was possible to establish a culture environment where DRG soma were partially separated from their nerve terminals, as intended (Figure. 37).
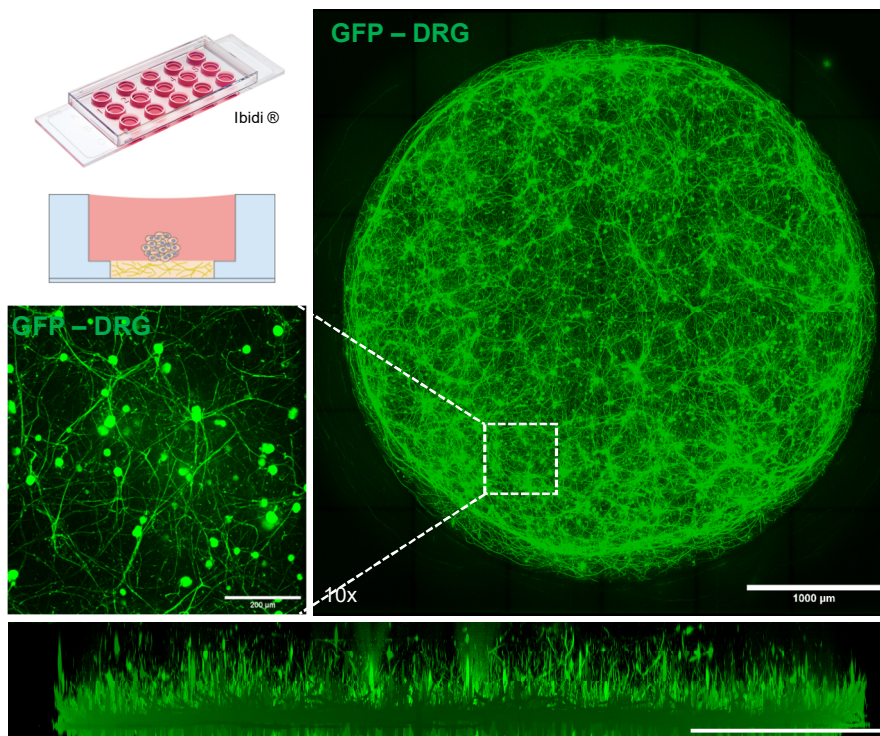
Figure. 37: 2.5D DRG neurons within the Ibidi® gel-plates. Specific geometry consists of a 4.0 mm well within a 5.0 mm well. Allows pipetting a 0.8 mm thick gel layer, supported by a proximal media layer. DRG neurites extended upwards towards the gel-liquid interface. Providing opportunity for interaction as the cancer tissues settle on top. ©IBIDI GMBH. All rights reserved.
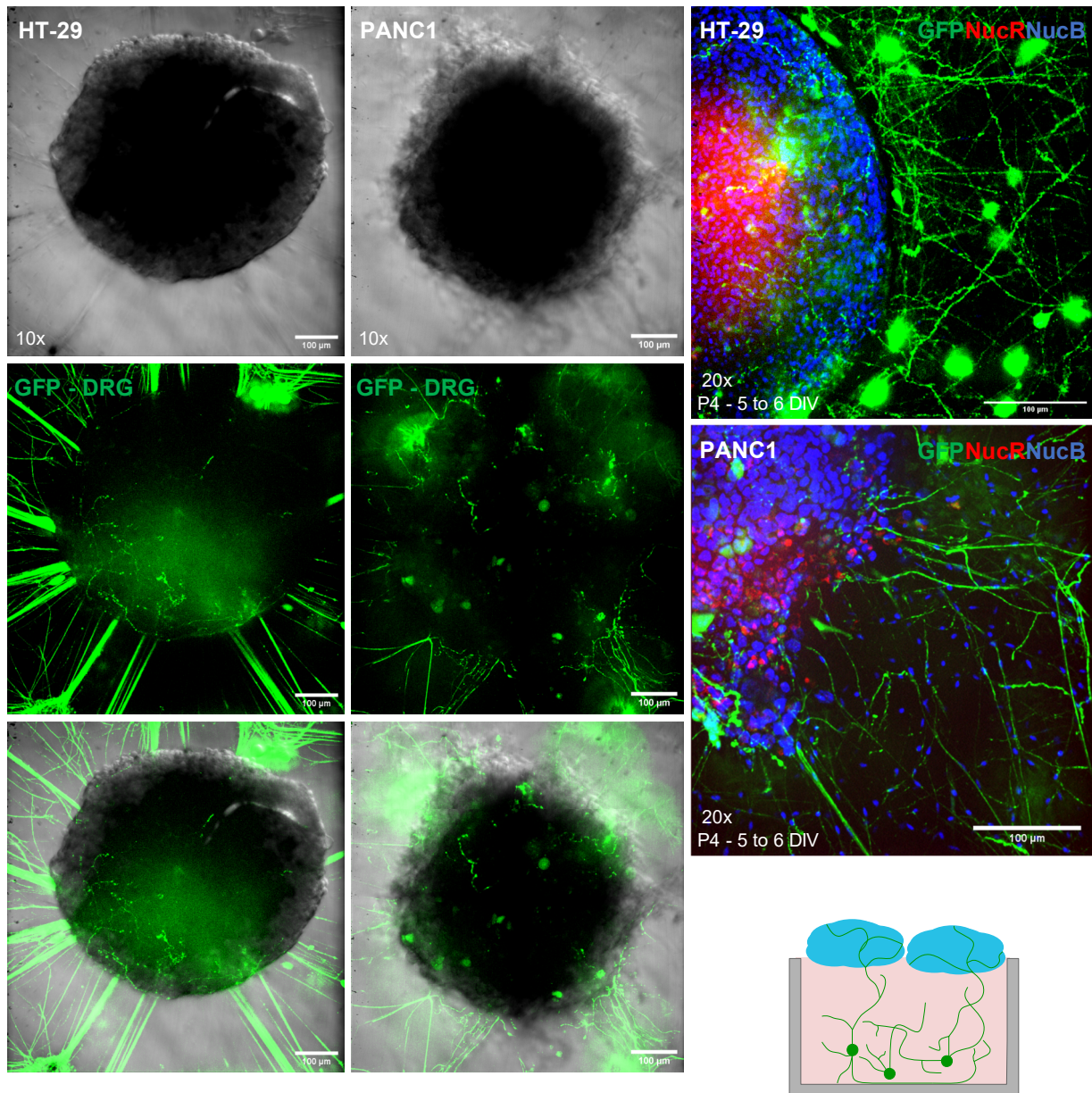
Figure. 38: Sensory nerve fibers innervate cancer spheroids at the gel-liquid interface. Both HT-29 and PANC1 spheroids attract nerve terminals to explore their surface and sporadically breach to grow inside them. DRG transduced with AAV1.Syn.EGFP (green) and cancers stained for nuclei (NucBlue - blue) and dead cells (NucRed - red)

An important foundation for the expectations regarding the interaction between cancer and sensory terminals is derived from the research conducted by Prof. Mantyh from the University of Arizona. Mantyh and colleagues presented clear evidence for sensory fiber sprouting and arborization associated with tumour-bearing limbs [51] [47]. In Figure. 38, a demonstration is

provided of similar phenomenon seen in the 3D cocultures. Instead of the sensory nerve terminals extending naturally, a fascinating behaviour was observed. Upon contacting cancer spheroids, the nerve terminals exhibited an almost stochastic growth pattern, showing characteristic crackling sprouts both on the surface and inside the cancer cells spheroids. Indicating that rather than cell-types simply crossing paths and continuing undisturbed, a real interaction is taking place that shapes the neuronal outgrowth. Additionally, looking at the colorectal cancer spheroids (HT-29), nerve fibers even form fasciculations (thicker parallel bundles) directed towards the cancer spheroids.

Studying the peripheral sprouting/directed growth of sensory terminals resulting from nerve-tissue interactions is a complex area of research that has traditionally relied on *in vivo* methods. For instance, scientists have looked at changes in nerve bundle proliferation, fiber sprouting and innervation density by immunofluorescent imaging of wounded skin (cutaneous) or diseased organ tissue biopsies [12, 145, 146]. In Prof. Mantyh's work, in bone cancer, techniques such as micro-computed tomography (µCT) are similarly combined with confocal immunofluorescence imaging of cancer-bearing limbs to locate and visualize the morphological changes induced by the tumour microenvironment in the associated fibers. Highly labor-intensive in nature and difficult for conducting larger studies on uncovering what this really means with regards to increases in localized pain and hypersensitivity. Furthermore, there is a scarcity of high-content, high(er)-throughput methods (in comparison to animal models) that can modulate these types of interactions to aid in drug discovery. Observing that current *in vitro* platform recapitulated what is seen *in vivo* confirms that this system can prove to be a counterpart to *in vivo* study of nerve-tissue interactions.

Obvious next step of realizing the same biological interplay in the single well nMPS with integrated electrodes, as shown in Figure. 25, turned out to be unfeasible due to the mismatch between the device's geometry, the plating protocol, and the physiological constraints of saturating a single well with both cell types. In Figure. 29A-B, the gel-layer geometry and the CMEs distributed along the surface are indicated, however overlaying the entire gel layer with spheroids of a specific size whilst following a standardized protocol brings difficulty. Spheroids end up misplaced, leaving me questioning whether obtaining a physical interaction (as observed *in vivo*) was possible. Also, due to the inability to systematically cover the 3D neurons with spheroids, some neurons were exposed to more foreign tissue than others, creating a non-uniform heterogeneous model of limited utility. Lastly, the limited supply of media now supporting both cell types, resulted in the rapid accumulation of catabolites, despite refreshing the media daily. It was observed that the

acidification of the liquid due to the rapid accumulation of waste, relative to the volume, ultimately indicated this was not a viable method for meeting morphological and electrophysiological endpoints. But it did, again, provide a clear glimpse into complex cancer-neuron crosstalk.
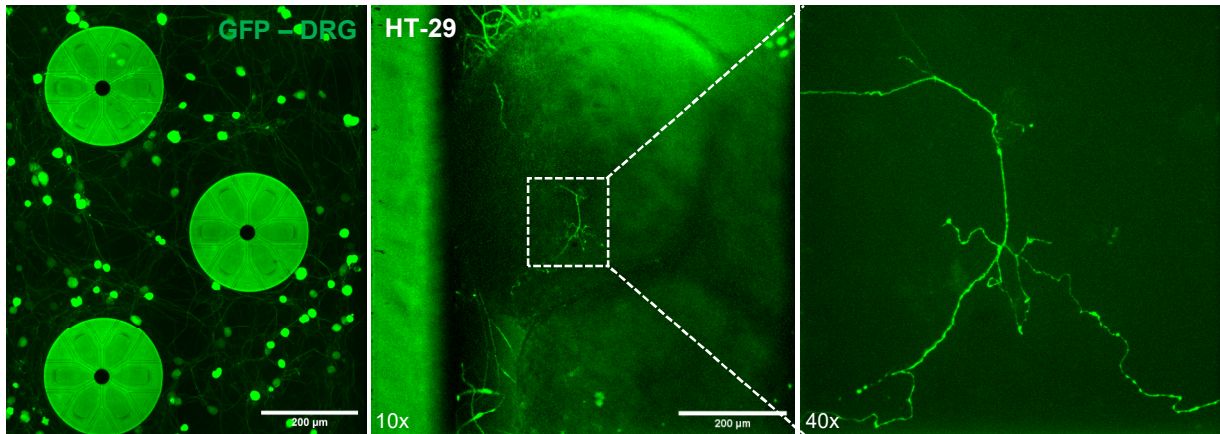
Figure. 39: Ratio of innervation to availability of cancer spheroids appears unfavorable in the MEA-nMPS platform. Only few neurons were able to establish contact with the spheroids. Some crackling sprouting of sensory fibers penetrating the cancer spheroids was observed, demonstrating dynamic interaction in the tumour microenvironment.

Encountering a lack of progress in the CME-inspired separating barrier approach (Chapter. 3 & 4), I opted to streamline the model and concentrate on replicating the biology with a more straightforward model. Now, with single well 3D (cancer-)sensory neuron culture findings analyzed, I returned to the separating barrier integrated coculture, commonly employed in the field of *in vitro* sensory neuron research [57, 58]. As mentioned, throughout this research I have always explored the direct integration of raised microtunnels (not continuous with the well-bottom) into the glass barrier and postulated a compatible recording approach. In the next chapter, I come to a consensus regarding the utility of combining CMEs with barrier-etched microtunnels with the added input generated from guiding sensory fibers towards the periphery by using (and rethinking) neurotrophin gradients in 3D. Development of the monolithic INV-MPS (SLE INV-MPS or IMGchip), a 3D-printed glass device, enabled me to rapidly improve and tune neurite outgrowth, employing NGF as a chemoattractant. This provided the understanding needed to effectively transition to the final MEA-integrated INV-MPS, considering that these higher-complexity devices are not as suitable for iterative improvement of culture parameters as simpler monolithic platforms.

Chapter 6: Monolithic Imaging Chip (IMGchip / SLE INV-MPS)

6.1 Introduction

Throughout this research, integration of microtunnels directly into the glass barrier starting ~100 μm (z-axis) from the substrate, has been investigated. Difficulty of this approach is finding a compatible recording setup, as incorporating microelectrodes along the barrier base is not possible in the absence of open tunnels to accommodate them. In Figure. 40 fluorescence microscopy data showcases the outcomes of seeding DRG neurons in various iterations of these 'Innervation Chips', generally featuring two compartments separated by a barrier with vertically spaced rows of etched microtunnels. Through collaboration with partners at FEMTOprint SA, I fine-tuned the parameters of the barrier and tunnels. However, degree of neurite outgrowth through the separating barrier into the axonal compartment remained relatively unpredictable. Seemingly straightforward approach of increasing microtunnel dimensions did not always result in a higher neurite count in the axonal compartment and additionally led to unfavourable crossing of non-neuronal cells. Resultingly, I found myself consistently balancing the relationship between outgrowth related phenomena and microtunnel parameters.

Key insights that facilitated improvement of observed neurite outgrowth in barrier-integrated chips came from observing cultures in monolithic glass innervation chips with a single row of tunnels at substrate height (tunnels continuous with well surface). These chips were created to function as a full glass copy of hypothetical geometry of MEA-integrated devices with electrodes located inside microtunnels underneath the separating barrier (as discussed in Chapter. 3 - Figure. 9). Producing this system enabled rapid improvement of methodology for guiding sensory fibers towards the periphery by rethinking/testing neurotrophin gradients in a 3D context – proving pivotal in this research.

Previously, the significant role of the interaction between the tropomyosin kinase A receptor and nerve growth factor (TrkA – NGF) in the induction of hyperexcitability in nerve fibers innervating diseased tissue has been emphasized. In this section, key findings related to TrkA-NGF and specifically *in vitro* and *in vivo* literature that discusses neuronal growth and guiding of peripheral nerve terminals will be highlighted.
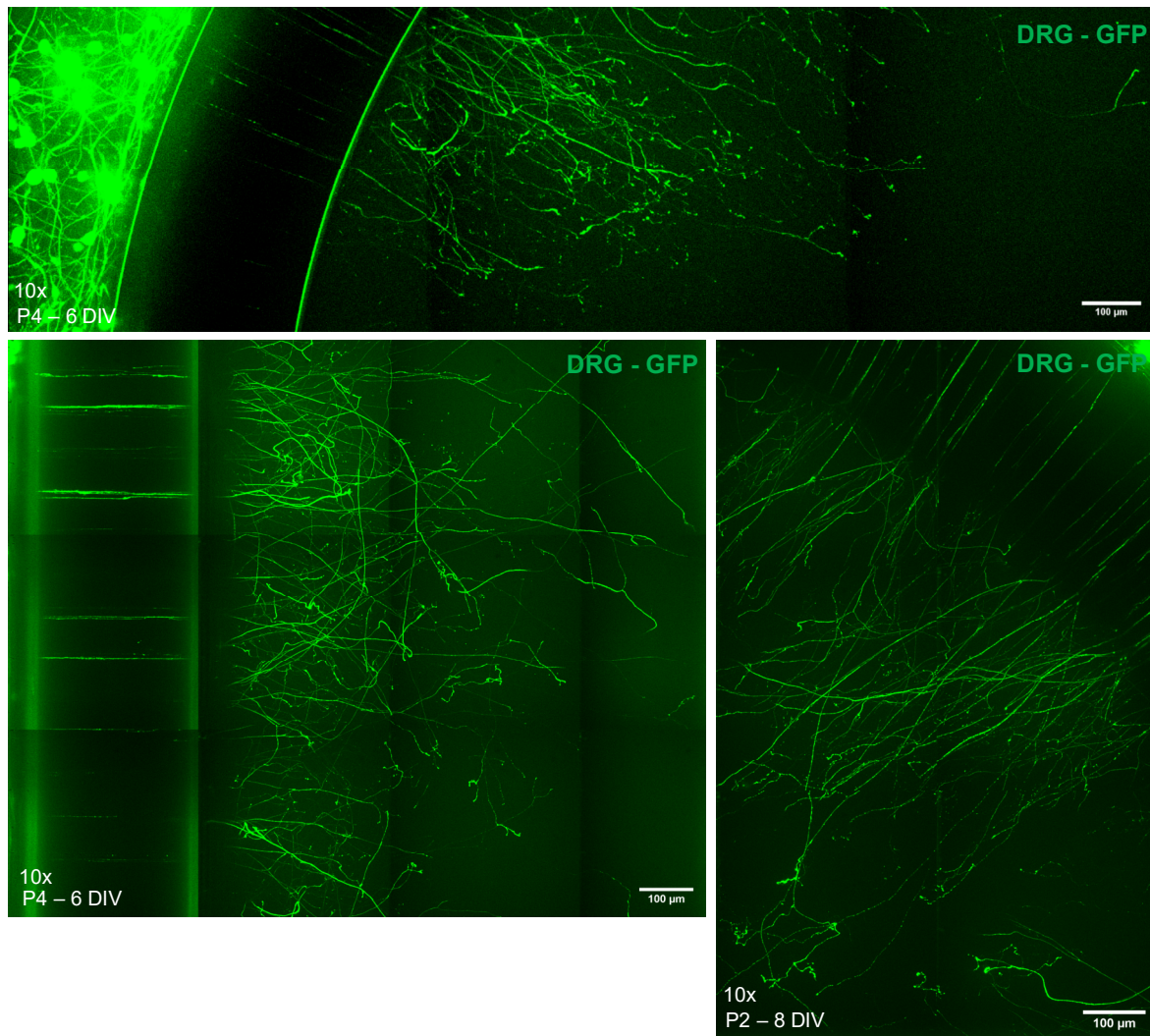
Figure. 40: DRG neurons seeded inside various Innervation Chips (or INV-MPSs). Fused silica microfluidic chips are bonded to a glass substrate via either epoxy adhesive or use of a thin coating of PDMS for fusion following plasma treatment.

NGF-TrkA

Neurotrophins play a central role in regulating aspects of neuronal development, including differentiation, survival, axonal and dendritic growth and synaptic plasticity. [147]. Most well-known neurotrophic factor is NGF (13 kDa protein), which was initially isolated from the mouse submandibular gland. Other members of the neurotrophin family include neurotrophin-(3/4/5/6) and BDNF (Chapter. 3 "Inflammatory mediators/modulators of pain" [20]). In the case of NGF, it binds to the TrkA receptor on nerve endings, leading to tyrosine kinase homodimerization, auto-phosphorylation and activation of downstream second-messenger cascades (Figure. 41) [148].

Cascades induce distal signalling and drive the transcriptional regulation of nociceptor genes involved in aforementioned processes. In parallel, NGF binding to TrkA triggers endocytosis of the complete ligand-receptor complex, followed by retrograde transport in endosomes to also exert nuclear effects [149]. Multiple studies have shown that approximately 40% of DRG cells express the NGF receptor TrkA and these cells are primarily of small diameter, indicating their role in pain sensing (also Figure. 41). Concordantly, animals lacking NGF or TrkA genes are born without nociception-associated CGRP and substance P-expressing small-diameter neurons [150].
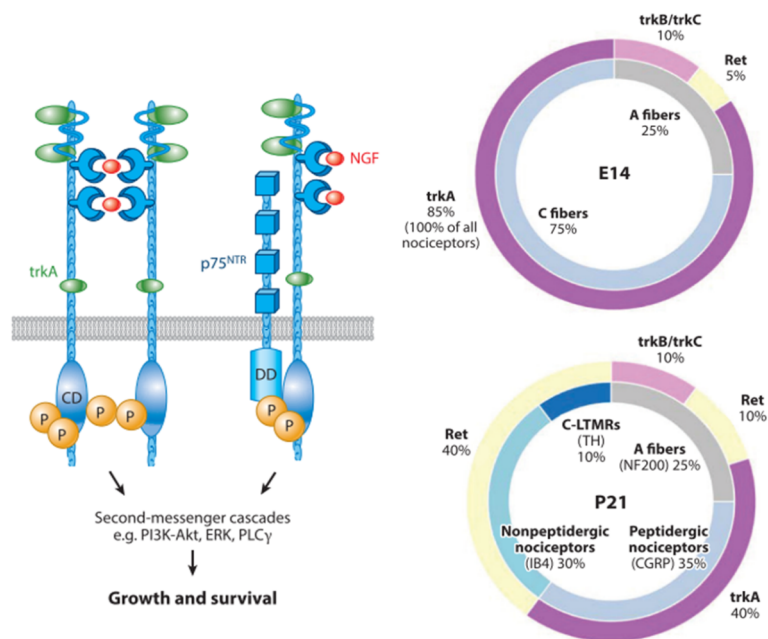
Figure. 41: NGF-TrkA ligand-receptor activation and receptor expression dynamics. p75 neurotrophin receptor (p75NTR) modulates survival/cell death response to NGF, working in conjunction with the Trk receptors. Majority of DRG neurons and all nociceptors require NGF for survival during development (E14), but lose dependence 1–2 weeks postnatally in rat or mouse. After birth, shifting towards GDNF (Ret receptor) expression, with half of the nociceptors losing TrkA expression and reducing their reliance on NGF. Reproduced from [148] with permission ©Annual Reviews (license num. 1449122-1).

During embryonic development, the realization of appropriate innervation in peripheral targets like e.g., bone and skin, involves NGF-dependent neurons receiving trace amounts of NGF from tissues, proportionate to the required innervation density [151]. Accordingly, transgenic mice overexpressing NGF in skin show increased nerve bundles and fibers (CGRP-reactive) throughout [152]. NGF in the epidermal target tissue-controlled innervation through neuronal

survival as transgenic mice showed 26 to 117% increase in cell counts compared to control mice. Interestingly, in adult mice, sensory neurons no longer rely on NGF for survival but remain responsive to its effects, enhancing the outgrowth of sensory axons *in vitro* [153, 154]. This suggests that the shaping of the innervation profile of specific tissue starts off relatively logical (pruning excessive innervation through apoptosis) but can later be affected by changes in neurotrophin solely driving neurite extension/guidance.

Changes in neurotrophin levels can be brought on by disease, as I previously discussed, as NGF-levels have been shown to rise in inflamed tissue. As demonstrated by Kinkelin et al. (2000) studying skin biopsies from patients with contact eczema [155], affected skin showed increased lengths of GAP43-positive (marker for axonal growth cones) nerve endings in both epidermis and dermis with elevated local NGF-content. Similarly, in the context of bone cancer pain, the previously mentioned work of Prof. Mantyh points at a mechanism involving tumour-mediated factor release modulating NGF-TrkA and 'hyperinnervation' [11, 47, 51]. Blocking NGF-TrkA pathway, in their setup, was highly efficacious for attenuating associated skeletal pain (proving its implication), but the exact contribution of nociceptor sprouting/hyperinnervation to chronic pain is still new territory [148]. However, what is well-known is the direct role of NGF in signalling cascades phosphorylating and trafficking specific receptors like e.g., TRPV-1, enhancing sensitivity to capsaicin and H^+ [156].

Building upon this existing knowledge of neurotrophin-mediated nerve guidance and input from various 2D microfluidic compartmentalization techniques for monitoring neurite outgrowth (see Chapter. 1 – Table. 2) [56, 57, 59], it was decided to employ the chemoattractive effects of NGF to induce the outgrowth through the separating barrier filled with polymerized Matrigel®. Interestingly, Matrigel® also contains a small amount of NGF that can potentially support some survival and growth [89]. In addition, I explored the potential of cancer-secreted neurotrophins (or other chemoattractive compounds) to mediate innervation by conducting further experiments, detailed in the Materials & Methods.

Furthermore, it is important to emphasize that conducting an in-depth analysis of molecules secreted by the cocultured tissues that induce a response in close proximity sensory fibers is beyond the scope of this thesis. While NGF, as well as other neurotrophins such as BDNF and GDNF, may be involved, a comprehensive exploration of implicated mediators would require detailed content analysis and multiple protein-based assay tools. Primary focus of this work is on the development of the platform itself and, therefore, such endeavours are currently not pursued.

6.2 Materials & Methods

SLE INV-MPS overview

Imaging INV-MPS (IMGchip) (Figure. 42), also known as the monolithic glass chip or imaging chip, developed in collaboration with FEMTOprint SA, shares general principles with the 9-well INV-MPS, outlined in Chapter. 4. Significant distinction lies in the fusion of the substrate and culture chambers, which allows the device to be utilized repeatedly (no bonding required), following a rigorous cleaning protocol as indicated in Molina-Martinez et al. (2022) [71]. Additionally, devices are now produced from a 5.8 mm thick glass sheet which enables increasing the media volumes supporting the GL (kept 1.0 mm x 1.0 mm).
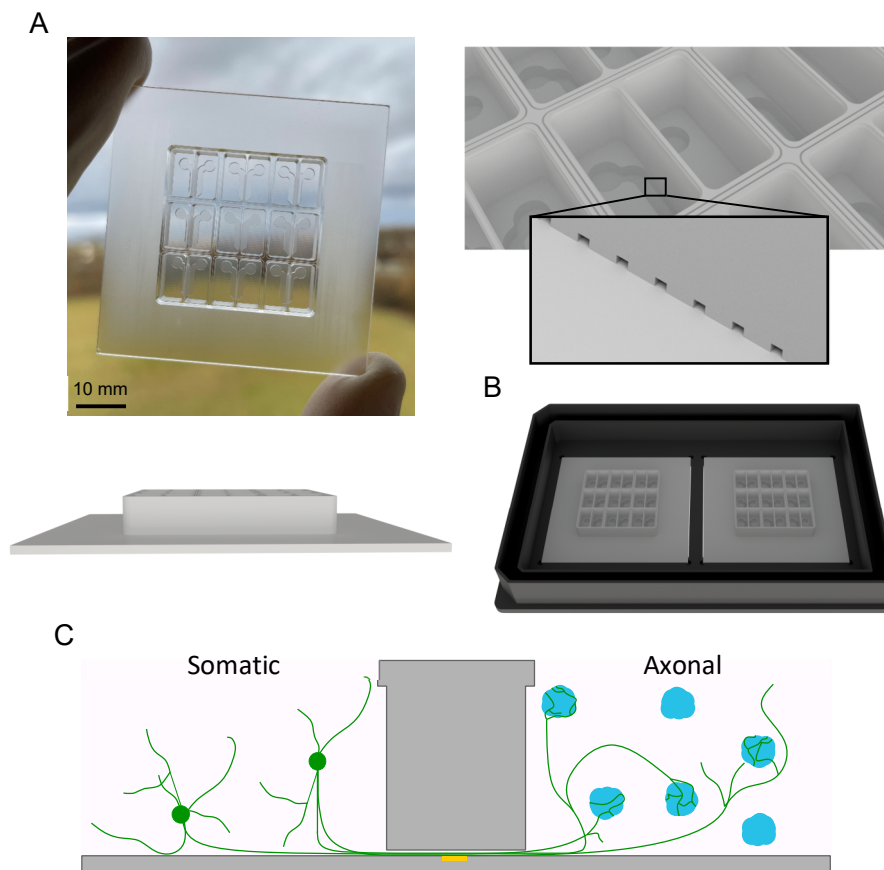
Figure. 42: Imaging INV-MPS overview. (A) 9 innervation experiments with GL ~8 µL and a ML ~110 µL within a compartment. A notable advancement compared to previous monoculture-focused studies was the incorporation of a thin 300 µm barrier containing a single row of over 100 microtunnels spanning ~4.0 mm. (B) 384 well microplate adaptor. (C) Microtunnels dimensions are 10 x 10 µm and feature no electrodes.

Neurite outgrowth

Primary DRG neurons are plated following standard protocol of isolation and dissociated mentioned previously (see Materials & Methods - Chapter. 2). Live-confocal fluorescence microscopy is performed on GFP-transduced neurons in 3D after 5 days and 7 days in culture, while reducing inter-chip variability as much as possible by imaging inside the 384 well microplate adaptor produced by Weerg Srl. (Italy), keeping 2 devices under humidity / CO_2 and temperature control (Figure. 42B). Neurobasal-A culture medium either contains no NGF (-/-), NGF in both somatic and axonal media compartments (+/+) or NGF only in the axonal media compartment (-/+) (100 ng/ml Nerve Growth Factor 2.5S). Neurite outgrowth assays quantification is performed on maximum intensity projections of 100 slices (AAV1-eGFP Alexa Fluor 488 - z-axis with 0,75 µm spacing – 20x) for 3 randomly selected ROIs (700 µm x 700 µm) starting at substrate-height. For each ROI, intensity profiles of vertical lines were plotted at 100 µm, 300 µm and 500 µm distance from distal tunnel exits and a 'Find Peaks' algorithm was then applied that returns the number of maxima (representing neurites – after background subtraction)

(available from https://github.com/tferr/Scripts#ij-bar/)

Cancer spheroid culture preparation

Human colorectal adenocarcinoma (ATCC, #SK809) and human pancreatic carcinoma (ATCC, #CRL1469) cells were grown in McCoy's 5A medium (Gibco, #16600082) and Dulbecco's Modified Eagle's medium (Gibco, #11965092), respectively, both supplemented with 10% Fetal Bovine Serum (Gibco, 10499044) and 1% Penicillin-Streptomycin (Sigma, #P4333). Cells were seeded onto uncoated T75 flasks at a density of $1.0 * 10^6$ cells per flask. On plating day, cells were detached with Trypsin-EDTA 0.25% (Sigma, T4049) for 3 min at 37 ◦C, enzymatic digestion was then blocked using DMEM (Gibco, 31966-021) with 10% FBS and cells were spun down before resuspending in designated cancer media. Distinction in these neuron-cancer coculture experiments compared to previous approaches is that I do not generate pre-formed spheroids prior to seeding the SLE INV-MPS devices. Instead, cancer cells are seeded as individual cells and allowed to aggregate and form cancer (micro) spheroids. This offers several advantages, including greater control over the homogeneous distribution of cancer cells within the well to avoid spatially biasing the system to certain channel section. It also allows the formation of smaller spheroid clusters with improved viability, minimizing the occurrence of necrotic cores that could negatively impact the culture conditions. Cell suspensions were counted using a NucleoCounter NC-200, mixed with Matrigel® 1 : 4 for stand. conc. of 500 cells/µL (2000 cells/µL before mixing) and kept cold while preparing SLE INV-MPS devices.

For neuron-cancer coculture experiments – after dispensing 8.5 μL of DRG solution into the proximal compartment, either HT-29 or PANC1 cell solution was dispensed into the distal compartment at RT and left to polymerize to ensure optimal 3D distribution. 100 μL cancer media w/wo NGF (100 ng/mL) was then added on top in the media layer and cells were closely monitored throughout the week to qualify their aggregation into cancer spheroids (Figure. 43). 3D cultures were maintained up to 1 week, by adding fresh medium every day (50/50) until imaging readout. Neuron-cancer cocultures undergo pre-incubation (2 drops/mL - 90 min at 37◦C) with NucRed Dead 647 ReadyProbes™ Reagent (TO-PRO-3 iodide) (Invitrogen, #R37113) for dead cells and NucBlue Live ReadyProbes™ Reagent (Hoechst 33342) (Thermo Fisher, #R37605) for all nuclei.
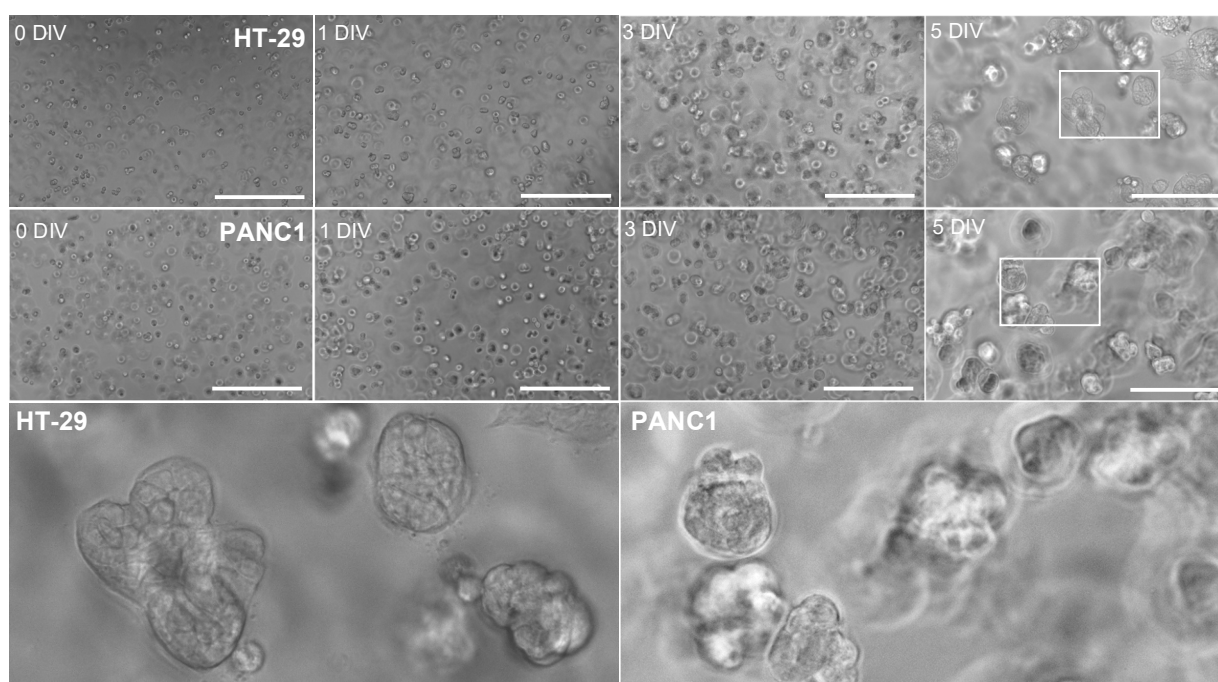
Figure. 43: Culturing dispersed cancer cells to (micro) spheroids. Gray scale images taken with EVOS® FL Cell Imaging System (Thermo, Germany) on the day of plating (0 DIV), 1 DIV, 3 DIV and 5 DIV for both HT-29 and PANC1 human cancer cell lines. (Scale bar: 400 μm.)

Statistical analysis

Statistical analysis was performed on the collected data using GraphPad Prism 8 developed by GraphPad Software Inc. (Boston, USA). For neurite outgrowth assay, conditions are represented as bar graphs with mean ± SEM. Differences were assessed by Brown-Forsythe and Welch's ANOVA test with post-hoc test Dunnett T3 ($n<50$) for comparison of means. Asterisks denote statistical significance as follows: *p < 0.05; **p < 0.01; ***p < 0.001; ****p < 0.0001.

6.3 Results & Discussion

NGF-gradient enhances neurite guidance

Before analysing the NGF-outgrowth data presented here, it is important to acknowledge that the next chapter, presenting the INV-MPS findings, incorporates content from this IMGchip (SLE INV-MPS) study. Results obtained with the IMGchip align with the electrophysiological data derived from the MEA-integrated official INV-MPS, contributing valuable morphological insights into the observed interaction between cancer cells and neurons in both devices.
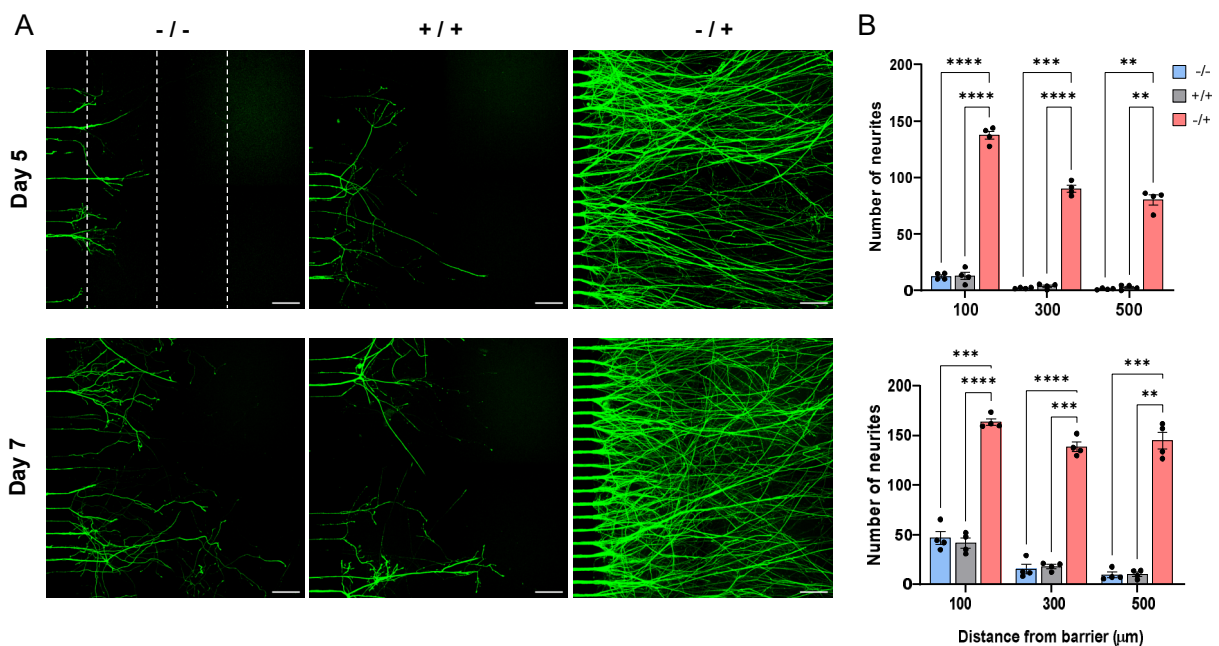
Figure. 44: Nerve fiber protruding into the axonal channel driven by NGF (A) Live-cell confocal images of GFP-transduced DRG neurons protruding from the barrier in 3D after 5 and 7 days in culture. (Scale bar: 75 µm.) Significant differences between mean values of groups are displayed as asterisks: *p < 0.05; **p < 0.01; ***p < 0.001; ****p < 0.0001; Brown-Forsythe and Welch's ANOVA test. Reproduced from reference [32] (CC BY 4.0) ©IOP Publishing.

In Figure. 44A & B, a summary is presented of neurite outgrowth assay results. In this particular culture setup, only DRG neurons are seeded in the somatic compartment, while the axonal compartment contains bare Matrigel®. Notably, I observe that NGF axonally (-/+) induces neurite protrusion of 10x more neurites than both the NGF-free condition (-/-) and the NGF-filled condition (+/+) after 5 days. Comparable growth observed in the NGF (-/-) condition and the NGF (+/+) condition suggests that the nerves in the NGF-free condition are not significantly impacted in terms of survival, which aligns with previous understanding of the independence of postnatal DRG neurons from the NGF-TrkA mechanism for survival [148]. Additionally, I analysed the cell counts and saw no clear difference in viability across conditions (see Chapter. 7 – Figure. S48). At day 7, the same pattern is seen repeated with an interesting note, the (+/+) and (-/-) conditions show moderate relative increase in density per ROI at 100 µm from the barrier with new fibers randomly finding unoccupied tunnels, whereas the NGF (-/+) condition shows relatively limited increase here because tunnels are nearly all saturated with neurites already.

This effective demonstration of the induction of vast 3D neurite outgrowth through utilization of neurotrophin gradients in the SLE INV-MPS played a vital role in current research. Insights from these NGF-gradient experiments formed the scientific basis for the approach of combining direct etching of microtunnels into the glass barrier with CME-based electrophysiological recording (as in Molina-Martinez et al. (2022) [71], for the INV-MPS study. Presence of a NGF-gradient should enable the attraction of a sufficient number of neurites for innervation of a resident axonal tissue while simultaneously recording from the same DRG neurons as they occupy tunnels inside CMEs located beneath in the somatic compartment (see Chapter. 7 – Figure. 46)

However, before commencing the production of appropriate MEA and culture chip for the INV-MPS platform, opportunity was exploited (with the IMGchip/SLE INV-MPS) to investigate, morphologically, cancer-mediated nerve outgrowth and innervation.

Cancer-spheroid Neuron coculture outgrowth

The rationale behind the selection of pancreatic and colorectal cancer for the study of cancer pain in this research is that the initial focus of the project was specifically on bone cancer, and these types of cancers are found to metastasize to bone. Cancer metastasis to bone remains highly relevant for this study, as it is particularly painful and researchers point to the high percentage of TrkA+ nociceptors innervating the different bone subtypes, particularly periosteum, mineralised bone and bone marrow.

Castaneda-Corral et al. (2011) reports that in the normal femur, both unmyelinated/thinly myelinated and myelinated sensory nerve fibers are present with 80% of thin fibers showing CGRP and TrkA immunoreactivity, and >50% in thick(er) fibers. Observing that the majority of sensory nerve fibers innervating the skeleton express TrkA+ may partially explain effectiveness of therapies blocking NGF/TrkA in attenuating skeletal pain [11]. Bone-cancer pain is, therefore, a commonly studied form of cancer-induced pain, also due to the ease with which *in vivo* behavioural studies are conducted when cancer can be localized to a single tumour-bearing limb.

Pancreatic cancer (or pancreatic ductal adenocarcinoma – PDAC) is frequently associated with high incidences of pain. Substance P staining of pancreatic tissue has indicated presence of sensory nerves, with researchers assessing their potential activation [157]. Pain in pancreatic cancer has been linked to perineural invasion (PNI – Chapter. 1) which serves as a negative prognostic factor for survival [158]. PNI is outside the scope of this research, but I postulate that the attraction between nerves and cancer can potentially proceed forms of PNI. Additionally, PNI in pancreatic cancer includes disruption of nerve topology which has been linked to inflammatory and neuropathic pain following remodelling of the affected nerve [159]. With pancreatic nerves, subject to pancreatic cancer (and pancreatitis) progression showing hypertrophy and increases in density, in combination with enhanced sensory neuron excitability. Contributing cancer-released molecules have been described, sensitizing sensory neurons, specifically targeting TRPV1. Among which, NGF, GDNF and artemin [160].

For colorectal cancer (CRC) - I initially found interesting literature reporting a series of three patients who presented with isolated bone and bone marrow metastasis (observed in FDG-PET scan and biopsy) as first presentation of an underlying CRC [161]. All three patients indicated near debilitating back pain with MRI data showing infiltration of malignant disease in the vertebra affecting nerves. Connecting CRC and nerve interaction - Albo et al. (2011) collected samples from 236 patients with colorectal cancer to see whether neurogenesis (staining for PGP9.5 – nerve marker) occurs in colorectal cancer and predicts an aggressive tumour phenotype [162]. Patients with stage II CRC and prominent neurogenesis had lower 5-year overall survival and disease-free survival compared with patients in stage III CRC with no neurogenesis. The gastrointestinal (GI) tract is a highly innervated organ system strongly connected to the CNS and also contains its own nervous system: the enteric nervous system (ENS). Furthermore, focusing on visceral afferents (DRG origin), retrograde neuronal tracing (tracer transported from nerve ending to soma) and multi-label immunohistochemistry in mice showed >75% jejunal and colonic afferents are medium-to-large diameter with 82% of jejunal afferents expressing TRPV1 – pointing

towards Aδ-fiber type II afferents [163]. However, gastrointestinal pain remains poorly understood and within the context of CRC specifically, there is a lot of mechanistic research (implicating sensory fiber-cancer interaction) still to be done.
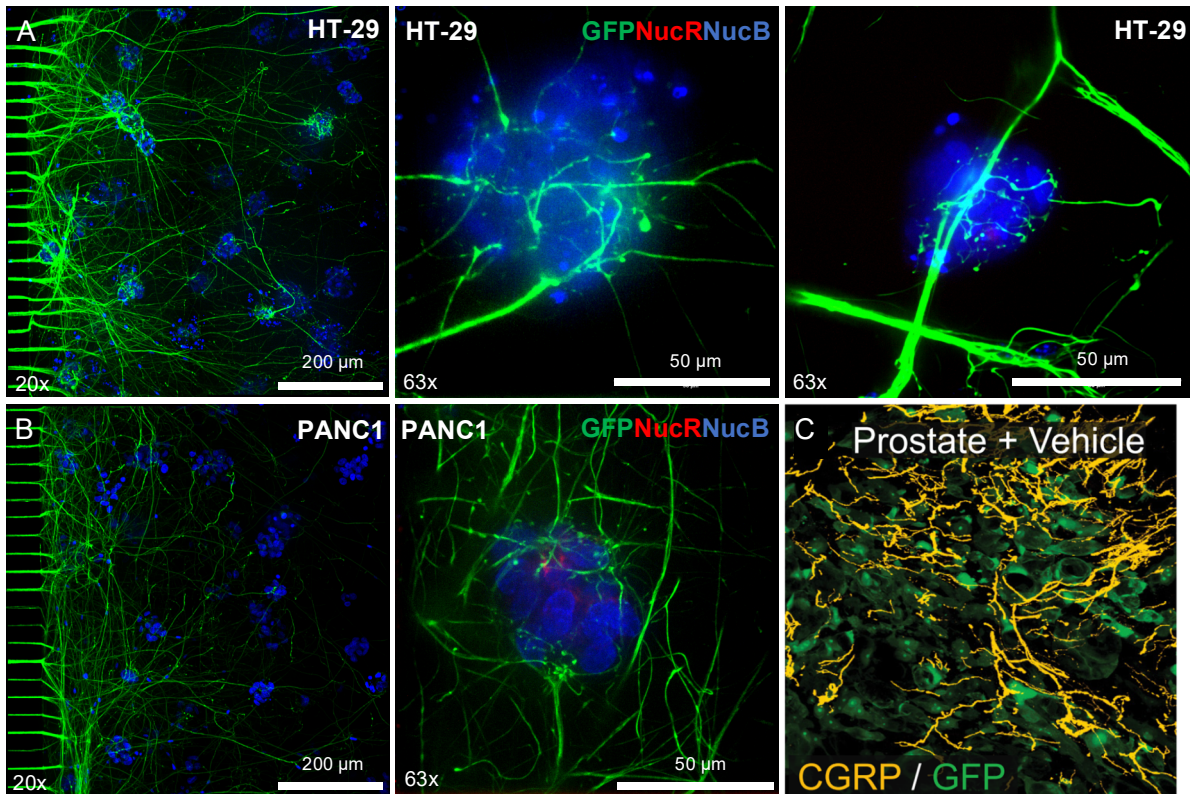
Figure. 45: *In vitro* **colorectal & pancreatic cancer innervation reminiscent of** *in vivo.* (A) Live-cell confocal images of GFP-transduced DRG neurons innervating either HT-29 or PANC1 cancer spheroids in 3D after 6 days in a NGF (-/+) culture. (B) DRG neurons innervating PANC1. Cancer spheroids are visualized using dyes staining nuclei (NucB) and dead cells (NucR). (C) Cancer cells induce sprouting innervation in Prof. Mantyh's work. --- Reproduced from reference [47] (CC BY 4.0) ©Society for Neuroscience.

In Figure. 45, results of preliminary neuron-cancer coculture experiments conducted in the SLE INV-MPS are presented. Sensory fibers establish contact with dispersed cancer spheroids in the axonal channel, periodically forming smaller sprouts or offshoots from larger fiber bundles (Figure. 45A and B). Fibers are also seen swirling erratically around the spheroids (enveloping) or growing in close proximity. In Jimenez-Andrade et al. (2010) CGRP+ neurons can be seen adopting a very similar phenotype - brought on by the injection of prostate cancer cells in the rat femur. Additionally, their control condition also shows less disturbed erratic behaviour from sensory fibers in the femur - similar to *in vitro* fibers from Figure. 40.

While these results provided encouragement to further investigate quantification of innervation, challenges emerged regarding the impact of different media formulations on neurons. Specifically, the presence of fetal calf serum (FCS) in the cancer media made it difficult to control the overgrowth of non-neuronal cells. Leading to issues such as gel shrinkage, waste accumulation and increased consumption of oxygen and media (shortening culture lifespan). In order to accurately quantify neurite outgrowth alongside electrophysiology across different conditions, it was decided to culture the entire system in FCS-free Neurobasal-A medium. Thereby, minimizing the differential effects of various media formulations on sensory neurons, only modulating the presence of NGF.

Additionally, in the INV-MPS section, a claim is made for the complete elimination of NGF (or strong control of) from standard *in vitro* DRG neuron culture procedures. It is posed that this will allow for a more sensitive exploration of the delicate cell-cell interactions that can potentially occur in a neuron-cancer coculture, without saturating the system with NGF, overriding cues, and drawing potentially inaccurate conclusions.

Chapter 7: Cancer-mediated Axonal Guidance of Sensory Neurons in a MEA-based Innervation MPS

7.1 Introduction

I here illustrate the culmination of knowledge from the 2022 publication [71] with newly obtained insights into neurotrophin driven neurite outgrowth, high-resolution fused silica etching and a rudimentary understanding of cancer-neuron coculture parameters for production of the 'Cancer-mediated Axonal Guidance of Sensory Neurons in a MEA-based Innervation MPS' article. This chapter contains a (partially modified) original draft of the INV-MPS publication written early 2023 and has, since then, been subjected to multiple rounds of rewrites and has been published in IOPScience Biofabrication.

This study showcases the INV-MPS, which consists of 9 barrier-separated pairs of channels for neuron-cancer hydrogel coculture with embedded MEA. As mentioned, I explored the integration of microtunnels into the glass barrier extensively but failed to develop a compatible recording approach. Here, manipulation of chemoattractive NGF-gradients and directing the growth of 3D neurites, allowed the combination of a barrier with etched microtunnels with arrangement of standard CMEs along the somatic channels. Combining neurite guidance techniques with this arrangement enabled trapping DRG neurons inside the CMEs while capturing axonally generated potentials from neurites extending through the barrier.

In short, a general device overview is given that functions as a starting point and outline of the novel MPS for 3D axon recording and manipulation. Neurons contained inside the glass microstructured platform are fluorescently labelled and grow neurites from the somatic compartment (with spaced CMEs) into the axonal compartment separating soma and nerve terminals. Subsequently, NGF-modulated nerve guidance and terminal excitability is addressed by first examining the effect of a stable NGF gradient across the barrier on enhancing 3D sensory fiber extension through etched microtunnels, followed by the axonal application of agonists on induction of measurable action potentials in DRG neurons to replicate peripheral activation of nociceptors. Here scientific data also includes results obtained with the monolithic IMGchip (renamed the SLE INV-MPS), as described in Chapter. 6. The SLE INV-MPS proved to be a valuable complement to the standard MEA-integrated INV-MPS by providing high-resolution morphological data.

Work continues with the study of the ability of cancer spheroids to induce sensory neurite outgrowth by monitoring the INV-MPS axonal compartment for nerve density and innervation of cancer in the neuron-cancer cocultures. Omission of exogenous NGF application uncovered that only a specific spheroid sub-type could induce significant sensory neurite outgrowth and establish *in vivo*-like innervation under current parametric INV-MPS constraints, highlighting its sensitivity. Monolithic SLE INV-MPS also played a significant role here, in quantifying conditional outgrowth and additionally facilitated screening cancer cell viability. Lastly, activation of sensory neurons by pain mediators is assessed in INV-MPS cocultures and findings showed that cancer played an active role in response generation at the periphery. Observing that 3D innervating fibers became active following the application of pain-inducing compounds after cancer spheroids had selectively stimulated initial outgrowth and terminal innervation. Future studies could explore the relevant mechanisms underlying potentially heightened sensitivity of neurons following coculture with cancer, considering carefully the cell-type specific interactions and signaling pathways involved.

This study is a collaborative effort between the Natural and Medical Sciences Institute in Reutlingen and FEMTOprint SA in Switzerland. The iterative process of enhancing the MF chip design (specifically) with intricate embedded etched structures and ensuring cost-effectiveness for future researchers interested in replicating this work has challenged the Swiss collaborators. Forcing them to dedicate significant efforts to optimizing their fabrication process whilst safeguarding the coverage of our specific requirements. With the INV-MPS publication, I hope to highlight the potential of monitoring innervation in various tissues, using cancer innervation as a case study. Noting that, I believe this microphysiological model holds promise for advancing human-relevant drug discovery in the general study of innervation in disease.

MEA-based Innervation MPS

MPSs have made significant strides in accurately representing organs and tissues for the investigation of complex biological interplay. Counterintuitively, there exists a general lack of emphasis on the important role of innervation in proper tissue function [2]. Peripheral innervation of skin, bone, muscles and visceral organs mediates response to changes in our environment and aids in safeguarding tissue homeostasis [3, 7, 14]. Nerve bundles also assist in arranging vascular networks by aligning blood vessels [164] and with regards to pathological conditions, aberrant innervation patterns in diseases like cancer can influence progression [165]. MPS-scientists should, therefore, carefully consider nerve incorporation for their 3D constructs. Arguably, compatible neuronal systems have been developed previously, these implement micropatterned structures separating soma from terminals for the manipulation of solely axons by

e.g., injury and/or growth factor cocktails [56, 57, 59, 62, 63, 166, 167]. Models are, however, limited to 2D space or neuron centric and not appropriate for innervation of intricate structures, such as organoids and spheroids. Additionally, systems are low-throughput and do not harbor electrophysiological readouts for monitoring activity of 3D tissue' innervating fibers. Shortcomings of existing literature are addressed by fabricating a compartmentalized 9-well INV-MPS for coculture of PNS neurons with choice tissues inside hydrogels on substrate-embedded MEA recording neuronal excitability at higher throughput than e.g., patch-clamp or calcium imaging [71]. Due to the vast literature available on nociceptive fibers and ethical concerns surrounding *in vivo* CIP research, we chose to investigate the sensory innervation of cancer spheroids. Interestingly, increased nerve density and nerve sprouting surrounding tumour tissues, following the release of attractive neurotrophic factors like e.g., NGF and prostaglandins, has been described to drive pain states [41, 47, 48, 51, 52, 168, 169]. However, this is a relatively new field with available literature limited to tumours of particular origin (mainly breast and prostate) and research is generally performed *in vivo*. 3D neuronal systems, such as the INV-MPS, provide an *in vitro* platform to ethically develop interventive therapies against cancer-induced axonal growth or nerve arborization and associated changes in neuronal electrophysiology. In brief, we bond a fused silica microfluidic chip to a non-standardized MEA creating two keyhole-shaped compartments separated by a micro tunneled barrier. Suspended in a hydrogel matrix (Matrigel®), DRG neurons and colorectal or pancreatic cancer cells are deposited inside and monitored via time-resolved live imaging and electrophysiological recording. Prior to incorporating cancer spheroids to model CIP, we ensure that our dissociated DRG culture is properly compartmentalized, 3D, utilizes minimal cells and enables chemoattraction of sensory fibers through the separating barrier by NGF. Model's ability to record distinct excitatory responses generated upon distal application was then also confirmed by exposing emanating nerve terminals to TRPV-1 agonists and inflammatory mediators. In the coculture, we demonstrate that colorectal cancer spheroids are similarly able to attract sensory neurites and become innervated. We also observe a substantial local sensitivity to chemical excitation following increased nociceptor density inside the tumour milieu. These findings suggest that cancer cells alone can drive a nociceptive phenotype, similar to NGF. Finally, visible Ca^{2+} transients in cancer-innervating fibers indicate neurites are responsive to noxious stimuli while interacting closely with cancer cells. Functional innervation of cancer spheroids by sensory fibers as shown here serves as a case study for the INV-MPS, an innovative 3D in vitro model amenable for exploring tissue-induced axonal growth, nerve sprouting and associated changes in neuronal electrophysiology. However, the platform has the potential to benefit a much broader community of micro-

physiological scientists who aim to recapitulate and explore the complexity of innervated tissues. Thus, the INV-MPS represents a significant advancement towards novel human-relevant drug discovery models, particularly in pathologies where tissue innervation plays a critical role.

7.2 Materials & Methods

Animals

Wild-type Swiss mice obtained from Janvier Labs (France) were housed in the animal facility of the institute. Mice were kept under standard conditions with controlled temperature and a 12-hour light-dark cycle, with ad libitum access to food and water. All experimental procedures described below were performed in compliance with the regulations outlined in the European Union (EU) legislation for the care and use of laboratory animals (Directive 2010/63/EU of the European Parliament on the protection of animals used for scientific purposes) and the German TierSchG (Tierschutzgesetz) with the latest revision in 2019.

Microfabrication

INV-MPS devices were prepared following the protocol described previously [14], with modifications. Briefly, compartmentalized microfluidic chips (Figure. S46A) were fabricated by SLE using fused silica. MEAs with integrated CME were produced by structuring two layers of permanent epoxy photoresist on gold microelectrodes. SU-8 2002 (MicroChem, USA) was spin-coated to achieve a thickness of approximately 3 µm (10 s at 500 rpm, then 30 s at 1000 rpm) (Figure. S46B). ADEX TDFS A20 (Micro Resist Technology GmbH, Germany) was then laminated onto the SU-8 layer using a pouch laminator (GMP Photonex@325, EF02015) at a temperature of 75°C. Microfluidic chips were bonded to the MEA using EPO-TEK 301-2FL (Epoxy Technology) after alignment with a Fineplacer® lambda (Finetech GmbH, Germany). The bonded devices were cured at 80°C for 3 hours. Prior to use, the devices were rinsed with bi-distilled water and incubated in a 1% Tergazyme solution for 3 hours. Subsequently, they were washed overnight with bi-distilled water. This cleaning process was repeated between experiments if the devices were deemed suitable for reuse. Alternatively, the devices were detached from the MEA substrate by immersion in concentrated sulfuric acid (H_2SO_4 ROTIPURAN® 98% - Carl Roth, # H290-H314) overnight and then reattached to a new MEA substrate. SLE INV-MPS devices do not acquire additional assembly as they are created from a monolithic fused silica substrate and lack microelectrodes.

Fabrication of fused silica microfluidic chips is based on a subtractive, direct-write microfabrication process. Exploiting a femtosecond laser and etching creates integrated 3D micro-systems with micrometer precision [76]. The process exploits highly localized material modifications, triggered by non-linear absorption during the laser exposure step. The size of the modified region is in the order of 2 μm in XY-axis and from 10 μm to 100 μm in Z-axis, depending on the optics used to focus the laser. These modifications cause a local increase of 'etching rate' in the exposed material. Since modification happens only within the focal spot (voxel) e.g., buried structures or free-form surfaces can be produced. The exposed material is later etched in KOH based solution to create 3D devices.

Barrier integrated microtunnels were analyzed using a 3D optical profiler (Contour GTK-A, Bruker UK Ltd.) equipped white light illumination and a 10x magnification objective. The instrument provides lateral resolution of 1 μm and Z resolution below 10.0 nm. Stylus profilometry (DektakXT, Bruker UK Ltd.) was performed to characterize CME height. Both SU8 (no ADEX cap) and SU8-ADEX (with cap) were measured by using a 2 μm tip. Both sets of measurements were processed and analyzed using dedicated Vision64 software (Bruker UK Ltd.).

3D DRG neuron culture

Dorsal root ganglion neurons were isolated and dissociated by modification of a previously published protocol [78]. Postnatal mice (P4-6) were sacrificed, in accordance with the European Union legislation, by decapitation with dissection scissors and disinfected with ethanol. Narrow incision through the skin and muscle of the back then exposed the spine, after which the ganglia could be removed using forceps for preservation in Hibernate™-A Medium (Thermo Fisher,#A1247501). Cleaned ganglia were then incubated in enzymatic solution(s) containing collagenase (IV) (Worthington, #LS004186) and dispase (Worthington, #LS02109), followed by manual dissociation in DNAse solution (Worthington, #LS002139). Lastly, gradient centrifugation was performed to remove dead cells and debris before mixing with plating media Neurobasal-A(Thermo Fisher, #10888-022) with GlutaMAX (Thermo Fisher, #35050-038), SM1 (Stemcell,#5711), N2 Supplement-A (Stemcell, #7152), 0.5% Penicillin-Streptomycin (Sigma, #P4333) and w/wo 100 ng/mL Nerve Growth Factor 2.5S (Promega, #G5141). Cell suspension was counted using a NucleoCounter NC-200 (ChemoMetec A/S, Denmark) and mixed with Matrigel® Growth Factor Reduced (Corning, #356230) at 1:4 ratio, resulting in a complex modulus of 20 ± 2 Pa(mean ± SD), and kept in a cold rack to prevent Matrigel® polymerization during seeding. Up to 5 INV-MPS devices were simultaneously sterilized / hydrophilized by air plasma treatment(Piccolo, Plasma Electronic GmbH). Low retention tips were used to dispense 8.5 μL of cell

solution into each proximal channel of a single compartmentalized experiment (gel layer 1000 µm thick - 9 total), followed by similar filling of the distal channel w/wo cancer cells. DRG neurons were plated at RT with stand. conc. 800 cells/µL (3200 cells/µL before mixing) and left to polymerize before addition of 100 µL Neurobasal-A to the media layer. 3D cultures were maintained up to 1 week by adding fresh Neurobasal-A medium every day (50/50) until electrophysiological or imaging readout. DRG neurons cultured in 3D were transduced immediately after plating with adeno-associated virus serotype 1 vectors containing either a transgene encoding enhanced green fluorescent protein or a G-protein coupled calcium indicator, both under control of the human Synapsin 1 promoter. Viral particles pAAV-hSynEGFP and pAAV-hSyn-GCaMP6f.WPRE.SV40, were obtained from Addgene (catalog #50465 and #100837, respectively). The multiplicity of infection used was 10^5. After 3-4 days in culture, DRG neurons exhibited homogeneous green fluorescence in the case of eGFP, while GCaMP6f-labeled DRG neurons showed fluorescence specifically upon Ca^{2+} transients.

Cancer spheroid culture preparation

Human colorectal adenocarcinoma (ATCC, #SK809) and human pancreatic carcinoma (ATCC, #CRL1469) cells were grown in McCoy's 5A medium (Gibco, #16600082) and Dulbecco's Modified Eagle's medium (Gibco, #11965092), respectively, both supplemented with 10% Fetal Bovine Serum (Gibco, 10499044) and 1% Penicillin-Streptomycin (Sigma, #P4333). Cells were seeded onto uncoated T75 flasks at a density of 1.0×10^6 cells per flask. On plating day, cells were detached with Trypsin-EDTA 0.25% (Sigma, T4049) for 3 min at 37 ◦C, enzymatic digestion was then blocked using DMEM (Gibco, 31966-021) with 10% FBS and cells were spun down before resuspending in complementary cancer media or Neurobasal-A for plating. As described in "3D DRG neuron culture", cell suspensions were similarly counted using a NucleoCounter NC-200, mixed with Matrigel® 1:4 for stand. conc. of 500 cells/µL (2000 cells/µL before mixing) and kept cold while preparing INV-MPS devices. For neuron-cancer coculture experiments – after dispensing 8.5 µL of DRG solution into the proximal compartment, either HT-29 or PANC1 cell solution was dispensed into the distal compartment at RT and left to polymerize to ensure optimal 3D distribution. 100 µL Neurobasal-A w/wo NGF (100 ng/mL) (or cancer media for live-dead assays) was then added on top in the media layer and cells were closely monitored throughout the week to qualify their aggregation into cancer spheroids. 3D cultures were maintained up to 1 week, by adding fresh medium every day (50/50) until electrophysiological or imaging readout.

Fluorescence imaging of neurite growth and innervation

3D structures were imaged by a spinning disk microscope (Zeiss Cell Observer®) equipped with ZEN software (blue edition, ZEISS), followed by quantitative analysis using open-source image processing software, FIJI (ImageJ, http://imagej.nih.gov/ij/) or qualitative reconstruction with IMARIS 4.6 (Bitplane AG, Oxford Instruments). A dedicated 384 well microplate adaptor was designed and produced by Weerg Srl (Italy) to simultaneously hold two devices while imaging under humidity/CO_2/temperature control (Figure. S47B).

Neurite outgrowth assays (Figure. S47C) were performed on maximum intensity projections of 100 slices (AAV1-eGFP Alexa Fluor 488 - z-axis with 0,75 μm spacing – 20x) for 3 randomly selected ROIs (700 μm x 700 μm) starting at substrate-height. For each ROI, intensity profiles of vertical lines were plotted at 100 μm, 300 μm and 500 μm distance from distal tunnel exits and a 'Find Peaks' algorithm was then applied that returns the number of maxima (representing neurites – after background subtraction) (available from https://github.com/tferr/Scripts#ij-bar/). Neuron-cancer cocultures were quantified for neuronal outgrowth by identical image generation and processing with additional pre-incubation (3 drops/mL for 90 min at 37°C) of NucRed Dead 647 ReadyProbes™ Reagent (TO-PRO-3 iodide) (Invitrogen, #R37113) for dead cells and NucBlue Live ReadyProbes™ Reagent (Hoechst 33342) (Thermo Fisher, #R37605) for all nuclei.

Dextran diffusion

Barrier permeability assay was performed using 2 different fluorescently labelled dextran moieties. 4 kDa FITC-Dextran and 20 kDa Rhodamine-Dextran (100 μg/mL diluted in growth media) were administered and tracked simultaneously upon pipetting of 50 μL tracer solution into 50 μL bare culture media in the media layer (2x final conc.). A 1x5 tilescan (350 μm x 1750 μm – center tile containing the 300 μm barrier) was taken at substrate-height every 10 minutes for 12 hrs with T=0 min directly after application. Diffusion was quantified at selected timepoints by generating intensity profiles for rectangular ROIs right outside the microtunnels (somatic and axonal compartments) and in the bulk (somatic). Time-dependent tracer loss to the somatic channel was then accounted for by measuring the fluorescent intensity development in both compartments and normalized as a % of the highest value measured axonally (at T=12 hrs).

Calcium imaging

Neuron-cancer cocultures were transduced as described in "AAV1-eGFP and AAV1-GCaMP6f transduction". Adeno-associated virus expressing GCaMP6f as Ca^{2+} indicator was imaged before and immediately after application of inflammatory/excitatory compounds using a spinning disk Zeiss Cell Observer® System (20x/63x objective) and processed in FIJI. At 5-6 days in culture, cocultures were placed inside the 384 well microplate adaptor and left to acclimate. ROI (350 μm x 350 μm) was selected by qualifying the presence of innervated cancer spheroids at various heights within the gel layer before stimulation with either 4 μM Bradykinin (Tocris/Biotechne, #3004) or 1 μM Capsaicin (Tocris/Biotechne, #0462). Acquisition time was set at ~2 frames per second.

MEA-based electrophysiological recordings

Electrophysiology of 3D innervating fibers was recorded using a USB-MEA 120-System (Multi Channel Systems MCS GmbH, Germany) at 4 – 6 days in culture for DRG monocultures and at 6 days in culture for cancer cocultures. During experiments, a customized MEA incubation chamber (Okolab Srl, Italy) was used to continuously monitor temperature, CO^2 and humidity. The temperature was set to 36°C, humidity at 85% and CO^2 at 5%. MEAs were allowed to acclimate inside the MEA chamber before applying agonists and inflammatory mediators to the axonal compartment. Agonists were applied 30 seconds into a recording to identify spontaneously active electrodes. Inflammatory mediators were applied 5 minutes before recording. Recordings were acquired using MC_Rack v. 4.6.2 (Multichannel Systems MCS GmbH, Germany) and filtered using a fourth-order bandpass filter (60-6000 Hz), before processing with NeuroExplorer (version 5.300) for spike detection and further analysis.

Statistical analysis

Statistical analysis was performed on the collected data using GraphPad Prism 8 developed by GraphPad Software Inc. (Boston, USA). Degree of normality of the data distribution was assessed both visually and quantitatively by employing quantile-quantile plots, frequency histograms, and Shapiro-Wilks tests. Within the neurite outgrowth assay domain, conditions are represented as bar graphs with mean ± SEM. Differences were assessed by Brown-Forsythe and Welch's ANOVA test with post-hoc test Dunnett T3 (n<50) for comparison of means. Electrophysiological data were represented as either bar graphs comparing conditions or connected-points for temporal dynamics with mean ± SEM. Differences were assessed similarly by either Brown-Forsythe and Welch's ANOVA with post hoc test Dunnett T3 (n< 50) or Welch's unpaired t-tests for comparison of means. Asterisks denote statistical significance as follows: $*p < 0.05$; $**p < 0.01$; $***p < 0.001$; $****p < 0.0001$.

7.3 Results

A novel MPS with integrated electrodes for 3D axon manipulation and recording from sensory neuron cultures

Innovation of *in vitro* PNS models has remained rather stagnant as integration of effective readouts in complex 3D cultures remains challenging. However, it is imperative for effective collaboration within the MPS-field that neuroscientists strive to improve existing models for e.g., tissue innervation. We hypothesized that we could advance the standard 2D neurite outgrowth models (separating soma and axons) using a 3D approach while integrating a non-invasive electrophysiological readout. This includes promoting the growth of peripheral neurons within 3D space and facilitating their projection through a barrier as they ultimately locate and integrate with axonally residing tissue (Figure. 46A). For this, we produce a high-resolution (<1 μm) fused silica 3D culture chip that integrates with MEA-substrate, as described previously [71]. The MPS includes pairs of adjacent two-layer tissue wells (somatic and axonal compartment) featuring defined hydrogel layers (GL; approx. 8.0 μL) below media layers (ML; approx. 110.0 μL). Distinction from past monoculture focus - is the incorporation of a thin 300 μm barrier, which holds 12 rows of 110 microtunnels (10 x 10 μm cross-section) each, over a surface area of approx. 4.0 x 1.0 mm (Figure. 46B and Figure. S46A). This 3D-arrangement of μ-tunnels is possible due to the unique capabilities of SLE that enables the selective removal of glass from a monolithic piece in 3D. Microtunnels exclusively allow the passage of DRG neurites to the GL of the axonal compartment (Figure. 46C). To record from gel-embedded 3D neurons inside the INV-MPS, we effectively trap axons as they regrow after seeding using CMEs placed at the bottom of the somatic compartment (Figure. 46D). Proportion of neurons occupying CMEs also extend towards

the barrier and cross into the adjacent compartment. Using live-cell confocal fluorescence microscopy in combination with transducing DRG neurons with adenoviral vectors encoding eGFP, we confirmed soma and nerve terminals are spatially separated while still organizing in 3D space (Figure. 46E). Furthermore, neurites become trapped inside CMEs with confined spaces (5 μm x 3 μm) granting the resolve of extracellular signals (up to ~100 μV) generated upon firing of action potentials (Figure. S46B). Each micropatterned glass microfluidic piece was bonded onto a 49.0 x 49.0 mm glass substrate containing 117 embedded recording electrodes. Thirteen recording-CMEs and a reference electrode are distributed inside the somatic compartment of a coculture experiment (9 in total) and lead to edge-pads securing connection to pins of the MEA-recording system (Figure. 46F and G).
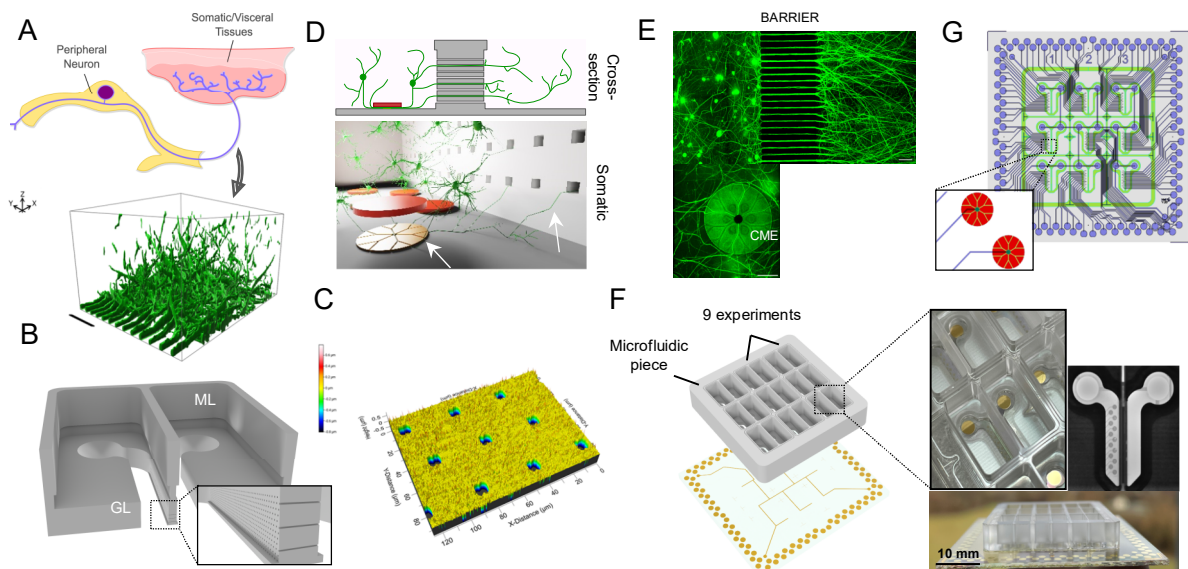
Figure. 46: A novel MPS with integrated electrodes for 3D axon manipulation and recording from sensory neuron cultures (A) Recapitulating the innervation of soft tissues by the peripheral nervous system. 3D-surface rendering of DRG terminals extending into 3D space in the axonal compartment. Dimensions 600 × 450 × 300 μm. (Scale bar: 100 μm.). (B) Both somatic and axonal compartments are filled with a soft 3D scaffold inside the gel layer (GL). Supporting media is added on top in both media layers (ML) (width: 300 μm.). (C) High magnification color map of micro tunneled barrier profilometry data. (D) DRG neurons grow neurites through the barrier while simultaneously projecting neurites into recording CMEs residing in the somatic compartment. (E) Live-cell confocal images of GFP-transduced DRG homogeneously distributed in the somatic compartment with neurites traversing the barrier and entering CMEs (Scale bar: 75 μm.). (F) INV-MPS holds 9 identical cocultures with 13 CMEs and assembles by bonding on top of the dedicated 120-electrode MEA. (G) Technical drawings of MEA-CME production photomasks.
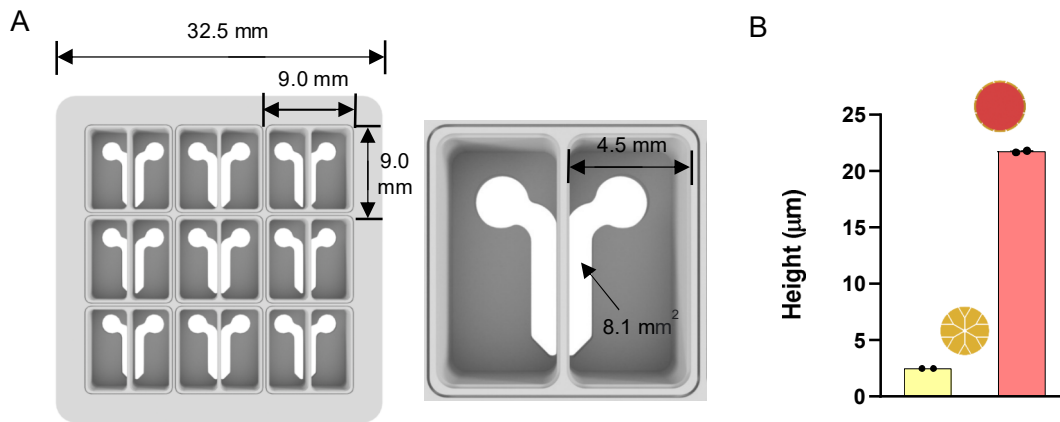
Figure. S46 INV-MPS overview. (A) Important parameters given as input for SLE of fused silica microfluidic chips (B) Stylus profilometry of subsequent photoresist layers constituting a CME. Data in B is represented as mean ± SEM.

3D axonal guidance and nerve terminal excitability modulated by NGF inside the MPS
We investigated the responsiveness of 3D gel-embedded DRG neurons to neurotrophic gradients, which may have implications for tissue innervation under various pathophysiological conditions *in vivo*. NGF is one of four known neurotrophic factors found in mammals and has been shown to steer the development of neuronal growth cones *in vitro* and can enhance survival *in vitro* [147, 154]. Here, experiments were performed using an INV-MPS without integrated electrodes (SLE INV-MPS - Figure. S47C), which features a single row of tunnels at the bottom of the barrier, allowing for accurate comparison of neurite outgrowth and microtunnel diffusion kinetics. To analyze the impact of NGF on 3D sensory fiber` extension into the axonal compartment, we supplemented NGF solely axonally (NGF -/+), thereby creating a stable gradient over the barrier for one week. We found a significant increase in fibers crossing the barrier (Figure. 47A and B and Figure. S47A) with limited variability in survival across different conditions (Figure. S47B). When NGF was supplied to both compartments (NGF +/+), few axons extended through the barrier and neurites predominantly grew within the somatic compartment, likely due to the lack of a chemoattracting gradient. Responsible fluidic separation could also be partially recapitulated by monitoring the diffusion of fluorescently labelled dextran moieties in the SLE INV-MPS. To mimic a NGF gradient across adjacent wells, we monitored the concentration of fluorescently labelled dextran moieties (applied to the axonal compartment) for 12 hours and observed a ~10x lower concentration of both 4 kDa and 20 kDa tracers in the somatic compartment.

Noteworthy that the actual concentration in the bulk of the somatic compartment is considerably lower following dilution into the larger volume. After optimizing culture conditions in the SLE INV-MPS, we transitioned to the INV-MPS with integrated MEA for electrophysiological recordings following manipulation of 3D nerve terminals in a NGF -/+ condition (Figure. 47D). Application of TRPV-1 agonist capsaicin (burning pain [35]) to the axonal compartment of the INV-MPS resulted in measurable action potentials in the majority of CMEs located in the somatic compartment (Figure. 47E). Signifying that current 3D culture system replicates desirable expression of both receptors and ion channels involved in transmitting excitability from nerve terminals to the soma. Additionally, recorded action potentials appeared within a timeframe of 3 - 5 seconds from administration of capsaicin, indicating the system's ability to rapidly detect and measure axonally-evoked changes in neuronal activity. We also demonstrate the ability to differentiate between rapid onset-offset effects of an agonist vs. prolonged effects induced by pain-associated inflammatory milieus, by recording action potentials continuously for up to 30 minutes by the majority of electrodes (NGF -/+ otherwise silent), after application of an inflammatory mediator cocktail (bradykinin, prostaglandin, serotonin and histamine) (Figure. 47F). Examining electrode response rates following capsaicin application, we found that a response rate of over 80% can be achieved within 6 days from plating. Understandably, the 3D system takes slightly longer to organize itself in comparison to conventional 2D cultures (2 - 3 days), as the additional time course is determined by presence of growing neurons in the axonal compartment (Figure. 47G and H). Subsequently, a capsaicin dose-response curve (0.1 - 1.0 µM) generated at day 6 indicates concentration directly affects the number of responses observed, confirming usefulness for assessment of acute dose responses in drug screening applications (Figure. 47I and J). In summary, the INV-MPS could be utilized to study the engagement of specific ligand-gated receptors or voltage-gated ion channels that may play a role in modulating pain states, as well as to monitor the potential of various factors to induce neuronal outgrowth or nerve degeneration in toxicity studies.
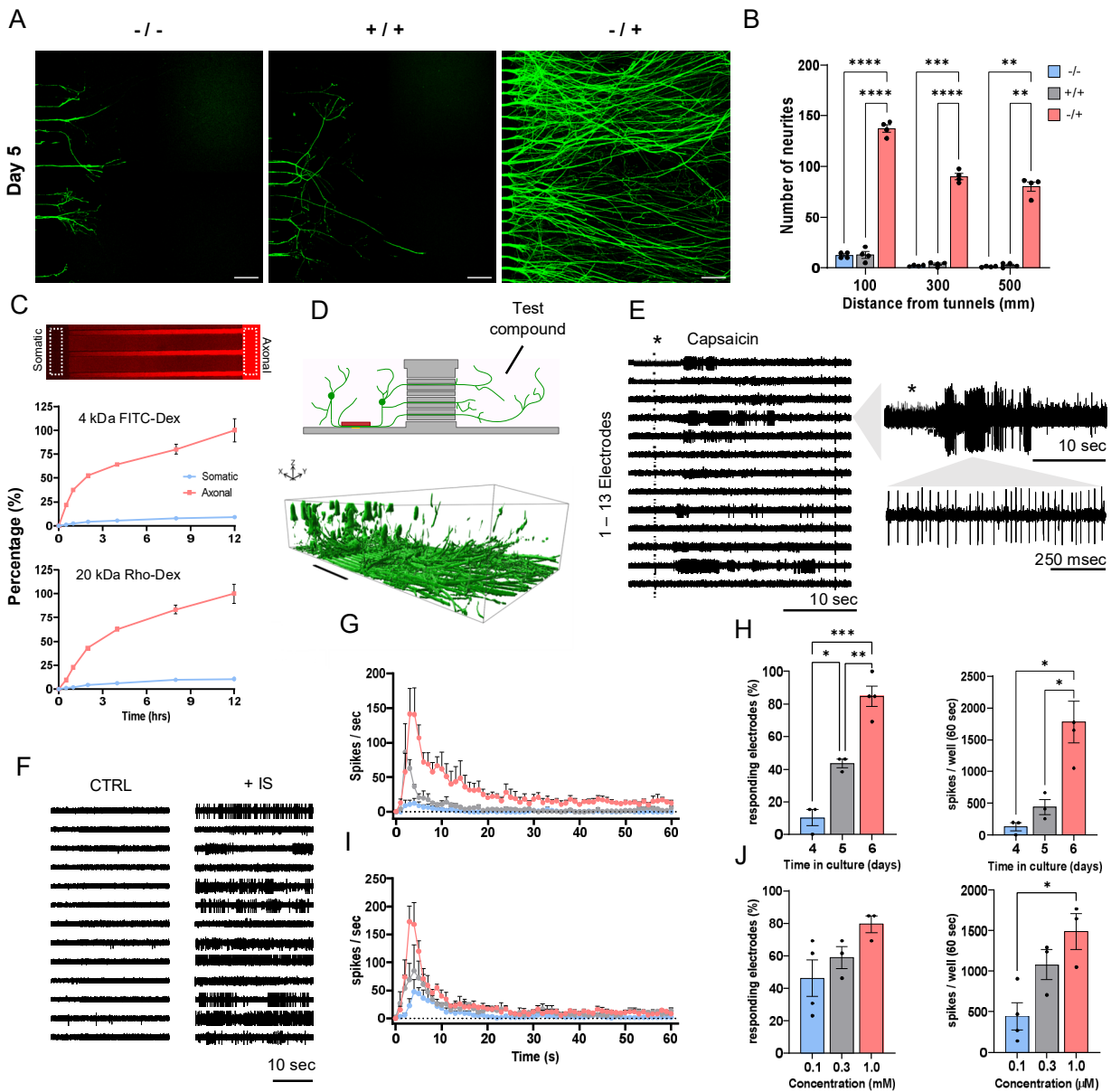
Figure. 47: 3D axonal guidance and nerve terminal excitability modulated by NGF inside the MPS
(A) Live-cell confocal images of GFP-transduced DRG neurons protruding from the barrier in 3D after 5 days in culture. Neurobasal-A culture medium either contains no NGF (-/-), NGF in both somatic and axonal media compartment (+/+) or NGF only in the axonal media compartment (-/+) (Scale bar: 75 µm.) (B) Quantification of neurite outgrowth after 5 days in culture. Total number of neurites was measured at 100 µm, 300 µm, and 500 µm distance from the barrier – perpendicular to the neurite development. Bar graphs represent mean ± SEM (n=4 wells) (C) Micrograph shows diffusion of Dextran-FITC (MW: 4 kDa) or Dextran-Rhodamine B (MW: 20 kDa) through the micro-tunnel barrier from axonal (right) to somatic (left). Fluorescent intensity profiles generated from ROIs entering and exiting the micro tunnel-barrier plotted against time as percentages (normalized to intensity at T = 12 hrs). Data is represented as mean ± SEM (n=3 wells). (D) Excitatory compounds are applied to the media layer atop the 3D nerve terminals of a NGF -/+ culture in the axonal compartment. 3D-surface rendering of DRG neurons and their soma.

Dimensions 1450 × 750 × 300 µm. (Scale bar: 300 µm.) (E) Trace plots representing the activity recorded by 13 CMEs after application of 1 µM Capsaicin (black asterisk) at different time scales. (F) Trace plots comparing control to activity recorded 5 minutes after application of inflammatory soup (IS containing: 3 µM Bradykinin, 3 µM Prostaglandin, 3 µM Serotonin and 3 µM Histamine). (G) Temporal dynamics of Capsaicin (1 µM) responses in -/+ cultures of DRG neurons after 4 (blue), 5 (grey) and 6 (red) days. Dots represent the mean spikes per second per well over a 60-second span post-application (n=3-4 wells). (H) Bar graphs comparing the development of CME-occupancy with DRG neurons responding to axonal stimuli (percentage of responding electrodes) and total spikes recorded per well in the 60-second span post application. (I) Dose-response curves comparing temporal dynamics following application of 0.1 (blue), 0.3 (grey) and 1 (red) µM capsaicin in -/+ cultures of DRG neurons (n=3-4 wells). (J) Bar graphs comparing excitability of CMEs occupied with DRG neurons responding to axonal stimuli (percentage of responding electrodes) and total spikes recorded per well in the 60-second span post application. In B, H, and J, significant differences between mean values of groups are displayed as asterisks: *p < 0.05; **p < 0.01; ***p < 0.001; ****p < 0.0001; Brown-Forsythe and Welch's ANOVA test.
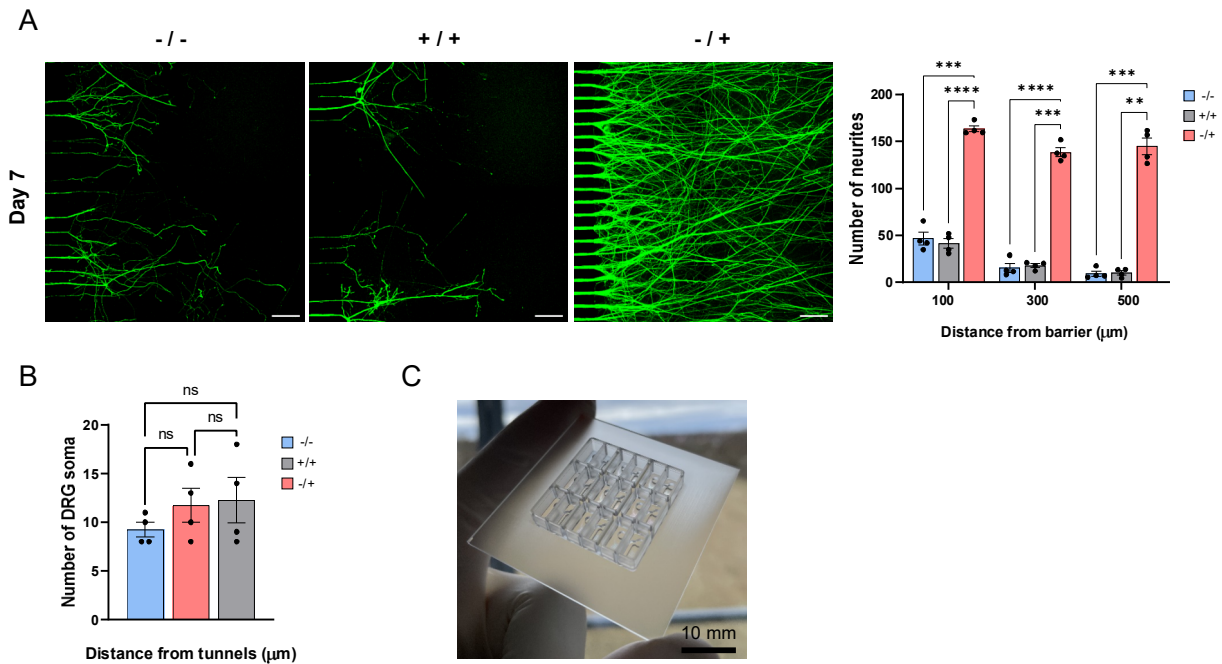
Figure. S47 Axonal outgrowth and survival. (A) DRG neurons extending in 3D inside the axonal compartment after 7 days in culture with quantification. (n = 4 wells) (Scale bar: 75 µm.) (B) Comparison of neuronal survival inside the somatic compartment by counting eGFP-fluorescent DGR soma. (n = 4 wells) (C) SLE INV-MPS without electrodes used for growth quantification and diffusion. In A and B, bar graphs represent mean ± SEM and significant differences between mean values of groups are displayed as asterisks: *P < 0.05; **p < 0.01; ***p < 0.001; ****p < 0.0001; Brown-Forsythe and Welch's ANOVA test.

Induction of sensory neurite outgrowth by colorectal cancer spheroids in the absence of NGF supplementation

We now discuss the INV-MPS' potential for investigating outgrowth of peripheral neurons, specifically mediated by conditions that relate to pathological pain *in vivo*. DRG neurons (NGF -/+) were seeded inside the electrode-free SLE INV-MPS, together with HT-29 or PANC1 spheroids and monitored as neurites are attracted to traverse the barrier and innervate targets in the axonal compartment. By quantifying sensory fiber outgrowth in a 3D environment while cancer spheroids are present, we hypothesize using the SLE INV-MPS for improving comprehension of the underlying neuronal mechanisms involved in pathological pain *in vivo* [158, 162, 170, 171]. Based on the results shown in Figure. 48A and B, however, no cancer-mediated increases of neural growth into the axonal compartment relative to the NGF -/+ control condition could be observed. Suggesting that the presence of NGF in the media of the axonal compartment can saturate the outgrowth potential of nerve fibers and override guidance clues, as previously described for *in vitro* systems [172]. We thus elected to remove NGF from the system. In absence of neurotrophin supplementation – a significant increase in nerve fiber density in the axonal compartment of HT-29 cancer spheroid 3D cocultures could be observed. Notably here, innervation and complete envelopment of individual cancer spheroids as seen *in vivo* [47, 51], could simultaneously be demonstrated (Figure. 48C and D). 3D representations of nerve fibers extending into the axonal compartments among resident cancer spheroids further verify that quantified cell-cell interactions are not simply planar but occur in all dimensions (Figure. 48E and F). Furthermore, for optimal neuronal outgrowth conditions and standardization, cells were cultivated in neuronal media instead of cancer media without clear negative effects on viability of the cancer spheroids (Figure. S48A and B). Interestingly, while HT-29 cancer spheroid 3D cocultures exhibited a significant induction of neuronal outgrowth in the absence of NGF, this effect was not observed in PANC1 cancer spheroid cocultures (Figure. 48C and D). This observation suggests that innervation can be highly cell-type-specific, possibly due to the presence of different molecular or paracrine cues associated to the microenvironment of each cancer type.
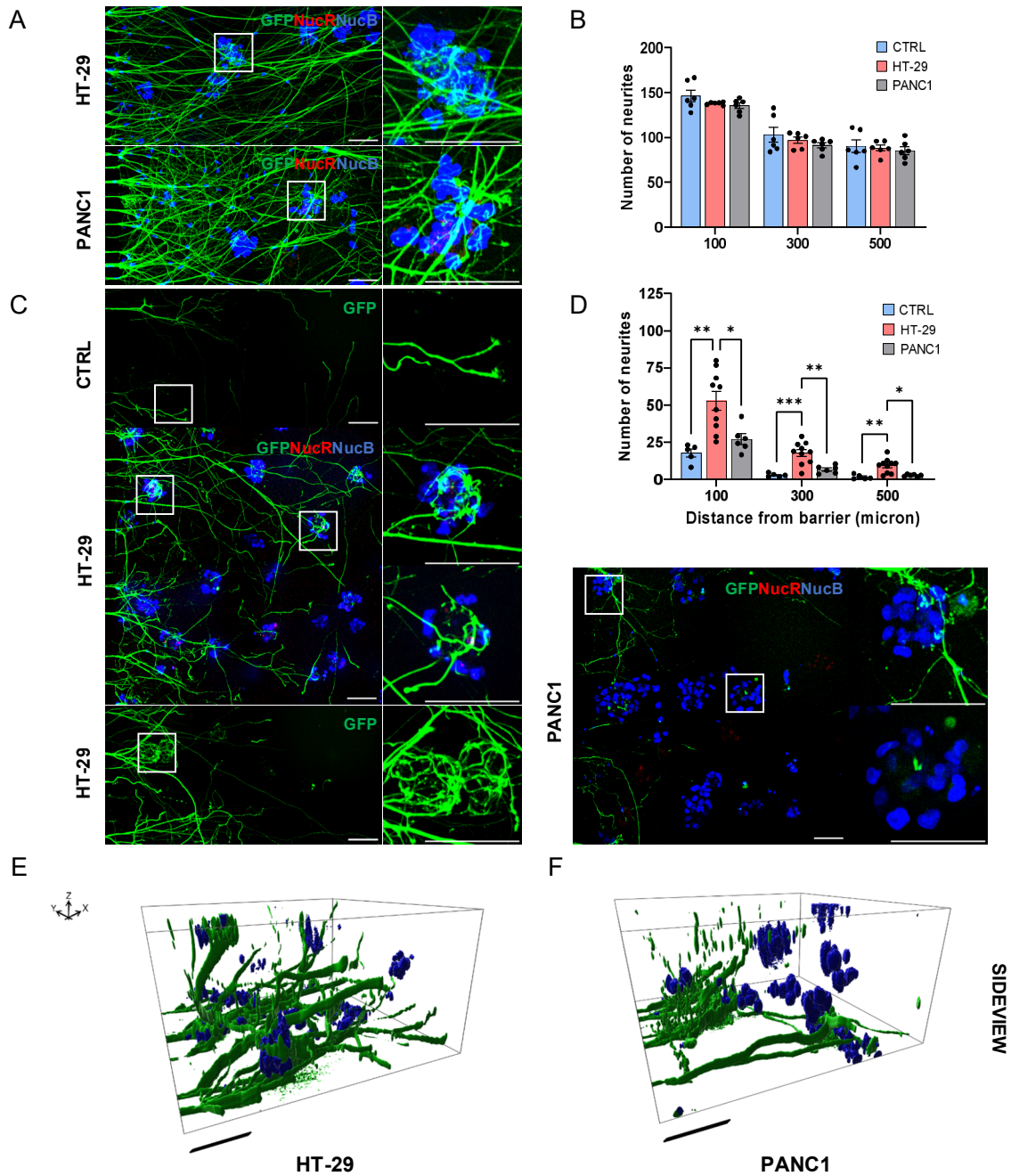
Figure. 48: Induction of sensory neurite outgrowth by colorectal cancer spheroids in the absence of NGF supplementation (A) Live-cell confocal images of GFP-transduced DRG neurons protruding from the micro tunnel-barrier and innervating either HT-29 (colorectal) or PANC1 (pancreatic) cancer spheroids in 3D after 6 days in a NGF -/+ culture. Cancer spheroids are visualized using dyes staining nuclei (NucB) and dead cells (NucR). (Scale bar: 75 μm.) (B) Quantification of neurite outgrowth after 6 days in culture. CTRL represents a DRG-only (NGF -/+) culture at day 5 & 6. Bar graphs represent mean ± SEM (n=6 wells) (C) Live-cell confocal images of DRG neurons protruding from the microtunnel-barrier and innervating either

HT-29 or PANC1 cancer spheroids after 6 days in a NGF -/- culture. (D) Quantification of neurite outgrowth after 6 days in culture. CTRL represents a DRG-only (NGF -/-) culture (n=5-10 wells). (E) Sideview of 3D-surface renderings of sensory neurites innervating HT-29 or (F) PANC1 cancer spheroids. Dimensions 400 x 400 x 200 µm. (Scale bar: 100 µm.) In B and D, significant differences between mean values of groups are displayed as asterisks: *p < 0.05; **p < 0.01; ***p < 0.001; ****p < 0.0001; Brown-Forsythe and Welch's ANOVA test.
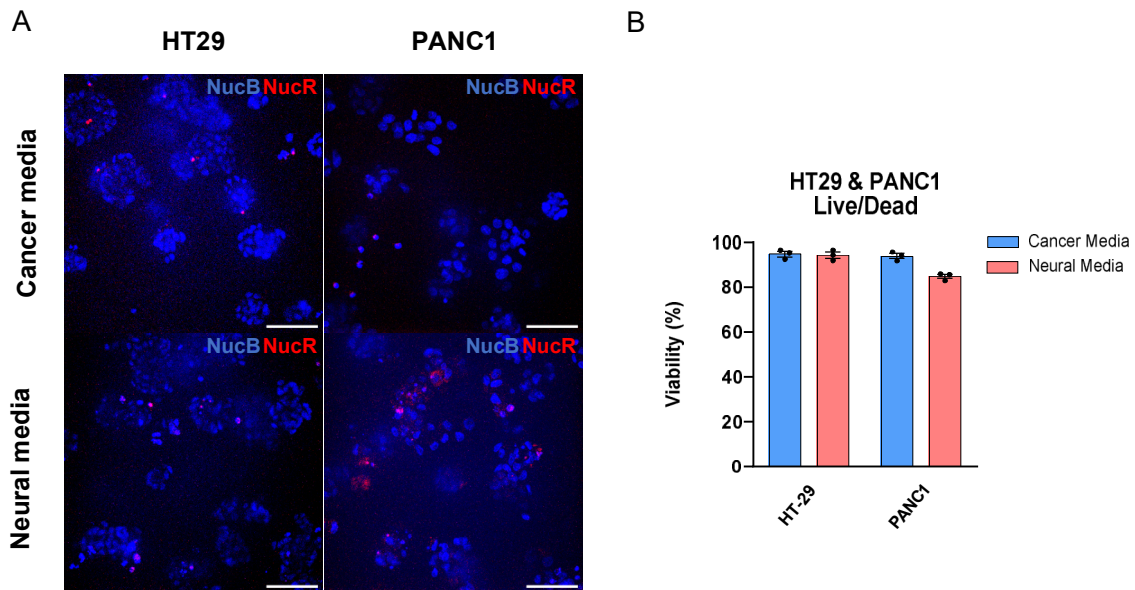
Figure. S48 Cancer viability study. (A) Cancer spheroids are imaged after 6 days in culture using dyes staining nuclei (NucB) and dead cells (NucR). HT-29 and PANC1 are either cultivated in their own media or neuronal media (Scale bar: 75 µm.). (B) Live/dead quantification (Total Cells - Dead cells/Total Cells * 100%). Bar graphs represent mean ± SEM (n = 3 wells).

Sensory neurons innervating 3D colorectal cancer spheroids can be activated by pain mediators
As stated in Molina-Martínez et al. (2022) [71], the combination of electrical and image-based readouts play a critical role in providing information about neuronal function. However, image-based monitoring of activity from 3D tissues, such as through calcium imaging, is often limited to solely qualitative analysis. In this study, we demonstrate the potential of the MEA-integrated INV-MPS for screening purposes in pain research. As shown in Fig. 48, cancer spheroids occupying the axonal compartment of the SLE INV-MPS can stimulate nerve growth, raising the question of whether nerve terminals also exhibit excitability.

To address this, we applied either capsaicin or bradykinin to the axonal compartment of MPSs containing DRG (NGF-/-) with or without cancer spheroids. Prior, we observed that HT-29 did not cause any rise in spontaneous activity (Figure. S49A). After chemical excitation, recordings demonstrated distinct responses to both compounds in axonally extended nerve fibers among cancer spheroids, whilst control group saw no response (Figure. 49A and B). Although less abundant than what we observe from NGF -/+ DRG monocultures (Figure. 49E and J), it is striking that addition of HT-29 cancer spheroids can similarly induce an increase in axonal nerve density sensitive to chemical excitation. Response to both depolarizing stimuli was quantified for DRG & HT-29 coculture vs. the DRG-alone control (Figure. 49C and D and Figure. S49B). For the capsaicin response in HT-29 coculture, we see a less pronounced initial cumulative peak and a lower responsiveness in comparison to NGF -/+ conditions (Figure. 47I and J), which correlates with the difference in neurite outgrowth (<50%). Analysis of time-course, number of responses elicited and response rate for both compounds in presence of HT-29 cancer spheroids (NGF -/-) vs. DRG-alone (NGF -/-) control revealed colorectal cells have the capacity to enhance outgrowth of nociceptive fibers that occupy multiple somatic CMEs and respond characteristically to noxious stimuli [20]. In order to establish a closer link between nerve terminal excitability and cancer innervation, we utilized AAV-GCaMPf6 to directly visualize calcium transients induced by application of chemical agonists in DRG neurons innervating cancer spheroids. Nerves that innervate cancer spheroids respond to chemical stimuli applied to the axonal compartment (Figure. 49E). Confirming the physiological relevance of our approach, which closely mimics neuro-oncological interactions. As discussed, although Ca^{2+} imaging can provide a direct measure of nerve terminal activation, monitoring responses in a multiplexed 3D setting remains technically challenging and time-consuming. This emphasizes the advantage of the INV-MPS platform, with regards to quantifying electrical excitability in 3D microtissues.
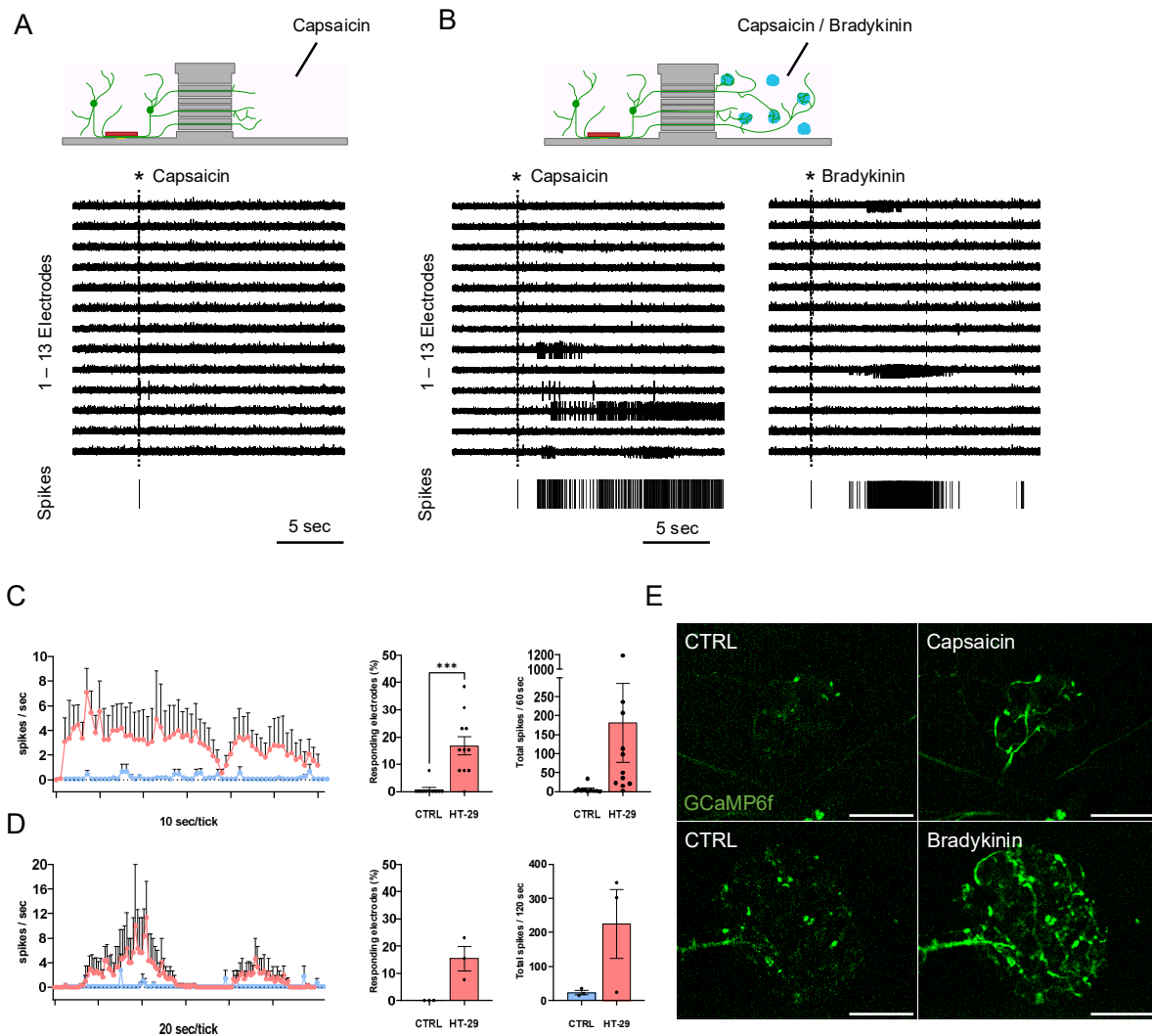
Figure. 49: Sensory neurons innervating 3D colorectal cancer spheroids can be activated by pain mediators (A) Trace plots representing individual CMEs (1 to 13) and cumulative raster after application of 1 µM Capsaicin (black asterisk) to a DRG-only culture (NGF -/-) after 6 days. (B) Trace plots and cumulative raster after application of 1 µM Capsaicin or 1 µM Bradykinin to DRG neurons innervating HT-29 cancer spheroids (NGF -/-) after 6 days. (C) Temporal dynamics of capsaicin responses in DRG neurons innervating HT-29 cancer spheroids (NGF -/-). Dots represent the mean spikes per second per well over a 60-second span post-application (n =10-11 wells). Bar graphs comparing excitability of DRG neurons responding to axonal stimuli (percentage of responding electrodes) and total spikes recorded per well in the 60-second span post application. (D) Temporal dynamics of bradykinin responses in NGF -/- cultures of DRG neurons innervating HT-29 cancer spheroids. Dots represent the mean spikes per second per well over a 120-second span post-application (n=3 wells). Bar graphs comparing excitability of DRG neurons responding to axonal stimuli (percentage of responding electrodes) and total spikes recorded per well in the 120-second span post application. (E) Live-cell confocal images of GCaMP6f-transduced DRG neurons innervating HT-29 cancer spheroids after 6 days in a NGF -/- culture. Application of 1 µM Capsaicin and 4 µM Bradykinin induces Ca^{2+} transients.

In C and D, significant differences between mean values of groups are displayed as asterisks: *p < 0.05; **p < 0.01; ***p < 0.001; ****p < 0.0001; Brown-Forsythe and Welch's ANOVA test.
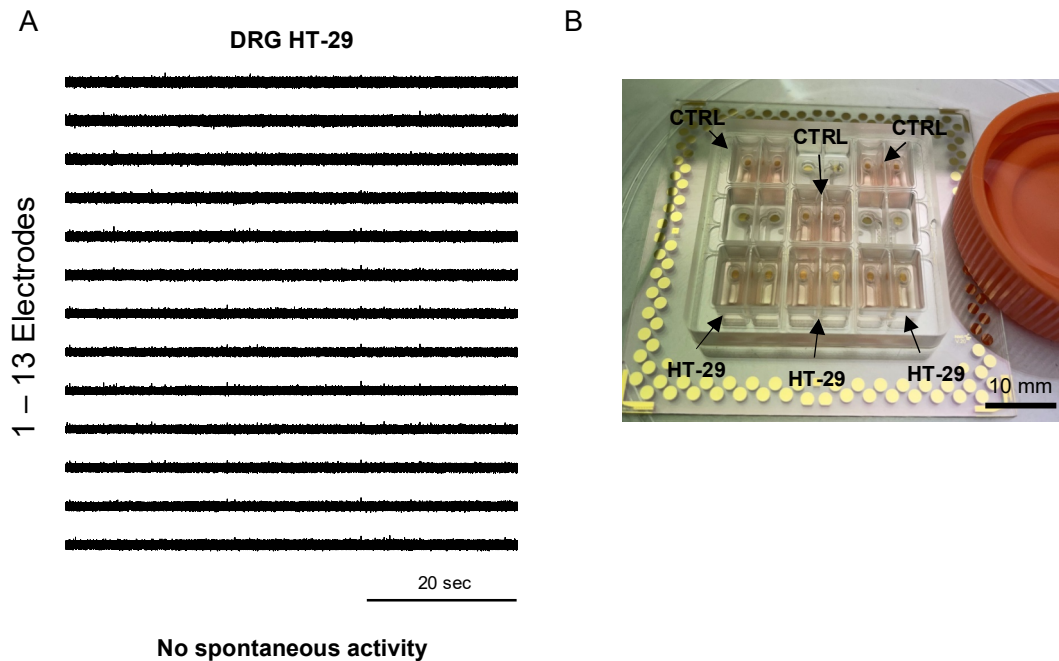
Figure. S49 Sensory innervation of cancer spheroids case study. (A) Spheroids do not induce spontaneous activity in DRG neurons that extend into the axonal compartment (B) Overview of INV-MPS setup on a recording day

7.4 Discussion

Objective of the MPS-field is to replicate organ functions that are challenging to simulate/study using conventional cell cultures or animal models [173]. However, recapitulating the ingrowth of nerve fibers in MPSs is not generally attempted due to the added complexity of incorporating nerve fibers. This is unfortunate as innervation could bring benefits to many therapeutic domains such as wound healing, adipocyte metabolism and endometriosis [174]. Decoding of the role of the PNS could prove valuable in all of these contexts. Furthermore, it requires specialized expertise to effectively bring together peripheral neurons and target tissues while simultaneously integrating a robust electrophysiological readout consistent with neurons. Leveraging our experience in combining custom MEA, high-resolution glass etching and 3D neuronal cultures ([71]) enabled us to create an innervation platform that recognizes the progression of the MPS-field towards creating intricate tissue models and integrates a microelectrode-based recording method. Reiterating that MEA systems designed for 2D axonal outgrowth cultures do not translate

well to 3D and available 3D *in vitro* electrophysiological recording methods generally do not scale to meet necessary requirements for enhanced throughput, simple handling and seamless integration across platforms. We describe the development of the INV-MPS with embedded CMEs, enabling electrophysiological recording from peripheral nerve fibers innervating target tissues in 3D. Additionally, our technology successfully integrates a glass microfluidic barrier that compartmentalizes 3D hydrogel-embedded sensory neurons, separating soma and terminals [57]. The INV-MPS avoids the use of patterned polymers generally employed in microfluidics like PDMS, which is susceptible to small molecule absorption and involves laborious molding processes. Instead, we designed an easy-to-assemble, reusable device utilizing a glass microfluidic chip with barrier-etched microtunnels and MEA. Guidance of axonal growth through the barrier was mediated by NGF and demonstrated how the INV-MPS system recapitulates physiologically relevant directed growth of neurons along neurotrophin gradients [151]. In addition, we were able to non-invasively capture the excitability of 3D extended fibers and showed response profiles to pain mediators are similar to what is observed *in vivo* and *ex vivo* [134, 175]. Taken together, this indicates that the INV-MPS can be used to study the engagement of specific receptors and ion channels (terminal vs. somatic) modulating nociception, while monitoring the effects of neurotrophic factors/inhibitors on neuronal spouting and arborization. This is a necessary step towards reducing the use of animal models within nociception research. We then aimed to expand on the unique readout capabilities of the INV-MPS by studying more delicate and pathological neuron-cancer interaction in CIP. It was quickly observed that when cancer spheroids and neurons were cocultured in the presence of NGF, the growth of nerve fibers was primarily driven by the exogenously applied neurotrophin pool. Upon its removal, we observed the remarkable ability of colorectal cancer spheroids (HT-29), specifically, to drive neural outgrowth and ultimately the innervation of individual structures as observed *in vivo* [47, 51]. While an increase in nerve fiber density could only be demonstrated for colorectal cancer, it would be premature to conclude that pancreatic cancer cannot exhibit similar phenomena within the INV-MPS setting [159]. Cancer type and associated stromal cells/components (immune cells, inflammation etc.) synergistically harbor the capacity to induce axonal growth via specific neurotrophin release, with certain tumours requiring more additional components than others [42-44, 176]. We conclude that the difference in 3D innervation between pancreatic and colorectal cancer spheroids, we observe, underlines the sensitive ability of the system to discriminate between the attractive forces generated by cancer environments.

Important to note that, although we have shown that neuronal outgrowth strongly depends on exogenously applied NGF, we can only merely suggest that the cancer-mediated outgrowth we observe also depends on NGF. This would be in line with general consensus [148] and it is also known that both HT-29 and PANC1 release similar amounts of NGF *in vitro* [46, 177], however, the observed disparity in innervation might appropriately suggest that various chemoattractants are relevant in this specific context. Expanding on this by investigating potentially implicated paracrine mediators and upregulated RNA expression/protein synthesis of receptors and ligands is outside of the scope of this study. In the HT-29 - DRG neuron coculture we further assessed the capacity of innervating fibers to respond to noxious stimuli, mimicking acute/chronic pain in cancer patients that can be triggered by the compounding of cancer progression and e.g., inflammation related low pH (H^+), ATP release and loading of the tumour-bearing limb [52]. We tested the response of fibers to capsaicin and bradykinin and found that terminals of nerves innervating the axonal compartment were excitable and measured responses were remarkably greater (duration and frequency) than those observed in cultures without cancer and exogenously applied NGF. Finally, the physiological relevance of the INV-MPS as a tool for investigating CIP was demonstrated by live-imaging of evoked calcium transients occurring in 3D cancer-innervating fibers. Calcium imaging in the INV-MPS successfully brought together the concepts of tumour innervation and neuronal activity in a highly qualitative manner complementary to the MEA-based readout. Moreover, in this work we extensively demonstrate the electrophysiological effects of sensory innervation in cancer spheroids, but emerging evidence indicates that peripheral neurons can also modulate cancer homeostasis / dissemination [45]. It is thus plausible to consider utilizing the INV-MPS to gain insights into perturbations of tumour progression by neural involvement. Finally reiterating, our focus has been on studying nerve-cancer interaction, but the INV-MPS can also be applied to closely monitor innervation in other pain-generating tissues (e.g., somatic and visceral organs). Our system is not limited by overcomplexity, but effectively provides a user-friendly and scalable workflow with a robust tissue-relevant readout. Focusing on preclinical studies, stable electrophysiological readouts for innervation in 3D microtissues has competitive translational potential considering the difficulty of manipulating innervation *in vivo*. This is why we are convinced that our microphysiological model has potential for human-relevant drug discovery, particularly in pathologies where tissue innervation has been implicated. Furthermore, the INV - MPS is purposefully designed to facilitate the exploration of complex *in vitro* biology, presenting great potential for researchers in the MPS field who seek to understand the intricate interactions between the PNS and innervated organs.

Chapter 8: Concluding Insights

8.1 General Comments

With the INV-MPS research published in scientific journal *Biofabrication*, our aim is to establish ourselves as knowledgeable on facilitating tissue innervation in the context of OoC and MPS science. In the manuscript, I choose to use the term MPS instead of OoC because OoC typically refers to a specific type of MPS, which incorporates perfusion and is designed to replicate the microenvironment of a particular organ or tissue, such as the lung, heart, liver, kidney or brain. OoCs are generally composed of a clear and flexible polymer with microfluidic channels often lined with living cells derived from organ or tissue. This dynamic environment mimics the mechanical and chemical behaviours of functional units inside. On the other hand, MPS is a broader term that encompasses OoCs but is not limited to a single organ or tissue and does not necessarily include perfusion. MPS can include multi-organ systems, tissue-tissue interfaces and more complex models that set out to replicate interconnected body systems, simulating human physiology. Therefore, when referring to the INV-MPS platform in the work titled "Cancer-mediated Axonal Guidance of Sensory Neurons in a MEA-based Innervation MPS," I believe it falls under the MPS umbrella. Noting that, specific nomenclature ascribed to the platform sometimes depends on the exact application and the scope of the research being conducted, so both terms; OoC and MPS, can fit in different contexts [178].

Main line of the thesis; developing *in vitro* models for sensory innervation of cancer, is similarly followed in the INV-MPS publication, while also making a larger case for general tissue-innervation and including relevant results from both the SLE INV-MPS and MEA-integrated INV-MPS. It is believed that the requirements outlined for the desired INV-MPS in the general introduction can be effectively met by combining the developed platforms for specific applications (SLE INV-MPS for imaging and INV-MPS for electrophysiology/imaging). In the introduction to this thesis, I describe designing a device to support the coculture of DRG neurons and cancer spheroids for the study of pain, which is PDMS-free and instead constructed from glass with necessary incorporation of photoresist [179]. Additionally, device should be compartmentalized, separating adjacent tissue wells and connect them via microtunnels. Key aspect of the device is the ability to provide MEA-based electrophysiological recordings from neurons cultured in 3D hydrogels within a reusable and scalable environment.

Hence, with the (SLE) INV-MPS study, I argue that I was able to meet the requirements specified for the desired INV-MPS in the introduction. Noting that imaging can also be performed in the INV-MPS, but the thicker substrate of 1.0 mm vs. 150 µm would require a longer working distance objective, with reduced image quality. Furthermore, this approach enables inclusion of all proposed material characteristics and functionality requirements (see Chapter. 1 – Figure. 5), coculturing both cell types in a CME-integrated and compartmentalized 3D hydrogel platform, which is reusable and scalable. As the electrophysiological and morphological readouts can be carried out inside a 384 well microplate adaptor for robotic workflows and the SLE INV-MPS can be used repetitively whilst the INV-MPS can be used ~10x with appropriate cleaning. Limited use lies in CME and glue deterioration with repeated hydration of the system. Initially, the epoxy-based adhesion method for bonding the microfluidic piece and MEA was poor and alternatives were explored due to concerns regarding bond strength and standardization (See Chapter. 2 & 3). However, progress made in addressing these concerns by incorporating a designated glue guide, etched into the bonding surface of the microfluidic piece manufactured by FEMTOprint SA, eliminated these concerns. The INV-MPS is, therefore, not glue-free but the use of the epoxy adhesive, with some modifications, proved satisfactory.

With regards to the MEA-based recordings, I took on a challenge by examining sensory innervation, considering that DRG neurons do not directly synapse with other DRG neurons *in vivo* but rather solely with neurons in the CNS (example of DRGs synapsing *in vitro* does exist but needs more research [180]). This means that when a signal is recorded within a somatic CME, the same neuron must, generally, extend across the barrier into the axonal compartment, either through the same neurite or another neurite after the signal is processed near the soma. Hypothesis was that neurons that do synapse and form connections, such as hippocampal neurons, may exhibit a higher response rate in the *in vitro* model. It should, therefore, be possible to effectively study the associated electrophysiological behaviour of innervation patterns in different brain regions using the INV-MPS. I also acknowledge that placing microelectrodes inside the microtunnels of the separating barrier would be the preferred method for accurately monitoring terminal inputs. Therefore, I continue to explore a low-temperature fusion bonding technique to ensure a secure seal between the microfluidic chip and the MEA to guarantee such reliable measurements.

8.2 Therapeutic Strategies

Pain management approaches summarized by the world health organization (WHO) include non-opioid analgesics like NSAIDs or acetaminophen for mild pain, weak opioids (hydrocodone and codeine) with or without non-opioid analgesics for moderate pain and potent opioids like morphine, methadone and fentanyl for severe pain [181]. However, since they cannot treat the mechanisms underlying pain initiation and primary afferent sensitization, drugs that target peripheral tissues are favored. With the avoidance of central side effects as an obvious desirable benefit of targeting the PNS specifically in CIP [52].

Findings in the INV-MPS study reveal that neural outgrowth is inducible in cancer spheroid-neuron cocultures and a potential driver might be the presence of neurotrophin NGF, but it would require extensive additional research to confirm which guidance molecules and exact mechanisms are involved. More importantly, I argue that interplay between cancer and the PNS is delicate and scientists should be conscious of exogenously applied NGF and other growth factors masking cell-cell crosstalk in coculture models. Understanding the release of growth factors and inflammatory mediators in CIP is potentially key for elucidating mechanisms of nerve-cancer interaction driving pathological pain and identifying therapeutic targets to block this engagement.

In a news article called "Cancer–neuronal crosstalk and the startups working to silence it" [174], published by Elie Dolgin in Nature Biotechnology, he discusses biotech startups taking aim at the neuronal signaling that drives cancer growth and progression. Thus, focusing more on neurons affecting cancer rather than vice versa or CIP specifically, but the article is still highly relevant as it discusses the potential blocking of connections that the tumour cells make with surrounding neuronal tissue. With its lead small molecule candidate, Divide & Conquer (a company in the cancer neuroscience space) has set out to block the signaling pathway involved in activating growth-associated protein-43, a regulator of synaptic plasticity that is also essential for formation and function of tumour protrusions. The article also details how startups are, similarly, coculturing primary neurons with both tumour and immune cells to visualize tumour innervation. Interventive therapies aimed at blocking nerve-cancer interplay then involve manipulating tumour-associated neurons with viral vectors, CRISPR-based screens of neuronal genes involved in regulating neural contact formation, transmission and axonal guidance and neural focused bioinformatics.

Furthermore, throughout this work and particularly in the general introduction, I mention the work of Prof. Patrick W Mantyh on cancer metastasis affecting the sensory nerves innervating bone [47, 51]. His work demonstrates the pathological sprouting and reconfiguration of TrkA expressing sensory nerve fibers in murine tumour-bearing tissue. He and his team point towards the NGF-

TrkA mechanism driving this adaptation and accordingly they used anti-NGF antibodies to effectively ameliorate sprouting and pain. Effectiveness of anti-NGF treatments in reducing pain in the clinic has already been shown with Tanezumab, an intravenously administered NGF monoclonal antibody for treatment of osteoarthritis pain [54]. However, Tanezumab showed only mild improvement compared to NSAIDs and opioids for pain treatment, causing regulators to state the current risks (reporting sensation abnormalities and RPOA - rapid onset osteoarthritis) outweigh the benefits. This calls for the study of downstream signaling proteins specific to the pain cascade, excluding those with involvement in other pathways, to avoid off-target effects.

Targeting specific Navs (sodium channels) involved in initiating and propagating action potentials in nociceptive neurons presents challenges. Only certain Nav isoforms, such as NaV1.7, NaV1.8, and NaV1.9 are mostly expressed in sensory afferents responsible for transmitting nociceptive signals. Consequently, extensive efforts have been made to discover selective inhibitors for these specific Nav subtypes. Selectivity is important for drug safety since, again, off-target effects on other Nav isoforms involved in central and peripheral conduction, skeletal muscle contraction and cardiac processes could be harmful. Pain sensation is closely associated with Nav1.7, as loss-of-function mutations have been linked to insensitivity to pain, while increased Nav1.7 activity is associated with heightened pain sensitivity [182]. Blocking Nav1.7 activity may thus hold promise for pain treatment. SiteOne Therapeutics, Inc., for example, has patented a non-hydrated ketone inhibitor of Nav1.7 and is currently conducting a Phase 1 clinical trial to assess its safety, tolerability, and pharmacokinetics [183].

Similarly difficult is developing compounds to target TRPV1 to reduce sensitivity to thermal and mechanical (breakthrough) pain, as it has been faced with the significant challenge of block causing hyperthermia (high body temperature) as a side effect [184]. Other strategies involve targeting pro-inflammatory cytokines like e.g., IL-1β, TNF-α, and IL-6, which play a role in the development and maintenance of cancer pain. Neutralizing antibodies against these cytokines have shown pain attenuation in rodents. Additionally, blocking tumour-derived vascular endothelial growth factor (VEGF) from binding to VEGFR1 in sensory neurons has demonstrated pain reduction with genetic deletion and silencing of VEGFR1 specifically mitigating cancer pain [185].

Concluding that this field continuously seeks new mechanistic insights and can benefit from the potential of MPSs to explore novel avenues for therapeutic interventions in cancer-related pain and pain management in general.

8.2 Innervation in Microfluidics & Outlook

This thesis primarily focuses on modelling the interaction between cancer microtissues and sensory neuron innervation using MPS technology. Within the INV-MPS study, I aimed to demonstrate the platform's potential to address the broader goals of the MPS-field, which involves replicating organ functions that are challenging to recapitulate using traditional cell cultures. I additionally describe the INV-MPS as a tool to overcome the complexities associated with replicating nerve fiber ingrowth in MPSs. Emphasizing the need for similar platforms that can effectively integrate peripheral neurons and target tissues while providing reliable electrophysiological readouts aligned with neuronal activity. I state that this INV-MPS platform specifically overcomes limitations of conventional systems, enabling close mimicry of *in vivo* nerve-tissue interaction through 3D peripheral nerve fibers innervating hydrogel-embedded targets combined with a reliable microelectrode array based readout.

Through this comprehensive work encompassing the research article and thesis, the team at the Natural and Medical Sciences Institute positions itself as a general facilitator for investigating the innervation of (already) complex *in vitro* biological systems and associated electrophysiology. While also advocating for the strong consideration of innervation in OoC and MPS research. Correspondingly, a 2019 review by Park et al. published in Trends in Biotechnology, highlights the integration of tissue innervation as a frontier for enhancing Organ-on-Chip systems [2]. The review differentiates between modeling neuron-neuron connections (synapses), neuroeffector junctions involving non-neuronal cells as the receiver of innervation and neuromuscular junctions involving muscle fibers. Promising innervation approaches are summarized in a table with the majority of the presented strategies incorporating electrophysiological readouts. Further underlining current approach as a relevant method that should hold potential for researchers in the MPS field wanting to explore the impact of innervation.

MPSs that integrate innervated tissues serve as a valuable alternative to animal models and can facilitate the translation of preclinical research to human applications. Next evolution of the INV-MPS could incorporate e.g., fully human iPSC-derived sensory neurons and patient-derived cancer tissues, paving the way for even more ethically sustainable and innovative research into viable targeted therapies. Ultimately, active consideration of the pivotal role that nerve fibers play in numerous organs and tissues is key and the incorporation of innervation within MPSs can truly advance accurate modeling of human physiology *in vitro*.

References

[1] S. Das *et al.*, "Innervation: the missing link for biofabricated tissues and organs," *NPJ Regen Med,* vol. 5, p. 11, 2020, doi: 10.1038/s41536-020-0096-1.

[2] D. Park, J. Lee, J. J. Chung, Y. Jung, and S. H. Kim, "Integrating Organs-on-Chips: Multiplexing, Scaling, Vascularization, and Innervation," *Trends Biotechnol,* vol. 38, no. 1, pp. 99-112, Jan 2020, doi: 10.1016/j.tibtech.2019.06.006.

[3] S. Takahashi *et al.*, "Homeostatic pruning and activity of epidermal nerves are dysregulated in barrier-impaired skin during chronic itch development," *Sci Rep,* vol. 9, no. 1, p. 8625, Jun 13 2019, doi: 10.1038/s41598-019-44866-0.

[4] B. Laverdet, A. Danigo, D. Girard, L. Magy, C. Demiot, and A. Desmouliere, "Skin innervation: important roles during normal and pathological cutaneous repair," *Histol Histopathol,* vol. 30, no. 8, pp. 875-92, Aug 2015, doi: 10.14670/HH-11-610.

[5] E. Lepore, I. Casola, G. Dobrowolny, and A. Musaro, "Neuromuscular Junction as an Entity of Nerve-Muscle Communication," *Cells,* vol. 8, no. 8, Aug 16 2019, doi: 10.3390/cells8080906.

[6] B. A. Cisterna *et al.*, "Active acetylcholine receptors prevent the atrophy of skeletal muscles and favor reinnervation," *Nature Communications,* vol. 11, no. 1, 2020, doi: 10.1038/s41467-019-14063-8.

[7] X. Guo *et al.*, "Tissue engineering the mechanosensory circuit of the stretch reflex arc with human stem cells: Sensory neuron innervation of intrafusal muscle fibers," *Biomaterials,* vol. 122, pp. 179-187, Apr 2017, doi: 10.1016/j.biomaterials.2017.01.005.

[8] A. Erickson *et al.*, "Voltage-gated sodium channels: (Na(V))igating the field to determine their contribution to visceral nociception," *J Physiol,* vol. 596, no. 5, pp. 785-807, Mar 1 2018, doi: 10.1113/JP273461.

[9] S. M. Brierley, T. J. Hibberd, and N. J. Spencer, "Spinal Afferent Innervation of the Colon and Rectum," *Front Cell Neurosci,* vol. 12, p. 467, 2018, doi: 10.3389/fncel.2018.00467.

[10] J. M. Brazill, A. T. Beeve, C. S. Craft, J. J. Ivanusic, and E. L. Scheller, "Nerves in Bone: Evolving Concepts in Pain and Anabolism," *J Bone Miner Res,* vol. 34, no. 8, pp. 1393-1406, Aug 2019, doi: 10.1002/jbmr.3822.

[11] G. Castaneda-Corral *et al.*, "The majority of myelinated and unmyelinated sensory nerve fibers that innervate bone express the tropomyosin receptor kinase A," *Neuroscience,* vol. 178, pp. 196-207, Mar 31 2011, doi: 10.1016/j.neuroscience.2011.01.039.

[12] S. W. Nam, Song, H. J., Back, S. J., Kim, T. H., Cho, S. H., Han, J. Y., Chung, K. W., "Decreased Hepatic Nerve Fiber Innervation in Patients with Liver Cirrhosis," *Gut and Liver,* 2007, doi: 10.5009/gnl.2007.1.2.165.

[13] K. Mizuno and Y. Ueno, "Autonomic Nervous System and the Liver," *Hepatol Res,* vol. 47, no. 2, pp. 160-165, Feb 2017, doi: 10.1111/hepr.12760.

[14] P. S. Rajendran *et al.*, "Identification of peripheral neural circuits that regulate heart rate using optogenetic and viral vector strategies," *Nat Commun,* vol. 10, no. 1, p. 1944, Apr 26 2019, doi: 10.1038/s41467-019-09770-1.

[15]   S. Kapa, C. V. DeSimone, and S. J. Asirvatham, "Innervation of the heart: An invisible grid within a black box," *Trends Cardiovasc Med,* vol. 26, no. 3, pp. 245-57, Apr 2016, doi: 10.1016/j.tcm.2015.07.001.

[16]   A. Guerrero-Moreno, C. Baudouin, S. Melik Parsadaniantz, and A. Reaux-Le Goazigo, "Morphological and Functional Changes of Corneal Nerves and Their Contribution to Peripheral and Central Sensory Abnormalities," *Front Cell Neurosci,* vol. 14, p. 610342, 2020, doi: 10.3389/fncel.2020.610342.

[17]   K. J. Paunicka, J. Mellon, D. Robertson, M. Petroll, J. R. Brown, and J. Y. Niederkorn, "Severing corneal nerves in one eye induces sympathetic loss of immune privilege and promotes rejection of future corneal allografts placed in either eye," *Am J Transplant,* vol. 15, no. 6, pp. 1490-501, Jun 2015, doi: 10.1111/ajt.13240.

[18]   Y. Wang *et al.*, "The role of somatosensory innervation of adipose tissues," *Nature,* vol. 609, no. 7927, pp. 569-574, Sep 2022, doi: 10.1038/s41586-022-05137-7.

[19]   A. Guilherme, F. Henriques, A. H. Bedard, and M. P. Czech, "Molecular pathways linking adipose innervation to insulin action in obesity and diabetes mellitus," *Nat Rev Endocrinol,* vol. 15, no. 4, pp. 207-225, Apr 2019, doi: 10.1038/s41574-019-0165-y.

[20]   M. K. S. B. McMahon, I. Tracey and D. C. Turk, *Wall and Melzack's textbook of pain*. Elsevier, 2013.

[21]   J. H. S. E. R. Kandel, T. M. Jessell, *Principles of neural science*, 4th ed. McGraw-Hill, 2013, p. 1414.

[22]   S. N. Raja *et al.*, "The revised International Association for the Study of Pain definition of pain: concepts, challenges, and compromises," *Pain,* vol. 161, no. 9, pp. 1976-1982, Sep 1 2020, doi: 10.1097/j.pain.0000000000001939.

[23]   C. Paolo, McNaughton, P., "Peripheral pain mechanisms.," *Current Opinion in Neurobiology,* 1997, doi: 10.1016/S0959-4388(97)80028-1.

[24]   A. I. Basbaum, D. M. Bautista, G. Scherrer, and D. Julius, "Cellular and molecular mechanisms of pain," *Cell,* vol. 139, no. 2, pp. 267-84, Oct 16 2009, doi: 10.1016/j.cell.2009.09.028.

[25]   R. S. Martin Schmelz, Hermann O. Handwerker and H. Erik Torebjork, "Encoding of burning pain from capsaicin-treated human skin in two categories of unmyelinated nerve fibres," *Brain* 2000, doi: 10.1093/brain/123.3.560.

[26]   E. Cavalli, S. Mammana, F. Nicoletti, P. Bramanti, and E. Mazzon, "The neuropathic pain: An overview of the current treatment and future therapeutic approaches," *Int J Immunopathol Pharmacol,* vol. 33, p. 2058738419838383, Jan-Dec 2019, doi: 10.1177/2058738419838383.

[27]   M. A. Fitzcharles, S. P. Cohen, D. J. Clauw, G. Littlejohn, C. Usui, and W. Hauser, "Nociplastic pain: towards an understanding of prevalent pain conditions," *Lancet,* vol. 397, no. 10289, pp. 2098-2110, May 29 2021, doi: 10.1016/S0140-6736(21)00392-5.

[28]   R. L. Chimenti, Frey-Law, L. A., & Sluka, K. A., "Mechanism Based Approach to Pain Management," *Physical Therapy,* 2018, doi: 10.1093/ptj/pzy030.

[29]   M. Devor, "Unexplained peculiarities of the dorsal root ganglion," *Pain,* 1999.

[30]   R. V. Haberberger, C. Barry, N. Dominguez, and D. Matusica, "Human Dorsal Root Ganglia," *Front Cell Neurosci,* vol. 13, p. 271, 2019, doi: 10.3389/fncel.2019.00271.

[31]   B. P. Bean, "The action potential in mammalian central neurons," *Nat Rev Neurosci,* vol. 8, no. 6, pp. 451-65, Jun 2007, doi: 10.1038/nrn2148.

[32]   M. van der Moolen, A. Lovera, F. Ersoy, S. Mommo, P. Loskill, and P. Cesare, "Cancer-mediated axonal guidance of sensory neurons in a microelectrode-based innervation MPS," *Biofabrication,* Jan 23 2024, doi: 10.1088/1758-5090/ad218a.

[33]   T. Bioscience. "Ion Channels Involved in Pain. ." News-Medical. Retrieved on February 04, 2024. https://www.news-medical.net/whitepaper/20190817/Ion-Channels-Involved-in-Pain.aspx.

[34]   D. J. A. I. Basbaum, "Molecular mechanisms of nociception," *Pain,* 2001, doi: 10.1038/35093019.

[35]   E. Cao, M. Liao, Y. Cheng, and D. Julius, "TRPV1 structures in distinct conformations reveal activation mechanisms," *Nature,* vol. 504, no. 7478, pp. 113-118, 2013, doi: 10.1038/nature12823.

[36]   A. L. H. Hodgkin, A. F. , "A quantitative description of membrane current and its application to conduction and excitation in nerve," *J. Physiol.,* 28-08-1952 1952, doi: 10.1113/jphysiol.1952.sp004764.

[37]   E. E. Benarroch, "Ion channels in nociceptors," *Neurology,* 20-02-2015 2015, doi: 10.1212/WNL.0000000000001382.

[38]   C. H.-R. Sonja Kilo, Kenneth M. Hargreaves a,b, Christopher M. Flores, "Peripheral CGRP release as a marker for neurogenic inflammation a model system for the study of neuropeptide secretion in rat paw skin," *Pain,* 1997, doi: 10.1016/S0304-3959(97)00108-5.

[39]   H. Y. Sheng and Y. Q. Zhang, "Emerging Molecular Targets for the Management of Cancer Pain," *Neurosci Bull,* vol. 36, no. 10, pp. 1225-1228, Oct 2020, doi: 10.1007/s12264-020-00526-2.

[40]   M. Madeo *et al.*, "Cancer exosomes induce tumor innervation," *Nat Commun,* vol. 9, no. 1, p. 4284, Oct 16 2018, doi: 10.1038/s41467-018-06640-0.

[41]   S. M. Gysler and R. Drapkin, "Tumor innervation: peripheral nerves take control of the tumor microenvironment," *J Clin Invest,* vol. 131, no. 11, Jun 1 2021, doi: 10.1172/JCI147276.

[42]   X. Chu *et al.*, "Blocking Cancer-Nerve Crosstalk for Treatment of Metastatic Bone Cancer Pain," *Adv Mater,* vol. 34, no. 17, p. e2108653, Apr 2022, doi: 10.1002/adma.202108653.

[43]   X. Li *et al.*, "Targeting tumor innervation: premises, promises, and challenges," *Cell Death Discov,* vol. 8, no. 1, p. 131, Mar 25 2022, doi: 10.1038/s41420-022-00930-9.

[44]   D. A. Silverman, V. K. Martinez, P. M. Dougherty, J. N. Myers, G. A. Calin, and M. Amit, "Cancer-Associated Neurogenesis and Nerve-Cancer Cross-talk," *Cancer Res,* vol. 81, no. 6, pp. 1431-1440, Mar 15 2021, doi: 10.1158/0008-5472.CAN-20-2793.

[45]   H. Wang *et al.*, "Role of the nervous system in cancers: a review," *Cell Death Discov,* vol. 7, no. 1, p. 76, Apr 12 2021, doi: 10.1038/s41420-021-00450-y.

[46]   Z. Zhu *et al.*, "Nerve growth factor and enhancement of proliferation, invasion, and tumorigenicity of pancreatic cancer cells," *Mol Carcinog,* vol. 35, no. 3, pp. 138-47, Nov 2002, doi: 10.1002/mc.10083.

[47]   J. M. Jimenez-Andrade *et al.*, "Pathological sprouting of adult nociceptors in chronic prostate cancer-induced bone pain," *J Neurosci,* vol. 30, no. 44, pp. 14649-56, Nov 3 2010, doi: 10.1523/JNEUROSCI.3300-10.2010.

[48] Q. Zheng, D. Fang, J. Cai, Y. Wan, J. S. Han, and G. G. Xing, "Enhanced excitability of small dorsal root ganglion neurons in rats with bone cancer pain," *Mol Pain,* vol. 8, p. 24, Apr 3 2012, doi: 10.1186/1744-8069-8-24.

[49] S. A. T. Mitchell, L. A. Majuta, and P. W. Mantyh, "New Insights in Understanding and Treating Bone Fracture Pain," *Curr Osteoporos Rep,* vol. 16, no. 4, pp. 325-332, Aug 2018, doi: 10.1007/s11914-018-0446-8.

[50] P. W. Mantyh, M. Koltzenburg, L. M. Mendell, L. Tive, and D. L. Shelton, "Antagonism of nerve growth factor-TrkA signaling and the relief of pain," *Anesthesiology,* vol. 115, no. 1, pp. 189-204, Jul 2011, doi: 10.1097/ALN.0b013e31821b1ac5.

[51] A. P. Bloom *et al.*, "Breast cancer-induced bone remodeling, skeletal pain, and sprouting of sensory nerve fibers," *J Pain,* vol. 12, no. 6, pp. 698-711, Jun 2011, doi: 10.1016/j.jpain.2010.12.016.

[52] R. Haroun, J. N. Wood, and S. Sikandar, "Mechanisms of cancer pain," *Front Pain Res (Lausanne),* vol. 3, p. 1030899, 2022, doi: 10.3389/fpain.2022.1030899.

[53] M. K. Patel, A. D. Kaye, and R. D. Urman, "Tanezumab: Therapy targeting nerve growth factor in pain pathogenesis," *J Anaesthesiol Clin Pharmacol,* vol. 34, no. 1, pp. 111-116, Jan-Mar 2018, doi: 10.4103/joacp.JOACP_389_15.

[54] M. C. Hochberg *et al.*, "Long-Term Safety and Efficacy of Subcutaneous Tanezumab Versus Nonsteroidal Antiinflammatory Drugs for Hip or Knee Osteoarthritis: A Randomized Trial," *Arthritis Rheumatol,* vol. 73, no. 7, pp. 1167-1177, Jul 2021, doi: 10.1002/art.41674.

[55] J. W. Park, B. Vahidi, A. M. Taylor, S. W. Rhee, and N. L. Jeon, "Microfluidic culture platform for neuroscience research," *Nat Protoc,* vol. 1, no. 4, pp. 2128-36, 2006, doi: 10.1038/nprot.2006.316.

[56] A. J. Clark *et al.*, "Functional imaging in microfluidic chambers reveals sensory neuron sensitivity is differentially regulated between neuronal regions," *Pain,* vol. 159, no. 7, pp. 1413-1425, Jul 2018, doi: 10.1097/j.pain.0000000000001145.

[57] N. Vysokov, S. B. McMahon, and R. Raouf, "The role of Na(V) channels in synaptic transmission after axotomy in a microfluidic culture platform," *Sci Rep,* vol. 9, no. 1, p. 12915, Sep 9 2019, doi: 10.1038/s41598-019-49214-w.

[58] R. B. Campenot, K. Lund, and S. A. Mok, "Production of compartmented cultures of rat sympathetic neurons," *Nat Protoc,* vol. 4, no. 12, pp. 1869-87, 2009, doi: 10.1038/nprot.2009.210.

[59] A. Klusch, C. Gorzelanny, P. W. Reeh, M. Schmelz, M. Petersen, and S. K. Sauer, "Local NGF and GDNF levels modulate morphology and function of porcine DRG neurites, In Vitro," *PLoS One,* vol. 13, no. 9, p. e0203215, 2018, doi: 10.1371/journal.pone.0203215.

[60] Z. Ao *et al.*, "Human Spinal Organoid-on-a-Chip to Model Nociceptive Circuitry for Pain Therapeutics Discovery," *Anal Chem,* vol. 94, no. 2, pp. 1365-1372, Jan 18 2022, doi: 10.1021/acs.analchem.1c04641.

[61] Y. Lei *et al.*, "An on-chip model for investigating the interaction between neurons and cancer cells," *Integr Biol (Camb),* vol. 8, no. 3, pp. 359-67, Mar 14 2016, doi: 10.1039/c5ib00309a.

[62] E. Neto *et al.*, "Osteoclast-derived extracellular vesicles are implicated in sensory neurons sprouting through the activation of epidermal growth factor signaling," *Cell Biosci,* vol. 12, no. 1, p. 127, Aug 14 2022, doi: 10.1186/s13578-022-00864-w.

[63]   A. D. Sharma *et al.*, "Engineering a 3D functional human peripheral nerve in vitro using the Nerve-on-a-Chip platform," *Sci Rep,* vol. 9, no. 1, p. 8921, Jun 20 2019, doi: 10.1038/s41598-019-45407-5.

[64]   A. Guichard, N. Remoué, and T. Honegger, "In Vitro Sensitive Skin Models: Review of the Standard Methods and Introduction to a New Disruptive Technology," *Cosmetics,* vol. 9, no. 4, 2022, doi: 10.3390/cosmetics9040067.

[65]   E. NEHER, SAKMANN, B. , "Single-channel currents recorded from membrane of denervated frog muscle fibres," *Nature,* 1976, doi: 10.1038/260799a0.

[66]   C. Py *et al.*, "From understanding cellular function to novel drug discovery: the role of planar patch-clamp array chip technology," *Front Pharmacol,* vol. 2, p. 51, 2011, doi: 10.3389/fphar.2011.00051.

[67]   A. H. Cecilia Farre, Claudia Haarmann, Sonja Stoelzle, Mohamed Kreir, and A. B. a. N. F. Michael George, "Port-a-Patch and Patchliner High Fidelity Electrophysiology for Secondary Screening and Safety Pharmacology," *Combinatorial Chemistry & High Throughput Screening,* 2009, doi: 10.2174/138620709787047966.

[68]   C. Tsantoulas, C. Farmer, P. Machado, K. Baba, S. B. McMahon, and R. Raouf, "Probing functional properties of nociceptive axons using a microfluidic culture system," *PLoS One,* vol. 8, no. 11, p. e80722, 2013, doi: 10.1371/journal.pone.0080722.

[69]   H. Rubaiy, "A Short Guide to Electrophysiology and Ion Channels," *J Pharm Pharm Sci. ,* 2017, doi: 10.18433/J32P6R.

[70]   M. W. Kucharczyk, K. I. Chisholm, F. Denk, A. H. Dickenson, K. Bannister, and S. B. McMahon, "The impact of bone cancer on the peripheral encoding of mechanical pressure stimuli," *Pain,* vol. 161, no. 8, pp. 1894-1905, Aug 2020, doi: 10.1097/j.pain.0000000000001880.

[71]   B. Molina-Martinez *et al.*, "A multimodal 3D neuro-microphysiological system with neurite-trapping microelectrodes," *Biofabrication,* vol. 14, no. 2, Jan 24 2022, doi: 10.1088/1758-5090/ac463b.

[72]   J. T. Russell, "Imaging calcium signals in vivo: a powerful tool in physiology and pharmacology," *Br J Pharmacol,* vol. 163, no. 8, pp. 1605-25, Aug 2011, doi: 10.1111/j.1476-5381.2010.00988.x.

[73]   D. M. Treiman, "GABAergic mechanisms in epilepsy," *Epilepsia,* vol. 42 Suppl 3, pp. 8-12, 2001, doi: 10.1046/j.1528-1157.2001.042suppl.3008.x.

[74]   U. E. H. Hammerle, A . Mohr & W. Nisch, "Extracellular recording in neuronal networks with substrate integrated," *Biosensors & Bioelectronics,* 1994, doi: 10.1016/0956-5663(94)80067-7.

[75]   M. Dipalo *et al.*, "Intracellular and Extracellular Recording of Spontaneous Action Potentials in Mammalian Neurons and Cardiac Cells with 3D Plasmonic Nanoelectrodes," *Nano Lett,* vol. 17, no. 6, pp. 3932-3939, Jun 14 2017, doi: 10.1021/acs.nanolett.7b01523.

[76]   Y. Bellouard, "The Femtoprint Project," *Journal of Laser Micro/Nanoengineering,* vol. 7, no. 1, pp. 1-10, 2012, doi: 10.2961/jlmn.2012.01.0001.

[77]   J. M. K. Ng, Gitlin, I., Stroock, A. D., & Whitesides, G. M. , "Components for integrated poly(dimethylsiloxane) microfluidic systems," *Electrophoresis,* 2002, doi: 10.1002/1522-2683(200210)23:20<3461::AID-ELPS3461>3.0.CO;2-8.

[78]   J. N. Sleigh, G. A. Weir, and G. Schiavo, "A simple, step-by-step dissection protocol for the rapid isolation of mouse dorsal root ganglia," *BMC Res Notes,* vol. 9, p. 82, Feb 11 2016, doi: 10.1186/s13104-016-1915-8.

[79] S. Meltzer, C. Santiago, N. Sharma, and D. D. Ginty, "The cellular and molecular basis of somatosensory neuron development," *Neuron,* vol. 109, no. 23, pp. 3736-3757, Dec 1 2021, doi: 10.1016/j.neuron.2021.09.004.

[80] M. B. Bunge, M. I. Johnson, M. D. Ard, and N. Kleitman, "Factors influencing the growth of regenerating nerve fibers in culture," *Prog Brain Res,* vol. 71, pp. 61-74, 1987, doi: 10.1016/s0079-6123(08)61814-2.

[81] C. Jensen and Y. Teng, "Is It Time to Start Transitioning From 2D to 3D Cell Culture?," *Front Mol Biosci,* vol. 7, p. 33, 2020, doi: 10.3389/fmolb.2020.00033.

[82] A. Ribeiro, S. Vargo, E. M. Powell, and J. B. Leach, "Substrate three-dimensionality induces elemental morphological transformation of sensory neurons on a physiologic timescale," *Tissue Eng Part A,* vol. 18, no. 1-2, pp. 93-102, Jan 2012, doi: 10.1089/ten.tea.2011.0221.

[83] R. Sedlak. "Photoresist Developing." RD Chemical Company. http://rdchem.com/chemical-milling-processes/photoresist-developing.html

[84] H. P. Cleaners. "PDMS Bonding." Harrick Plasma. https://harrickplasma.com/pdms-bonding/#:~:text=Process%20time%3A%2015%2D60%20seconds,plasma%20treating%20similar%20PDMS%20materials.

[85] X. Jiang, Zheng, H., Gourdin, S., Hammond, P.T., "Polymer on Polymer Stamping Universal Approaches to Chemically Patterned Surfaces," *Langmuir,* 2002, doi: 10.1021/la011098d.

[86] D. B. Howard and B. K. Harvey, "Assaying the Stability and Inactivation of AAV Serotype 1 Vectors," *Hum Gene Ther Methods,* vol. 28, no. 1, pp. 39-48, Feb 2017, doi: 10.1089/hgtb.2016.180.

[87] S. Kugler, E. Kilic, and M. Bahr, "Human synapsin 1 gene promoter confers highly neuron-specific long-term transgene expression from an adenoviral vector in the adult rat brain depending on the transduced area," *Gene Ther,* vol. 10, no. 4, pp. 337-47, Feb 2003, doi: 10.1038/sj.gt.3301905.

[88] M. Lange, Y. Zeng, A. Knight, A. Windebank, and E. Trushina, "Comprehensive Method for Culturing Embryonic Dorsal Root Ganglion Neurons for Seahorse Extracellular Flux XF24 Analysis," *Front Neurol,* vol. 3, p. 175, 2012, doi: 10.3389/fneur.2012.00175.

[89] Corning, "Certificate of Analysis Matrigel," 2022.

[90] N. F. A. Zainal, S. A. Lai, and C. H. Chan, "Melt Rheological Behavior and Morphology of Poly(ethylene oxide)/Natural Rubber-graft-Poly(methyl methacrylate) Blends," *Polymers (Basel),* vol. 12, no. 3, Mar 24 2020, doi: 10.3390/polym12030724.

[91] G. Stojkov, Z. Niyazov, F. Picchioni, and R. K. Bose, "Relationship between Structure and Rheology of Hydrogels for Various Applications," *Gels,* vol. 7, no. 4, Dec 9 2021, doi: 10.3390/gels7040255.

[92] R. K. Willits and S. L. Skornia, "Effect of collagen gel stiffness on neurite extension," *J Biomater Sci Polym Ed,* vol. 15, no. 12, pp. 1521-31, 2004, doi: 10.1163/1568562042459698.

[93] P. Bednarczyk, I. Irska, K. Gziut, and P. Ossowicz-Rupniewska, "Novel Multifunctional Epoxy (Meth)Acrylate Resins and Coatings Preparation via Cationic and Free-Radical Photopolymerization," *Polymers (Basel),* vol. 13, no. 11, May 24 2021, doi: 10.3390/polym13111718.

[94]   P. Vulto, T. Huesgen, B. Albrecht, and G. A. Urban, "A full-wafer fabrication process for glass microfluidic chips with integrated electroplated electrodes by direct bonding of dry film resist," *Journal of Micromechanics and Microengineering,* vol. 19, no. 7, 2009, doi: 10.1088/0960-1317/19/7/077001.

[95]   E. E. S.-. Resistechno, "Technical Data Sheet_Ordyl_SY300_dry_film.pdf," ed: Resistechno, 2022.

[96]   B. J. Lin, "Deep uv lithography," *Journal of Vacuum Science and Technology,* vol. 12, no. 6, pp. 1317-1320, 1975, doi: 10.1116/1.568527.

[97]   A. Ribas-Massonis, M. Cicujano, J. Duran, E. Besalu, and A. Poater, "Free-Radical Photopolymerization for Curing Products for Refinish Coatings Market," *Polymers (Basel),* vol. 14, no. 14, Jul 13 2022, doi: 10.3390/polym14142856.

[98]   M. Chen, M. Zhong, and J. A. Johnson, "Light-Controlled Radical Polymerization: Mechanisms, Methods, and Applications," *Chem Rev,* vol. 116, no. 17, pp. 10167-211, Sep 14 2016, doi: 10.1021/acs.chemrev.5b00671.

[99]   A. Olziersky *et al.*, "Insight on the SU-8 resist as passivation layer for transparent Ga2O3–In2O3–ZnO thin-film transistors," *Journal of Applied Physics,* vol. 108, no. 6, 2010, doi: 10.1063/1.3477192.

[100]   J. M. Ripalda, R. Á. , and a. M. L. Dotor, "Ether cleavage and chemical removal of SU-8," *SciPost Chemistry,* 2022, doi: 10.26434/chemrxiv-2022-49n7z.

[101]   K. Y. Lee *et al.*, "Micromachining applications of a high resolution ultrathick photoresist," *Journal of Vacuum Science & Technology B: Microelectronics and Nanometer Structures Processing, Measurement, and Phenomena,* vol. 13, no. 6, pp. 3012-3016, 1995, doi: 10.1116/1.588297.

[102]   G. Genolet *et al.*, "Soft, entirely photoplastic probes for scanning force microscopy," *Review of Scientific Instruments,* vol. 70, no. 5, pp. 2398-2401, 1999, doi: 10.1063/1.1149767.

[103]   S. J. S. Carl J. Houtman, Jihui Guo, Helen Xu, Larry Gwin, "Properties of water-based acrylic pressure sensitive adhesive films in aqueous environments," 26-09-2007 2007.

[104]   A. A. Issa, M. El-Azazy, and A. S. Luyt, "Kinetics of alkoxysilanes hydrolysis: An empirical approach," *Sci Rep,* vol. 9, no. 1, p. 17624, Nov 26 2019, doi: 10.1038/s41598-019-54095-0.

[105]   M. K. Jan Schmidt*, "Highest-quality surface passivation of low-resistivity p-type silicon using stoichiometric PECVD silicon nitride," *Solar Energy Materials & Solar Cells,* 2001, doi: 10.1016/S0927-0248(00)00145-8.

[106]   J. Y. C. P.K. Chua, b, L.P. Wanga and N. H. , "Plasma-surface modification of biomaterials," *Materials Science & Engineering,* 2002, doi: 10.1016/S0927-796X(02)00004-9.

[107]   "What is a plasma." © PLASMA ELECTRONIC GmbH. https://plasma-electronic.com/en/what-is-a-plasma/

[108]   "Post Exposure Bake," in "Basics of Microstructuring," MicroChemicals GmbH.

[109]   N. G. Paul Vulto, Luigi Altomare, Jacqueline Bablet, Gianni Medoro, et al.. "Dry film resist for fast fluidic prototyping," presented at the 8th International Conference on Miniaturized Systems in Chemistry and Life Sciences - Micro Total Analysis Systems (µTAS), 2004.

[110]   J. Pine, "Recording action potentials from cultured neurons with extracellular microcircuit electrodes," *Journal of Neuroscience Methods,* 1979, doi: 10.1016/0165-0270(80)90042-4.

[111] J. P. Neto *et al.*, "Does Impedance Matter When Recording Spikes With Polytrodes?," *Front Neurosci,* vol. 12, p. 715, 2018, doi: 10.3389/fnins.2018.00715.

[112] D. A. ROBINSON, "The Electrical Properties of Metal Microelectrodes," *Proceedings of the IEEE,* 1968, doi: 10.1109/PROC.1968.6458.

[113] M. Mierzejewski, H. Steins, P. Kshirsagar, and P. D. Jones, "The noise and impedance of microelectrodes," *J Neural Eng,* vol. 17, no. 5, p. 052001, Oct 15 2020, doi: 10.1088/1741-2552/abb3b4.

[114] J. O. Jon Sinclair, Johan Pihl, and Owe Orwar, "Stabilization of high resistance seals in patch clamp recordings by laminar flow," *Anal Chem,* 2003, doi: 10.1021/ac0346611.

[115] A. d. Campo and C. Greiner, "SU-8: a photoresist for high-aspect-ratio and 3D submicron lithography," *Journal of Micromechanics and Microengineering,* vol. 17, no. 6, pp. R81-R95, 2007, doi: 10.1088/0960-1317/17/6/r01.

[116] K. A. Materials, "SU-8 Permanent Negative Epoxy Photoresist Formulations 2 - 25," 2020. https://kayakuam.com/wp-content/uploads/2020/09/KAM-SU-8-2-25-Datasheet-9.3.20-final.pdf

[117] M. GmbH, "Basics of Microstructuring - Exposure of Photoresists," 2013. [Online]. Available: https://www.microchemicals.com/technical_information/exposure_photoresist.pdf

[118] D. M. Inc., "ADEX® Thin Film Rolls or Sheets," 2020. https://djmicrolaminates.com/wp-content/uploads/2020/06/ADEX-Data-Sheet-June-2020.pdf

[119] "301-2FL Epoxy Adhesive," 2021. https://www.epotek.com/docs/en/Datasheet/301-2FL.pdf

[120] "Eppendorf_Liquid-Handling_SOP Manual pipettes dispensers Standard operating procedure manual dispensing systems," Eppendorf SE, Germany, 2022. https://www.eppendorf.com/product-media/doc/en/155258_SOP/Eppendorf_Liquid-Handling_SOP_Manual-pipettes-dispensers_Standard-operating-procedure-manual-dispensing-systems.pdf

[121] H. L. Daniel J. Cavanaugha, Liching Lob, Shannon D. Shieldsa, Mark J. Zylkad, Allan I. Basbauma and David J. Anderson, "Distinct subsets of unmyelinated primary sensoryfibers mediate behavioral responses to noxiousthermal and mechanical stimuli," *PNAS,* 2008, doi: 10.1073/pnas.0901507106.

[122] L. Djouhri and S. N. Lawson, "Abeta-fiber nociceptive primary afferent neurons: a review of incidence and properties in relation to other afferent A-fiber neurons in mammals," *Brain Res Brain Res Rev,* vol. 46, no. 2, pp. 131-45, Oct 2004, doi: 10.1016/j.brainresrev.2004.07.015.

[123] V. Prato *et al.*, "Functional and Molecular Characterization of Mechanoinsensitive "Silent" Nociceptors," *Cell Rep,* vol. 21, no. 11, pp. 3102-3115, Dec 12 2017, doi: 10.1016/j.celrep.2017.11.066.

[124] M. A. B. Cooper, R. M. Friedman, and J. Labanc, "Properties of high-threshold mechanoreceptors in the goat oral mucosa. II. Dynamic and static reactivity in carrageenan-inflamed mucosa," *Journal of Neurophysiology,* 1991, doi: 10.1152/jn.1991.66.4.1280.

[125] F. P. Magerl W, Meyer RA, Treede RD., "Roles of capsaicin-insensitive nociceptors in cutaneous pain and secondary hyperalgesia," *Brain,* 2001, doi: 10.1093/brain/124.9.1754.

[126] J. V. Priestley, G. J. Michael, S. Averill, M. Liu, and N. Willmott, "Regulation of nociceptive neurons by nerve growth factor and glial cell line derived neurotrophic factor," *Can J Physiol Pharmacol,* vol. 80, no. 5, pp. 495-505, May 2002, doi: 10.1139/y02-034.

[127] P. Allan I. Basbaum, "Basic mechanisms," in *Pain Management Secrets*, Third ed.: Mosby, 2009, ch. 3.

[128] D. Usoskin *et al.*, "Unbiased classification of sensory neuron types by large-scale single-cell RNA sequencing," *Nat Neurosci,* vol. 18, no. 1, pp. 145-53, Jan 2015, doi: 10.1038/nn.3881.

[129] R. A. M. RD Treede, J. N. Campbell, "Myelinated mechanically insensitive afferents from monkey hairy skin heat response properties," *Journal of Neurophysiology,* 1998, doi: 10.1152/jn.1998.80.3.1082.

[130] M. C. Reddan and T. D. Wager, "Modeling Pain Using fMRI: From Regions to Biomarkers," *Neurosci Bull,* vol. 34, no. 1, pp. 208-215, Feb 2018, doi: 10.1007/s12264-017-0150-1.

[131] R. H. W. Rochelle Ackerley, *Microneurography: Recordings from single neurons in human peripheral nerves* (Somatosensory Research Methods). 2023.

[132] R. A. MEYER, "Myelinated Nociceptive Afferents Account for the Hyperalgesia That Follows a Burn to the Hand," 1981, doi: 10.1126/science.7280675.

[133] R. A. M. a. J. N. Campbell, "Peripheral neural coding of pain sensation," *Johns Hopkins APL Technical Digest,* 1981.

[134] R. A. M. K. D. Davis, J. N. Campbell, "Chemosensitivity and Sensitization of Nociceptive Afferents that Innervate the Hairy Skin of Monkey," *Journal of Neurophysiology,* 1993, doi: 10.1152/jn.1993.69.4.1071.

[135] M. C. C. J. Woolf, "Transcriptional and posttranslational plasticity and the generation of inflammatory pain," presented at the National Academy of Sciences colloquium 1999.

[136] L. M. Mendell, "The Path to Discovery of Windup and Central Sensitization," *Front Pain Res (Lausanne),* vol. 3, p. 833104, 2022, doi: 10.3389/fpain.2022.833104.

[137] T. K. Kaan *et al.*, "Systemic blockade of P2X3 and P2X2/3 receptors attenuates bone cancer pain behaviour in rats," *Brain,* vol. 133, no. 9, pp. 2549-64, Sep 2010, doi: 10.1093/brain/awq194.

[138] E. C. Urch, T. Donovan-Rodriguez, and H. A. Dickenson, "Alterations in dorsal horn neurones in a rat model of cancer-induced bone pain," *Pain,* vol. 106, no. 3, pp. 347-356, Dec 2003, doi: 10.1016/j.pain.2003.08.002.

[139] F. W. B. S.R. Chaplan, J.W. Pogrel. J.M. Chung, T.L. Yaksh, "Quantitative assessment of tactile allodynia in the rat paw," *Journal of Neuroscience Methods* 1994, doi: 10.1016/0165-0270(94)90144-9.

[140] G. Czanner *et al.*, "Measuring the signal-to-noise ratio of a neuron," *Proc Natl Acad Sci U S A,* vol. 112, no. 23, pp. 7141-6, Jun 9 2015, doi: 10.1073/pnas.1505545112.

[141] T. KAYANO, N. K. , T. MORIYA, T. K. , Y. K. , Emil C., TOESCU, and I. S. , "Chronic NGF treatment induces somatic hyperexcitability in cultured dorsal root ganglion neurons of the rat," *Biomedical Research,* 2013, doi: 10.2220/biomedres.34.329.

[142] S. M. G. Weiguo Zhu, Jeffrey C. Petruska, Gerry S. Oxford, and Lorne M. Mendell, "A developmental switch in acute sensitization of small dorsal root ganglion neurons to capsaicin or noxious heating by NGF," *Journal of Neurophysiology,* 2004, doi: 10.1152/jn.00356.2004.

[143] A. D. a. M. Perkins, "Bradykinin and inflammatory pain," *Trends in Neurosciences,* 1993, doi: 10.1016/0166-2236(93)90133-7.

[144] B. Liu *et al.*, "The acute nociceptive signals induced by bradykinin in rat sensory neurons are mediated by inhibition of M-type K+ channels and activation of Ca2+-activated Cl- channels," *J Clin Invest,* vol. 120, no. 4, pp. 1240-52, Apr 2010, doi: 10.1172/JCI41084.

[145] M. H. Nina Bohm-Starke, Christian Falconer, Eva Rylander, "Increased intraepithelial innervation in women with vulvar vestibulitis syndrome," *Gynecol Obstet Invest,* 1998, doi: 10.1159/000010045.

[146] M. LARS V. WESTROM, PhD, ROGER WILLEN, MD, PhD, "Vestibular Nerve Fiber Proliferation in Vulvar Vestibulitis Syndrome," *Obstet Gynecol.,* vol. 94, no. 4, pp. 572-576, 1998.

[147] E. J. Huang and L. F. Reichardt, "Neurotrophins: roles in neuronal development and function," *Annu Rev Neurosci,* vol. 24, pp. 677-736, 2001, doi: 10.1146/annurev.neuro.24.1.677.

[148] F. Denk, D. L. Bennett, and S. B. McMahon, "Nerve Growth Factor and Pain Mechanisms," *Annu Rev Neurosci,* vol. 40, pp. 307-325, Jul 25 2017, doi: 10.1146/annurev-neuro-072116-031121.

[149] D. D. Ginty and R. A. Segal, "Retrograde neurotrophin signaling: Trk-ing along the axon," *Curr Opin Neurobiol,* vol. 12, no. 3, pp. 268-74, Jun 2002, doi: 10.1016/s0959-4388(02)00326-4.

[150] C. C. S. D. S. M. C. N. K. S. C. S. P.-M. M. P. A. L. H. L. S. B. M. D. L. Shelton; Arthur D. Levinson; Heidi S. Phillips, "Mice lacking nerve growth factor display perinatal loss of sensory and sympathetic neurons yet develop basal forebrain cholinergic neurons," *Cell,* 1994, doi: 10.1016/0092-8674(94)90378-6.

[151] D. AM, "The emerging generality of neurotrophic hypothesis," *Trends in Neurosciences,* 1988, doi: 10.1016/0166-2236(88)90099-9.

[152] D. Kathryn M. Albers and a. B. M. D. E. Wright, "Overexpression of nerve growth factor in epidermis of transgenic mice causes hypertrophy of the peripheral nervous system," *Journal of Neuroscience,* 1994, doi: 10.1523/JNEUROSCI.14-03-01422.1994.

[153] R. M. Lindsay, "Nerve Growth Factors NGF BDNF Enhance Axonal Regeneration but are not required for survival of adult sensory neurons," *Journal of Neuroscience,* 1988, doi: 10.1523/JNEUROSCI.08-07-02394.1988.

[154] T. J. Price *et al.*, "Treatment of trigeminal ganglion neurons in vitro with NGF, GDNF or BDNF: effects on neuronal survival, neurochemical properties and TRPV1-mediated neuropeptide secretion," *BMC Neurosci,* vol. 6, p. 4, Jan 24 2005, doi: 10.1186/1471-2202-6-4.

[155] I. Kinkelin, S. Motzing, M. Koltenzenburg, and E. B. Brocker, "Increase in NGF content and nerve fiber sprouting in human allergic contact eczema," *Cell Tissue Res,* vol. 302, no. 1, pp. 31-7, Oct 2000, doi: 10.1007/s004410000202.

[156] J. A. F. Winter, C. Sternberg, Julia; Lindsay, Ronald M. , "Nerve growth factor (NGF) regulates adult rat cultured dorsal root ganglion neuron responses to the excitotoxin capsaicin," *Neuron,* 1988, doi: 10.1016/0896-6273(88)90154-7.

[157] H. J. Chien *et al.*, "Human pancreatic afferent and efferent nerves: mapping and 3-D illustration of exocrine, endocrine, and adipose innervation," *Am J Physiol Gastrointest Liver Physiol,* vol. 317, no. 5, pp. G694-G706, Nov 1 2019, doi: 10.1152/ajpgi.00116.2019.

[158] G. Gasparini *et al.*, "Nerves and Pancreatic Cancer: New Insights into a Dangerous Relationship," *Cancers (Basel),* vol. 11, no. 7, Jun 26 2019, doi: 10.3390/cancers11070893.

[159]   I. E. Demir, H. Friess, and G. O. Ceyhan, "Neural plasticity in pancreatitis and pancreatic cancer," *Nat Rev Gastroenterol Hepatol,* vol. 12, no. 11, pp. 649-59, Nov 2015, doi: 10.1038/nrgastro.2015.166.

[160]   S. A. Malin, B. M. Davis, and D. C. Molliver, "Production of dissociated sensory neuron cultures and considerations for their use in studying neuronal function and plasticity," *Nat Protoc,* vol. 2, no. 1, pp. 152-60, 2007, doi: 10.1038/nprot.2006.461.

[161]   R. Assi, D. Mukherji, A. Haydar, M. Saroufim, S. Temraz, and A. Shamseddine, "Metastatic colorectal cancer presenting with bone marrow metastasis: a case series and review of literature," *J Gastrointest Oncol,* vol. 7, no. 2, pp. 284-97, Apr 2016, doi: 10.3978/j.issn.2078-6891.2015.092.

[162]   D. Albo *et al.*, "Neurogenesis in colorectal cancer is a marker of aggressive tumor behavior and poor outcomes," *Cancer,* vol. 117, no. 21, pp. 4834-45, Nov 1 2011, doi: 10.1002/cncr.26117.

[163]   L. L. Tan, J. C. Bornstein, and C. R. Anderson, "Distinct chemical classes of medium-sized transient receptor potential channel vanilloid 1-immunoreactive dorsal root ganglion neurons innervate the adult mouse jejunum and colon," *Neuroscience,* vol. 156, no. 2, pp. 334-43, Oct 2 2008, doi: 10.1016/j.neuroscience.2008.06.071.

[164]   W. J. Oh and C. Gu, "Establishment of neurovascular congruency in the mouse whisker system by an independent patterning mechanism," *Neuron,* vol. 80, no. 2, pp. 458-69, Oct 16 2013, doi: 10.1016/j.neuron.2013.09.005.

[165]   M. Balood *et al.*, "Nociceptor neurons affect cancer immunosurveillance," *Nature,* vol. 611, no. 7935, pp. 405-412, Nov 2022, doi: 10.1038/s41586-022-05374-w.

[166]   H. A. Enright *et al.*, "Long-term non-invasive interrogation of human dorsal root ganglion neuronal cultures on an integrated microfluidic multielectrode array platform," *Analyst,* vol. 141, no. 18, pp. 5346-57, Sep 21 2016, doi: 10.1039/c5an01728a.

[167]   R. Atmaramani *et al.*, "Investigating the Function of Adult DRG Neuron Axons Using an In Vitro Microfluidic Culture System," *Micromachines (Basel),* vol. 12, no. 11, Oct 27 2021, doi: 10.3390/mi12111317.

[168]   P. W. Mantyh, "Mechanisms that drive bone pain across the lifespan," *Br J Clin Pharmacol,* vol. 85, no. 6, pp. 1103-1113, Jun 2019, doi: 10.1111/bcp.13801.

[169]   Y. F. Zhu *et al.*, "Differences in electrophysiological properties of functionally identified nociceptive sensory neurons in an animal model of cancer-induced bone pain," *Mol Pain,* vol. 12, 2016, doi: 10.1177/1744806916628778.

[170]   A. Horn, Dahl, O., & Morild, I. , "Venous and neural invasion as predictors of recurrence in rectal adenocarcinoma," *Diseases of the colon & rectum,* 1991, doi: 10.1007/BF02051074.

[171]   R. E. Stopczynski *et al.*, "Neuroplastic changes occur early in the development of pancreatic ductal adenocarcinoma," *Cancer Res,* vol. 74, no. 6, pp. 1718-27, Mar 15 2014, doi: 10.1158/0008-5472.CAN-13-2050.

[172]   H.-j. S. Guo-li Ming, N. I. Benedikt Berninger, and a. M.-m. P. Marc Tessier-Lavigne, "Phospholipase C-g and Phosphoinositide 3-Kinase Mediate Cytoplasmic Signaling in Nerve Growth Cone Guidance," *Neuron,* 1999, doi: 10.1016/s0896-6273(00)80760-6.

[173]   D. Huh, B. D. Matthews, A. Mammoto, M. Montoya-Zavala, H. Y. Hsin, and D. E. Ingber, "Reconstituting organ-level lung functions on a chip," *Science,* vol. 328, no. 5986, pp. 1662-8, Jun 25 2010, doi: 10.1126/science.1188302.

[174]   E. Dolgin, "Cancer–neuronal crosstalk and the startups working to silence it," *Nat Biotechnol,* vol. 38, no. 2, p. 116, Feb 2020, doi: 10.1038/s41587-020-0429-z.

[175]   X.-L. Shu, A.; Mendell, L. M.*, "Effects of trkB and trkC neurotrophin receptor agonists on thermal nociception a behavioral and electrophysiological study," *PAIN,* 1999, doi: 10.1016/S0304-3959(99)00042-1.

[176]   Z. Gil *et al.*, "Paracrine regulation of pancreatic cancer cell invasion by peripheral nerves," *J Natl Cancer Inst,* vol. 102, no. 2, pp. 107-18, Jan 20 2010, doi: 10.1093/jnci/djp456.

[177]   L. S. Caroline Brunetto de Fariasa, Rodrigo Cruz Limaa, Flávio Kapczinskic, Gilberto Schwartsmann and Rafael Roesler, "Reduced NGF Secretion by HT-29 Human Colon Cancer Cells Treated with a GRPR Antagonist," *Protein & Peptide Letters,* 2009, doi: 10.2174/092986609788490177.

[178]   C. M. Leung *et al.*, "A guide to the organ-on-a-chip," *Nature Reviews Methods Primers,* vol. 2, no. 1, 2022, doi: 10.1038/s43586-022-00118-6.

[179]   M. Radisic and P. Loskill, "Beyond PDMS and Membranes: New Materials for Organ-on-a-Chip Devices," *ACS Biomater Sci Eng,* vol. 7, no. 7, pp. 2861-2863, Jul 12 2021, doi: 10.1021/acsbiomaterials.1c00831.

[180]   F. K. Bayat, B. Polat Budak, E. N. Yigit, G. Ozturk, H. O. Gulcur, and A. Guvenis, "Adult mouse dorsal root ganglia neurons form aberrant glutamatergic connections in dissociated cultures," *PLoS One,* vol. 16, no. 3, p. e0246924, 2021, doi: 10.1371/journal.pone.0246924.

[181]   "Cancer Pain Relief," World Health Organization 1986. 9241561009_eng.pdf

[182]   G. Goodwin and S. B. McMahon, "The physiological function of different voltage-gated sodium channels in pain," *Nat Rev Neurosci,* vol. 22, no. 5, pp. 263-274, May 2021, doi: 10.1038/s41583-021-00444-w.

[183]   B. E. Blass, "Inhibitors of Na(v)1.7 for the Treatment of Pain," *ACS Med Chem Lett,* vol. 13, no. 4, pp. 532-533, Apr 14 2022, doi: 10.1021/acsmedchemlett.2c00088.

[184]   L. S. Premkumar, "Targeting TRPV1 as an alternative approach to narcotic analgesics to treat chronic pain conditions," *AAPS J,* vol. 12, no. 3, pp. 361-70, Sep 2010, doi: 10.1208/s12248-010-9196-y.

[185]   D. Selvaraj *et al.*, "A Functional Role for VEGFR1 Expressed in Peripheral Sensory Neurons in Cancer Pain," *Cancer Cell,* vol. 27, no. 6, pp. 780-96, Jun 8 2015, doi: 10.1016/j.ccell.2015.04.017.